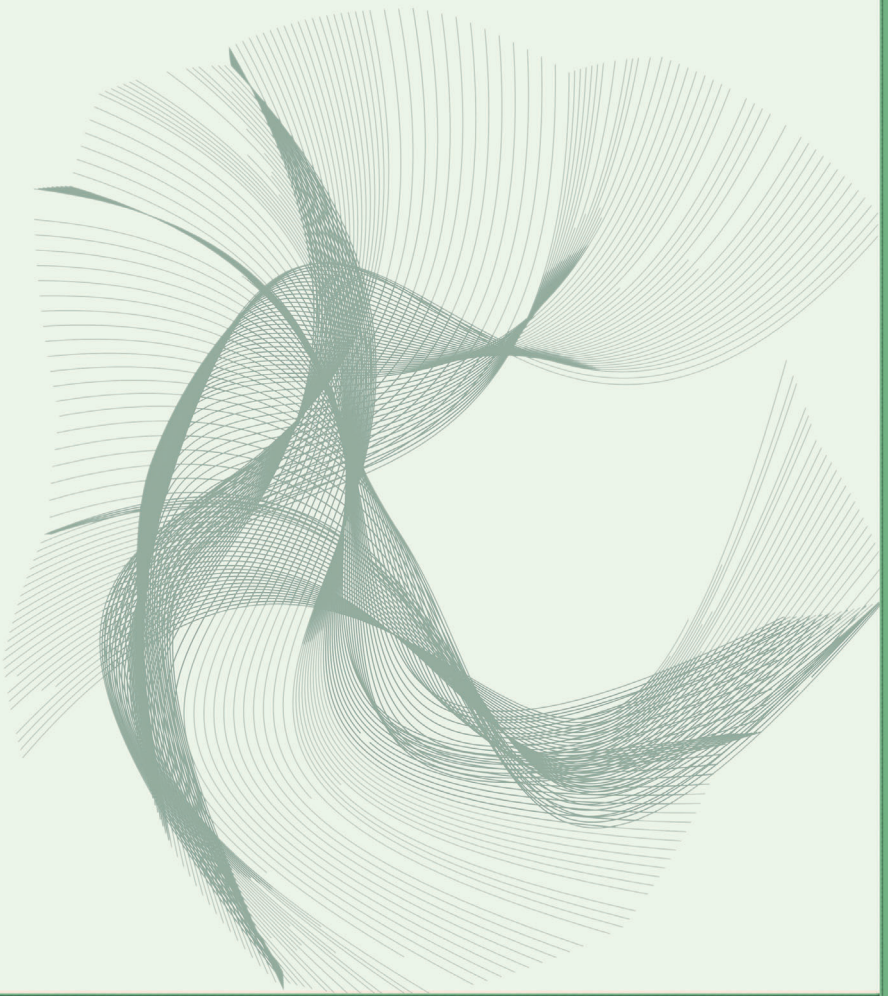

Department of Applied Chemistry
Cochin University of Science and Technology
Kochi -22

STUDIES ON THE PREPARATION OF SUPPORTED NICKEL CATALYSTS USING BIS(ETHYLENEDIAMINE)NICKEL(II) COMPLEXES AS PRECURSORS

Ph.D Thesis

STUDIES ON THE PREPARATION OF SUPPORTED NICKEL CATALYSTS USING BIS(ETHYLENEDIAMINE)NICKEL(II) COMPLEXES AS PRECURSORS

By

ROBINSON P PONMINIESSARY

Department of Applied Chemistry
Cochin University of Science and Technology
Kochi - 22

JUNE 2010

Studies on the preparation of supported nickel catalysts using bis(ethylenediamine)nickel(II) complexes as precursors

Thesis submitted to the
Cochin University of Science and Technology
In partial fulfillment of the requirements for the degree of

Doctor of Philosophy

In

Chemistry

Under the Faculty of Science

By

Robinson P Ponminiessary

Department of Applied Chemistry
Cochin University of Science and Technology
Kochi-682022

June 2010

O' Lord you are good and you do good.

Teach me your statutes!

(Psalm 119:68). The Bible.

Certificate

This is to certify that the thesis entitled ***"Studies on the preparation of supported nickel catalysts using bis(ethylenediamine)nickel(II) complexes as precursors"*** *is an authentic record of research work carried out by Mr. Robinson P Ponminiessary under my supervision, in partial fulfillment of the requirements for the degree of Doctor of Philosophy of Cochin University and Science and Technology, and further that no part thereof has been presented before for any other degree.*

Kochi,

18th June 2010.

Dr. K. K. Mohammed Yusuff,

(Supervising Guide)

Declaration

I hereby declare that the work presented in this thesis entitled **"Studies on the preparation of supported nickel catalysts using bis(ethylenediamine)nickel(II) complexes as precursors"** is entirely original and was carried out by me independently under the supervision of Dr. K. K. Mohammed Yusuff, (former Professor of Catalysis, Department of Applied Chemistry, Cochin University of Science and Technology) and has not been included in any other thesis submitted previously for the award of any degree.

Kochi, ***Robinson P Ponminiessary***

18th June 2010.

Acknowledgement

I was glad to come back to active catalysis research, as I received a warm welcome from the research group of ***Dr. K K Mohammed Yusuff.*** *Sir, I would like to express my sincere gratitude for the trust you had in me that I will complete this work. The constant encouragement, the thorough guidance and the freedom which you gave to me, played a significant role in finishing this work. I will ever remember the patience you were showing to correct my incomplete manuscripts in between your busy schedules as The Dean, Faculty of Science.*

I am grateful to ***Dr. K Sreekumar****, Head of the Department, Department of Applied Chemistry, and to* ***Dr. S Sugunan****,* ***Dr. M R Prathapachandra Kurup,*** *and* ***Dr. K Girish Kumar*** *former Heads of the Department for providing me the necessary facilities. I would like to express my sincere gratitude to all teaching and non-teaching staff of Department of Applied Chemistry.*

I express my sincere thanks to ***Mr. Somnath*** *(Chemistry Manager, Emirates Industrial Laboratory, Dubai) and* ***Mr. Andrew Fake*** *(Engineering Supridentant, Dubai Natural Gas Limited, Dubai) for allowing me to pursue my studies.*

And then dear ***Dr. Arun****, I wouldn't have completed this work without your help. I gratefully remember that, whenever I needed a help you and* ***Manju*** *were there.* ***Dr. Annu Anna, Leeju, Varsha*** *and* ***Digna*** *thanks for making our lab a better place. I would like to give special thanks to* ***Dr. K. K Abdul Rashid, Dr. Anas*** *and Mr.* ***M.V Baiju*** *of Research and Develpoment Division, Sud Chemie India Ltd for their kind support. And hey* ***Mr. Aniz*** *(Sud Chemie) our team work on TPR and those discussions were really interesting.*

My sincere thanks to all Research Scholars and M.Tech students of the department for the friendship offered to me. I am greatly indebted to ***Mr. Sudheesh*** *(CSMCRI, Bhavnagar),* ***Mr. Jayakumar*** *(Oslo University, Norway) and* ***Mr. Sujith Krishnan*** *(IISC, B'lore) for their readiness to send the literature papers. I am thankful to Department of Science and Technology, India for providing the*

instrumental facilities of Sophisticated Analytical Instrument Facility (SAIF) at the Sophisticated Test and Instrumentation centre (STIC), Cochin University of Science and Technology, Cochin. I sincerely thank ***Dr. Shibu and Melwin*** *(STIC, CUSAT) for their cooperation in recording XRD and SEM. The encouragement and goodwillness of* ***Mohammed Al Jawi****,* ***Krishnamurthy****,* ***Nithin*** *and* ***Mohammed Mansouri*** *of DUGAS lab is greatly acknowledged.*

Special thanks to chettan and chechi for all those good words and support, and to Immanuel and Issabella for pressurizing me to wind up the work. Dear amma, how much you and Pappa suffered for my studies from kindergarten to this level. It will be a sin if I try to express my feelings in words. So better keep silent. And finally dear Alice thanks for not complaining about my absence at home, for the consolations whenever I was tired and for the encouragement when I was lazy. So finally you are the woman behind this man's successful dissertation.

And O' Lord I bow before You for the lesson 'Knowledge about You is worth than a hundred thesis'. And so it's time to search for the real knowledge.

Robinson

Contents

.....✵.....

Preface

Transforming the art of catalyst preparation in to a science has been one of the major challenges faced by the catalyst researchers of all periods. The chemical reactions occurring in the solution state and in the solid state during catalyst preparation are extremely complex and are also poorly understood. Scientific knowledge on the 'happenings' of a catalyst synthesis can become the stepping stone towards the development of efficient catalysts or the improvement of the existing ones. Main theme of the present work is the consequences of using different precursors for the preparation of supported nickel catalysts.

The precursors used were bis(ethylenediamine) complexes of nickel(II) with varying counter ions. Migration of metal ions to the support structure is one of the crucial factors determining the activity and selectivity of supported catalysts and efforts were made in this study to determine the influence of counter ions on metal migration. The unsupported nickel complexes were subjected to almost the same heat treatment as in catalyst preparation and the properties of the product obtained were studied. The effect of these metal complexes on the macrodistribution of active species obtained by impregnation, on preformed catalyst support were also investigated. Furthermore an attempt was made to study the structure-activity correlations by carrying out the reactions like hydrogenation and dehydrogenation on these catalysts. In short the work presented in this thesis is a humble effort to add 'a little input' to the catalyst preparation science.

Chapter 1

INTRODUCTION

Contents

More than 90% of all chemical and environmental processes use catalysts in at least one step, and there is a trend to replace older stoichiometric processes by clean catalytic ones. Heterogeneous catalysis is used widely in chemical, refinery and pollution control processes. Current world wide catalyst usage is about 10 billion $ annually with approximately 3 % annual growth. For a 1 $ worth of catalyst consumed, about 200$- 1000$ worth of products are manufactured [1]. Because of ease of separation of catalysts, more and more homogeneous processes are being converted to heterogeneous processes.

1.1 Nickel catalysts in industry

Nickel catalysts play a major role in chemical industry. For example, out of the nine catalytic processes in an ammonia plant, five of them namely hydrodesulphurization ($NiMo/Al_2O_3$), pre reforming, primary reforming, secondary reforming and methanation, make use of nickel catalysts. The development of homogeneous nickel complex catalysis was mainly initiated by Reppe and Wilke, who synthesized a series of organo-nickel complexes for polymerization reactions [2]. It was in 1899, that Paul Sabatier for the first time used Raney nickel for the hydrogenation of unsaturated organic compounds. He was awarded the Nobel Prize in 1912 for his work on nickel catalysts. Hearing about the work of Sabatier, Wilhelm Norman conducted hydrogenation of fats using nickel catalysts in 1901. The first commercial plant based on Wilhelm's work was constructed in United Kingdom by Joseph Crosfield and Sons Ltd, Crosfield UK. The first year production of hydrogenated fats and fatty acids were 3000 tons, whereas presently 15 million tons of hydrogenated products are produced world wide. However due, to its pyrophoric properties, Raney nickel was unsuitable for many organic hydrogenations.

1.1.1 Supported nickel catalysts

The discovery of supported metal catalysts was based on accidental observation that unknowingly added diatomaceous earth increased the activity of Raney nickel catalysts. The following excerpt by G.C Bond, [3] describes supported catalysts in the following most elegant way.

> *"Supported metal catalysts comprise 0.1-20 weight percent of a metal of group 8 or 9 dispersed over the surface of a* ***support,*** *which is typically a high-surface area oxide. They are widely used on an industrial scale and in research laboratories. Principal large-scale uses include hydrogenation of animal and vegetable oils (fat hardening), petroleum reforming to make high-octane gasoline, and treatment of*

vehicle exhaust to minimize environmental pollution. These materials are effective as catalysts because the active metallic phase is present as extremely small particles, having a ***degree of dispersion*** *(that is, the fraction of atoms exposed at the surface) of 10-100%. They are firmly anchored to the support and are widely separated from each other, and hence do not readily coalesce, or sinter."*

Supported nickel catalysts are used in modern chemical industry for some key processes. A few processes are discussed below.

1.1.2 Hydrogenation

Sabatier's discovery of nickel hydrogenation catalyst [4] led to the establishment of commercial hydrogenation processes. Large scale processes include hydrogenation of benzene to cyclohexane, hydrogenation of aldehydes and acids to alcohols and hydrogenation of cyclododecatriene to cyclododecane for manufacture of plasticizers. A large number of pharamaceutical intermediates and bioactive substances also rely on nickel hydrogenation catalysts for their commercial production. Nickel catalysts are the most abundantly used ones in gas-phase and liquid-phase hydrogenation. Catalysts based on noble metals (Pt, Pd, Rh, and Ru) are usually more active and less sensitive to poisons. But they are more expensive and hence used less.

Hydrogenation of aromatics is very important in upgradation of coal liquids and diesel fuels. These processes have been studied over nickel and noble metal catalysts [5, 6]. Exhaust particles from diesel engines contain powerful carcinogens which are mainly generated by combustion of aromatics. The hydrogenated aromatics can increase the cetane number of diesel. Thus deep aromatic saturation is very much relevant in industrial research. Effect of different nickel precursors on the hydrogenation of naphthalene (which is considered as a model aromatic compound of diesel) was studied by Li *et al.* [7]. The reduction patterns were different when the precursors were changed and the studies indicated that the catalysts with high reduction degree had high activity. The same reaction was studied by Kirumakki *et*

al. [8] on Ni/SiO_2-Al_2O_3 catalysts. Two types of nickel sites were identified by temperature programmed reduction studies: one with no interaction with the support and the other having interaction with the support. They observed a direct correlation between hydrogenation activity and NiO with no interaction. This indicates Ni crystallites generated from reduction of free NiO have high hydrogenation capability.

1.1.3 Steam Reforming

Steam reforming of naphtha, LPG, methanol and CO_2 has been reported on nickel catalysts. Low temperature steam reforming technology is of much application in fuel cell systems. The reaction is industrially operated at high temperature around 800 °C to achieve reasonable conversion for this endothermic process [9]. Generally Ni/α-Al_2O_3 catalysts are used for high temperature steam reforming. The poor dispersion of nickel species on α-Al_2O_3 forces one to test other high surface area forms of alumina like γ-Al_2O_3. Steam reforming nickel catalysts require operating conditions such as high temperature and high steam to carbon ratio. These conditions facilitate the easy sintering of nickel metal crystallites and deposition of carbon on them leading to severe deactivation. Also these catalysts require fuels with high quality (<0.5 ppm S). Because of their low activity, high volume of catalysts has to be used for high conversions.

In steam reforming, the decomposition of hydrocarbon to a carbon species is regarded as the first step in the reaction. In the second step, the carbon species react with steam or surface oxygen of catalyst to form carbon oxides and gets desorbed from the surface.

Steam reforming is an equilibrium limited reaction and the removal of hydrogen from reaction system can significantly increase the conversion of hydrocarbons. This can result in low reaction temperatures for significant conversions. Membrane reactors have been proposed to effectively separate hydrogen [10]. By using such a membrane reactor Uemiya *et al.* [11] achieved methane conversion close to 90 % at 500 °C. If the reaction temperatures can be bought to such low temperatures, high surface area oxides can be used without

affecting the stability of the reaction. Silica, γ-Al_2O_3 and zirconia were used as supports for nickel catalysts for steam reforming of methane at 500 °C by Matsumura and Nakamori [12]. Ni/Zirconia was found to be the most effective catalyst. Their mechanistic studies have shown that the surface hydroxyl groups play the major role in the reaction pathway. Zirconia can accumulate significant quantities of water on its surface by dissociation of Zr-O-Zr with H_2O to 2Zr-OH. These hydroxyls then migrate to the reduced nickel atoms to form Ni-OH, which then reacts with methane to form carbon dioxide.

In a recent study, steam reforming of LNG (liquefied natural gas) was conducted on nickel catalysts supported on mesoporous γ-aluminas prepared by hydrothermal method [13]. The well-developed mesopores and strong metal support interaction on the catalysts gave good stability for the reaction conducted at 600 °C. It was found that a high pore volume and large pore size of the support facilitate the internal mass transfer, which significantly increases the rate of the reaction.

1.1.4 Methanation

The first literature on methanation appeared in the literature in 1902 [14]. Methanation catalysts are used industrially on a large scale in ammonia synthesis plants to remove traces of carbon oxides that would otherwise poison the ammonia synthesis catalysts [15]. Methanation process is also used in refineries and caprolactam plants where high purity hydrogen is required. The preferred industrial catalyst is still the Ni/Al_2O_3, despite the years of research to find new ones.

Computational screening studies by Anderson *et al.* indicated that Ni-Fe alloy can function as more effective catalyst for methanation [16]. Later it was experimentally verified, and found that the best catalysts have a Ni/Fe ratio above 1 and that the pure iron catalyst is much less active than the pure nickel catalyst. Thus, the activity pattern can be described as a volcano curve.

1.2 New areas of performance

The energy requirements and environmental constraints of this century have forced application of supported nickel catalysts for some new processes. In this section potential applications of supported nickel catalysts are presented.

1.2.1 Partial oxidation of methane

Large volumes of methane gas are flared out in oil rigs and refineries, mainly because of the difficulty in transportation. Moreover methane is a unreactive molecule, due to the difficulty in C-H bond activation. As more oil is used for energy purposes, modern technologists now rely on natural gas (of which methane is the major component) for synthesis of chemicals. Scientists are partially successful in converting methane to syngas by steam reforming, partial oxidation and carbon dioxide reforming. Partial oxidation of methane (POM) is an important reaction for the production of syngas, but has not been commercialized.

$$CH_4 + \tfrac{1}{2}\, O_2 \rightarrow CO + 2H_2 \qquad ; \Delta H°_{298} = -36 \text{ kJ mol}^{-1}$$

The reaction is slightly exothermic, which is a major advantage over the strongly endothermic steam reforming process. The produced syngas has a ratio H_2:CO = 2:1 which is suitable for Fischer-Tropsch synthesis. Generation of waste gases is also less compared to steam reforming. Coking is the major reason for the deactivation of POM catalysts. Carbon deposition mainly comes from methane decomposition and CO disproportionation (Boudart) reactions.

$$CH_4 \rightarrow C_s + 2H_2$$

$$2CO \rightarrow C_s + CO_2$$

The catalysts studied for the reaction include supported noble metals [17, 18], supported nickel [19, 20] and pervoskite oxides [21, 22].

Tang *et al.* [23] studied the POM reaction on nickel supported on MgO, CaO or CeO_2. They studied the reaction under thermodynamically severe conditions (CH_4/O_2 = 2.5, a higher CH_4 to O_2 than the stoichiometric ratio) and observed

Ni/MgO catalysts were resistant to carbon formation. These Ni/MgO catalysts have low reducibility, but they have uniform dispersion and weak donor ability of nickel, which make them effectively resistant towards carbon deposition. Magnesium-Aluminum layered double oxides were used as supports for nickel catalysts in POM reaction [24]. Such double oxides have basic character which makes the catalyst more resistant towards coke formation.

The MgO precoated Ni/Al_2O_3 catalysts prepared by Chowdhari *et al.* [25] exhibit stable performance for POM reaction due to the formation of stable $NiMg_2O_4$ spinel protective layer. This protective layer hinder the formation of $NiAl_2O_4$. POM is a very fast reaction, and hence eggshell catalysts are proposed to give higher conversion and stability [26]. The studies by Qiu *et al.* suggested that small nickel crystallites and large pores are necessary for a stable catalyst for the POM reaction.

Use of oxygen permeating ceramic membrane as catalyst is another advancement in the research on POM reaction. Ishihara and Takita [27] used basic $LaGaO_3$ oxide as mixed ionic and electronic conducting membrane to obtain pure oxygen from air. Perovskite oxides of $LaGaO_3$ doped with Sr for a La site and Fe, Co, or Ni for a Ga site, are promising as the oxygen-separating membrane for methane partial oxidation because of high stability in a reducing atmosphere and high permeability of oxygen.

1.2.2 Carbon dioxide reforming of methane

Both carbon dioxide and methane are green house gases and their release to atmosphere is restricted by legislature. Carbon dioxide reforming of methane (CRM) is proposed to be an attractive process for effective utilization of both the gases [28, 29]. The process produces syngas with equal mols of CO and H_2 which is ideal for methanol and Fischer-Tropsch synthesis. The natural gas reservoirs contain, in addition to methane, a large fraction of CO_2. Thus natural gas can be directly used as the feed for the process with some purification. The use of CO_2 provides a clean and cheaper source of oxygen, which eliminates the costly separation process required

for partial oxidation of methane. Even though much research has been done in last two decades, no industrial technology has been established. Catalyst deactivation due to coke formation is the main hurdle to overcome, and the use of noble metals was a choice to reduce the deactivation [30]. But, the high cost of noble metals has driven the research towards developing nickel based catalysts.

Nickel/Zeolite catalysts were made by both solid state reaction and impregnation [31]. Catalyst prepared by solid state reaction was much active than the other and gave 90 % conversion and an operational period of 140 hours at 800 °C without much deactivation. Effect of nickel precursors on the activity of Ni/La_2O_3 catalysts was studied by Ruckenstein and Hu [32]. Catalyst prepared from chloride precursor was more active than the one prepared from nitrate precursor. The effect of supports on the activity was studied by Wang and Lu [33]. The deactivation rates of the catalysts were in the following order: $Ni/MgO < Ni/\gamma\text{-}Al_2O_3 < Ni/SiO_2 < Ni/\alpha\text{-}Al_2O_3$. Both carbon deposition and metal sintering were responsible for catalyst deactivation. The types of carbon (amorphous or graphitic) formed on the catalysts depended on the nature of the support. The carbon formed on Ni/MgO catalyst was amorphous and could be oxidized at low temperatures. Nano ZrO_2 was used as support to prepare Ni/ZrO_2 catalysts which exhibited extreme stability for CRM [34, 35]. Size limit of the nano ZrO_2 was determined to be 25 nm. It was proposed that the higher metal/oxide boundaries or perimeters on the nanocomposite catalysts rendered the high stability. The oxidative removal of carbon atoms to produce CO increases with the area of metal/oxide boundaries.

The most promising catalysts for the reaction are NiO-MgO solid solutions [36, 37]. A solid solution of composition $Ni_{0.03}Mg_{0.97}O$ showed stability for more than 100 days of operation [38]. In a recent study by Wang *et al.* [39], it was suggested that complete reaction of NiO with the support MgO to form solid solution ($Ni_xMg_{1-x}O$; x=0.06-0.25) is essential to get stable Ni/MgO catalysts for CRM reaction. They also showed that the turnover frequency increased with decreasing crystallite size.

1.2.3 Steam reforming of ethanol

Steam reforming of ethanol is highly relevant in the modern technology because of its application in hydrogen generation. Some futurists believe that hydrogen play a significant role in future energy sector. Proton exchange membrane (PEM) fuel cell which uses hydrogen as fuel is almost certain to meet future low emission targets for NOx, SOx and COx. Ethanol, a form of biomass, which is easy to obtain and to transport can be used for generation of hydrogen. Moreover, ethanol is a bye product of biofuel synthesis and a surge in its production is expected by next decade when many biofuel projects become operational.

In a recent study, mesoporous yttria stabilized zirconia was used as support for nickel catalysts for steam reforming of ethanol [40]. The support with a Y/Zr molar ratio 0.1 was superior in catalytic performance because of its high reducibility and structural stability. Akande *et al.* [41] reformed crude ethanol on Ni/γ-Al_2O_3 catalysts prepared by precipitation, coprecipitation and impregnation. The highest conversion was obtained for the precipitated catalyst which was having high reducibility and small crystallite size. However, in terms of hydrogen yield, coprecipitated catalysts were better ones.

1.2.4 Enantioselective hydrogenation

A large number of pharmaceuticals and bioactive molecules are chiral. Synthesis of chiral compounds with required enantiomeric excess (ee) has always been a challenging task to synthetic chemists. The heterogeneous enantioselective catalysts are advantageous over homogeneous ones because of their ease of separation. However, in most cases the heterogeneous catalysts give low ee.

Polycrystalline nickel surface gives racemic products. It can be made chirally selective by suitable modification with chirally active modifiers like naturally occurring cinchona alkaloids and tartaric acid. The most reported heterogeneous enantioselective nickel catalyst consists of Raney nickel modified by L-tartaric acid. They were used for hydrogenation of unfunctionalized and β-functionalized ketones

[42, 44]. Most of the enantioselective reactions are conducted in liquid phase, but a few are reported in vapor phase also [45]. Hydrogenation of 2-butanone to chiral 2-butanol was reported in vapor phase on Ni/Y-Zeolite and Ni/SiO_2 catalysts. Even though freshly activated catalysts generated racemic products, the in situ and ex situ modification by methanolic solution of L-tartaric acid increased the enantioselectivity. The specific activity increased with average nickel particle size. Nickel supported on graphite was used for enantioselective hydrogenation of methyl acetoacetate by Wolfson *et al.* [46]. Their studies also revealed the dependence of particle size of nickel crystallites.

1.3. Catalyst design-'Selection of precursors'

Many aspects of catalyst manufacturing are still poorly understood. There is a lack of a scientific basis of catalyst manufacture, and the process design often relies on empiricism and trial and error. Clearly, advances and improvements of many key catalyst manufacturing steps could potentially have a large impact on the entire chemical industry. There should be a focused effort to get a better scientific basis for catalyst manufacture.

The main motivations for the development or improvement of an industrial catalyst are a) change in market conditions, b) change in government legislature such as for pollution control and c) to improve the performance of an existing process plant. To satisfy these motivations, an efficient catalyst design should be performed.

According to D.L Trimm [47], one of the pioneers in modern catalysis, '*Catalyst design is described as the application of established concepts to the problem of choosing a catalyst for a given reaction*'. The '*established concepts*' are the theoretical and practical knowledge acquired through years of prior research. A proper design of catalyst requires a multidisciplinary approach from fields of inorganic chemistry, organic chemistry, physical chemistry, solid state chemistry and chemical reaction engineering.

The first task in catalyst design is to identify the suitable inorganic compounds that can catalyze the target organic reaction. Once the primary components are identified, the next task is to prepare the catalyst in suitable form of activity and selectivity. To prepare industrial catalysts with long term activity and selectivity is a challenging task. The first step in achieving this is to identify the starting compounds. The starting compound of the active precursor or better termed as 'catalyst precursor' should have certain properties that would make their selection worthwhile. The precursor should be capable of getting transformed to active component with desired physical and chemical properties like surface area, pore volume, particle size and metal support interaction. The availability and the economic cost should be taken to consideration to reduce the burden on the capital investment. Precursor should be easily convertible to the active component without usage of much time and energy. The environmental regulations restrict the use of some precursors that generate toxic gases and waste materials. These criteria make the '*selection of precursor*' a difficult task to the catalyst designer.

1.3.1 Effect of nickel precursor

Innumerous articles could be found in the literature citing the effect of catalyst precursors on the activity and selectivity of catalysts. For the preparation of supported nickel catalysts, the common precursors used industrially are nickel nitrate and nickel carbonate. The transformation of nickel nitrate to nickel oxide and nickel metal has been studied in detail by many researchers [48-50]. As per their studies, nickel nitrate can decompose in two ways depending upon the drying temperature and atmosphere used. It can decompose by removal of water and nitrogen oxides (N_2O_5, NO_2) simultaneously or by eliminating them in different steps. If the decomposition happens at reduced pressure, dehydration of nickel nitrate occurs as the first step and anhydrous intermediates are obtained. When the decomposition is carried out in presence of water both dehydration and hydropyrolytic reactions occur together and basic nickel nitrates such as $2Ni(NO_3)_2.Ni(OH)_2$ and $Ni(NO_3)_2.Ni(OH)_2$ are obtained as intermediates. The calcination of these intermediates results in the formation of NiO with varying

properties. Nickel oxide obtained by calcination of anhydrous nickel nitrate is reported to have a surface area fifty times higher than that of the oxide obtained by decomposition in static conditions. This indicates the importance of starting precursor and the heating environment.

Estelle *et al.* [51] carefully decomposed nickel nitrate hexahydrate to $Ni_3(NO_3)_2(OH)_4$, by heating in an air oven for 14 days. They proposed a sequential decomposition as follows

$$Ni(NO_3)_2.6H_2O \rightarrow Ni(NO_3)_2.4H_2O \rightarrow Ni(NO_3)_2.2H_2O \rightarrow Ni_2(NO_3)_2(OH)_2 2H_2O \rightarrow Ni_3(NO_3)_2(OH)_4$$

Subsequent calcination of this precursor, $Ni_3(NO_3)_2(OH)_4$, yielded homogeneous octahedral NiO particles. The direct calcination of the $Ni(NO_3)_2.6H_2O$ resulted in formation of low surface area NiO with octahedral particles having different sizes.

The same preparation route was followed to prepare NiO-MgO systems and it was found that when $Ni_3(NO_3)_2(OH)_4$ was used as precursor, homogeneous particles with higher surface area and reducibility were obtained [52]. Argon atmosphere was used for calcination by the same authors in another study [53]. By calcining $Ni_3(NO_3)_2(OH)_4$/MgO under a flowing argon atmosphere, they obtained NiO/MgO systems with higher surface area and reducibility. The highly disadvantageous NiO-MgO solid solution formation could be avoided by this method. Also the particles were of smaller size and homogeneous in shape.

Calcination in an atmosphere other than static air is found to be better, when nickel nitrate is used as precursor. In a recent study by the researchers of the Utrecht University, calcination of catalyst precursor was done in static air, He or NO/He atmosphere to prepare nickel supported on SBA-15 catalysts [54]. They obtained highly dispersed catalysts on using NO/He atmosphere. Nickel nitrate decomposition is highly endothermic. The *in situ* XRD and DSC studies proved that

the nitric oxide atmosphere lowered the decomposition rate and made it less endothermic due to the exothermic scavenging of oxygen by NO.

The high solubility of nickel nitrate and its ability to decompose completely in air atmosphere makes them attractive candidates as catalyst precursors. However, there are studies which reveal that the catalysts made from nickel nitrate have poor metal dispersion. This poor metal dispersion arises from redistribution during drying and sintering during air calcination [55-58]. Moreover, the stringent environmental regulations against the release of nitrogen oxides during calcination make them less attractive.

The nickel salts like nickel chloride, nickel acetate, nickel hydroxide and nickel citrate were also used as precursors to make unsupported and supported NiO. The effect of different precursors on the properties of NiO was studied by Estelle *et al.* [51]. Their studies revealed that NiO prepared from nickel hydroxide precursor had high surface area and sponge like morphology. Nickel acetate precursor after calcining yields partially reduced NiO.

Eliche-Quesada *et al.* studied the influence of nickel citrate precursor for the preparation of supported nickel zirconium-doped mesoporous silica catalysts [59]. The aqueous solution of nickel citrate yielded catalysts with high nickel specific surface area. When compared with catalysts made of nickel nitrate in aqueous and ethanolic solutions, the physical properties (surface area and porosity) were almost the same. The only difference was in the crystallite sizes, which accounted for the high reactivity of the catalysts made using the citrate.

Supported Ni/γ-Al_2O_3 catalysts were prepared by impregnation of nickel nitrate, nickel chloride or nickel sulfate, and their activity for hydrodechlorination of 1,1,2 trichloroethane was studied by Kim *et al.* [60]. The nitrate precursor yielded catalyst with high initial activity but low stability. The sulfate and chloride precursors gave catalysts with large particles of NiO, which were resistant to deactivation. The use of chloride precursor resulted in Ni^{2+} migration to lattice leading to the formation of nickel aluminate. Bifunctional Ni/Al MCM-41 catalysts

prepared by using nickel citrate precursor for hydroconversion of n-dodecane exhibit higher catalytic activity than the catalysts prepared by using nickel nitrate or alkaline tetraamminenickel nitrate [56]. The catalyst; prepared using nickel citrate as the precursor possesses strong metal support interaction and high metal dispersion. This catalyst is reported to have an intimate interaction with metal and acid functions which improve its activity and isomerisation selectivity.

Three different precursors, nickel(II) nitrate hexahydrate, nickel(II) acetylacetonate and nickel(II) phthalocyanine were used to prepare Ni/KL-Zeolite catalysts for selective hydrogenation of citral [61]. Partially oxidized nickel species (Ni^{n+}) were formed, when nickel(II) phthalocyanine was used as the precursor. These species lead to the formation of byproducts like isopulegol, menthol and linalool during the initial phase of the reaction. Nickel nitrate, nickel acetate and nickel chloride were used as precursors to prepare Ni/α-Al_2O_3 catalysts for the oxidative steam reforming of methane [62]. Nickel particle sizes measured by both hydrogen adsorption and XRD were high for the catalysts prepared from nickel chloride precursor. Industrially hydrodearomatization is conducted mainly on nickel or noble metal supported systems. In a recent study Li *et al.* [7] prepared Ni/γ-Al_2O_3 catalysts for hydrogenation of naphthalene to decalin. They studied the use of three nickel precursors, nickel nitrate, nickel acetate and nickel acetate plus citric acid. The catalyst prepared with nickel acetate precursor reduced without calcination was much better with respect to reduction behavior, adsorption-desorption behavior of hydrogen and catalytic activity.

In a more recent study, researchers from Laboratoire de Réactivité de Surface, France, compared the properties of Ni/MCM-41 and Ni/Al-MCM-41 catalysts prepared by nickel nitrate and nickel acetate [63]. Problems generally associated with preparation of catalysts using nickel nitrate, redistribution while drying and poor metal dispersion, could be avoided by the usage of nickel acetate precursor. In the case of nickel acetate, the pH of the impregnating solution is found to be high, which favors the electrostatic interaction between the nickel ions and the

support and result in high metal dispersion. When Al-MCM-41 was used as support, acetate ions could dissolve and extract Al^{3+} ions from the support which partially destroys the support structure.

1.3.2 Metal chelates as catalyst precursors

The above discussion clearly reveals the importance of *'selection of precursors'* in the preparation of supported nickel catalysts. But these studies do not reveal what properties of a precursor make them better or worse than others. The properties of the precursors should be studied more intrigue to add the knowledge to the '*established concepts*' which can be later used for effective catalyst design. However there are some studies already done in this direction, especially in the case of metal chelates [55]. The two important properties which make them attractive as precursors are

i) The viscosity of the impregnating solution increases rapidly on drying due to gelation. Chelating ligands also can form bridging between the metal ions, which further increases the viscosity. The highly viscous, partially dried solution can inhibit the redistribution of active component. This property can be made use of to prepare uniform distribution over catalyst pellets [64].

ii) Upon further drying, the chelated metal complex forms a gel like phase (unlike in the case of usual metal salts which changes in to the crystalline form), which on calcination gives highly dispersed active component [65].

The high viscosity of the chelated solution enabled the preparation of Ni/MCM-41 catalysts with very small nickel particle size [66, 67]. When nickel nitrate was used as precursor, because of the low viscosity the ions migrated from the pores and got deposited on the support surface. In the case on nickel citrate, a thin film of the complex is formed inside the micropores of MCM-41, which upon calcination results in a fine dispersion of nickel.

The most common chelating agents used for the preparation of supported catalysts from aqueous solution are citric acid [66], nitrilotriacetic acid [68, 69], ethylenediamine [70], and ethylenediaminetetraacetic acid [71]. As our study is centered on the use of the ethylenediamine complexes as precursors, further discussion on this aspect will be limited to the application of the complexes of chelating ligand, ethyelenediamine.

1.4 Nickel chelates of ethylenediamine as precursors

Interactions of different types can occur when a transition metal complex is in contact with the support. Six types of interactions are clearly illustrated by Negrier *et al.* [70]. These interactions (Figure 1) between ligand, counter ion, metal and support during drying and calcination determine the final structure and activity of the catalyst.

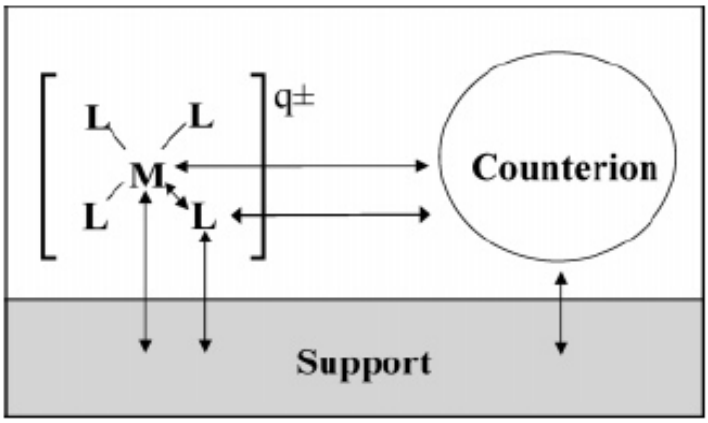

Figure1. Six possible interactions between ligand, metal, counter ion and support during an impregnation process (from Reference [70])

It was reported that Ni^{2+} species coordinated with three or four surface O^{2-} are formed up on calcinations of the surface grafted complexes [72]. These species can be reduced to unusual oxidation state Ni^{+} and are known to be active for olefin diemrization [73]. When Ni(II)tris(ethylenediamine) was used to ion exchange H-ZSM-5 support, a high nickel dispersion was achieved [74]. However the acidity of the support was lowered by ethylenediamine ligands, which resulted in a decrease in

the activity for hydroisomerisation of n-decane; probably the rate controlling step in this case is influenced by acid sites. Nickel(II)bis(ethylenediamine) complexes were used to prepare Ni/γ-Al_2O_3 catalysts by Che group [75]. The final calcinations were done in inert atmosphere and they obtained partially reduced and highly dispersed catalysts.

1.4.1 Effect of number of chelating ligands

One, two or three ethylenediamine ligands can be accommodated in the nickel(II) octahedral complexes as indicated below.

$$[Ni(H_2O)_6]^{2+} \rightarrow [Ni(H_2O)_4(en)]^{2+} \rightarrow [Ni(H_2O)_2(en)_2]^{2+} \rightarrow [Ni(en)_3]^{2+}$$

The logarithmic formation constants *log* β_1, *log* β_2 and *log* β_3 of the three stepwise complexation reactions are 7.60, 14.08 and 19.13 respectively [76]. This indicates that these complexes can be prepared almost stoichiometrically in aqueous solution. The coordinated water molecules are labile and can be easily substituted by different functional groups of the support surface. As the number of H_2O ligands varies, the reactivity towards the surface also varies. The effect of number of ethylenediamine ligands on the preparation of supported nickel catalysts was studied in detail by Sun *et al.* [77]. Their studies indicate that, even though the formation constants of complexes are large and well separated, complexes with different stoichiometries can coexist at any particular en:Ni ratio. Thus when the en:Ni ratio increases from 1 to 3, the most abundant complex is $[Ni(en)(H_2O)_4]^{2+}$ (64% of all Ni complexes), $[Ni(en)_2(H_2O)_2]^{2+}$ (81%) and $[Ni(en)_3]^{2+}$ (61%), respectively. Thus during impregnation, even at a fixed en:Ni ratio, the adsorption of other en complexes on the support cannot be avoided. The complex $[Ni(en)_3]^{2+}$, cannot be absorbed or grafted on the support as it does not contain any labile H_2O ligands.

The complex $[Ni(H_2O)_4(en)]^{2+}$ on grafting on the silica support formed the complex $[Ni(H_2O)_2(SiO)_2(en)]^{2+}$ which on calcination formed NiO and nickel phyllosilicate. Subsequent reduction of this material gave metallic nickel with varying sizes and poor dispersion. The grafting of the complex $[Ni(H_2O)_2(en)_2]^{2+}$

resulted in formation of $[Ni(SiO)_2(en)_2]^{2+}$, which does not contain any labile ligands. Calcination and reduction of this material led to formation of nickel crystallites well separated from each other and was having uniform size and shape. Thus it appears that the precursor complex with en:Ni stoichiometry, 2:1, is much better than the others.

In a recent work, Negrier *et al.* [78] studied the effect of number of ligands on Ni/γ-Al_2O_3 catalysts. They could not find significant changes in the properties of the final catalysts by varying the number of chelating ligands. However, with higher number of ligands, higher degrees of reduction were observed.The effect of number of ethylenediamine ligands on the macrodistribution on γ-Al_2O_3 catalyst pellets and nickel speciation was studied by Espinosa-Alonso *et al.* [79]. The nickel profiles on the dried pellets were measured by SEM–EDX (Figure 2).

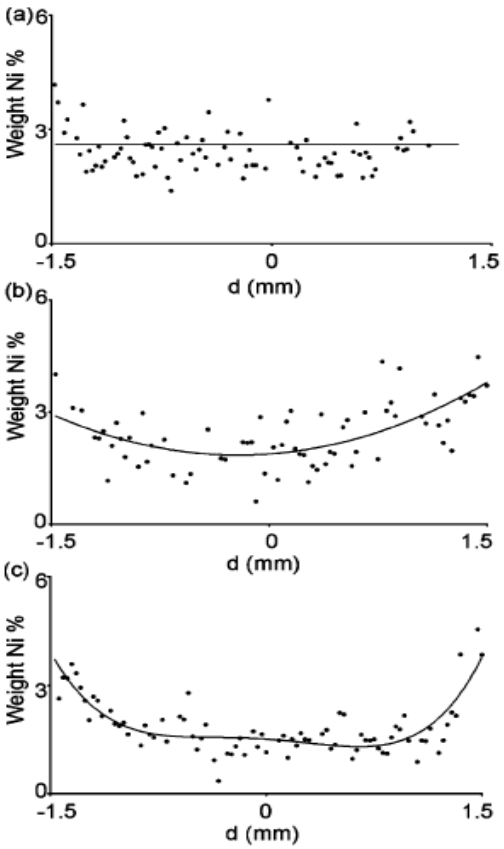

Figure 2. Ni profiles as measured by SEM-EDX (a) en:Ni=1:1, (b) en:Ni=2:1 and (c) en:Ni=3:1. (from Reference [79]).

During the drying process the complexes undergo redistribution, if the adsorption strength is less. In such cases, the uniform distribution obtained immediately after the impregnation step changes during drying. The profiles (Figure 2) also indicate the mobility of ethylenediamine complexes and the mobility is in the order en:Ni=1:1 < en:Ni=2:1 < en:Ni=3:1. During drying, $[Ni(en)_3]^{2+}$ complex is transported together with the solvent toward the outer surface of the pellets, because of the absence of interactions between this complex and alumina in the impregnation step. In the case of $[Ni(en)_2(H_2O)_2]^{2+}$ or $[Ni(en)(H_2O)_4]^{2+}$, the transport of Ni^{2+} toward the outer surface during the drying step is not possible because of the stronger interactions between these complexes and the support. For en:Ni molar ratio 1 and 2 the pH of the impregnating solution was below the *pzc* (point of zero charge) of Al_2O_3. At this pH, the acidic OH groups of the alumina protonate the NH_2 groups of ethylenediamine ligand leading to the decomposition of the complex. Thus by controlling the en:Ni ratios, either egg shell or uniform catalyst pellets could be prepared.

1.4.2 Equilibrium adsorption

When complexes are deposited on support by equilibrium adsorption, they are allowed to react with the surface groups of the support. The counter ions are removed in a washing step and they do not interfere in process. The mechanism of adsorption of complex on the support is a new exciting area in coordination chemistry termed as interfacial coordination chemistry. Lambert *et al.* [80] studied in detail the interfacial coordination chemistry of $[Ni(en)_2(H_2O)_2]^{2+}$ on various supports. They concluded that hydrogen bonding between the H_2O and ethylenediamine ligands on the one hand and surface S-OH groups on the other hand plays important role in the adsorption mechanism during deposition. Upon drying the labile H_2O ligands are replaced by surface groups. The grafted complexes may be written *cis*-$[Ni(en)_2(SO)_2]^{x+}$, where (SO) denotes a surface oxide or hydroxide. The surface species thus enter the coordination sphere as ligands. They even suggested a spectrochemical series of supports as

$$\Delta_0(Cl) < \Delta_0(AlO) < \Delta_0(ZO) < \Delta_0(SiO) = \Delta_0(H_2O)$$

where AlO, SiO and ZO are surface groups of alumina, silica and zeolite respectively.

These surface complexes are transformed to different nickel species after calcination. Their studies also suggested that in saponite clays, because of their lamellar structure, $[Ni(en)_2]^{2+}$ exists as a square planar complex in the interlayer space.

1.4.3 Incipient wetness- Effect of counter ions

Incipient wetness impregnation is the most common method to prepare catalysts and consists of filling the void volume of support with a solution of metal salt. When catalyst supports are subjected to incipient wetness impregnation all the interactions depicted in Figure 1 can occur. The presence of counter ions complicates the adsorption and decomposition mechanisms. The detailed study by Negrier *et al.* [70] shed some light in to complex mechanisms happening during decomposition in the presence of counter ions. Figure 3 shows the mechanism of deposition, drying and final calcinations when $[Ni(H_2O)_2(en)_2]Y$; $Y=NO_3^-$or Cl^- was used as the precursor.

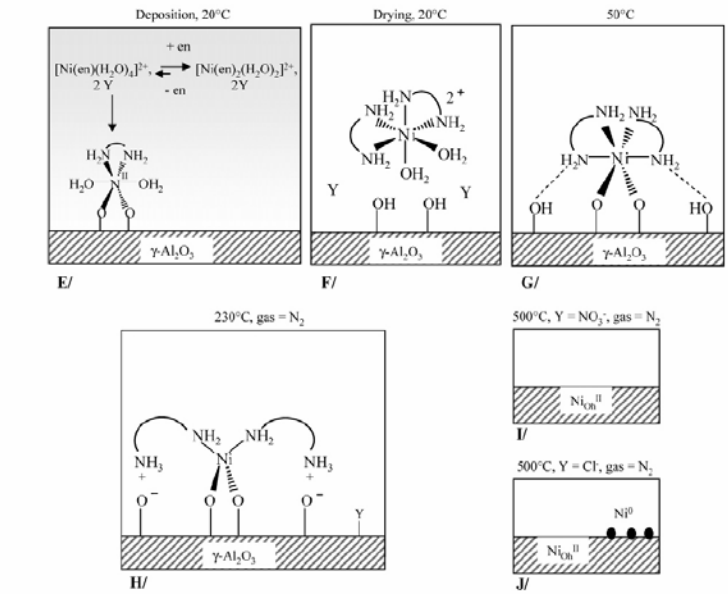

Figure 3. Interactions between support, ligands, metal ions and counterions during preparation by incipient wetness (from Reference [70]).

During deposition, the bis(ethylenediamine) complex forms a mono (ethylenediamine) complex and this complex grafts on to the surface. Upon drying as H_2O ligands are removed, the bis(diamine) complexes graft on to alumina by second sphere interactions. When the temperature is raised to 230 °C the second sphere interactions become strong and lead to the dissociation of ligands from Ni^{2+}. During these interactions of the metal complex, the counter ions are also grafted to the complex. At temperatures above 230 °C the counter ions destroy the ligand by reacting with it. Here the nature of counter ions comes in to action. The NO_3^- ion because of its oxidizing character, oxidize the ethylendiamine ligand and Ni^{2+} ions are deposited on the surface. Chloride counter ion does not have that ability. The ethylenediamine ligands are good reservoir of hydrogen [81]. Hydrogen evolution from the ligands were proposed as

$$R\text{-}CH_2\text{-}NH_2\text{-}Ni^{II}\text{-}O\text{-}Al \rightarrow H_2 + R\text{-}CH{=}NH\text{-}Ni^{II}\text{-}O\text{-}Al$$

$$R\text{-}CH{=}NH\text{-}Ni^{II}\text{-}O\text{-}Al \rightarrow H_2 + R\text{-}CN + Ni^{II}\text{-}O\text{-}Al$$

The nitrate counter ion resulted in deposition of Ni^{2+} species, while chloride ion could reduce some of the Ni^{2+} to metallic state. Thus counter ions can definitely influence the decomposition mechanism which influences the final state of active component.

The thermochemistry of the decomposition reaction can have definite influence on the final state of metal ions. If the decomposition reaction is strongly exothermic the heat generated locally can promote sintering. This locally generated heat can also promote the migration of metal ions in to the support structure. Migration of metal ions deeper in to the support is disadvantageous as may lead to stable compound formation like $NiAl_2O_4$ in case of alumina or NiO-MgO solid solution formation in case of MgO. Thus the judicial selection of the ligands and counter ions can help the design of supported nickel catalyst.

1.4.4 Effect of calcining atmosphere

In most of the work reported on the use of ethylenediamine precursors to prepare catalysts, the final calcinations were done in inert atmosphere. Schimpf *et al.* [82] prepared Ni/SiO_2 catalysts by impregnation of $[Ni(en)_3](NO_3)_2$ for hydrogenation of glucose. Drying and calcination were done in inert atmosphere. The catalyst was thermally treated in two ways; direct reduction and calcination before reduction. Lower conversion for glucose hydrogenation was observed on directly reduced catalysts. XPS studies on directly reduced catalysts revealed the presence of a nitrogen compound on them. These catalysts gave stable performance and were resistant towards leaching.

Argon atmosphere was used in the work of Negrier *et al.* [78]. Carbon contents of 2 to 3 wt% were observed after the heat treatment of the catalysts. The use of inert atmosphere results in partial formation of metallic nickel. However a post treatment in hydrogen was necessary to convert most of the Ni^{2+} to nickel metal and remove the carbonaceous species. An exposure to air atmosphere oxidized many of the Ni^0 crystallites, but a second treatment in hydrogen increased the percentage of reduced nickel.

These studies clearly indicate that, even though the heat treatment under inert atmosphere is beneficial for formation of metallic nickel, the remnants of ligand decomposition still show their presence on the catalysts. A second treatment either in hydrogen or in air followed by hydrogen is necessary for the maximum utilization of the nickel component.

1.5 Scope of the present investigation

The above discussions reveal that counter ions in cationic metal complexes influences the final structure and activity of the catalyst. These ions which are present during the heat treatment make significant changes in the decomposition patterns of the precursors. However, no systematic study has been carried out to know the actual role of counter ions in the preparation of nickel catalysts.

Furthermore most of the investigations reported in the literature deal with nickel catalysts with low percentage of metal loading. Majority of the supported catalysts used in industry have large metal loadings (20 wt%). Furthermore the calcinations in many of these cases were done in inert atmosphere which is costly and difficult to maintain. It was therefore thought worthwhile to carryout detailed investigations on the role of counter ions in the preparation of nickel catalysts and also to prepare active nickel catalysts with high metal loadings. The calcination condition was selected to be in air atmosphere which is easy and cost effective. The en:Ni ratio was fixed to be 2:1. A control sample was prepared using nickel nitrate salt, which forms the hexa aqua complex in the solution. The main objectives of the present work are as follows.

i) To prepare and study the thermal decomposition of the nickel complexes of chelating ligands with different counter ions.

ii) to study the properties of nickel / nickel oxide obtained by the thermal decomposition of such complexes

iii) to study the kinetics of temperature programmed reduction of nickel oxide

iv) to study the influence of counter ions on the macrodistribution of nickel on γ-Al_2O_3 pellets after impregnation

v) to study the influence of counter ions on the structure and activity of Ni/α-Al_2O_3 catalysts

vi) to study the influence of counter ions on the migration of nickel ions to γ-Al_2O_3 to form nickel aluminate

vii) to study the influence of counterions on the solid solution formation in NiO/MgO systems

With the above mentioned objectives, we synthesized the following four complexes and studied their thermal decomposition.

a) $[Ni(H_2O)_6](NO_3)_2$

b) $[Ni(en)_2(H_2O)_2](NO_3)_2$

c) $[Ni(en)_2(H_2O)_2](CH_3COO)_2$

d) $[Ni(en)_2(H_2O)_2]Cl_2$

The influence of the counter ions on the structure and activity of the catalysts were also studied. We hope that these studies may result in some conclusions which would be helpful for the synthesis of more efficient supported metal catalysts.

References

[1] M. Moribdelli, A. Gavrillidis, A. Varma., *Catalyst Design: Optimal distribution of catalyst in pellets, reactors and membranes*. (2001) Cambridge University Press, Cambridge, U.K.

[2] W. Keim., Nickel: An Element with wide application in industrial homogeneous catalysis, *Angew. Chem. Int. Edn.* 29 (1990) 235-244

[3] G.C. Bond., Strategy of research on supported metal catalysts. Problems of structure-sensitive reactions in the gas phase., *Acc. Chem. Res.* 26 (1993) 490-495

[4] P. Sabatier., *Kataliz v organicheskoi khimii* (Catalysis in Organic Chemistry), (1932) Leningrad: Goskhimtekhizdat.

[5] R.C Santana, S. Jongpatiwut, W.E Alvarez, D.E Resasco., Gas-phase kinetic studies of Tetralin hydrogenation on Pt/Alumina., *Ind. Eng. Chem. Res.* 44 (2005) 7928-7934

[6] H. Wang, W. Li, M. Zhang, K. Tao., A novel Ni_2Mo_3N/MCM41 catalyst for the hydrogenation of aromatics., *Catal. Lett.* 100 (2005) 73-77

[7] F. Li, X. Yi, W. Fang., Effect of organic nickel precursor on the reduction performance and hydrogenation activity of Ni/Al_2O_3 Catalysts., *Catal. Lett.* 130 (2009) 335-340

[8] S.R. Kirumakki, B.G. Shpeizer, G.V. Sagar, K.V.R. Chary, A. Clearfield., Hydrogenation of Naphthalene over $NiO/SiO_2–Al_2O_3$ catalysts: Structure–activity correlation., *J. Catal.* 242 (2006) 319-331

[9] J.R. Rostrup-Nielsen, in : J.R. Anderson, M. Boudard, (Eds,), Catalysis Science and Technology, vol. 5, Springer, New York, 1984, pg. 3

[10] E. Kikuchi., Membrane reactor application to hydrogen production., *Catal. Today* 56 (2000) 97-101

[11] S. Uemiya, N. Sato, H. Ando, T. Matsuda, E. Kikuchi., Steam reforming of methane in a hydrogen-permeable membrane reactor., *Appl. Catal.* 67 (1990) 223-230

[12] Y. Matsumura, T. Nakamori., Steam reforming of methane over nickel catalysts at low reaction temperature., *Appl. Catal. A: General.* 258 (2003) 107-114

[13] J.G. Seo, M.H. Youn, S. Park, J.C. Jung, P. Kim, J.S. Chung, I.K. Song., Hydrogen production by steam reforming of liquefied natural gas (LNG) over nickel catalysts supported on cationic surfactant-templated mesoporous aluminas., *J. Power Sources.* 186 (2009) 178–184

[14] P. Sabatier, J.B. Senderens., *C. R. Acad. Sci. Paris* 134 (1902) 514

[15] Nielsen, A. (Ed.), *Ammonia: Catalysis and Manufacture*, Springer, 1995

[16] M.P. Andersson, T. Bligaard, A. Kustov, K.E. Larsen, J. Greeley, T. Johannessen, C.H. Christensen, J.K. Nørskov., Toward computational screening in heterogeneous catalysis: Pareto-optimal methanation catalysts., *J. Catal.* 239 (2006) 501-506

[17] D.A. Hickman, L.D. Schmidt., Production of Syngas by direct catalytic oxidation of methane., *Science.* 259 (1993) 343-346

[18] D.A. Hickman, L.D. Schmidt., Synthesis gas formation by direct oxidation of methane over Pt monoliths., *J. Catal.* 138 (1992) 267-282

[19] V.R. Choudhary, A.M. Rajput, B. Prabhakar., Low temperature oxidative conversion of methane to syngas over NiO-CaO catalyst., *Catal Lett.* 15 (1992) 363-370

[20] D. Dissanayake, M.P. Rosynek, K.C.C. Kharas, J.H. Lunsford., Partial oxidation of methane to carbon monoxide and hydrogen over a Ni/Al_2O_3 catalyst., *J. Catal.* 132 (1991) 117-127

[21] Å. Slagtern, U. Olsbye., Partial oxidation of methane to synthesis gas using La-M-O catalysts., *Appl. Catal. A: General.* 110 (1994) 99-108

[22] T. Hayakawa, A.G. Andersen, M. Shimizu, K. Suzuki, K. Takehira., Partial oxidation of methane to synthesis gas over some titanates based perovskite oxides., *Catal. Lett.* 22 (1993) 307-317

[23] S. Tang, J. Lin and K.L. Tan., Partial oxidation of methane to syngas over Ni/MgO, Ni/CaO and Ni/CeO_2., *Catal. Lett.* 51 (1998) 169-175

[24] K.M. Lee, W.Y. Lee., Partial oxidation of methane to syngas over calcined Ni–Mg/Al layered double hydroxides, *Catal. Lett.* 83 (2002) 65-70

[25] V.R. Choudhary, B.S. Uphade, A.S. Mamman., Large enhancement in methane-to-syngas conversion activity of supported Ni catalysts due to precoating of catalyst supports with MgO, CaO or rare-earth oxide., *Catal. Lett.* 32 (1995) 387-390

[26] Y. Qiu, J. Chen, J. Zhang., Effect of calcination temperature on properties of eggshell Ni/MgO–Al_2O_3 catalyst for partial oxidation of methane to syngas., *Catal. Lett.* 127 (2009) 312–318

[27] T. Ishihara, Y. Takita., Partial oxidation of methane into syngas with oxygen permeating ceramic membrane reactors, *Catal. Surv. Jpn*. 4 (2001) 125-133

[28] A.T. Ashcroft, A.K. Cheetham, M.L.H. Green, P.D.F. Vernon., Partial oxidation of methane to synthesis gas using carbon dioxide., *Nature.* 352 (1991) 225-228

[29] M.C.J. Bradford, M.A. Vannice., CO_2 Reforming of CH_4., *Catal. Rev. Sci-Eng.* 41 (1991) 1-42

[30] S. Wang, G.Q.(Max) Lu, G.J. Millar., Carbon dioxide reforming of methane to produce synthesis gas over metal-supported catalysts: State of the Art., *Energy & Fuels.* 10 (1996) 896-904

[31] J-S. Chang, S-E. Park, K-W. Lee, M.J. Choi., Catalytic reforming of methane with carbon dioxide over pentasil zeolite-supported nickel catalyst., *Stud. Surf. Sci. Catal.* 84 (1994) 1587-1594

[32] E. Ruckenstein, Y.H. Hu., Interactions between Ni and La_2O_3in Ni/La_2O_3 catalysts prepared using different Ni precursors., *J. Catal.* 161 (1996) 55-61

[33] S. Wang, G.Q.M. Lu., CO_2 reforming of methane on Ni catalysts: Effects of the support phase and preparation technique., *Appl. Catal. B: Environmental.* 16 (1998) 269-277

[34] J-M. Wei, B-Q. Xu, J-L. Li, Z-X. Cheng, Q-M. Zhu., Highly active and stable Ni/ZrO_2 catalyst for syngas production by CO_2 reforming of methane., *Appl. Catal. A: General.* 196 (2000) L167 – L172

[35] B-Q. Xu, J-M. Wei, Y-T. Yu, Y. Li, J-L. Li, Q-M. Zhu., Size limit of support particles in an oxide-supported metal catalyst: Nanocomposite Ni/ZrO_2 for utilization of natural gas., *J. Phys. Chem. B.* 107 (2003) 5203-5207

[36] Y.H. Hu, E. Ruckenstein., Binary MgO-based solid solution catalysts for methane conversion to syngas., *Catal. Rev. Sci-Eng.* 44 (2002) 423-453

[37] B-Q. Xu, J-M. Wei, H-Y. Wang, K-Q. Sun, Q-M. Zhu., Nano-MgO: novel preparation and application as support of Ni catalyst for CO_2 reforming of methane., *Catal. Today*. 68 (2001) 217-225

[38] K. Tomishige, O. Yamazaki, Y. Chen, K. Yokoyama, X. Li, K. Fujimoto., Development of ultra-stable Ni catalysts for CO_2 reforming of methane., *Catal. Today*. 45 (1998) 35-39

[39] Y-H.Wang, H-M. Liu, B-Q. Xu., Durable Ni/MgO catalysts for CO_2 reforming of methane: Activity and metal–support interaction., *J. Mol. Catal. A: Chemical.* 299 (2009) 44–52

[40] M.H. Youn, J.G. Seo, J.C. Jung, S. Park, I.K. Song., Hydrogen production by auto-thermal reforming of ethanol over nickel catalyst supported on mesoporous yttria-stabilized zirconia., *Int. J. Hydrogen Energy.* 34 (2009) 5390-5397

[41] A.J. Akande, R.O. Idem, A.K. Dalai., Synthesis, characterization and performance evaluation of Ni/Al_2O_3 catalysts for reforming of crude ethanol for hydrogen production, *Appl. Catal. A: General.* 287 (2005) 159-175

[42] A.Tai, T. Sugimura, in *Chiral Catalyst Immobilization and Recycling*; D. E. De Vos, I.F.J Vankelecom, P.A Jacobs., Eds.; Wiley-VCH: Weinheim, 2000; p 173.

[43] T. Sugimura., Recent progress in tartaric acid‐modified Raney nickel system for enantio-differentiating hydrogenation., *Catal. Surv. Jpn.* 3 (1999) 37-42

[44] T. Osawa, T. Harada, O.Takayasu., Asymmetrically modified nickel catalyst for the enantio-differentiating hydrogenation of prochiral ketones., *Curr. Org. Chem.* 10 (2006) 1513-1531

[45] A. Lopez-Martınez, M.A. Keane., The gas phase hydrogenation of 2-butanone over supported nickel catalysts: introduction of enantioselectivity., *J. Mol. Catal. A: Chemical.* 153 (2000) 257–266

[46] A. Wolfson, S. Geresh, M.V. Landau, M. Herskowitz., Enantioselective hydrogenation of methyl acetoacetate catalyzed by nickel supported on activated carbon or graphite., *Appl. Catal. A: General.* 208 (2001) 91–98

[47] D.L. Trimm., *Design of Industrial Catalysts*., Elsevier Scientific Publishing Company, Amsterdam, 1980

[48] F. Paulik, J. Paulik, M. Arnold., Investigation of the phase diagram for the system $Ni(NO_3)_2$-H_2O and examination of the decomposition of $Ni(NO_3)_2 \cdot 6H_2O$., *Thermochim. Acta.* 121 (1987) 137-149

[49] M.A.A. Elmasry, A. Gaber, E.M.H. Khater., Thermal Decomposition of Ni(II) and Fe(III) Nitrates and their Mixture., *J. Therm. Anal.* 52 (1998) 489-495

[50] P.L. Llewellyn, V. Chevrot, J. Ragaı¨, O. Cerclier, J. Estienne, F. Rouque´rol., Preparation of reactive nickel oxide by the controlled thermolysis of hexahydrated nickel nitrate., *Solid State Ionics*. 101–103 (1997) 1293

[51] J. Estelle, P. Salagre, Y. Cesteros, M. Serra, F. Medina, J.E. Sueiras., Comparative study of the morphology and surface properties of nickel oxide prepared from different precursors., *Solid State Ionics.* 156 (2003) 233– 243

[52] M. Serra, P. Salagre, Y. Cesteros, F. Medina, J.E. Sueiras., Study of preparation conditions of NiO–MgO systems to control the morphology and particle size of the NiO phase., *Solid State Ionics.* 134 (2000) 229–239

[53] M. Serra, P. Salagre, Y. Cesteros, F. Medina, J.E. Sueiras., Design of NiO–MgO materials with different properties., *Phys. Chem. Chem. Phys.* 6 (2004) 858-864

[54] J.R.A. Sietsma, H. Friedrich, A. Broersma, M. Versluijs-Helder, A. Jos van Dillen, P.E. de Jongh, K. P. de Jong., How nitric oxide affects the decomposition of supported nickel nitrate to arrive at highly dispersed catalysts., *J. Catal.* 260 (2008) 227–235

[55] A.J. Van Dillen, R.J.A.M. Terörde, D.J. Lensveld, J.W. Geus, K.P. De Jong., Synthesis of supported catalysts by impregnation and drying using aqueous chelated metal complexes., *J. Catal.* 216 (2003) 257–264

[56] K. Fang, J. Ren, Y. Sun., Effect of nickel precursors on the performance of Ni/AlMCM-41 catalysts for *n*-dodecane hydroconversion., *J. Mol. Catal.* 229 (2005) 51-58

[57] J. Van de Loosdrecht, S. Barradas, E.A. Caricato, N.G. Ngwenya, P.S. Nkwanyana, M.A.S. Rawat, B.H. Sigwebela, P.J. Van Berge, J.L. Visagie., Calcination of Co-based Fischer–Tropsch synthesis catalysts., *Top. Catal.* 26 (2003) 121–127

[58] I. Chen, S.Y. Lin, D.W. Shiue., Calcination of nickel/alumina catalysts., *Ind. Eng. Chem. Res.* 27 (1988) 926-929

[59] D. Eliche-Quesada, J. Me´rida-Robles, P. Maireles-Torres, E. Rodrı´guez-Castello, A.J.Lo´pez., Hydrogenation and ring opening of Tetralin on supported nickel zirconium-doped mesoporous silica catalysts**.** Influence of the nickel precursor., *Langmuir.* 19 (2003) 4985-4991

[60] P. Kim, H. Kim, J.B. Joo, W. Kim, I.K. Song, J. Yi., Effect of nickel precursor on the catalytic performance of Ni/Al_2O_3 catalysts in the hydrodechlorination of 1,1,2-trichloroethane., *J. Mol. Catal. A: Chemical.* 256 (2006) 178–183

[61] J.A. lvarez-Rodriguez, M. Cerro-Alarcon, A. Guerrero-Ruiz, I. Rodrıguez-Ramos, A. Arcoya., Effect of nickel precursor and the copper addition on the surface properties of Ni/KL-supported catalysts for selective hydrogenation of citral., *Appl. Catal. A: General.* 348 (2008) 241–250

[62] B. Li, R. Watanabe, K. Maruyama, K. Kunimori, K. Tomishige., Thermographical observation of catalyst bed temperature in oxidative steam reforming of methane over Ni supported on α-alumina granules: Effect of Ni precursors., *Catal. Today.* 104 (2005) 7–17

[63] E. Marceau, M. Che, J. Cejka, A. Zukal., Nickel(II) Nitrate vs. Acetate: influence of the precursor on the structure and reducibility of Ni/MCM-41 and Ni/Al-MCM-41 Catalysts., *Chem Cat Chem.* 2 (2010) 413-422

[64] N. Kotter, L. Riekert., The influence of impregnation, drying and activation on the activity and distribution of CuO on α-Alumina., *Stud. Surf. Sci. Catal.* 3 (1978) 51-63

[65] R. Takahashi, S. Sato, T. Sodesawa, M. Kato, S. Takenaka, S. Yoshida., Structural and catalytic properties of Ni/SiO_2 prepared by solution exchange of wet silica gel., *J. Catal.* 204 (2001) 259-271

[66] D.J. Lensveld, J.G. Mesu, A.J. van Dillen, K.P. de Jong., Synthesis and characterisation of MCM-41 supported nickel oxide catalysts., *Microporous. Mesoporous. Mater.* 44–45 (2001) 401-407

[67] D.J. Lensveld, J.G. Mesu, A.J. van Dillen, K.P. de Jong., The application of well-dispersed nickel nanoparticles inside the mesopores of MCM-41 by use of a nickel citrate chelate as precursor., *Stud. Surf. Sci. Catal.* 143 (2002) 647

[68] M.S. Thomson., European Patent 0181035, 1986.

[69] S.P.A Louwers, M.W.J Craje, A M. Vanderkraan, C. Geantet, R. Prins., The Effect of passivation on the activity and structure of sulfided hydrotreating catalysts., *J. Catal.* 144 (1993) 579-596

[70] F. Negrier, E. Marceau, M. Che, J-M. Giraudon, L. Gengembre, A.F. Lofberg., A systematic study of the interactions between chemical partners (Metal, Ligands, Counterions, and Support) involved in the design of Al_2O_3-supported nickel catalysts from diamine-Ni(II) chelates., *J. Phys. Chem. B.* 109 (2005) 2836-2845

[71] H. Zhao, Z. Zhang, F. Shemshaki, J. Zhang, Z. Ring., Aqueous interfacial chemistry in the catalyst preparation of NiMo/Al2O3 system by EDTA-containing impregnation., *Energy & Fuels.* 20 (2006) 1822-1827

[72] M. Che, Z. X. Cheng, C. Louis., Nucleation and particle growth processes involved in the preparation of silica-supported nickel materials by a two-step procedure., *J. Am. Chem. Soc.* 117 (1995) 2008-2018

[73] L. Bonneviot, D. Olivier, M. Che., Dimerization of olefins with nickel-surface complexes in X-type zeolite or on silica., *J. Mol. Catal.* 21 (1993) 415-430

[74] M.D. Romero, A. de Lucas, J.A. Calles, A. Rodriguez., Bifunctional catalyst Ni/HZSM-5: effects of the nickel incorporation method., *Appl. Catal. A: General.* 146 (1996) 425-441

[75] F. Negrier, E. Marceau,; M. Che, D. de Caro., Role of ethylenediamine in the preparation of alumina-supported Ni catalysts from $[Ni(en)_2(H_2O)_2](NO_3)_2$: from solution properties to nickel particles., *C. R. Chimie.* 6 (2003) 231-240

[76] J.P. Jones, P.W. Margerum., Relaxation kinetic study of the equilibrium between diaquobis(ethylenediamine)nickel(II) and tris(ethylenediamine)nickel(II)., *J. Am. Chem. Soc.* 92 (1970) 470-475

[77] K-Q. Sun, E. Marceau and M. Che., Evolution of nickel speciation during preparation of Ni–SiO_2 catalysts: effect of the number of chelating ligands in $[Ni(en)_x(H_2O)_{6-2x}]^{2+}$ precursor complexes., *Phys. Chem. Chem. Phys.* 8 (2006) 1731–1738

[78] F. Negrier, E. Marceau, M. Che, J-M. Giraudon, L. Gengembre, A. Lofberg., From Al_2O_3-supported Ni(II)-ethylenediamine complexes to CO hydrogenation catalysts: importance of the hydrogen post-treatment evidenced by XPS., *Catal. Lett.* 124 (2008) 18–23

[79] L. Espinosa-Alonso, K.P. de Jong, and B. M. Weckhuysen., Effect of the nickel precursor on the impregnation and drying of γ-Al_2O_3 catalyst Bodies:A UV-vis and IR microspectroscopic study., *J. Phys. Chem. C.* 1.12 (2008) 7201-7209

[80] J-F. Lambert, M. Hoogland, and M. Che., Control of the Ni^{II}/Surface interaction in the first steps of supported catalyst preparation: The interfacial coordination chemistry of $[Ni(en)_2(H_2O)_2]^{2+}$., *J. Phys. Chem. B.* 101 (1997) 10347-10355

[81] G. Riahi, D. Guillemot, M. Polisset-Thfoin, D. Bonnin, J. Fraissard., Gold-based mono-and bimetallic nanoparticles on HY zeolites., *Stud. Surf. Sci. Catal.* 135 (2001) 141

[82] S. Schimpf, C. Louis and P. Claus., Ni/SiO_2 catalysts prepared with ethylenediamine nickel precursors: Influence of the pretreatment on the catalytic properties in glucose hydrogenation., *Appl. Catal. A: General*. 318 (2007) 45-53

Chapter 2

SYNTHESIS AND CHARACTERIZATION OF NICKEL/NICKEL OXIDE BY THERMOLYSIS OF ETHYLENEDIAMINE COMPLEXES.

Contents

2.1 Introduction

Transition metal oxides and metals have been researched extensively due to their interesting catalytic, electronic and magnetic properties. Nanometer sized metal oxides and metals find wide applications in data storage devices, catalysis, drug delivery and biomedical imaging [1-4].

2.1.1 Nickel oxide and nickel metal

Nickel oxide is a promising material for applications in fuel cells [5] and catalysis [6]. Non-stoichiometric nickel oxide, because of its defect structure is a p-type semiconductor and finds application as gas sensor for H_2 [7]. Above 523 K NiO

has an fcc (NaCl type) crystal structure under the space group *Fm3m*. As the Neel temperature of NiO is 523 K, it can be applied for room temperature spin valve devices [8].

Majority of the nickel metal produced world wide finds its use in making steel. Application of nickel metal in its freshly prepared form (Raney nickel) for hydrogenation is very well known. Nano nickel has very high catalytic activity at small particle sizes, and is physically and chemically robust. They are potential candidates to replace expensive Pt catalysts [9]. Nickel nanostructures having one-dimensional structures are used as efficient materials for making nanotubes and arrays for hydrogen storage [10, 11].

2.1.2 Synthesis of metal oxides/metal by thermolysis of metal complexes

Various methods like mechanochemical processing [12], metal alkoxide hydrolysis [13], nonhydrolytic sol–gel reaction process [14], non aqueous synthesis [15] and salt-assisted aerosol decomposition [16] have been used to synthesize nano metal oxides. The thermal decomposition of metal complexes is also a viable route and generally metal alkoxides are used for the synthesis [17]. Metal salts are rarely used for this purpose, as their decomposition yields bulk materials as products [18, 19]. Furthermore, the products formed are poorly crystalline and exhibit broad particle size distribution. Unlike metal complexes of organic ligands, the inorganic salts yield sintered products after thermal decomposition. If the nanoparticles formed during decomposition are capped by organic ligands, the sintering can be reduced and stable nanoparticles can be synthesized [20, 21]. Starting from metal nitrates and using triethyl amine and *N*-cetyl-*N*,*N*,*N* trimethyl ammonium bromide (CTAB) as capping ligands Zhou *et al.* prepared metal oxides and mixed metal oxides of nano size range [22].

There is a continuing interest in easy synthesis of metallic nano nickel. Nickel nanoparticles were synthesized from nickel nitrate hexahydrate with hydrogen, formic acid, and ethanol as the reducing agents by using low pressure spray pyrolysis [23]. Recently, Wang *et al.* [24] reported the synthesis of nano

nickel by thermal decomposition of nickel acetate along with a surfactant hexadecylamine. They obtained nano sized nickel (7 nm) with a product purity of approximately 74.3 %.

Nickel nano particles were also obtained by controlled evaporation of nickel-oleylamine complex solution [25]. Such preparation methods employ costly surfactants and the product is usually contaminated with organic species. Thermolysis of ethylenediamine (en) complexes usually gives NiO [26]. Recently the ethylenediamine complexes of nickel(II) have been used in the preparation of supported nickel catalysts [27, 28]. The preparation method involves decomposition of catalyst precursors (the support and the nickel complex) in an inert atmosphere. Partially reduced nickel species on the support surface was obtained by the method.

The scope of the present chapter is to study the decomposition properties of the bis(ethylenediamine)nickel(II) complexes with varying counter ions.

The four complexes studied were, complex A $[Ni(H_2O)_6](NO_3)_2$ (hexaaqua nickel(II) nitrate), complex B $[Ni(en)_2(H_2O)_2](NO_3)_2$ (diaquabis(ethyelenediamine) nickel(II) nitrate), complex C $[Ni(en)_2(H_2O)_2](CH_3COO)_2$ (diaquabis(ethyelenedia mine)nickel(II) acetate) and complex D $[Ni(en)_2(H_2O)_2]Cl_2$ (diaquabis(ethyelene diamine)nickel(II) chloride) ; (en = ethylenediamine). The complex A in the solid state will be $NiNO_3.6H_2O$

Properties of the product obtained (nickel metal and nickel oxide) were also studied to gain insight about usage of these complexes as catalyst precursors.

2.2 Experimental

2.2.1 Synthesis of metal complexes

Complex A was prepared by recrystallizing $NiNO_3.6H_2O$ from water. It was then washed with ethanol and dried over vacuum. Complex B, C and D were prepared according to the reported procedure [29] by adding stoichiometric amounts of ethylenediamine (2.05g) (en/Ni=2) to solutions of nickel nitrate (4.956g), nickel acetate (4.240g) or nickel chloride (4.050g) in distilled water (50 mL) with stirring.

The solutions were kept in an ice bath for 4 hours. The complexes formed were then washed with dry ethanol and dried over vacuum.

2.2.2 Thermal studies (TG, DTG and DTA) of metal complexes

The thermal decomposition patterns of the complexes were recorded on a Pyris Diamond TG of Perkin Elmer make. An air flow of 200 mL min^{-1} was maintained and the heating rate employed was 10 °C min^{-1} from 100 °C to 800 °C. The DTG-DTA patterns of the complexes are given from Figure 1 to Figure 4. Complex A shows endothermic decompositions in several stages. The major event of decomposition happens at 305 °C, and the decomposition is complete by 400 °C. For complex B the decomposition occurs in a single stage at 250 °C, and the event is highly exothermic. A mass gain is registered at 355 °C due to oxidation of metallic nickel. The metal complexes of ethylenediamine ligand and nitrate counter ion come under the class of energetic compounds [30]. Nitrate counter ion is a powerful oxidizing agent and can decompose the ethyelenediamine ligands in a single exothermic step. The decomposition of ethylenediamine ligands would have resulted in hydrogen or in any reducing gas which reduced a part of Ni^{2+} to Ni^{0}. There are two exothermic weight losses for the decomposition of complex C and the decomposition is complete by 410 °C. Acetate has a less oxidizing power than that of nitrate and the major decomposition occurs at 365 °C. Complex D decomposes in several stages starting from 200 °C to 600 °C. An endothermic event is seen at 270 °C.

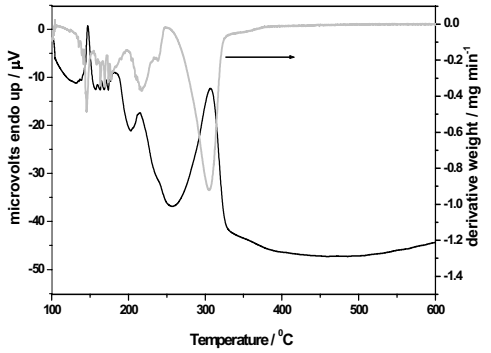

Figure 1. DTG-DTA of complex A

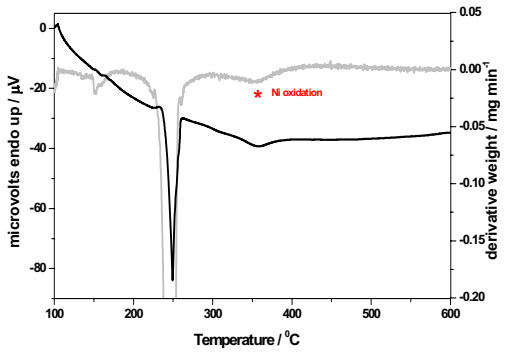

Figure 2. DTG-DTA of complex B

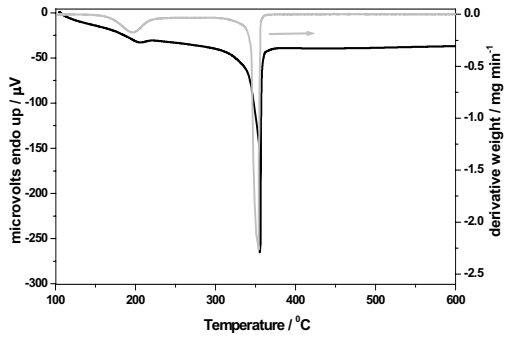

Figure 3. DTG-DTA of complex C

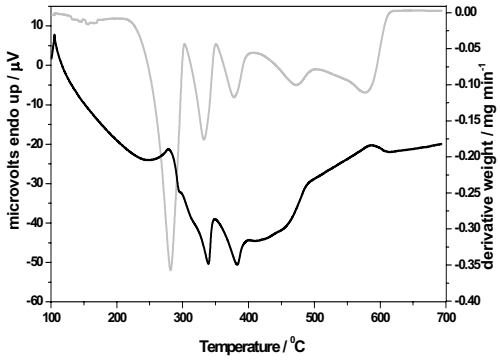

Figure 4. DTG-DTA of complex D

2.2.3 Thermolysis procedures

In the present work we adopted two procedures for thermolysis

Procedure 1. The dried complexes were decomposed at their decomposition temperatures for two hours. The temperature ramp of 5 °C min^{-1} from room temperature to decomposition temperature was adopted. The decomposition temperatures selected for the complexes were, complex A - 400 °C, complex B - 200 °C, complex C - 410 °C and complex D - 600 °C. (Even though the decomposition temperature for complex B was 250 °C; in an accidental observation it was noted that complex B decomposed at 200 °C in the muffle furnace).

Procedure 2._In this procedure, the complexes were decomposed in the muffle furnace at 600 °C for four hours. The heating rate was 5 °C min^{-1} starting from room temperature. The aim of this procedure was to subject the nickel complexes to the same heat treatment used in the catalyst preparation as these complexes are to be used as precursors to prepare supported nickel catalysts. In an impregnation method to prepare the catalyst, the dried precursor (which is a compact mixture of the support and the metal precursor) is calcined in a furnace in air atmosphere. Usually calcination temperature of 400 to 600 °C or above is used to convert the nickel precursor to nickel oxide.

The products obtained after subjecting the thermolysis procedure 1 are termed as intermediate stage products and the products obtained after thermolysis procedure 2 are termed as final stage products.

2.2.4 Intermediate stage – XRD and surface area

The X-ray diffractogram of the intermediate stage products are given in Figure 5.

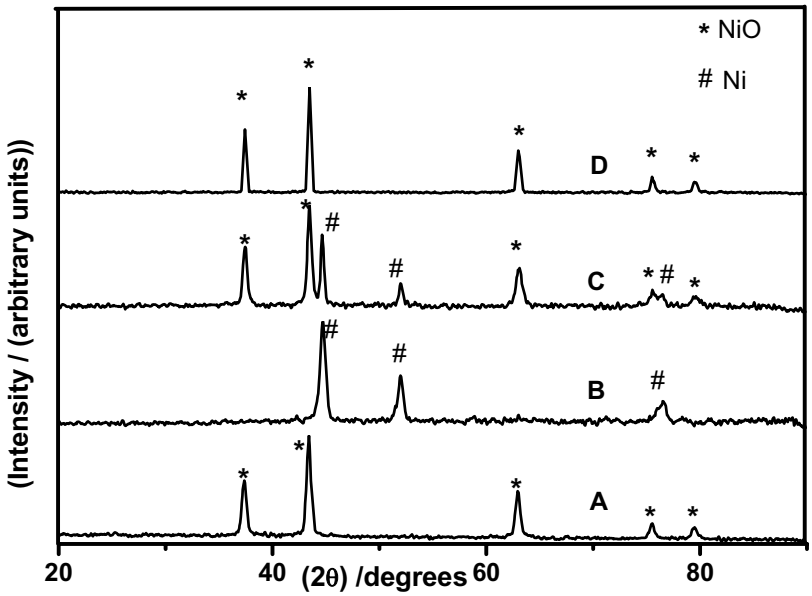

Figure 5. XRD patterns of intermediate stage products.

Both complex A and D yielded only NiO (JCPDS card No :47-1049) as the final product. Phase pure nickel (JCPDS card No :04-0850) metal was obtained

during the thermolysis of complex B. Both NiO and Ni phases were present in the decomposition product of complex C. Table 1 gives the BET surface areas, phases present and the decomposition temperatures used for the thermolysis.

Table 1. Decpmposition temperatures and properties of the products obtained after thermolysis Procedure 1.

Complex used	A	B	C	D
Decomposition temperatures	400 °C	200 °C	410 °C	600 °C
Crystalline phases present	NiO	Ni	NiO, Ni	NiO
BET surface area (m^2 gm^{-1})	8.1	1.0	2.8	1.6

2.3 Nickel metal from $[Ni(en)_2(H_2O)_2](NO_3)_2$

The direct transformation of complex B to phase pure metallic nickel is very interesting. Usually the exothermic decomposition of metal complexes in air atmosphere yields metal oxides. However, there are cases in which the complexes were transformed directly to metal [24]. The temperature of decomposition in our experiment (200 °C) is less than the real decomposition temperature of the complex (250 °C). The decomposition procedure (heating rate and temperature) is important, as decomposition at lower temperatures yielded a black charred mass, while the decomposition at higher temperatures resulted in partial formation of nickel oxide. We tried to simulate the formation of nickel crystallites in static furnace by carrying out the decompositions in TG furnace as described below.

2.3.1 TG studies on $[Ni(en)_2(H_2O)_2](NO_3)_2$

In one TG run, the nickel complex was heated from room temperature to 200 °C at a rate of 5 °C min^{-1} and was maintained at 200 °C for three hours with an air flow of 50 ml min^{-1} (Figure 6A). Even after three hours the product obtained from TG was a black mass corresponding to a percentage mass loss of 47.7.

$$[Ni(en)_2(H_2O)_2](NO_3)_2 \xrightarrow{in\ TG\ furnace\ 200\ ^0C\ isothermal} \text{gaseous products + partially decomposed product}$$

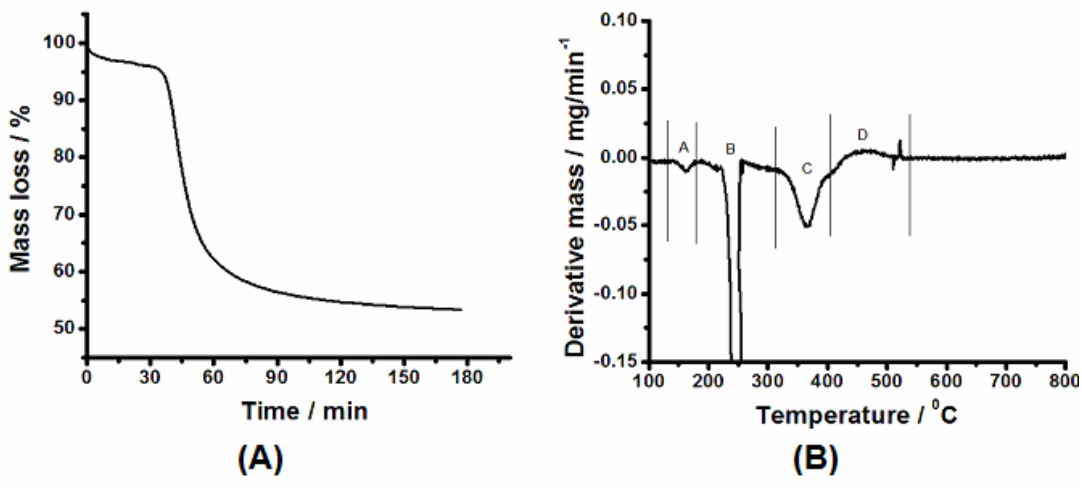

Figure 6 A- isothermal weight loss of $[Ni(en)_2(H_2O)_2](NO_3)_2$ at 200^0C, **B** - DTG graph of thermolysis of $[Ni(en)_2(H_2O)_2](NO_3)_2$ (TG program; air flow = 50 mL min^{-1}; temperature 100 $^0C \rightarrow$240 ^0C at a rate 5 $^0C\ min^{-1}$; isothermal at 240 ^0C for 1 hour; 240 $^0C \rightarrow$800 ^0C at a rate of 10 $^0C\ min^{-1}$)

We did another TG run with a heating program (air flow = 50 mL min^{-1}; temperature 100 °C → 240 °C at a heating rate of 5 °C min^{-1}; isothermal at 240 °C for 1 hour; 240 °C → 800 °C at a rate of 10 °C min^{-1}). Our DTG results (Figure 6B) in air atmosphere shows four stages of mass loss/gain. Stage A corresponds with mass loss of water, stage B corresponds to explosive decomposition, stage C corresponds to mass loss and reduction of Ni^{2+} and stage D corresponds to mass gain due to nickel oxidation. We isolated the product after stage B and its XRD gave characteristic reflections due to Ni and NiO.

The CHN elemental analyses (C, 8.1; H, 4.6; and N, 1.5 mass %) indicated a carbon rich contaminant is formed on the surface. The mass loss around 350 °C (stage C) can be due to decomposition of carbon remains along with evolution of hydrogen [29]. The mass increase from 400 to 550 °C (stage D) is due to nickel oxidation. The elemental analysis (CHN< 0.5 mass %) of final product showed practically no contaminants.

Thus decomposition in stage A and B can be written as

$[Ni(en)_2(H_2O)_2](NO_3)_2 \xrightarrow{in\ TG\ furnace\ 100°C-240°C} Ni^0 + NiO +$ Carbon containing contaminants (13.2 %) + gaseous products

And in stage C and D as

$Ni^0 + NiO +$ Carbon containing contaminants $+ O_{2\ (TG\ gas)} \xrightarrow{in\ TG\ furnace\ 240\ °C-800\ °C}$ NiO + gaseous products

Thus we could not observe the formation of phase pure nickel metal in the temperature range 200 °C – 240 °C in the thermolysis experiments done in TG furnace. The preparation of nickel nanocrystallites was done by isothermal decomposition in a muffle furnace with dimensions 22 cm × 20 cm × 20 cm and a sample mass of 8g. Partial decomposition of ethylenediamine ligands by nitrate ions/oxygen (present initially in small amount) occurs as the first step of the isothermal decomposition. The high sample/space in furnace and the partial decomposition creates an atmosphere devoid of air around the sample which prevents the formation of NiO. We propose an autogeneous temperature increase occurred in static furnace due to the partial oxidation of ethylenediamine ligands. This temperature rise initiated a self-propagating reaction by which all the ligands were decomposed to gaseous products including hydrogen, which act as reducing agents for the complete reduction of Ni^{2+} to $Ni^0_{(metal)}$. This might be the reason for the formation of nickel metal in a static furnace.

$[Ni(en)_2(H_2O)_2](NO_3)_2 + O_{2\ (atmos)} \xrightarrow{in\ static\ furnace\ 200°C} Ni^0 + H_2(g) +$ other gaseous products + contaminants (8.9 %)

This direct transformation of the metal complex at low temperature to nanocrystallites of nickel is interesting as the preparation route is simple.

2.3.2 Characterisation of nickel metal

XRD analysis

There were no peaks due to NiO or the starting complex in the XRD of the intermediate stage product of complex B (Figure 5), indicating phase pure product has been obtained. The peaks were subjected to Lorentzian curve fit, and the fwhm (τ) were determined after deducting the instrumental broadening. The calculated lattice constant from the 2θ values was 3.5192 Å. The crystallite sizes were calculated from the (111), (200) and (220) reflections by the well known Scherrer equation (for line broadening),

$d_{vol} = \frac{0.9\lambda}{\tau \cos\theta}$; d_{vol} = Volume average crystallite size; λ = wavelength of X-Ray.

and the values were 15.0, 16.1 and 9.8 nm respectively. The variation in crystallite size for different crystallographic planes indicates that the crystallite sizes and shapes are not homogeneous. The X-ray line broadening can be due to size effect or/and strain effect. We did the Williamson-Hall method, [31] to separate the strain contribution from the total fwhm. Williamson-Hall method to separate the broadening due to size and strain is based on the equation.

$$\text{fwhm} = \tau_{size+\,strain} = \tau_{size} + \tau_{strain}$$

$$\tau_{size+\,strain} = \frac{K\lambda}{\cos\theta * d_{vol}} + \eta \tan\theta\,; \quad where\ \eta tan\theta = \tau_{strain}$$

$$\tau_{size+\,strain} * cos\theta = \frac{K\lambda}{d_{vol}} + \eta \sin\theta$$

where K is the shape factor usually 0.9 and η is the microstrain.

Thus a plot of $\tau_{size+\,strain} * cos\theta$ against $sin\theta$ gives a straight line with slope η. From the y-intercept the crystallite size corrected for microstrain can be calculated.

The W-H plot for our sample is shown in Figure 7. The calculated average crystallite size from the y- intercept of the W-H plot was 18.1 nm. This value is

greater than the ones calculated by usual Scherrer equation indicating considerable microstrain in our sample.

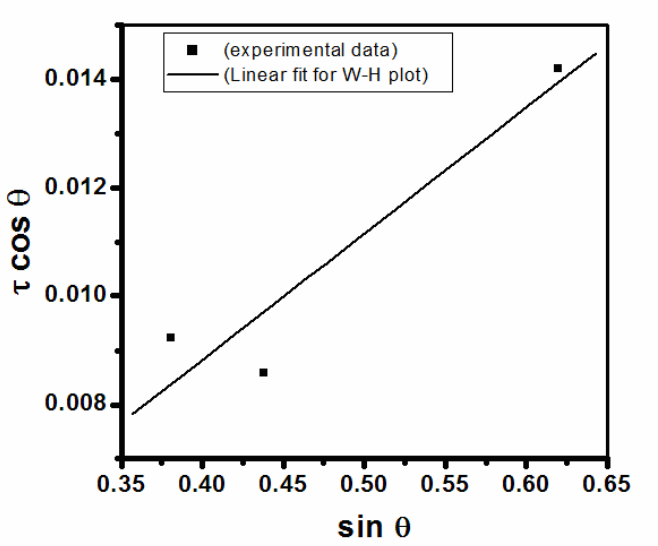

Figure 7. Williamson-Hall plot for metallic nickel

The positive slope of the plot gave the microstrain (η = 0.0235) which was significant. Points not lying along the straight line indicate anisotropic strain. The XRD analysis of the sample thus indicates formation of nanocrystalline phase pure nickel with significant anisotropic microstrain.

TG, IR and SEM

The mass gain (Figure 8) observed in the TG curve due to oxidation of the nickel was 20.1 % against the theoretical mass gain of 27.3 % (if the product was 100% nickel).

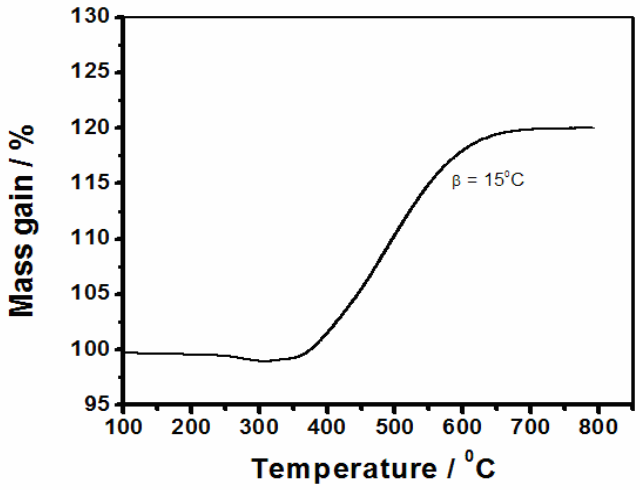

Figure 8. The mass gain curve during oxidation

The CHN analysis of the product yielded the results as C, 2.2; H, 1.2; and N, 5.5 %. Combining both the above results, purity of the nickel metal is ≈ 93 % which is higher than the reported values for similar preparation methods [24].

The infra-red spectrum of the product is shown in Figure 9. The absence of Ni—O stretching vibrations in the region 420 - 470 cm^{-1} confirms the absence of nickel oxide formation in the product which is in accordance with the XRD results [32].

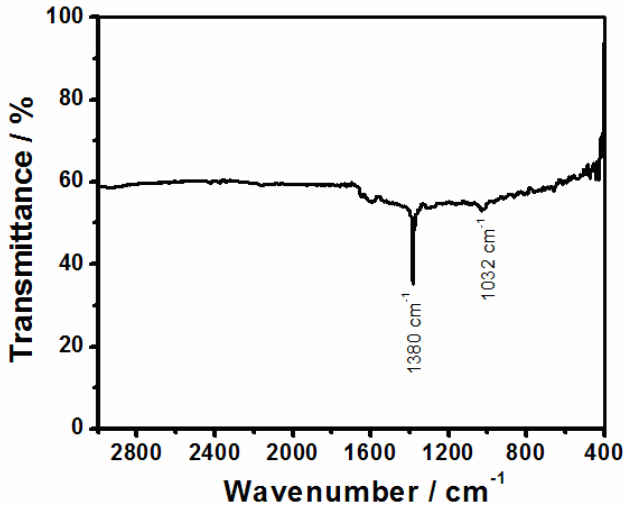

Figure 9. IR spectra of the prepared nickel nanocrystallites

The peaks at 1380 cm^{-1} and 1032 cm^{-1} may be due to the $\nu_a(NO_2)$ and $\nu_s(NO_2)$ vibrations of unidentate N-bonded nitro groups [33]. The absence of extra peaks from ligands confirms that the decomposition was almost complete. The scanning electron micrograph (Figure 10) shows foam like structure which has been formed by the aggregation of nickel crystallites. The foam has been made up of thin film like structures.

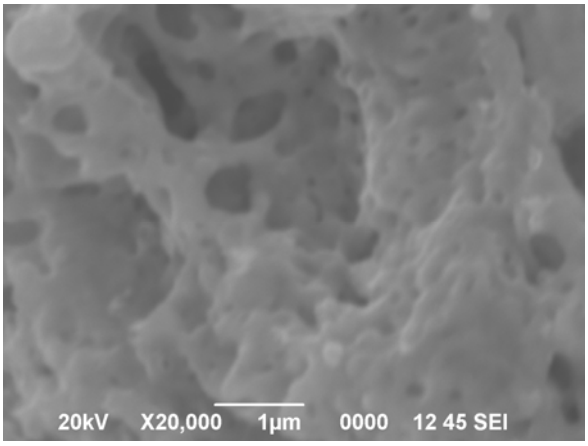

Figure 10. SEM of metallic nickel

2.3.3 Kinetics f nickel oxidation

Metals in nanometer scale have high surface area and are more probable to oxidation at a faster rate than their bulk counterparts. As the use of nano sized metals is gaining importance, their corrosion and activity loss due to oxidation is worth for studies. Oxidation kinetics of bulk nickel has been studied by Atkinson and Taylor [34]. Oxidation kinetics of nickel nanoparticles has gained renewed interest as it is a potential candidate for chemical looping combustion [35-37]. The oxidation resistance of nickel is important, as resistant metal will be more stable at room temperature. Size dependent kinetics for nano nickel oxidation has been studied by Karmhag *et al.* [38].

Oxidation of nickel nanocrystallites

The unusual morphology of the nickel nanocrystallites obtained by thermolysis procedure 1 for complex B (thin film like three dimensional structure) prompted us to study the kinetics of oxidation of the material. The differential thermogravimetric (DTG) plots for the oxidation of metallic nickel (product obtained from the static furnace) at various heating rates are shown in the Figure 11. There was an initial mass loss of around 0.3 % near 300 °C, which is due to the combustion of contaminants covering the surface. This mass loss was deducted before the kinetics calculations were made. The conversion ratios at given temperatures are determined from the TG data by assuming stoichiometric oxidation reaction. We did not consider any oxide layer if initially present on the surface and took sample mass as that of pure nickel. Complete oxidation was assumed at the attainment of maximum mass.

The mass increase due to oxidation of nickel started in between 320 °C to 360 °C depending on the heating rates. This temperature of initial oxidation is less compared to bulk nickel oxidation values and is attributed to the nano scale dimensions of the sample [39]. The temperature of peak maximum in the DTG plot shifted to higher values when the heating rate was increased.

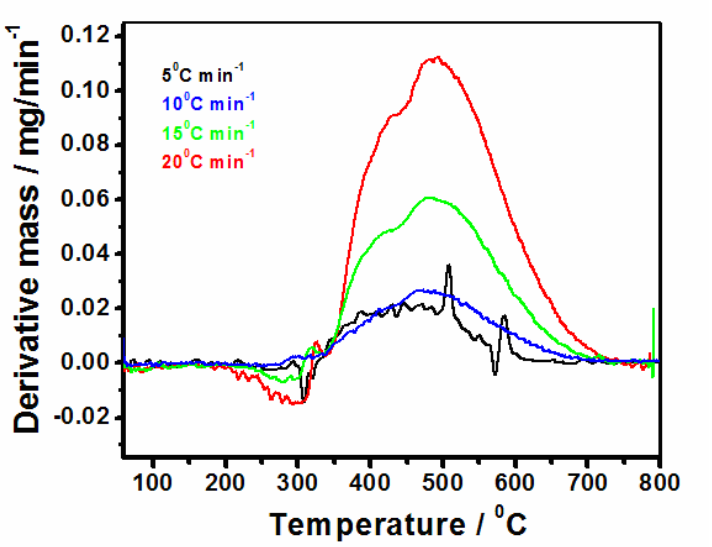

Figure 11. DTG plot of Nickel oxidation at different heating rates

Oxidation kinetics

a. Determination of activation energy by model-free isoconversional methods and Kissinger method.

The basic assumption of model-free isoconversional methods is that the reaction rate at a constant conversion is only a function of temperature, and that the reaction model is not dependent on temperature or heating rate. Flynn-Wall-Osawa (FWO) [40] and Kissinger-Akahira-Sunose (KAS) [41] equations are generally used to study the kinetics of solid state reactions. This method allows the estimation of activation energy without choosing a reaction model and reaction order. The FWO equation in its differential form is as below.

$$\frac{d \ln \beta}{d(1/T)} = \frac{1.052 * E_a}{R} \; ;$$

β = linear heating rate, E_a = activation energy and R = gas constant

The method is based on measurement of temperatures for each conversion degree α and different heating rates β. The plots of ln β versus 1/T at constant α will give straight line and from the slope activation energies are determined.

The integral form of KAS equation is

$$\ln\left(\frac{\beta}{T^2}\right) = \ln \frac{A}{E_a * g(\alpha)} - \frac{E_a}{RT}$$

A = Arrhenius frequency factor, $g(\alpha)$ = mechanism function

A plot of $\ln\left(\frac{\beta}{T^2}\right)$ against 1/T gives a straight line with slope = $-\frac{E_a}{R}$.

Friedman differential method [42] is based on the intercomparison of the rates of conversion, dα/dT for a given degree of conversion α, at different heating rates. This method requires measurement of both temperatures and conversion rates, at different heating rates.

$$\ln\left(\beta\frac{d\alpha}{dT}\right)=\ln[Af(\alpha)]-\frac{E_a}{RT}$$

The activation energies were calculated by the above three equations and are plotted against each conversion degree (Figure 12). Activation energy increases first with conversion ratios, attains a maximum ≈ 45 % conversion and decreases afterwards. Similar values for activation energy were obtained for both KAS and FWO methods. The differential Friedman method yielded slightly lower values for activation energies. The activation energies calculated by FWO method falls between 1.3 and 2.1 eV. For nanocrystallites, as the reaction proceeds, reactants may undergo changes in reactivity due to crystal defect formation, intracrystalline strain and particle disintegration [35]. The reactivity of nickel nanocrystallites may not remain constant during the full course of the reaction. This may be the reason for the varying activation energies obtained at different conversions. However, the exact reason for a maximum in the curve could not be explained at this stage.

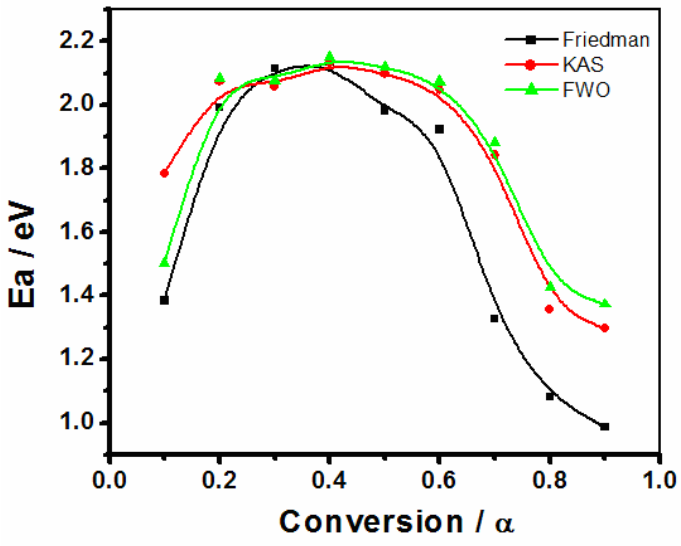

Figure 12. Variation of activation energy with conversion for model free isoconversional equations

Kissinger equation [43] which yields a single value of activation energy was also used to determine the activation energy.

$$\ln\left(\frac{\beta}{T^2_{\max}}\right) = \ln\frac{AR}{E_a} - \frac{E_a}{RT_{\max}};$$

where T_{max} = Temperature of peak maximum from the DTG graph.

A plot of $\ln\left(\frac{\beta}{T^2_{\max}}\right)$ against $1/T_{max}$ gives the Arrhenius (Figure 13) plot from the slope of which activation energy can be determined.

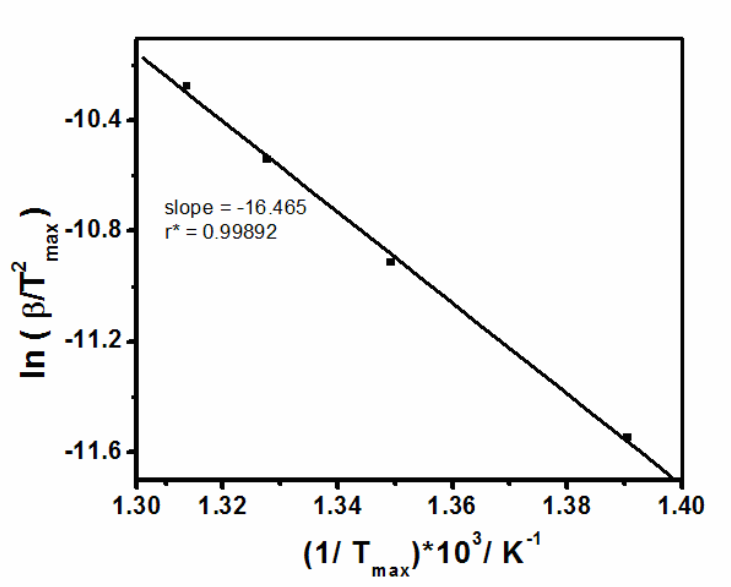

Figure 13. Arrhenius plot using Kissinger equation

The activation energy obtained was 136.8 kJ mol^{-1} (1.42 eV) which is within the range obtained by other methods.

b. ***Master plot method to study kinetics.***

To study the reaction kinetics of nickel oxidation we used the conventional master plot technique [44].

The $f(\alpha) / f(\alpha)_{0.5}$ were plotted for various differential $f(\alpha)$ functions against fractional conversion α. The experimental curve was plotted using variable activation energies obtained from FWO method and using the equation

$$\frac{f(\alpha)}{f(0.5)} = \frac{(d\alpha/dT)_{\alpha} e^{E/RT_{\alpha}}}{(d\alpha/dT)_{0.5} e^{E/RT_{0.5}}}$$

The master plots of various differential functions and the experimental curve is shown in Figure 14. Table 2 illustrates the various differential equations plotted in the master plot.

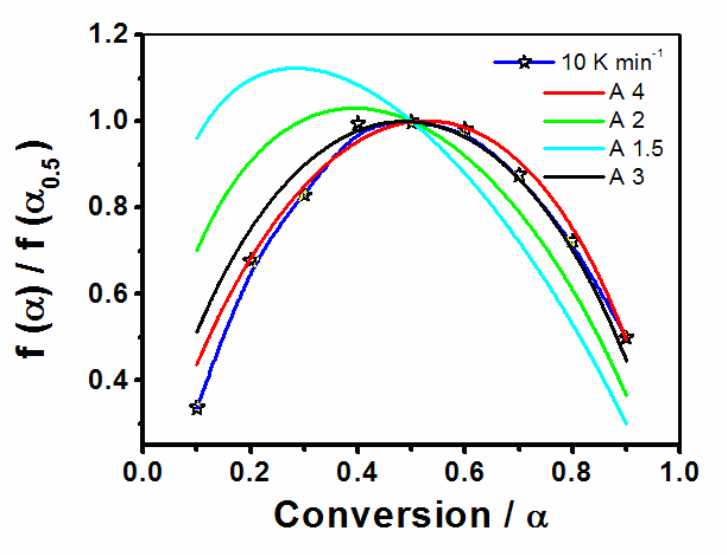

Figure 14. Kinetic model fitting for nickel nano crystallites using differential equations in Table 2.

Unlike for spherical nickel nano particles which generally obeys Jander equation [36] we got best fit for Johnson- Mehl- Avrami (JMA) equation of the form

$f(\alpha) = m(1-\alpha)[-\ln(1-\alpha)]^{1-1/m}$ where m = avrami exponent

The equation with m = 4 gave best fit at conversion < 0.5 while m = 3 gave good fitting for conversions > 0.5. We suggest the film like morphology and the crystallite strain present on the sample should be the reason for this type of oxidation kinetics. Similar type of JMA kinetics was observed by Courtade *et al.* for the growth of NiO from Ni films [45]. As in our case, change in kinetics with lattice strain was recently reported for decomposition of ultrafine calcite by Ren *et al.* [46].

Table 2. Differential equations of JMA kinetics with varying m values

symbol	f (α)	m
A 1.5	$3/2(1-\alpha)[-\ln(1-\alpha)]^{1/3}$	1.5
A 2	$2(1-\alpha)[-\ln(1-\alpha)]^{1/2}$	2
A 3	$3(1-\alpha)[-\ln(1-\alpha)]^{2/3}$	3
A 4	$4(1-\alpha)[-\ln(1-\alpha)]^{3/4}$	4

2.4 Final stage

The results of characterization of the nickel oxides obtained by thermolysis Procedure 2 is discussed in this section.

2.4.1 Final stage – XRD and Surface area

The nickel oxides obtained after thermolysis procedure 2 are named as NiO-A, NiO-B, NiO-C and NiO-D respectively, in the case of complex A, complex B, complex C and complex D. The XRD patterns of nickel oxides are given in Figure 15.

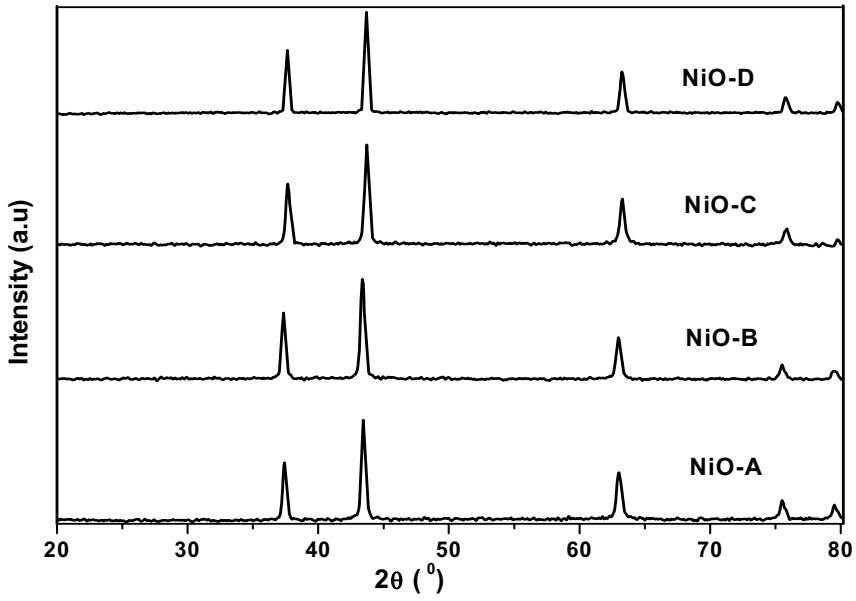

Figure 15. XRD patterns of nickel oxides (Final stage)

The diffraction patterns correspond to fcc NiO (bunsenite phase- JCPDS card No :47-1049). The peaks corresponded to (111), (200), (220), (311) and (222) peaks of NiO. The lattice constant for each sample was determined by Cohen's Analytical procedure [47]. The size-strain separation was done by Williamson-Hall (W-H) plot method. Figure 16 shows the Williamson-Hall plots for NiO-A, NiO-B, NiO-C and NiO-D. The (311) point for NiO-B and (111) point for NiO-C lies away from the W-H in indicates much strain present along that direction.

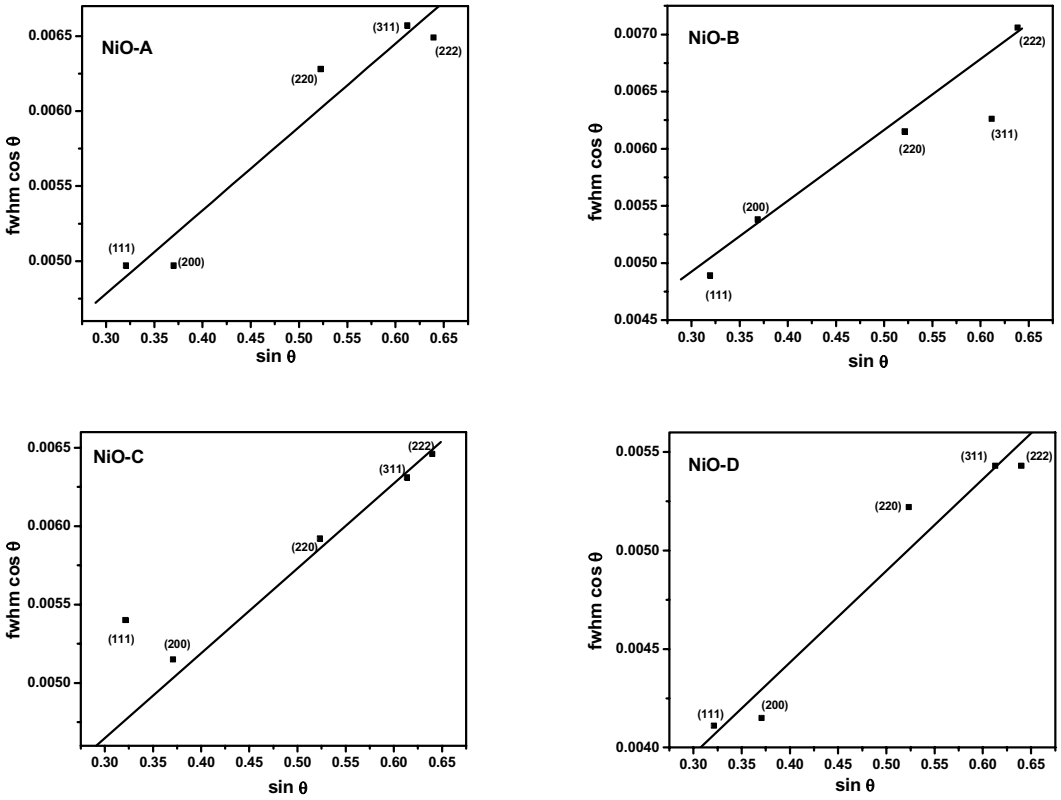

Figure 16. W-H plots of NiO-A, NiO-B, NiO-C and NiO-D.

The summary of XRD results and the BET surface areas are given in Table 3. The crystallite sizes of the samples did not vary much. NiO-D (chloride counter ion) has a crystallite size higher than others. The microstrain was highest for NiO-B where as the change in lattice constant was more for NiO-C. Sample NiO-D, which has the highest crystallite size, has the lowest surface area. It can be seen that the change in counter ions of the complexes had a profound influence on the crystal

structure and surface area of the final products. The decomposition properties of the complexes definitely influenced the crystal structure. Complex D which decomposed at higher temperatures had lowest surface area and highest crystallite size. Conversely complex B which decomposed at low temperature had a higher surface area. If we compare the surface area values of the intermediate stage and final stage products (Table 1 and Table 3) some important conclusions can be made. The surface area values did not change much between the Procedure 1 and procedure 2 except for NiO-B. The primary particles are formed during the intermediate stage itself. After this stage the heat treatment does not have much influence on the final properties. However, for NiO-B there is an increase of surface area, as the nickel oxide is formed mainly by oxidation of low surface area nickel metal.

Table 3. Results of XRD analysis and surface area

Sample	Crystallite size (nm)	Microstrain × 1000	Lattice constant 'a' Å	Change in lattice constant $(a_0\text{-}a) \times 100$	BET surface area m^2gm^{-1}
NiO-A	29.7	5.77	4.1771	-0.02	5.9
NiO-B	29.5	6.31	4.1794	-0.25	6.2
NiO-C	28.6	5.66	4.1709	+0.60	2.6
NiO-D	36.1	4.65	4.1733	+0.35	1.4

fcc NiO lattice constant - 4.1769 Å

2.4.2 Final stage - SEM

The SEM images of the samples are given in Figure 17. Sample NiO-A consists of octahedral particles with size less than 1μm. The crystallites show mainly the (111) planes. Particles are of same shape for NiO-D, but are of bigger size. NiO-D shows a bimoday particle size distribution. The SEM image of NiO-C shows an amorphous like structure without any well defined particle shape. For sample NiO-B, foam like structure has been formed by the aggregation of particles. The change in counter ions had a dramatic influence on the morphology of nickel oxides [48].

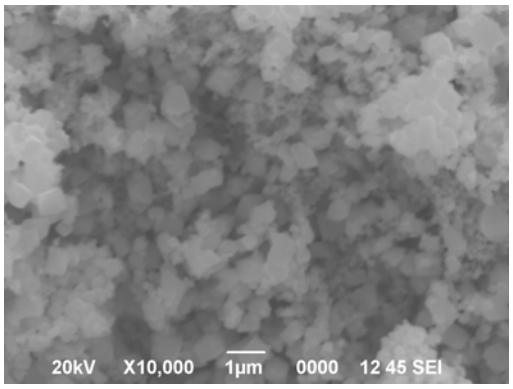

NiO-A

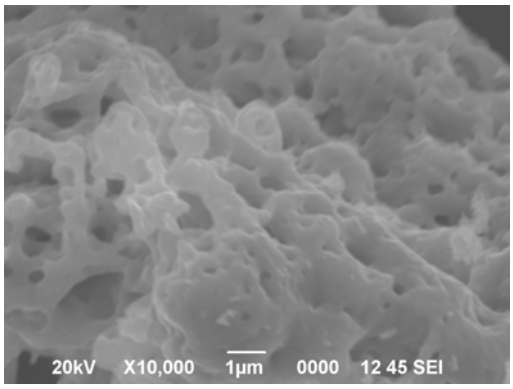

NiO-B

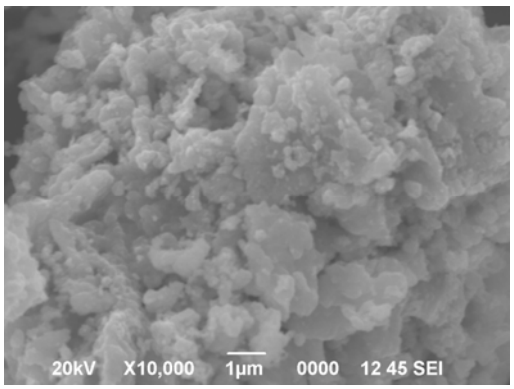

NiO-C

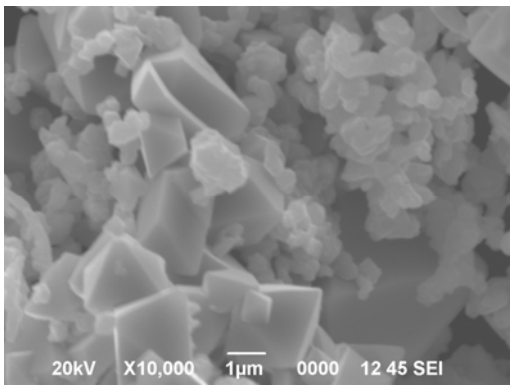

NiO-D

Figure 17. SEM of nickel oxides

2.5 Conclusions

i) The counter ions present on the complexes can influence the decomposition properties of the complexes

ii) Properties of the final product are influenced by the decomposition properties of the complexes.

iii) The nickel complex $[Ni(en)_2(H_2O)_2](NO_3)_2$ gave nickel metal upon decomposition.

iv) Oxidation studies conducted on the nanonickel formed suggest that the kinetics is influenced by the morphology of nickel nanocrystallites.

References

[1] K.M. Dooley, S.Y. Chen., J.R.H. Ross., Stable nickel-containing catalysts for the oxidative coupling of methane., *J. Catal.* 145 (1994) 402-408

[2] T. Hyeon., Chemical synthesis of magnetic nanoparticles., *Chem. Commun.* (2003) 927–934

[3] S. Sun., Recent advances in chemical synthesis, self-assembly, and applications of FePt nanoparticles., *Adv. Mater.* 18 (2006) 393–403

[4] Y-W. Jun, J-H. Lee, J. Cheon., Chemical design of nanoparticle probes for high-performance magnetic resonance imaging., *Angew. Chem., Int. Ed.* 47 (2008) 5122–5135

[5] L. Daza, C.M. Rangel, J.Baranda, M.T. Casais, M.J. Martínez, J.A. Alonso., Modified nickel oxides as cathode materials for MCFC., *J. Power Sources.* 86 (2000) 329-333

[6] Y. Wang, J. Zhu, X. Yang, L. Lu, X. Wang., Preparation of NiO nanoparticles and their catalytic activity in the thermal decomposition of ammonium perchlorate., *Thermochim. Acta.* 437 (2005) 106-109

[7] M. Matsumiya, F. Qiu, W. Shin, N. Izu, N. Murayama, S. Kanzaki., Thin-film Li-doped NiO for thermoelectric hydrogen gas sensor., *Thin Solid Films.* 419 (2002) 213-217

[8] J. Nogues, I.K. Schuller., Exchange Bias., *J. Magn. Magn. Mater.* 192 (1999) 203-232

[9] P. Mitchell., Nano-nickel catalysts: nano-nickel could replace a significant portion of the platinum catalyst market, and sales could be worth $500-$1bn in five years., *Chemistry and Industry.* (2005) 22-24

[10] S-Z. Chu, K. Wada, S. Inoue, S. Todoroki, Y.K. Takahashi, K. Hono., Fabrication and characteristics of ordered Ni nanostructures on Glass by anodization and direct current electrodeposition., *Chem. Mater.* 14 (2002) 4595-4602

[11] M. Green, P. O'Brien., The preparation of organically functionalised chromium and nickel nanoparticles., *Chem. Commun.* (2001) 1912-1914

[12] P.G. McCormick, T. Tsuzuki, J.S. Robinson, J. Ding., Nanopowders synthesized by mechanochemical processing., *Adv. Mater.* 13 (2001) 1008-1010

[13] H. Kominami, M. Kohno, Y. Takada, M. Inoue, T. Inui, Y. Kera., Hydrolysis of titanium alkoxide in organic solvent at high temperatures: A new synthetic Method for nanosized, thermally stable Titanium(IV) Oxide., *Ind. Eng. Chem. Res.* 38 (1999) 3925-3931

[14] J. Tang, J. Fabbri, R.D. Robinson, Y. Zhu, I.P. Herman, M.L. Steigerwald, L.E. Brus., Solid-Solution Nanoparticles: Use of a nonhydrolytic sol−gel synthesis to prepare HfO_2 and $Hf_xZr_{1-x}O_2$ nanocrystals., *Chem. Mater.* 16 (2004) 1336-1342

[15] M. Niederberger, N. Pinna, J. Polleux, M. Antonietti., A general soft-chemistry Route to perovskites and related materials: synthesis of $BaTiO_3$, $BaZrO_3$, and $LiNbO_3$ nanoparticles., *Angew. Chem. Int. Ed*. 43 (2004) 2270-2273

[16] B. Xia, I.W. Lenggoro, K. Okuyama., Novel route to nanoparticle synthesis by salt-assisted aerosol decomposition., *Adv. Mater.* 13 (2001) 1579-1582

[17] M. Aslam, L. Fu, M. Su, K. Vijayamohanan, V.P. Dravid., Novel one-step synthesis of amine-stabilized aqueous colloidal gold nanoparticles., *J. Mater. Chem*. 14 (2004) 1795-1797

[18] M.Z.-C. Hu, M.T. Harris, C.H. Byers., Nucleation and growth for synthesis of nanometric zirconia particles by forced hydrolysis., *J. Colloid Interf. Sci*. 198 (1998) 87-99

[19] Y. Jiang, Y. Wu, B. Xie, Y. Xie, Y. Qian., Moderate temperature synthesis of nanocrystalline Co_3O_4 via gel hydrothermal oxidation., *Mater. Chem. Phys*. 74 (2002) 234-237

[20] T.J. Trentler, T.E. Denler, J.F. Bertone, A. Agrawal, V.L. Colvin., Synthesis of TiO_2 nanocrystals by nonhydrolytic solution-based reactions., *J. Am. Chem. Soc*. 121 (1999) 1613-1614

[21] J. Rockenberger, E.C. Scher, A.P. Alivisatos., A new nonhydrolytic single-precursor approach to surfactant-capped nanocrystals of transition metal oxides., *J. Am. Chem. Soc*. 121 (1999) 11595-11596

[22] L. Zhou, J. Xu, X. Li, F. Wang., Metal oxide nanoparticles from inorganic sources via a simple and general method., *Mater. Chem. Phys.* 97 (2006) 137–142

[23] W-N. Wang, Y. Itoh, I.W. Lenggoro, K. Okuyama., Nickel and nickel oxide nanoparticles prepared from nickel nitrate hexahydrate by a low pressure spray pyrolysis., *Mater. Sci. Eng., B.* 111 (2004) 69–76

[24] H. Wang, X. Jiao, D. Chen., Monodispersed nickel nanoparticles with tunable phase and size: synthesis, characterization, and magnetic properties. *J. Phys. Chem. C.* 112 (2008) 18793-18797

[25] J. Park, E. Kang, S.U. Son, H.M. Park, M.K. Lee, J. Kim, K.W. Kim, H-J. Noh, J.H. Park, C.J. Bae, J.G. Park**,** T. Hyeon., Monodisperse nanoparticles of Ni and NiO: synthesis, characterization, self-assembled superlattices, and catalytic applications in the suzuki coupling reaction., *Adv. Mater.* 17 (2005) 429-434

[26] K.S. Rejitha, S. Mathew., Thermal deamination kinetics of tris(ethylenediamine) nickel(II) sulphate in the solid-state. *J. Therm. Anal. Calorim.* 93 (2008) 213-217

[27] S. Schimpf, C. Louis, P. Claus., Ni/SiO_2 catalysts prepared with ethylenediamine nickel precursors: Influence of the pretreatment on the catalytic properties in glucose hydrogenation., *Appl. Catal. A: General.* 318 (2007) 45-53

[28] F. Negrier, E. Marceau, M. Che, J.M. Giraudon, L. Gengembre, A. Lofberg., A systematic study of the interactions between chemical partners (metal, ligands, counterions, and support) involved in the design of Al_2O_3-supported nickel catalysts from Diamine−Ni(II) chelates., *J. Phys. Chem. B.* 109 (2005) 2836-2845

[29] F. Negrier, E. Marceau, M. Che, D. de Caro., Role of ethylenediamine in the preparation of alumina-supported Ni catalysts from $[Ni(en)_2(H_2O)_2](NO_3)_2$: from solution properties to nickel particles. *C. R. Chimie* 6 (2003) 231-240

[30] G. Singh and D. K. Pandey., Studies on energetic compounds Part 27: Kinetics and mechanism of thermolysis of bis(Ethylenediamine) metal nitrates and their role in the burning rate of solid propellants., *Propellants.. Explos. Pyrotech.* 28 (2003) 231-239

[31] C. Suryanarayana, M.G. Norton., X-Ray diffraction a practical approach. New York: Plenum Press; 1998 pg 253.

[32] G.L. Guerlou, C. Delmas., Structure and properties of precipitated nickel-iron hydroxides. *J. Power Sources.* 45 (1993) 281-289

[33] K. Nakamoto., Infrared and raman spectra of inorganic and coordination compounds part B: applications in coordination, organometallic, and bioinorganic chemistry. 5th ed. New York: John Wiley and Sons; 1997

[34] A. Atkinson, R.I. Taylor., The diffusion of ^{63}Ni along grain boundaries in nickel oxide., *Philos. Mag. A.* 43 (1981) 979-998

[35] L. Zhou, A. Rai, N. Piekiel, X. Ma, M.R. Zachariah., Ion-mobility spectrometry of nickel nanoparticle oxidation kinetics: application to energetic materials., *J. Phys. Chem. C.* 112 (2008) 16209-16218

[36] P. Song, D. Wen, Z.X. Guo, T. Korakianitis., Oxidation investigation of nickel nanoparticles., *Phys. Chem. Chem. Phys.* 10 (2008) 5057-5065

[37] W. Suwanwatana, S. Yarlagadda, J.W. Gillespie., An investigation of oxidation effects on hysteresis heating of nickel particles., *J. Mater. Sci.* 38 (2003) 565-573

[38] R. Karmhag, T. Tesfamichael, E. Wackelgard, G.A. Niklasson, M. Nygren., Oxidation kinetics of nickel particles: comparison between free particles and particles in an oxide matrix., *Sol. Energy.* 68 (2000) 329-333

[39] R. Karmhag, G.A. Niklasson, M. Nygren., Oxidation kinetics of nickel nanoparticles., *J. Appl. Phys.* 89 (2001) 3012-3017

[40] J.H. Flynn, L.A. Wall., A quick, direct method for the determination of activation energy from thermogravimetric data., *J. Polym. Sci. Part B.* 4 (1996) 323-328

[41] T. Akahira, T. Sunose., Research Report of Chiba Institute Technology. 16 (1971) 22

[42] H.L. Friedman., New methods for evaluating kinetic parameters from thermal analysis data., *J. Polym. Sci. Part B. Ploym Lett.* 7 (1969) 41-46

[43] H.E. Kissinger., Reaction kinetics in differential thermal analysis., *Anal. Chem.* 29 (1957) 1702-1706

[44] F.J. Gotor, J.M. Criado, J. Malek, N. Koga., Kinetic analysis of solid-state reactions: The universality of master plots for analyzing isothermal and nonisothermal experiments., *J. Phys. Chem. A.* 104 (2000) 10777-10782

[45] L. Courtade, Ch. Turquat, Ch. Muller, J.G. Lisoni, L. Goux, D.J. Wouters, D. Goguenheim, P. Roussel, L. Ortega., Oxidation kinetics of Ni metallic films:

formation of NiO-based resistive switching structures. *Thin Solid Films*. 516 (2008) 4083-4092

[46] Y.L. Ren, X. Wang, M. Shui, R.S. Li., The influence of morphology of ultra-fine calcite particles on decomposition kinetics., *J. Therm. Anal. Calorim.* 91 (2008) 867-871

[47] C. Suryanarayana, M.G. Norton., X-Ray diffraction a practical approach. New York: Plenum Press; 1998, pg. 159

[48] J. Estelle, P. Salagre, Y. Cesteros, M. Serra, F. Medina, J.E. Sueiras., Comparative study of the morphology and surface properties of nickel oxide prepared from different precursors., *Solid State Ionics.* 156 (2003) 233– 243

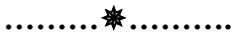

Chapter 3

KINETICS OF TEMPERATURE PROGRAMMED REDUCTION (TPR) OF NiO.

Contents

3.1 Introduction

Metal oxides are used as catalysts for a wide range of reactions as selective oxidation, dehydrogenation and ammoxidation. In such reactions the oxidation-reduction properties of metal oxides are very important in controlling the activity and selectivity. Non stoichiometric oxides are more active than stoichiometric oxides because of the presence of mixed valence states. The metal oxides which can change their oxidation state easily are considered as good materials to be used as selective oxidation catalysts. In many of the applications where metal acts as catalyst, the metal oxide is converted to metal by hydrogen at elevated temperatures. It is highly essential that metal should be in its metallic state (without getting oxidized) to maintain the stability of catalytic reaction. Detailed study on oxidation-reduction properties would be helpful in developing efficient oxidation catalysts.

Oxidation-reduction properties of metal oxides are made use of in their application in chemical looping combustion (CLC) as solid oxygen carriers [1]. Unlike most of other energy generating technologies, CLC can separate the green house gas, CO_2, more efficiently. In CLC a solid oxygen carrier is used to transfer the oxygen from air to fuel [2]. The CLC system (Figure 1) consists of two reactors connected together namely an air reactor and fuel reactor.

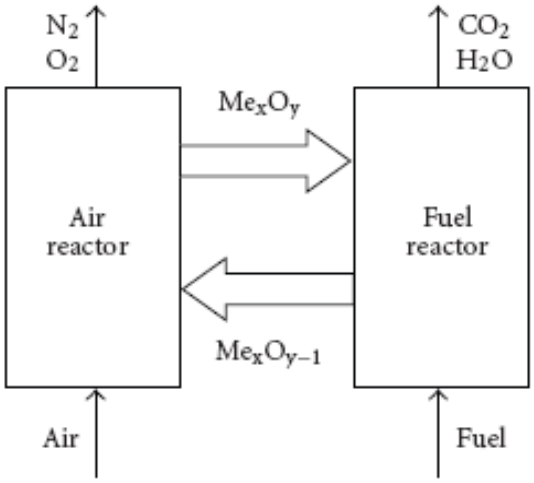

Figure 1. Chemical looping combustion (CLC)

In the fuel reactor, the metal oxide is contacted with hydrocarbon or hydrogen. The fuel is oxidized by the lattice oxygen of the metal oxide.

$$MO + \text{fuel} \rightarrow M + CO_2 + H_2O$$

The exothermic energy of this reaction can be used for power generation. As the exit gas consists of only CO_2 and H_2O, CO_2 can be easily separated by condensation. The reduced metal oxide is transported and oxidized in the air reactor.

$$M + ½\ O_2 \rightarrow MO$$

The whole process can be operated continuously generating power. In CLC, as combustion takes place without flame in two steps, NOx formation is avoided.

The suitable selection of an oxygen carrier is very much important in CLC. Among transition metals, oxides of Fe, Cu and Ni are widely studied for this purpose [3-5]. Recently $CaSO_4$ was also studied for application in CLC [6]. Pure NiO, NiO/YSZ (yttria stabilized zirconia) and $NiO/NiAl_2O_4$ are the materials studied for application in CLC [7, 8]. In view of the importance of reduction of NiO, the reduction kinetics of nickel oxide was studied in detail by non isothermal gravimetry and the results are discussed in this chapter.

3.1.1 Reduction mechanism of NiO

Hydrogen reduction of nickel oxide is only slightly exothermic.

$$NiO + H_2 \rightarrow Ni + H_2O$$

The reaction is irreversible, as in the temperature range 0 to 1000 °C the equilibrium constant (K_p) has values in the range 10^3 to 10^2. Unlike iron oxide, only two solid phases are involved. These facts make the reaction simple and easy to follow. Kinetics of nickel oxide reduction has always attracted the interest of researchers and technologists and is considered to be a model reaction for the reduction of transition metal oxides. In the first reported (1924) kinetic study of nickel oxide, Benton and Emmett [9] have pointed out the existence of a nucleation period, which depends on nature of sample, temperature of reduction, "autocatalytic effect" of nickel atoms and a reaction interface consisting of nickel oxide and previously reduced nickel. They monitored the reaction by following water formation as indication of extent of reaction. In 1932, Taylor and Starkweather studied NiO reduction by following hydrogen consumption and arrived at similar conclusions of existence of nucleation period and autocatalytic effect [10]. Koga and Harrison [11] suggested that the nucleation (induction) period is the time for generation of nickel atoms on surface of nickel oxide particles. These nickel atoms grow two dimensionally and coalesce. Recent studies by Jankovic *et al.* [12], also confirm the above mechanism consisting of induction period, autocatalytic effect and overlapping of growing nickel grains. The importance of hydrogen adsorption

sites on the stoichiometric surface of nickel oxide during reduction was pointed out by Fursteanu *et al.* [13]. The reaction is preceded by an induction period which is due to the scarcity of hydrogen adsorption sites on the stoichiometric surface. The hydrogen adsorption removes the surface oxygen and replacement of the depleted oxygen occurs through Fickian diffusion from the sub surface region. They proposed a mechanism based on the dissociation of hydrogen at a partially reduced nickel surface site, followed by hydroxylation of lattice oxygen and subsequent water condensation and desorption. Later Rodriguez *et al.* [14] confirmed the role of oxygen vacancies by in situ time-resolved XRD and NEXAFS/EXAFS studies. They also proposed an induction period in which surface defect sites are created which have high efficiency for dissociation of hydrogen. They observed a direct correlation between concentration of vacancies in NiO lattice and the rate of oxide reduction. Lee and Kim [15] reported the synthesis of nanocrystalline nickel by hydrogen reduction of nickel oxide and the related kinetics. Their studies showed that for nanoagglomerate of NiO, the reduction initially starts by the nucleation-growth process and then retards later due to the diffusion controlling process owing to porous structure of the nano agglomerate. No discussion about NiO reduction kinetics would be complete without mentioning the works of Richardson *et al.* [16]. In situ hot stage X- ray diffraction was used to measure the NiO depletion and Ni formation simultaneously during the reduction reaction. Their studies reveal that, after a small induction period, the kinetics is pseudo-frist-order up to conversion levels of 0.8. The remaining NiO crystallites are covered with the metallic nickel crystallites and the inaccessibility of NiO crystallites retards the rate. The retention of product, H_2O, on the surface also reduces the rate.

Influence of grain size and crystallite size

The two different models proposed for the reduction of metal oxides are i) nucleation model and the ii) interface controlled model. Grain size of the sample is of much important in the interface controlled model (also called as shrinking core model). As per this model, the Ni–NiO interface moves towards the center of the grain, leaving behind a porous metallic product layer through which H_2 diffuses in

and H_2O diffuses out. The rate equation will depend on the slowest process. When the chemical reaction at the interface is the slowest step the model is best described by the function

$$x_{NiO} = 1 - (1 - k_c t)^3$$

where $k_c = (kP_H)/R_g$; (R_g is the grain radius). Moriyama and Yamaguchi [17] found that reduction rate constants are inversely proportional to grain size above a diameter of about 10 μm.

In the nucleation model, the induction period is described as the generation of nickel atoms on the outer surface of NiO crystallites. After nucleation, the formed Ni clusters grow two-dimensionally across the surface. At this point the hydrogen dissociation is very fast and the interface proceeds quickly to the grain. This type of nucleation growth is best described by Avrami relationship [18] given as

$$x_{NiO} = 1 - exp(-kt^m)$$

where x_{NiO} is the fractional conversion at time t, k an overall rate constant, and m is an exponent whose value (0.5–4) depends on grain geometry and the limiting step (i.e. chemical nucleation or diffusion). Many sigmoidal reduction curves are best explained by the Avrami relationship. The reduction curve in the work of Benton and Emmet [9], was fitted with Avrami relation with an m value of 1.34. This value suggests instantaneous nucleation and three dimensional growth, with the rate controlled by diffusion across the interface.

Influence of crystallite size was studied by Richardson *et al.* [19]. They found out that the crystallite size had no dependence on T_{50} (temperature for 50 % reduction) and also inferred that NiO, from whatever source will exhibit the same type of reduction behaviour.

3.1.2 Solid state kinetics

The kinetics of solid state reactions is treated in a different way compared to kinetics of reactions in homogeneous solutions. In solid state reactions the reaction is considered to initiate and propagate at the interface of solids. Figure 2 shows the changes caused by the introduction of dimensionality to the rate equation.

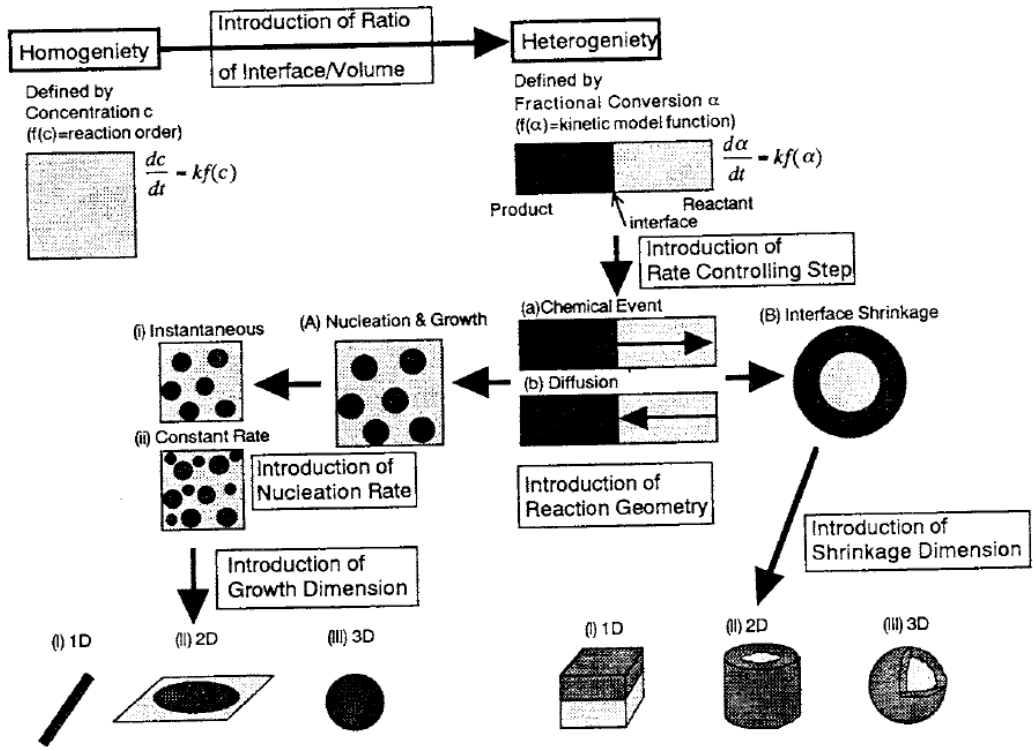

Figure 2. Introduction of dimensionality in solid state kinetics [From ref-20]

The molar concentration of reactants in the homogeneous solution kinetics is replaced by degree of conversion, α, which is usually defined as

$$\alpha_t = (C_t - C_0) / (C_\infty - C_0)$$

Where, C is the concentration of reactants or any other physical property chosen to study the system. The subscripts in the above equation correspond to the value at initial time (t = 0) and final time ($t \rightarrow \infty$), respectively. The time dependence of α is obviously expressed in the form of a differential equation

$$d\alpha/dt = k\ f(\alpha)$$

where k is the Arrhenius rate constant and f(α) is the kinetic model, which is an algebraic function describing the mechanism of the process. There are various models for solid state kinetics and a few are listed in Table 1.

Table 1. Different models of solid state reactions and corresponding f(α) functions

Model name	f(α)
Random nucleation	$(1-\alpha)$
Generalized n^{th} order	$(1-\alpha)^n$
Generalized Avrami- Erofeyev	$n(1-\alpha)(-\ln(1-\alpha))^{(n-1)/n}$
Contracting area Sharp interface controlled reaction	$(1-\alpha)^{1/2}$
Contracting volume Sharp interface controlled reaction	$(1-\alpha)^{1/3}$
Generalised model by Sestak	$\alpha^m(1-\alpha)^n(-\ln(1-\alpha))^p$
One dimensional diffusion	$1/2\alpha$
Two dimensional diffusion	$-\ln(1-\alpha)\ -1$
Three dimensional diffusion (Jander equation)	$3(1-\alpha)^{2/3}/2(1-(1-\alpha)^{1/3}))$
Three dimensional diffusion (Ginstling-Brounshtein equation)	$3/2((1-\alpha)^{-1/3}-1)$

3.1.3 Methodology – non isothermal thermogravimetry

Kinetics of nickel oxide reduction was followed by simple thermogravimetric experiments. There are several studies in literature, in which nickel oxide reduction was studied by thermogravimetry [21].

The fundamental rate equation for kinetics of solid state reactions is

$$\frac{d\alpha}{dt} = A \exp\left(\frac{-E_a}{RT}\right) f(\alpha)$$

where A is the pre exponential factor, T the absolute temperature, R the gas constant and f(α) is a function of the reacted fraction α. Under non isothermal conditions, temperature varies with time at a constant heating rate (β), where β = dT/dt and equation (1) changes to

$$\beta\left(\frac{d\alpha}{dT}\right) = A \exp\left(\frac{-E_a}{RT}\right) f(\alpha)$$

Though hydrogen reduction of nickel oxide is a gas solid reaction, under our experimental conditions the hydrogen concentration is a constant (large excess of hydrogen) and above equation is sufficient to describe the process. A complete kinetic analyses of solid state reaction should include determination of E_a, lnA and f(α) which are generally termed as the kinetic triplet.

Estimation of Activation energy E_a

Model free isoconversional methods based on multiple heating curves are considered to be better to determine activation energy than methods based on model fitting, which are based on single heating curves [22]. The assumptions of isoconversional methods are that the reaction rate at a constant conversion is only a function of temperature, and the reaction model is independent of the heating rate. Variation of heating rate causes changes in the reaction processes. The material spends more time at low temperature with low heating rates. At higher heating rates the reaction rates are faster, as the material is quickly exposed to elevated temperatures. This varying reaction rates at different heating rates can be used to estimate the activation energy of the process. The isoconversional methods can estimate activation energy at different conversions. For a single-stage reaction the activation energy (E_a) will be a constant throughout the conversion; but, for a reaction which consists of more than one stage, the activation energy varies with the

extent of reaction. This variation of E_a with alpha (α, extent of reaction) can be used to explain the reaction mechanism [23].

The Flynn-Wall-Osawa [24] method is an integral isoconversional method and the equation in its differential form is as below.

$$\frac{d\ln\beta}{d(1/T)} = \frac{1.052 * E_a}{R}$$

The method is based on measurement of temperatures for each degree of conversion, α, and different heating rates, β. The plots of ln β versus 1/T at constant α will give straight line and from the slope activation energies are determined.

Friedman differential method [25] is based on the intercomparison of the rates of conversion, dα/dT for a given degree of conversion α, at different heating rates. This method requires measurement of both temperatures and conversion rates, at different heating rates.

$$\ln\left(\beta\frac{d\alpha}{dT}\right) = \ln\left[A f(\alpha)\right] - \frac{E_a}{RT}$$

According to Budurgeac *et al.* [26], Friedman method is more suitable if activation energy depends on conversion. Moreover FWO method involves a systematic error, as it uses integral function which involves the history of the system.

Determination of f(α)

In the present chapter the suitable kinetic model (f(α)) was determined by Malek's procedure [27]. The procedure involves estimation of two special functions $Y(\alpha)$ and $Z(\alpha)$. These functions are as follows

$$Y(\alpha) = (d\alpha/dt) \times exp(x)$$

$$Z(\alpha) = \pi(x) \times (d\alpha/dt) \times T/\beta$$

$$where,\ x = E_a/RT$$

$\pi(x)$ is the approximation of the temperature integral [28] which has the form

$$\pi(x) = \frac{x^3 + 18x^2 + 88x + 96}{x^4 + 20x^3 + 120x^2 + 240x + 120}$$

The *Y(α)* function is proportional to f(α) function and the shape of *Y(α)* can be used as a diagnostic tool for kinetic model discrimination. The shapes of *Y(α)* functions for different kinetic models are depicted in Figure 3.

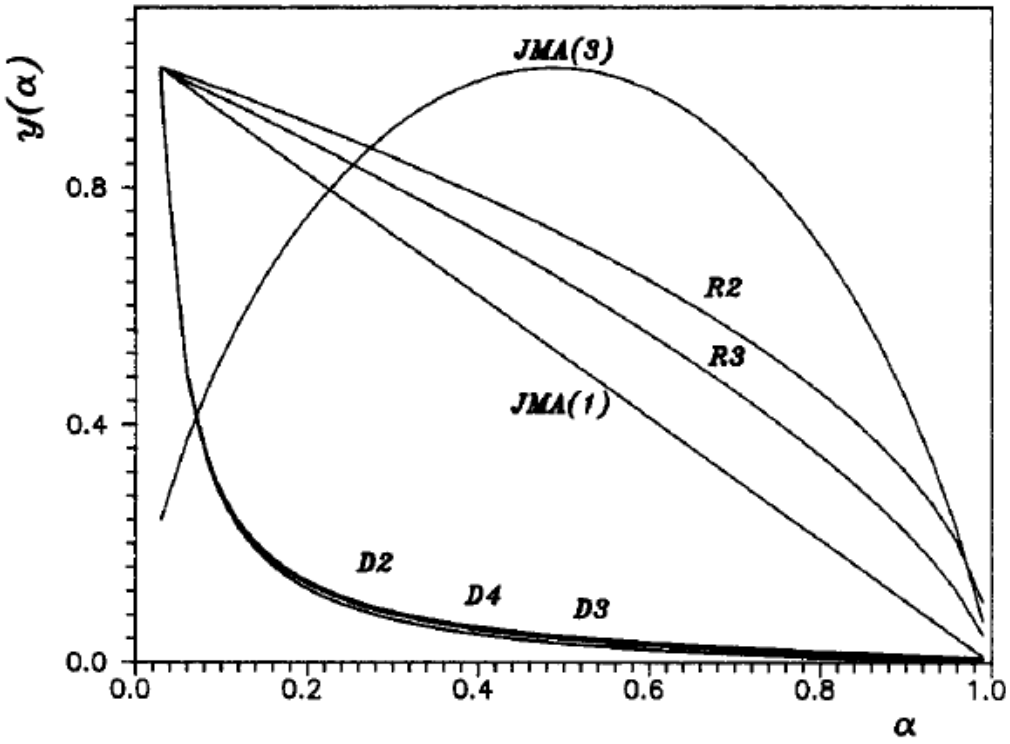

Figure 3. Shapes of *Y(α)* functions corresponding to different models; JMA(1), (3) (Johnson Mehl Avrami), R2, R3 (Reaction order), D2, D3, D4 (Diffusion).

The *Z(α)* function has a maximum for all the kinetic models. The maximum of *Z(α)*function termed as $(\alpha)_p$ has characteristic values corresponding to each kinetic model and some of them are given in Table 2.

Table 2. Values of $(\alpha)_p$ corresponding to different models

Kinetic model	Typical value of $(\alpha)_p$
Johnson Mehl Avrami (n=1, 2, 3)	0.632
Reaction order model (2 dimensional)	0.750
Reaction order model (3dimensional)	0.704
Diffusion (two dimensional)	0.834
Diffusion (three dimensional)	0.704
Diffusion (four dimensional)	0.776

The maximum $(\alpha)_m$ of the $Y(\alpha)$ function, maximum $(\alpha)_p$ of $Z(\alpha)$ function and the shape of $Y(\alpha)$ function can be used to select the best kinetic model of the process. Figure 4 shows a schematic diagram for the selection of suitable kinetic model from the values of $(\alpha)_m$ *and* $(\alpha)_p$.

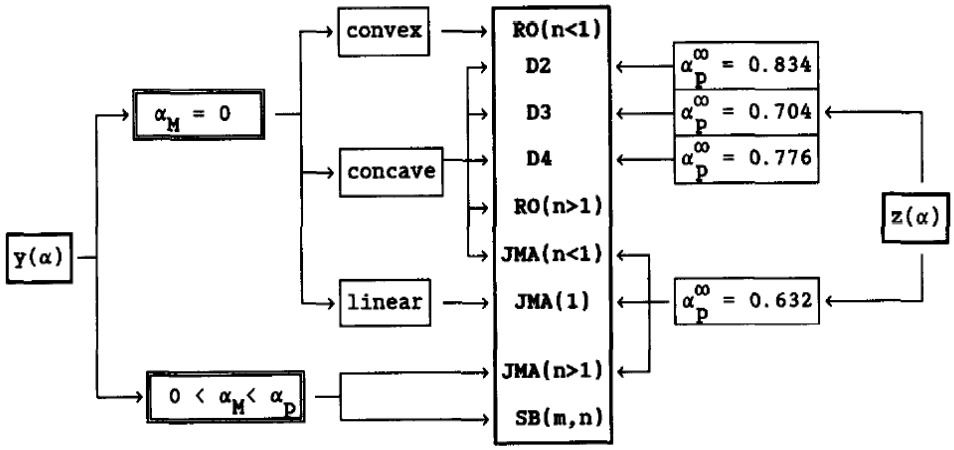

Figure 4. Kinetic model determination from values of $(\alpha)_m$ *and* $(\alpha)_p$.

The objectives of this study are

i) to study the influence of crystallite size on NiO reduction kinetics

ii) to study the influence of structural parameters of NiO (from different precursors-chapter 2) on the reduction kinetics.

3.2 Experimental

3.2.1 Preparation of nickel oxides

Synthesis of nickel oxide nanocrystallites

To obtain homogeneous NiO nanoparticles, the reported procedure of Estelle *et al.* [29] was adopted. $NiNO_3.9H_2O$ (Merck +99.5%) was dissolved in 50 mL distilled water and was slowly evaporated to get the crystals. The crystals were separated from the mother liquor and dried in an air oven at 120 °C for five days. The basic nickel nitrate – $Ni_3(NO_3)_2(OH)_4$ was formed which was confirmed by the single stage decomposition in theromgravimetry experiment (Figure 5) which is in accordance with the reported procedure. This basic nickel nitrate was then divided to three parts. One part was calcined at 400 °C, the second part at 600 °C and the third part was calcined at 800 °C in a static muffle furnace for two hours by heating at a rate of 5 °C min^{-1} from room temperature to the desired temperature and was named as NiO-400, NiO-600 and NiO-800 respectively.

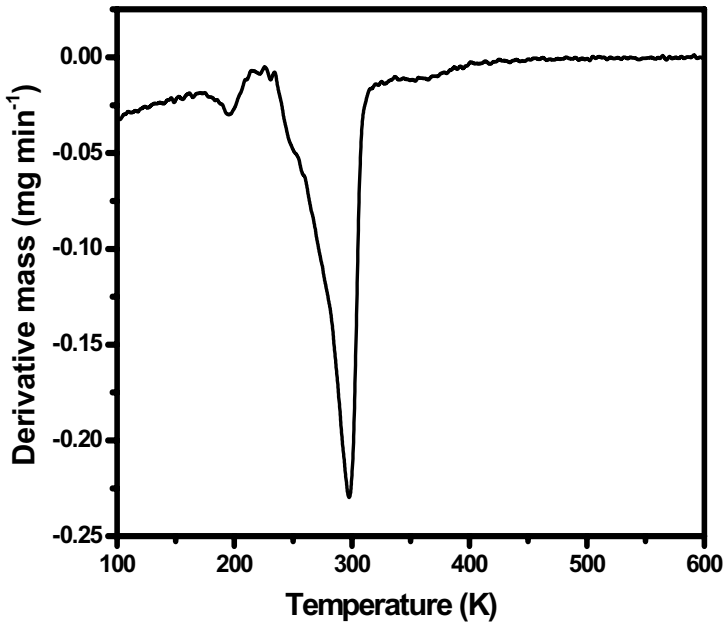

Figure 5. DTG graph of $Ni_3(NO_3)_2(OH)_4$

Nickel oxide from different precursors

Nickel oxides were prepared by thermal decomposition of the complexes. Details of the preparation are given Chapter 2. The samples were NiO-A, NiO-B, NiO-C and NiO-D.

3.2.2 Characterization techniques

The XRD patterns were recorded on Bruker model D8 (CuKα source) diffractometer. The peaks were subjected to Lorentzian curve fit, and the fwhm (τ) were determined after deducting the instrumental broadening. The X-ray line broadening analysis (XLBA) was done with the well known Scherrer equation to determine the crystallite size.

$$d_{vol} = \frac{0.9\lambda}{\tau \cos\theta} \ ;$$

d_{vol} = Volume average crystallite size; λ = wavelength of X'Ray; τ = fwhm (full width at half maximum)

SEM-EDX was recorded on Jeol JSM-6390 LA scanning electron microscope with EDX assembly. BET surface area was measured on a Micromeritics Tristar surface area analyzer.

3.2.3 Reduction reaction-experimental conditions

In a recent study on nickel oxide reduction kinetics, Erri *et al.* [30] identified the importance of diffusion effects on the reduction kinetics and recommend low heating rates for nonisothermal experiments. Recently Criado *et al.* have emphasized the use of low heating rates for processes involving overlapping reactions when using the isoconversional methods of kinetic analyses [31]. Utigard *et al.* [32] got varying kinetic results when they changed the hydrogen concentration. The TG

experiments were designed in such a way to eliminate the mass transfer limitations as far as possible.

The TG experiments were done on a Perkin Elmer TG-DTG Pyris Diamond instrument and the experimental conditions were, low sample mass (2.2±0.3 mg), low grain size (74μm-105μm (sieved through mesh size -100,+140)), high hydrogen concentration (99.95%), high hydrogen flow (500 mL min^{-1}), low heating rates (1,2,3 and 4 °Cmin^{-1}). Prior to each experiment the sample was dried in an air oven at 150 °C to avoid the presence of residual water. Necessary safety precautions were adopted as the studies involved hydrogen gas at high temperatures. The degree of conversion 'α' was calculated from the TG data as

$$\alpha = \frac{w_0 - w_T}{w_0 - w_f}$$

Where w_T is the mass of the sample at temperature T, and w_0 and w_f are mass of the sample at the beginning and at the end of the process respectively.

3.3 Results and Discussion

3.3.1 Kinetics of reduction of nickel oxide nanocrystallites

XRD & SEM

The XRD patterns in Figure 6 indicate decrease of fwhm (full width at half maximum) of the major peaks with increase of calcinations temperature. The crystallite sizes calculated by Scherrer equation were 13, 21 and 29 nm for samples NiO-400, NiO-600 and NiO-800 respectively.

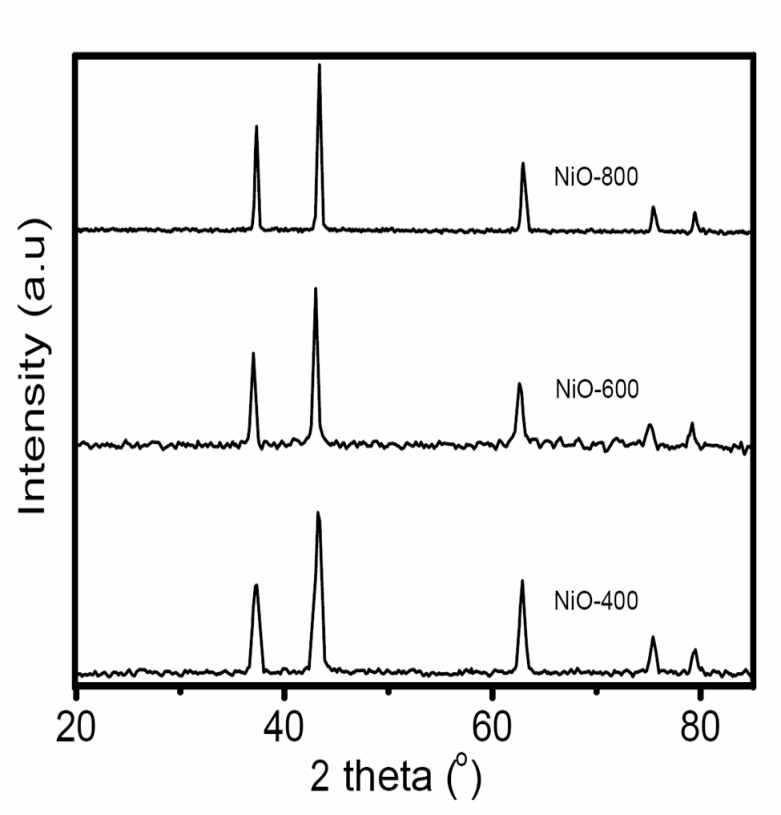

Figure 6. XRD patterns of nickel oxide calcined at 400 °C, 600 °C and 800 °C

The surface areas decreased as 20.2, 9.3 and 4.2 $m^2 g^{-1}$ with increasing calcination temperature. Particles were nearly in cubic shape as evidenced from SEM micrographs (Figure 7). The calcination temperature had less influence on particle shape; however the particles aggregated together as the temperature increased.

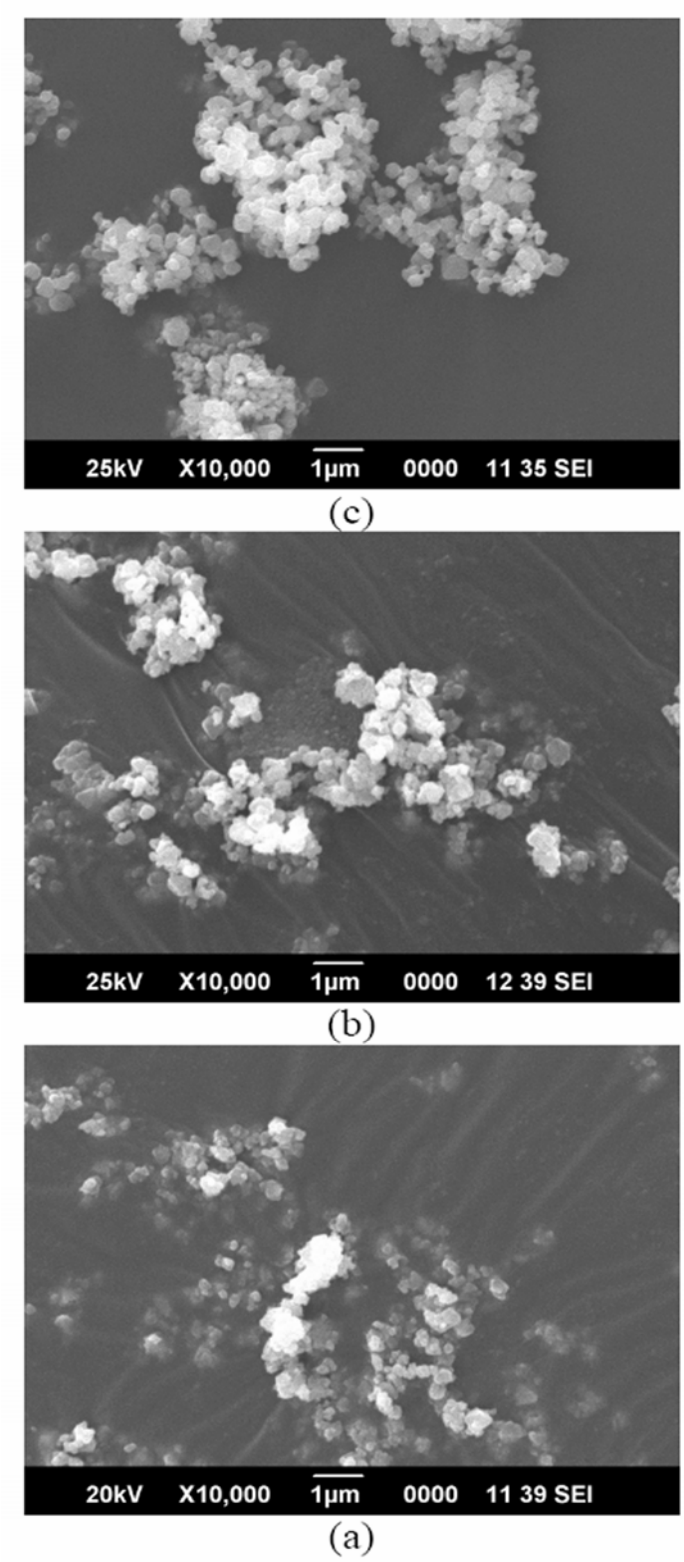

Figure 7. SEM of nickel oxide calcined at (a) 400 °C, (b) 600 °C and (c) 800 °C

Thermogravimetric results

The percentage mass losses during the temperature programmed reduction of the samples are shown in Figure 8 (a) to (c), and the corresponding α - T curves are shown in Figure 9 (a) to (c). An average of 21.5±0.2% of mass loss was recorded in all the experiments. The dependence of dα/dt versus T at different heating rates for the samples are shown in Figure 10 (a) to (c) and the results are summarized in Table 3. With increasing heating rate, the rate of reduction process of the samples increased. The T_{max} (temperature of peak maxima) and α_{max} (degree of conversion at T_{max}) read from α-T curve (Figure 8 (a) to (c)) shifted to higher values as the crystallite size increased. The ΔT values (peak width) decreased as the crystallite size increased.

More number of defects and vacancies are expected on NiO-400 sample because of its low crystallite size. This should be the reason for the low reduction temperatures for this sample and this observation is in accordance with the previously reported literature [13, 14] in which a direct correlation between reduction temperature and vacancies has been pointed out.

Table 3. Values of T_{max}, ΔT and α_{max} for the samples at different heating rates.

Heating rate °C min^{-1}	NiO-400			NiO-600			NiO-800		
	T_{max} (K)	ΔT	α_{max}	T_{max} (K)	ΔT	α_{max}	T_{max} (K)	ΔT	α_{max}
1	500.3	58.7	0.27	504.0	33.5	0.45	516.1	26.2	0.50
2	512.2	61.9	0.29	513.4	40.1	0.47	527.8	30.7	0.53
3	520.2	63.6	0.31	521.6	40.9	0.55	533.8	33.4	0.56
4	523.9	70.0	0.29	525.8	40.2	0.56	539.7	37.8	0.55

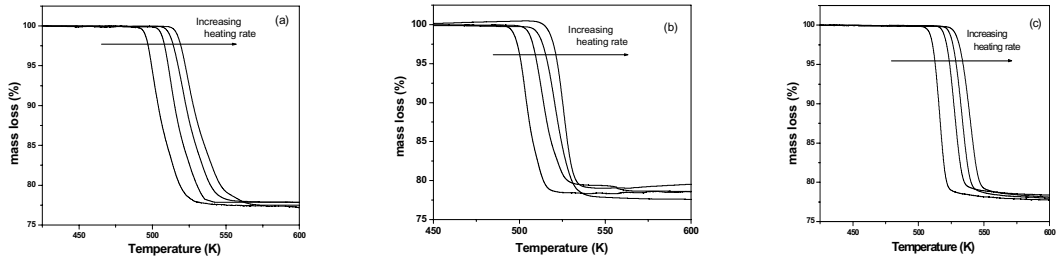

Figure 8 (a), (b) and (c). Mass loss curves of NiO-400, NiO-600 and NiO-800.

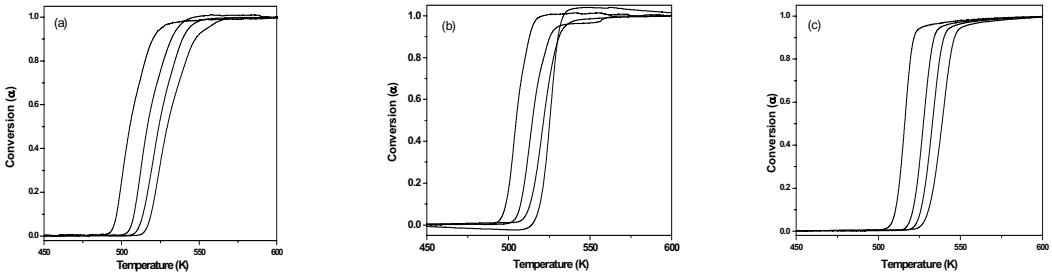

Figure 9 (a), (b) and (c). α - T curves of NiO-400, NiO-600 and NiO-800.

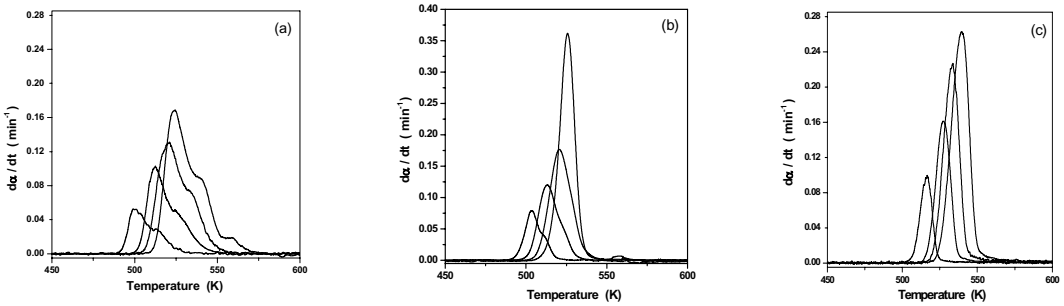

Figure 10 (a), (b) and (c). The experimental rate curves (dα/dt) of NiO-400, NiO-600 and NiO-800.

Activation energies

The activation energies were determined by Flynn-Wall-Osawa method and Friedman method for the samples and the values are plotted against α in the Figures 11 (a) to (c).

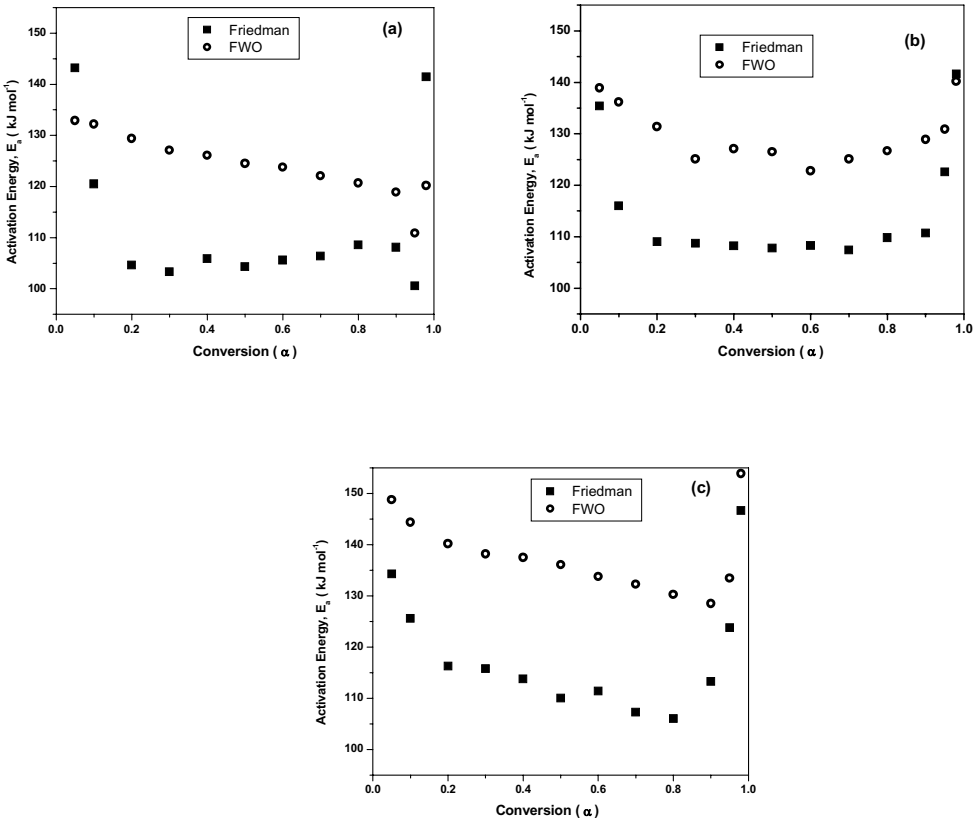

Figure 11 (a) NiO-400, (b) NiO-600 and (c) NiO-800. Variation of the Activation energy with conversion, determined by Friedman and FWO method.

The activation energies were determined within the range 0.05 to 0.95 α. For all samples the activation energies determined by Friedman method were lower than that of FWO method. Also it can be seen that the activation energy is a function of α with high values at both initial and final states. However, the variation with α were similar for both the methods. The activation energies for all samples were almost constant within the range 0.3 α to 0.7 α. The NiO-400 sample had the lowest activation energy and the activation energy increased as the crystallite size increased. The variation of Ea with α indicates the complex nature of the nickel oxide reduction. Vyazovkin [33] has assigned such an E_a - α dependence to occurrence of a parallel independent reaction which has higher activation energy. Comparing the curves, it can be seen that this step of higher activation energy is more important as

the crystallite size increases. As per the reported mechanism [12] of NiO reduction, the reduction in interfacial area of reduced phase and unreduced phase cause higher activation energy towards the end. In case of NiO-800 the overlapping of nickel grains will be difficult and the process will have high activation energy because of its higher crystallite size. The activation energy was averaged from the Friedman curve (in the range 0.3α to 0.7α) and was 105.1 kJ mol^{-1}, 108.4 kJ mol^{-1} and 111.6 kJ mol^{-1} for NiO-400, NiO-600 and NiO-800 respectively.

Note:- For the sample NiO-600 the rate curve at 4 °C min^{-1} is distinctively different from others, indicating a change in mechanism. For activation energy determination data from heating rates 1 °C min^{-1}, 2 °C min^{-1} and 3 °C min^{-1} was used.

Kinetic model by Malek's procedure

The $Y(\alpha)$ and $Z(\alpha)$ functions were calculated for NiO-400 sample. The normalized $Y(\alpha)$ and $Z(\alpha)$ were plotted against α in the Figure 12 (a) and (b).

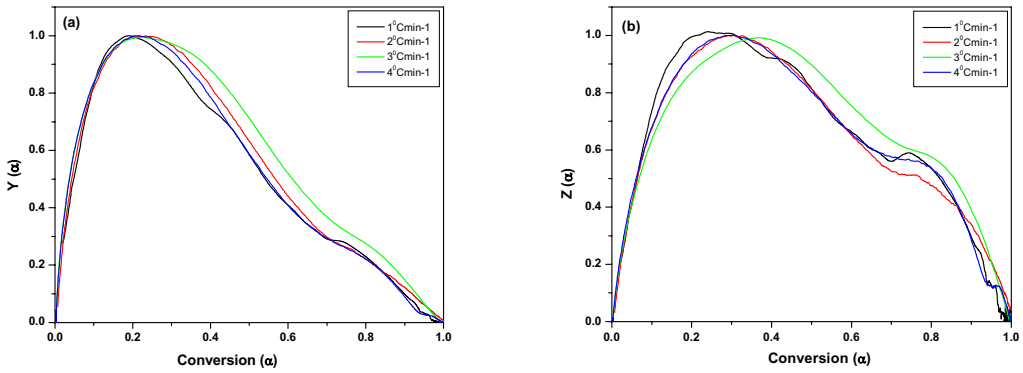

Figure 12 (a) $Y(\alpha)$ function and (b) $Z(\alpha)$ function *of NiO-400*

The values of $(\alpha)_m$ and $(\alpha)_p$ extracted from Figure 12 are given in Table 4.

Table 4. Values of $(\alpha)_m$ and $(\alpha)_p$ for NiO-400 different heating rates.

Heating rate °C min^{-1}	NiO-400	
	$(\alpha)_m$	$(\alpha)_p$
1	0.188	0.264
2	0.223	0.291
3	0.222	0.322
4	0.205	0.285

Considering the shape of $Y(\alpha)$ function and the fact that $(\alpha)_m$ values are lower than $(\alpha)_p$ values, the kinetic model can be either Johnson Mehl Avrami (JMA) or Sestak Berggren (SB). The fact that $(\alpha)_p$ value is lower than 0.632 indicates that Sestak Berggren model $f(\alpha)=\alpha^m(1-\alpha)^n$ is suitable for both samples. The ratio of kinetic exponents $s = m / n$ can be determined from $(\alpha)_m$ values as $s = (\alpha)_m / 1- (\alpha)_m$. To determine *n,* the following relation is used

$$\ln\left[\left(\frac{d\alpha}{dt}\right)\exp\left(\frac{E_a}{RT}\right)\right]=\ln A + n\ln\left[\alpha^s(1-\alpha)\right]$$

The pre exponential factor A and kinetic exponents *n* and *m* ($m=s \times n$) were determined at each heating rates and the results are presented Table 5.

Table 5. The kinetic parameters n, m and ln A for NiO-400 at different heating rates and their average values

Heating rate °C min^{-1}	NiO-400		
	n	**m**	**ln A (min^{-1})**
1	1.86	0.491	19.37
2	1.92	0.507	19.55
3	1.67	0.441	19.34
4	1.87	0.494	19.40
Average	**1.83**	**0.483**	**19.42**

The kinetic triplet obtained for the NiO-400 sample is

NiO-400 [Ea = 105.1 kJ mol^{-1}, ln A = 19.42 min^{-1}, $f(\alpha)=\alpha^{0.48}(1-\alpha)^{1.83}$]

Above procedure was repeated for NiO-600 and NiO-800 samples and the kinetic triplet obtained were

NiO-600 [Ea = 108.4 kJ mol^{-1}, ln A = 20.34 min^{-1}, $f(\alpha)=\alpha^{0.69}(1-\alpha)^{1.42}$]

NiO-800 [Ea = 111.6 kJ mol^{-1}, ln A = 20.56 min^{-1}, $f(\alpha)=\alpha^{0.60}(1-\alpha)^{0.91}$].

The validity of the obtained kinetic parameters can be checked by comparing the experimental curve with the calculated rate curve. The rate curve is calculated using the above kinetic triplet in the equation

$$\frac{d\alpha}{dt} = A\exp\left(\frac{-E_a}{RT}\right)f(\alpha)$$

Figure 13 shows the experimental and the calculated rate curves. It can be seen that the curves match very well within the range 0.01α to 0.9 α (the α was read from the corresponding α - T curves; Figure 9 (a), (b) and (c))

The solid state reaction of nickel oxide with hydrogen consists of various chemical and physical processes such as adsorption-desorption, reaction of hydrogen gas with nickel oxide, and polymorphous transition when nickel nuclei grows in nickel oxide lattice. Therefore, the effective activation energy of the process is generally a composite value determined by the activation energies of various processes as well as by the relative contributions of these processes to the overall reaction rate.

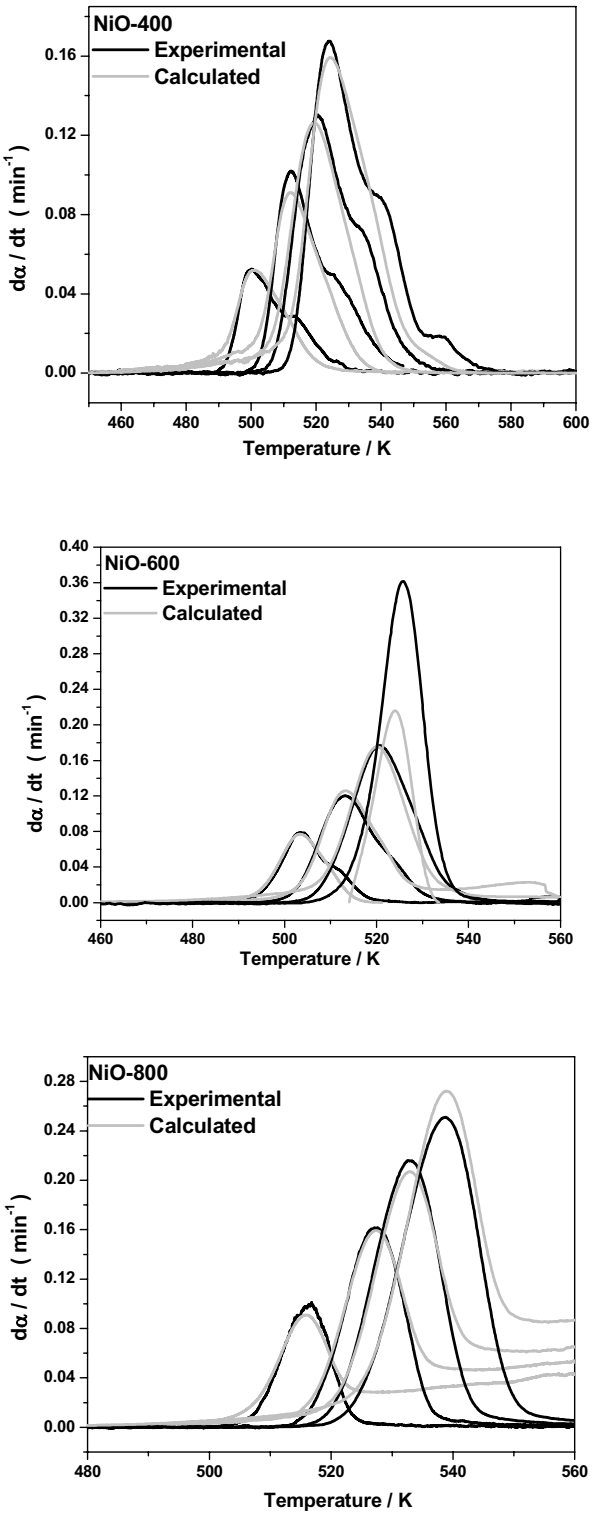

Figure 13. Experimental vs. Calculated rate curves

Discussion on kinetic parameters n, m and r

The empirical two parameter kinetic model of Sestak and Berggren [34] when proposed was of the form

$$f(\alpha) = \alpha^m (1-\alpha)^n [-\ln(1-\alpha)]^r$$

where n, m and r are the kinetic exponents. Mathematical analysis of above equation [35] has shown that only two kinetic exponents are necessary, and the above equation was reduced to the form

$$f(\alpha) = \alpha^m (1-\alpha)^n$$

where m and n are the kinetic exponents. Sestak Berggren model is usually denoted as SB (*m, n*). The kinetic exponent m and n should be linked with the mechanism of reduction process but due to the empirical nature of the Sestak Berggren model such links are hard to find in the literature. However some recent studies [36-38] has attempted to relate the SB (*m, n*) exponents to the structure of the material. Comparing the kinetic exponents, it can be seen that the n value decreases from 1.83 to 0.91 as crystallite size increases. It has been proposed such a shift of *n* value indicates the shift of mechanism from Langmuir-Hinshelwood to Eley-Rideal [38]. The *m* values increases from 0.48 to 0.60 as crystallite size increases. An increase of m value indicates the role of reduced phase in the overall reduction process.

The macroscopic process of reduction (nucleation/crystal growth) strongly depends on the concentration and distribution of nuclei in the sample. The nuclei can be of two types, surface nuclei and bulk nuclei. The surface nuclei are already present on the sample, while the bulk nuclei, termed as secondary nuclei, form during the course of reduction. Because of the low crystallite size and higher surface area of NiO-400 sample, these surface nuclei initiate the reaction early. Thus the reaction is more Langmuir-Hinshelwood type, as hydrogen dissociates rapidly on the surface nuclei and the dissociated hydrogen reacts with nickel oxide. For this case the important process is the reaction of adsorbed hydrogen and the surface nuclei-

probably the oxygen vacancies. This is indicated by a high value of *n*. For NiO-800 sample, the number of oxygen vacancies and correspondingly the surface nuclei are small. But as its reduction happens at a higher temperature a larger number of bulk nuclei are formed. These bulk nuclei which are present inside the NiO crystals, tend to grow faster. The higher value of *m* for NiO-800 sample indicates that the major reduction happens between the interphase of reduced and nonreduced phase.

The work of Sestak, Satava and Wendlandt [39] has shown that the SB (*m, n*) equation is equivalent to the JMA (*r*) equation to a first approximation. The empirical SB (*m, n*) model thus includes JMA (*r*) model as a special case [40] and the kinetic parameters are related as

$$r = \frac{1}{1 + \ln(n) - \ln(n+m)}$$

The average value of *r* and the m, n values for the samples are tabulated in Table 6.

Table 6. Calculated kinetic exponents

Sample	n	m	r
NiO-400	1.83	0.48	1.31
NiO-600	1.42	0.69	1.66
NiO-800	0.91	0.60	2.04

The JMA model is derived from first principles and hence, its parameter (*r*) has physical significance. The value of *r* depends on the shape of the nuclei and dimensionality of their growth, as well as on the rate of their formation [41]. The Avrami exponents of the samples show that the dimensionality of the reduction process increases as crystallite size increases. This indicates that under the

experimental conditions, the hydrogen reduction of nickel oxide takes place in a surface oriented fashion for NiO-400 sample. Thus the reduction mechanism of nickel oxide depends on the crystallite size of the sample under the studied experimental conditions.

A special mention on NiO-600

The α-T curve of NiO-600 shows that at low heating rates the reduction happens in two stages, but as the heating rate increases the two stages merges together to a single peak. This indicates a change in mechanism with heating rates and is attributed to the complex nature of the reduction process. The change in α_{max} values (Table 3) also indicates a change in reduction mechanism. The calculated rate curve deviates from the experimental one as shown in Figure 13. The shape of the experimental curve at 4 °C min^{-1} is more similar to that of NiO-800. The rate curve was again calculated with the kinetic model ($f(\alpha)=\alpha^{0.60}(1-\alpha)^{0.91}$) for NiO-800. Figure 14 shows that now the curve matched better with the experimental curve. This shows that the mechanism has changed at higher heating rate. Oxidation of tungsten carbide is shown to happen in two stages at low heating rates whereas as single stage on higher heating rates [42].

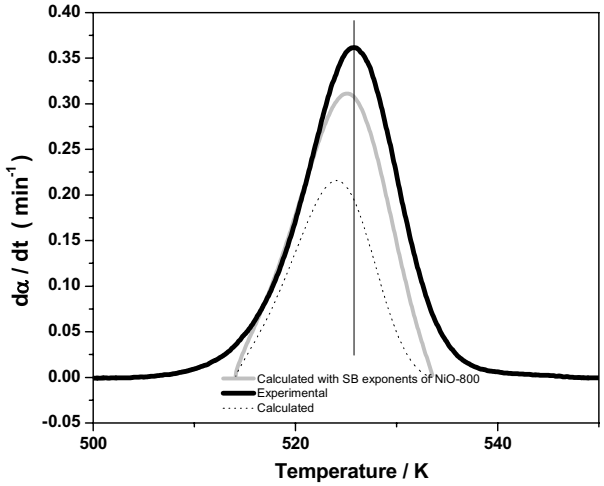

Figure 14. Experimental vs. Calculated rate curve of NiO-600 at 4 °C min^{-1}. When calculated with kinetic model of NiO-800; both T_{max} and shape matches better.

The relative contribution of the two competitive reactions to the overall process depends on the heating rate, as the reaction with higher activation energy will become dominant at higher temperatures. Thus while selecting the heating rates, one should be sure that the rate of individual processes does not vary within the selected heating rates.

3.3.2 Kinetics of reduction of nickel oxide derived from different precursors

The nickel oxides prepared by thermal decomposition of metal complexes (Chapter 2) were subjected to kinetic study. The procedure for kinetic analyses was same as that in the previous section, and only the results will be discussed in this section. The T_{max} values for the samples are given Table 7.

Table 7. The T_{max} values of nickel oxides.

Heating rate °C min^{-1}	**T_{max} (K)**			
	NiO-A	**NiO-B**	**NiO-C**	**NiO-D**
1	509.9	495.9	530.8	530.4
2	523.6	514.7	539.3	543.1
3	528.4	520.6	547.2	551.2
4	534.1	527.3	553.0	558.5

NiO-A (derived from $[Ni(H_2O)_6](NO_3)_2$

The kinetic triplet obtained for the sample was

NiO-A [Ea = 114.3 kJ mol^{-1}, ln A = 20.65 min^{-1}, $f(\alpha)=\alpha^{0.38}(1-\alpha)^{0.68}$]

The Ea-α curve and the rate curves are shown in Figure 15 and Figure 16 respectively.

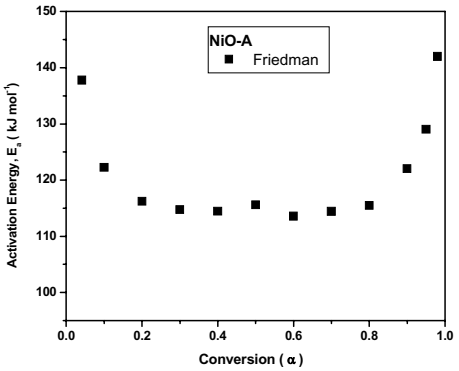

Figure 15. Ea-α curve of NiO-A

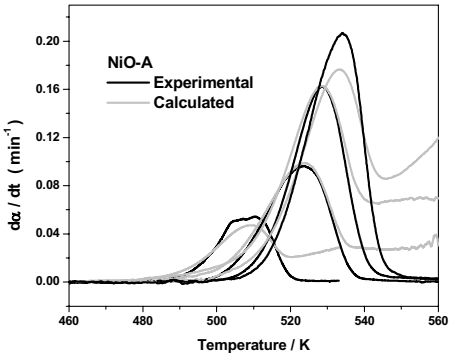

Figure 16. Rate curve of NiO-A

The experimental and calculated curves matched up to 0.87 α. After the conversion of 0.87 the calculated curves lie above the experimental ones. This may be due to higher activation energy involved in later stages of reduction. At higher conversions the remaining NiO is covered with Ni crystallites and it requires higher activation energy to reduce the deeply seated nickel oxide particles. This may be due to the difficulty for hydrogen to diffuse inside or the product water to diffuse outside [43, 16].

NiO-B (derived from $[Ni(en)_2(H_2O)_2](NO_3)_2$

The Ea-α dependence (Figure 17) is almost constant for NiO-B. The kinetic triplet obtained for the sample was

NiO-B [Ea = 88.5 kJ mol^{-1}, ln A = 20.14 min^{-1}, $f(\alpha)=\alpha^{0.81}(1-\alpha)^{1.28}$]

The activation energy was considerably low for this sample. The T_{max} values were also low. The rate curves (Figure 18) matched at all conversion values.

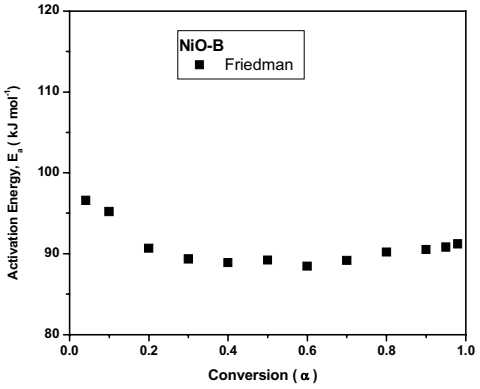

Figure 17. Ea-α curve of NiO-B

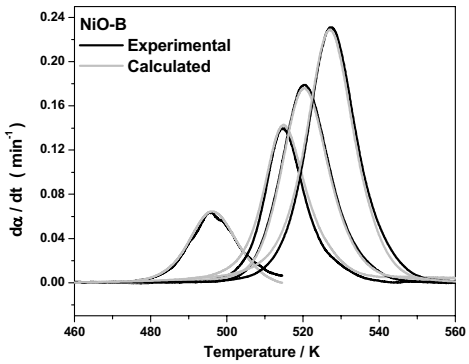

Figure 18. Rate curve of NiO-B

NiO-B was obtained by oxidation of nickel metal (Chapter 2). Some nickel crystallites remnant in the sample can act as nucleating sites. If the nucleating sites are present on the onset of reduction, the reduction can start early. The T_{max} values indicate a low induction period for the sample. The SEM of the sample (Chapter 2) shows it has foam like structure. This special structure can enhance the hydrogen diffusion inside and water diffusion outside, during the reduction reaction. The high value of SB parameter 'm' (0.81) indicates the increased dependence on the crystallized (Ni crystallites) phase.

NiO-C (derived from $[Ni(en)_2(H_2O)_2](CH_3COO)_2$

The kinetic triplet obtained for the sample was

NiO-C [Ea = 118.5 kJ mol^{-1}, ln A = 21.03 min^{-1}, $f(\alpha) = \alpha^{0.58}(1-\alpha)^{1.02}$]

Both T_{max} and activation energy was highest for this sample.

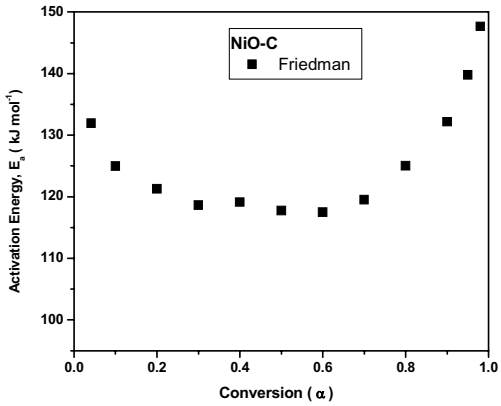

Figure 19. Ea-α curve of NiO-C

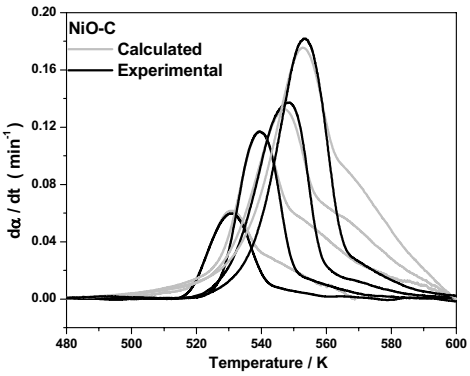

Figure 20. Rate curve of NiO-C

The SEM picture (Chapter 2) indicates a compact shape for the amorphous structured sample. This tough structure may be retarding the diffusion of hydrogen or water vapour; thus increasing the activation energy.

NiO-D (derived from $[Ni(en)_2(H_2O)_2]Cl_2$

The T_{max} values are higher compared to NiO-A (which has almost same morphology as NiO-D; Chapter 2), but the activation energy is lower. The kinetic triplet obtained for the sample was

NiO-D [Ea = 110.8 kJ mol^{-1}, ln A = 19.04 min^{-1}, $f(\alpha)=\alpha^{0.65}(1-\alpha)^{1.03}$]

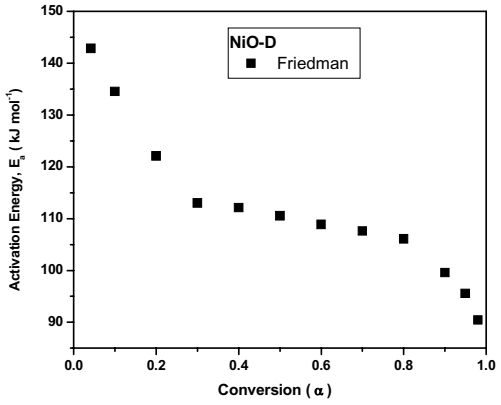

Figure 21. Ea-α curve of NiO-D

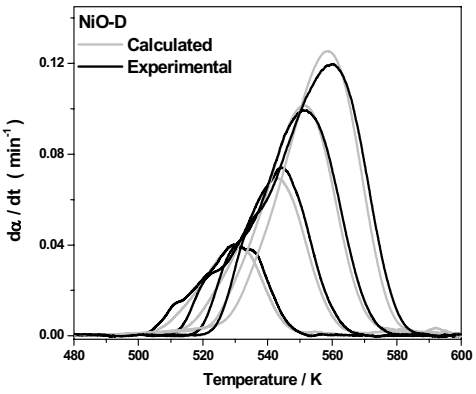

Figure 22. Rate curve of NiO-D

The EDX analysis of the NiO-D (Figure 23) sample before reduction indicates presence of chlorine in the sample (0.2 wt%). The reduced sample (Figure 24) does not contain any chlorine which indicates chlorine has escaped during the reduction.

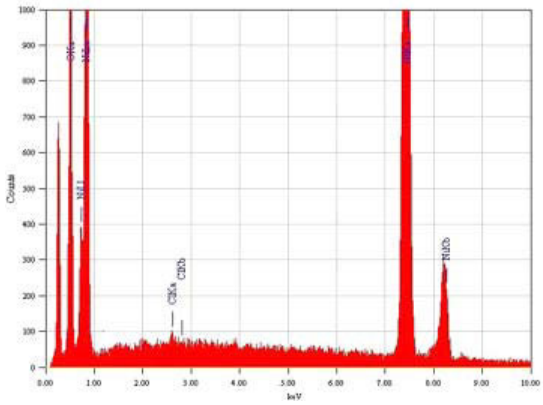

Figure 23. EDX results before reduction of NiO-D

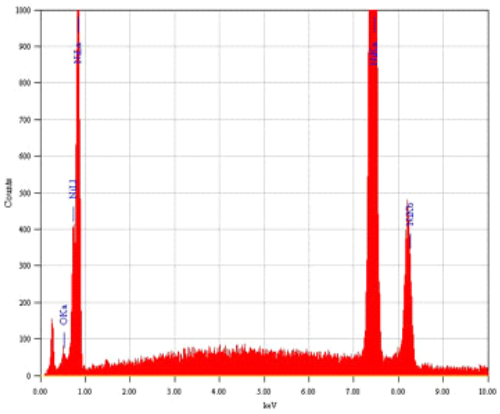

Figure 24. EDX results after reduction of NiO-D

The Ea-α values show decreasing dependence towards the end. Vyazovkin [44] has identified such decreasing dependence of activation energy due to diffusion limited process which involves conversion of solid → solid + gas. Generally a process becomes diffusion limited when the reaction rate is high. The low activation energy observed for the NiO-Cl sample should be because of the effect of chlorine, which acts as a catalyst for the reduction reaction. The following mechanism can be suggested. During the induction (nucleation) period the gas phase hydrogen dissociates on the NiO surface. The surface disorders like defects, kinks and vacancies activate this step on the NiO surface.

$$H_{2\ (g)} \rightarrow 2H_{\ (ads)}$$

In the nucleation step the adsorbed hydrogen reacts with nickel oxide to form nickel metal which acts as nucleating sites for the further steps of nucleation growth.

$$NiO + 2H_{\ (ads)} \rightarrow Ni_{\ (metal)} + H_2O_{\ (g)} \quad — \quad (2)$$

Chlorine is present on the nickel oxide as nickel chloride. The chlorine atoms present on the NiO lattice reduces the reactivity of NiO surface by its electron withdrawing property and the reduction starts at higher temperature on this sample. Once sufficient number of nuclei is formed, $Ni_{(metal)}$ acts auto catalytically and the reaction becomes faster. On the NiO-D sample the following reaction also takes place

$$NiCl_2 + 2H_{(ads)} \rightarrow Ni_{(metal)} + 2HCl_{(g)} \quad — \quad (3)$$

The formed HCl can either be transported away through the gas phase or can be adsorbed on NiO surface and Ni surface or may get dissolved in evolving H_2O. If HCl gets adsorbed on NiO it forms nickel chloride by the reaction

$$NiO + 2HCl_{(g)} \rightarrow NiCl_2 + H_2O_{(g)} \quad — \quad (4)$$

Activation energy for reduction of $NiCl_2$ is lower (54 kJ mol^{-1}) than that for NiO [45]. Thus during the process, a part of nickel oxide gets reacted as nickel chloride for which the activation energy is lower. This explains the lowering of activation energy as conversion increases. If the HCl gets dissolved in water it reduces the volatility of water vapour, consequently escape of water vapour from Ni surface becomes slow. During the process the HCl gets transported away through the gas phase. The final EDX analysis shows the absence of chlorine. As the particle size increases (by sintering) the diffusion of hydrogen to the reacting interphase (surface between nickel metal and nickel oxide) becomes the rate determining step in the latter stages. Because of the above reasons the reaction becomes more and more diffusion limited and the activation energy gets lower. The activation energy for diffusion is always lower than the activation energy for the reaction.

3.4 Conclusions

i) Crystallite size influences the NiO reduction mechanism.

ii) Reduction starts earlier for low crystallite sized sample probably due to higher number of surface nuclei.

iii) The SB (*m, n*) exponents vary with the crystallite size. Comparison of the exponents indicated that, when the crystallite size is lower the reduction follows a surface oriented mechanism under the experimental conditions.

iv) The NiO-B sample, which probably has the presence of Ni crystallites, reduces at a low temperature with low activation energy.

v) Nucleation period is longer for reduction on chlorine containing sample (NiO-D) as Cl^- reduces the reactivity of NiO surface by its electron withdrawing effect.

vi) The rate of reaction is much lower at the end for the NiO-D sample; which may be due to (a) inhibition of reaction because of slow water desorption or (b) difficulty in diffusion of hydrogen through the sintered nickel metal surface to the reaction interphase.

vii) There is an indication that morphology of the sample influences the reduction kinetics.

References

[1] H. Fang, L. Haibin, and Z. Zengli., Advancements in Development of Chemical-Looping Combustion: A Review., *International Journal of Chemical Engineering.* Hindawi Publishing Corporation, doi:10.1155/2009/710515

[2] H.J. Richter and K.F. Knoche., "Reversibility of combustion processes," in Efficiency and Costing: Second Law Analysis of Processes., 235 (1983) 71-85

[3] T. Mattisson, M. Johansson, A. Lyngfelt., Multicycle reduction and oxidation of different types of iron oxide particles - Application to chemical – looping combustion., *Energy Fuels.* 18 (2004) 628–637

[4] L. De Diego, F. Garcia-Labiano, J. Adanez, P. Gayan, A. Abad, B.M. Corbella, J.M Palacios., Development of Cu-based oxygen carriers for chemical-looping combustion., *Fuel.* 83 (2004) 1749–1757

[5] H. Jin, T. Okamoto, M. Ishida., Development of a novel chemical-looping combustion: Synthesis of a solid looping material of $NiO/NiAl_2O_4$., *Ind. Eng. Chem. Res.* 38 (1999) 126–132

[6] Q. Song, R. Xiao, Z. Deng., Chemical-looping combustion of methane with $CaSO_4$ oxygen carrier in a fixed bed reactor., *Energy Conversion and Management.* 49 (2008) 3178–3187.

[7] M. Ishida, H. Jin., A novel chemical-looping combustor without NO_x formation., *Ind. Eng. Chem. Res.* 35 (1996) 2469–2472

[8] R. Villa, C. Cristiani, G. Groppi., Ni based mixed oxide materials for CH_4 oxidation under redox cycle conditions., *J. Mol. Catal. A: Chemical.* 204-205 (2003) 637–646

[9] A.F. Benton, P.H Emmett., The reduction of nickelous and ferric oxides by hydrogen., *J. Am. Chem. Soc.* 46 (1924) 2728-2737.

[10] G.B. Taylor, H.W. Starkweather., Reduction of Metal oxides by hydrogen., *J. Am. Chem. Soc*. 52 (1930) 2314-2325

[11] Y. Koga, L.G Harrison, in: C.H. Bamford, C.F.H. Tipper, R.G. Compton,. (Eds.), *Comprehensive Chemical Kinetics*, vol. 21., Elsevier.: Amsterdam, 1984.

[12] B. Jankovic, B. Adnadevic, S. Mentus., The kinetic study of temperature programmed reduction of nickel oxide in hydrogen atmosphere., *Chem. Eng. Sci.* 63 (2008) 567-575

[13] R.P. Furstenau, G. Mcdougall., M.A. Langell., Initial stages of hydrogen reduction of Ni(100)., *Surf. Sci.* 150 (1985) 55-79

[14] J.A. Rodriguez, J.C. Hanson, A.I. Frenkel, J.Y. Kim, M. Perez., Experimental and theoretical studies on the reaction of H_2 with NiO: Role of O vacancies and mechanism for oxide reduction., *J. Am. Chem. Soc.* 124 (2002) 346-354

[15] J.S. Lee, B.S. Kim., Synthesis and related kinetics of nanocrystalline Ni by hydrogen reduction of NiO., *Mater. Trans. JIM.* 42 (2001) 1607-1612

[16] J.T. Richardson, R. Scates, M.V. Twigg., X-ray diffraction study of nickel oxide reduction by hydrogen., *Applied Catalysis A: General.* 246 (2003) 137–150

[17] J. Moriyama, A. Yamaguchi, *Nippon. Kinzoku. Gakkaishi.* 28 (1964) 831.

[18] M. Avrami., Kinetics of phase change. I., *J. Chem. Phys*. 7 (1939) 1103-1112

[19] J.T. Richardson, M.V. Twigg., Reduction of impregnated NiO/α-$A1_2O_3$ association of $A1^{3+}$ ions with NiO., *Applied Catalysis A: General.* 167 (1998) 57-64

[20] N. Koga, J. Malek, J. Sestak and H. Tanaka., Data treatment in non-isothermal kinetics and diagnostics limits in phenomenological models., *Netsu Sokutei.* 20(4) (1993) 210-223

[21] B. Jankovic, B. Adnadevic, S. Mentus., The kinetic analysis of non-isothermal nickel oxide reduction in hydrogen atmosphere using the invariant kinetic parameters method., *Thermochim. Acta*. 456 (2007) 48–55

[22] S. Vyazovkin, C.A. Wight., Model-free and model-fitting approaches to kinetic analysis of isothermal and nonisothermal data., *Thermochim. Acta.* 340/341 (1999) 53-68

[23] S. Vyazovkin, N. Sbirrazzouli, Kinetic methods to study isothermal and nonisothermal epoxy-anhydride cure., *Macromol. Chem. Phys.* 200 (1999) 2294-2303.

[24] J.H. Flynn, L.A. Wall., A quick, direct method for the determination of activation energy from thermogravimetric data., *J. Polym. Sci. Part B.* 4 (1996) 323-328

[25] H.L. Friedman., New methods for evaluating kinetic parameters from thermal analysis data., *J. Polym. Sci. Part B. Ploym Lett.* 7 (1969) 41-46

[26] P. Budrugeac, D. Homentcovschi, E. Segal., Critical analysis of the isoconversional methods for evaluating the activation Energy. I. Theoretical background., *J. Therm. Anal. Calorim.* 63 (2001) 457-463

[27] J. Málek, The kinetic analysis of nonisothermal data., *Thermochim. Acta.* 200 (1992) 257-269

[28] G.I. Senum., R.T. Yang., Rational approximations of the integral of the Arrhenius function., *J. Therm. Anal.* 11 (1977) 445-447

[29] J. Estelle, P. Salagre, Y. Cesteros, M. Serra, F. Medina, J.E. Sueiras., Comparative study of the morphology and surface properties of nickel oxide prepared from different precursors., *Solid State Ionics.* 156 (2003) 233– 243

[30] P. Erri, A. Varma., Diffusional effects in nickel oxide reduction kinetics., *Ind. Eng. Chem. Res.* 48 (2009) 4-6

[31] J.M. Criado, P.E. Sánchez-Jiménez, L.A. Pérez-Maqueda., Critical study of the isoconversional methods of kinetic analysis., *J. Therm. Anal. Calorim.* 92 (2008) 199-203

[32] T.A Utigard, M. Wu, Z.X Gao., Reduction kinetics of Goro nickel oxide using hydrogen., *Chem. Eng. Sci.* 60 (2005) 2061-2068

[33] S.V. Vyazovkin, V. Goryachko, A.I. Lesnikovich., An approach to the solution of the inverse kinetic problem in the case of complex processes. Part III. Parallel independent reactions., *Thermochim. Acta.* 197 (1992) 41-51

[34] J. Šesták, G. Berggren., Study of the kinetics of the mechanism of solid-state reactions at increasing temperatures., *Thermochim. Acta.* 3 (1971) 1–12

[35] V.M. Gorbachev., Some aspects of Šestak's generalized kinetic equation in thermal analysis., *J. Therm. Anal.* 18 (1980) 193-197

[36] G. Munteanu, L. Ilieva, R. Nedyalkova, D. Andreeva., Influence of gold on the reduction behaviour of Au–V_2O_5/CeO_2 catalytic systems: TPR and kinetic parameters., *Appl. Catal. A: General.* 227 (2004) 31–40

[37] G. Munteanu, P. Budrugeac, L. Ilieva, T. Tabakova, D. Andreeva, E. Segal., Kinetics of temperature programmed reduction of Fe_3O_4 promoted with copper: application of iso-conversional methods., *J. Mater. Sci.* 38 (2003) 1995–2000

[38] G. Munteanu, E. Segal., Sestak–Berggren function in temperature-programmed reduction., *J. Therm. Anal. Calorim.* doi 10.1007/s10973-009-0435-3

[39] J. Šesták, J. Šatava, W.W. Wendlandt., The study of heterogeneous processes by thermal analysis., *Thermochim. Acta.* 7 (1973) 333–336

[40] J. Sestak, J. Malek., Diagnostic limits of phenomenological models of heterogeneous reactions and thermal analysis kinetics., *Solid State Ionics.* 245 (1993) 63-65

[41] J. Sestak., Thermophysical properties of solids, their measurements and theoretical analysis, Elsevier, Amsterdam 1984. pg. 190.

[42] C.A. Ribeiro, W.R. de Souza, M.S. Crespi, J.A.G. Neto, F.L. Fertonani., Non-isothermal kinetic of oxidation of tungsten carbide., *J. Therm. Anal. Calorim.* 90 (2007) 801-805

[43] S. Sridhar, D. Sichen, S. Seetharaman, *Z. Metallkd.* 85 (1994) 616

[44] S. Vyazovkin., A unified approach to kinetic processing of nonisothermal data., *Int. J. Chem. Kinet.* 28 (1996) 95-101

[45] S.R. Stopic, I.B. Ilic, D.P Uskokovic., Effect of Pd, Cu, and Ni additions on the kinetics of $NiCl_2$ reduction by hydrogen., *Metall. Mater. Trans. B.* 28B (1997) 1241-1248

Chapter 4

THE ACTIVE PHASE DISTRIBUTION IN Ni/γ-Al_2O_3 CATALYSTS PREPARED BY IMPREGNATION OF BIS(ETHYLENEDIAMINE)NICKEL(II) COMPLEXES

Contents

4.1 Introduction

For a supported metal catalyst, the desirable distribution of active sites depends on the rate and nature of the catalytic reaction. In a heterogeneous catalytic reaction, the diffusion step becomes rate determining when the desired chemical reaction becomes fast enough [1]. It is advantageous to deposit the catalytically active particles at the external edge of the catalyst bodies for such reactions. Recently, Qiu *et al.* reported a better catalytic performance for partial oxidation of methane to synthesis gas on egg shell (active metal deposited at the external edge) Ni/Al_2O_3 catalysts compared to uniform catalysts [2]. A uniform distribution of active sites will be beneficial for slow reactions, as the transport limitations are minimal. For dehydrogenation of *n*-dodecane, uniform Pt/alumina catalysts had higher activity than those with egg-shell distributions [3]. Catalyst effectiveness factors larger than one can be achieved for exothermic reactions, if the active metal is located inside the support making advantage of heat transport resistances [4]. In a consecutive reaction, if the secondary product is undesirable, an eggshell distribution will be beneficial to increase the selectivity of the primary product. Thus

Komiyama *et al.* [5] obtained highest butene selectivity on egg shell catalysts for hydrogenation of 1,3- butadiene over Pt/γ-Al_2O_3 catalysts. Butane selectivity was high owing to the higher residence time of butenes in uniform catalyst pellets. If the reactant feed consists of catalytic poisons like sulphur compounds, it is better to deposit the active component inside the subsurface layer, and have an egg white distribution. A desired metal profile can be obtained by proper selection of impregnation parameters like choice of precursor, pH, time of contact and competitors. [6-9]. Different types of metal distributions in catalyst pellets are given in Figure 1.

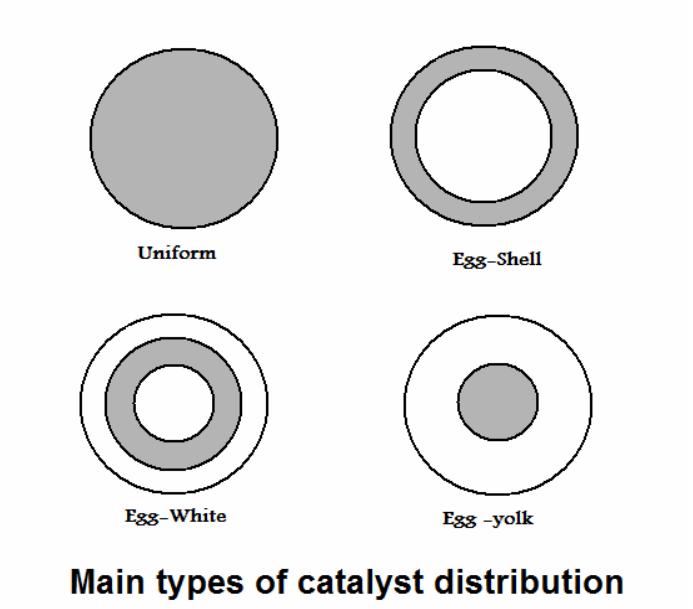

Figure.1 General types of catalyst distribution.

Among the several methods to prepare industrial catalysts, impregnation is important because of its simplicity and cost effectiveness. Depending upon the volume of the impregnation solution, impregnation can be divided to pore volume (dry or incipient wetness) impregnation (where the volume of the impregnating solution is equivalent to the pore volume of the support and the capillary forces

operate for the distribution of active component) and wet impregnation (where the volume of the impregnation solution used is much more than the pore volume and adsorption forces and diffusion of ions determine the active site distribution). Vincent and Merril [10] identified three different processes occurring simultaneously during pore volume impregnation process namely (a) transport of solution (convection) in the longitudinal direction of the pore (b) mass-transfer (diffusion) in the liquid-solid interface (c) adsorption of ions on the walls of the pores. When adsorption of the active metal ions is fast, it causes the concentration of the active metal to decrease in longitudinal direction and an egg shell profile results. If the adsorption processes are slow the metal ions are transported to farther end of pores with same initial concentration leading to a homogeneous uniform distribution of active sites. Thus by controlling the adsorption characteristics of the active precursor, the profile of metal distribution can be changed.

However, the subsequent drying and calcinations of the impregnated support may change the metal distribution obtained in the impregnation step. The impact of drying conditions on the final metal profile was studied in detail by Umera *et al.* [11] and Lekhal *et al.* [12]. Their studies confirmed that under conditions of strong adsorption, drying does not have a strong effect on the final metal profile. In the case of weak adsorption, the convective flow and diffusion becomes predominant and varying profiles are obtained depending upon the drying conditions. Recently, ethylenediamine (en) complexes of nickel have been used to prepare supported nickel catalysts, with low temperature of reduction, low particle size and high activity [13-15]. However, studies directed towards the impregnation profiles using these complexes are limited in literature [16]. In this chapter, the results of an experimental study on the impregnation of gamma alumina support with nickel ethylenediamine complexes having different counter ions.

4.2 Experimental

Spherical γ-Al_2O_3 pellets from Sud- Chemie India Pvt Ltd were used for the impregnation studies and their physical characteristics are given in Table 1.

Table 1: Physical characteristics of support

Physical Characteristics of γ-Al_2O_3 spheres	
Average Pellet diameter	0.38 cm
Apparent density	0.92 g cm^{-3}
Surface area*	230.1 m^2 g^{-1}
Pore volume*	0.34 cm^3 g^{-1}
Average pore radius*	58.4 Å

* Obtained by BJH adsorption method

The pzc (point of zero charge) of alumina was determined by mass titration method [17] and was found to be 8.5.

Incipient wetness

For pore volume impregnations the final nickel loading was targeted to be 1 weight percentage. The impregnating solution of $[Ni(H_2O)_6](NO_3)_2$, designated as Ni-A, was prepared by dissolving 0.1g $Ni(NO_3)_2.6H_2O$ in 0.7mL distilled water. The other impregnating solutions $[Ni(en)_2(H_2O)_2]X_2$,X= NO_3^-, CH_3COO^-, or Cl^- were prepared by adding ethylenediamine (Aldrich; 99+%) at a molar ratio en/Ni=2 to aqueous solution (0.7mL distilled water) of the nickel(II) salts (all from Merck ;99+%) $Ni(NO_3)_2.6H_2O$ (0.1g), $Ni(CH_3COO)_2.4H_2O$ (0.085g) or $NiCl_2.6H_2O$ (0.08g) and were named as named as Ni-B, Ni-C and Ni-D respectively. The alumina support (2g – calcined at 400 °C for 6 hours) was suddenly added to the impregnating solution in a glass vial and was thoroughly shaken to make a

homogeneous mixture. A portion of this mixture was separated to study the impregnation profile. Another portion was dried at 200 °C for 4 hours and then was subjected to impregnation profile studies.

Wet impregnation

The dried supports (4g) were incipiently wetted with distilled water (equivalent to the pore volume) in a glass flask and then contacted with 25mL of 0.055M impregnating solution of nickel nitrate, $[Ni(en)_2(H_2O)_2](NO_3)_2$, $[Ni(en)_2(H_2O)_2](CH_3COO)_2$ or $[Ni(en)_2(H_2O)_2]Cl_2$ for 30 minutes. The flask was kept on a shaker for total impregnation period. After the impregnation time the solution was removed, and the pellets were divided to two parts. One part was subjected immediately to profile analysis, while the other was calcined at 200 °C for 4 hours prior to the profile analysis.

Effect of solvent removal on viscosity

Initially 0.1M of all the impregnating solution was prepared and their viscosities were determined. This solution (100 mL) of one of the complex was taken in a graduated glass beaker and was slowly heated on a water bath to different degrees of solvent removal (50, 60, 70, 80 and 90 vol%). The solutions were then cooled to room temperature. The heating was discontinued once the solute precipitated and the corresponding volume was noted as precipitation volume. The measurements were carried out similarly for the other complexes. Viscosities were determined at each drying stages on a U-tube gravity (Ostwald) viscometer. The viscometer was calibrated with distilled water and all viscosity measurements were done at 30 ± 0.5 °C.

Impregnation profiles

The distribution profiles were measured on a Jeol JSM-6390 LA scanning electron microscope with EDX assembly. The impregnated spheres, were

mechanically rubbed to expose the cross section and quantitative microanalysis were done along the radial distances. This was done before the drying and after the drying of the spheres. To determine the penetration depth by optical micrographs, an alcoholic solution of 10 % dimethylglyoxime was applied on the cross-sectioned pellets [18]. This allowed the visual observation, and the surface was photographed and the penetration depths were measured, on a Leica DM 2500 M optical microscope.

Cyclohexanol decomposition

The cyclohexanol dehydrogenation was performed in a conventional glass reactor (10 mm id, fixed bed, down flow) operated at atmospheric pressure. To avoid chanelling, catalyst pellets (2g) were mixed with quartz powder (2g) and were immobilized in the middle of the reactor with glass wool. Cyclohexanol was introduced with a pre calibrated syringe pump (at a flow rate 3 mL hr^{-1}), and a flow of N_2 (20 mL min^{-1}) was maintained in the reactor by Bronkhaurst mass flow controller. The liquid products were collected at the bottom of the reactor in an ice cooled trap. Products were analysed after 30 minutes (to ensure mass balance) on a gas chromatograph (Chemito 8510) equipped with a carbowax column and flame ionization detector.

4.3 Results and Discussion

4.3.1 Pore volume impregnation

The optical micrographs and EDX spot analysis of the pore volume impregnated alumina spheres before drying are shown in Figure 2 and those of the spheres after drying at 200 °C are shown in Figure 3.

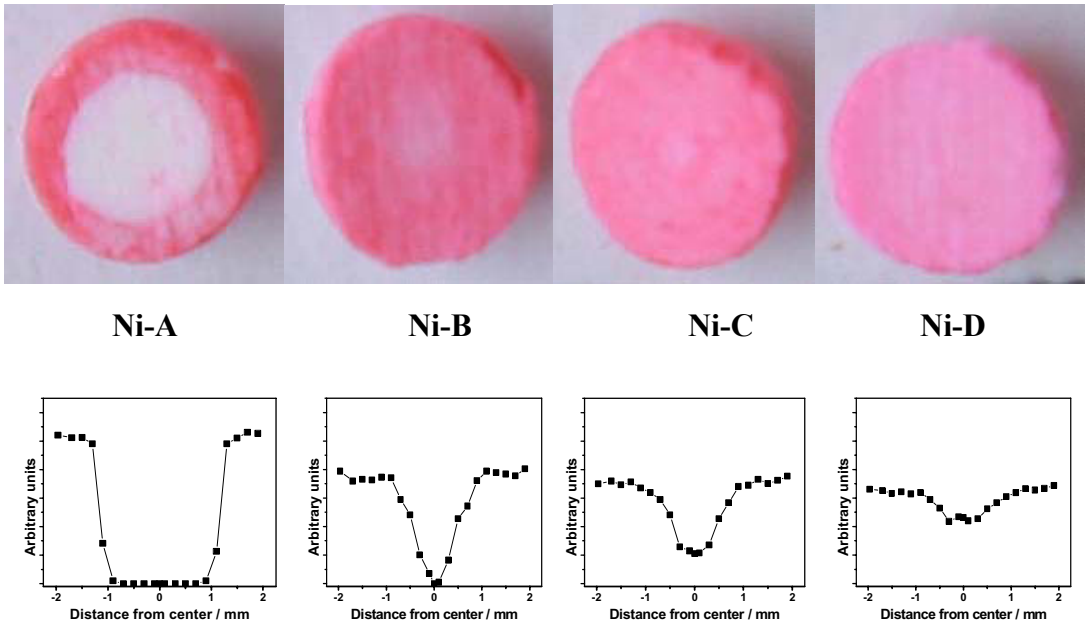

Figure 2. Optical micrographs and EDX spot analysis metal profiles of pore volume impregnated solids before drying.

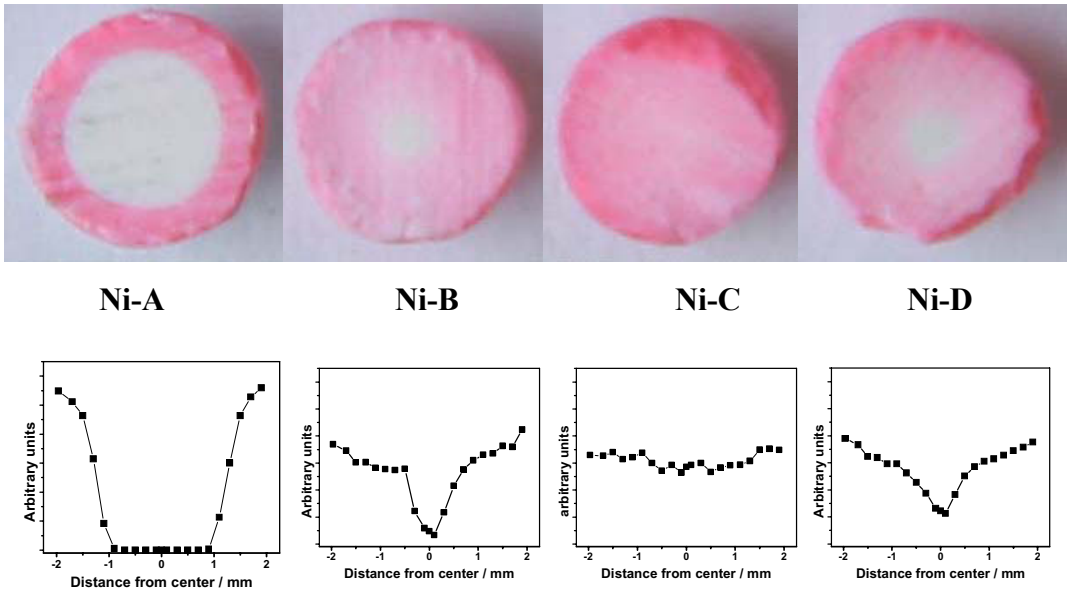

Figure 3. Optical micrographs and EDX spot analysis metal profiles of pore volume impregnated solids after drying at 200 °C for four hours.

The nickel nitrate impregnation (Ni-A) resulted in eggshell profiles, while the impregnation of ethylenediamine complexes resulted in uniform distribution. The viscosities of the impregnating solutions were determined as a function of the extent of drying and the results are shown in Figure 4.

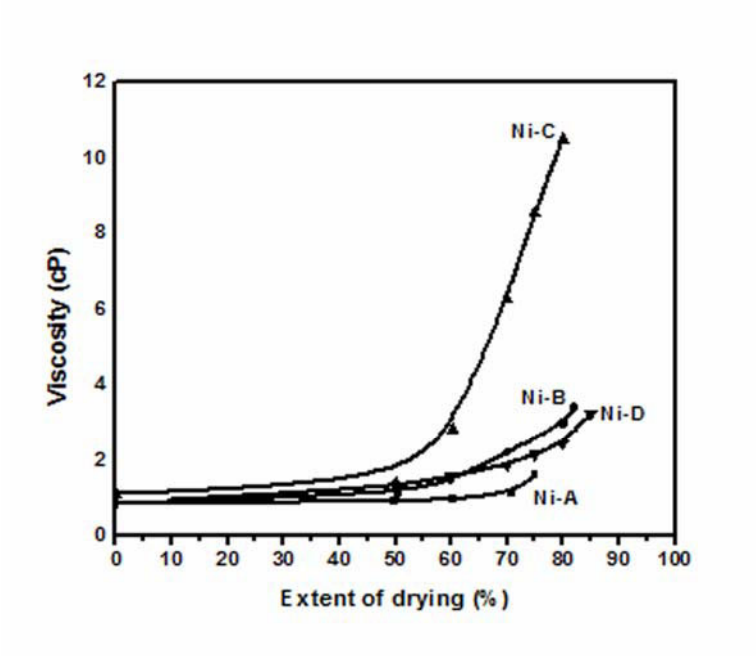

Figure 4. Change in viscosity during drying of impregnating solutions

For each curve, the last point denotes the viscosity just before precipitation. The initial viscosities of ethylenediamine complexes were higher than that of the nickel nitrate solution; while the nickel nitrate solution had a higher volume of precipitation (it precipitated at low concentration) than that of the ethylenediamine complexes. For a solution consisting of less viscous solvent, the solvent can diffuse faster than the solute, and lead to deposition of the solute [19]. Thus impregnation by Ni-A solution, which has low viscosity, derives eggshell distribution. The complexes of ligands with chelating behavior not only increase the viscosity but also prevent hydrolysis and flocculation of the active precursor [20]. van den Brink [20] demonstrated that the crystallization proceeds badly and small crystallites are formed with a uniform distribution for metal complexes of chelating ligands. The

ethylenediamine complexes are seen to diffuse deeper in to the core of alumina spheres achieving a diffuse eggshell or uniform distribution.

Final metal profile after drying depends on the relative strength of convection, diffusion, adsorption and evaporation. It is to be noticed that there was no significant changes in the distribution of the active species for all the pore volume impregnated catalysts. The redistribution was least in case of Ni-A sample, as most of the active species have been precipitated during the impregnation step itself. Further more, there is no dissolution of the active species during drying. If there were dissolution, the nickel species would have migrated outwards because of low viscosity of the solution which makes easier the convective transport by capillary forces [21]. There are chances that nickel nitrate gets precipitated as Ni(II) hydroxides during the impregnation step as pH level of the solution gets easily increased due to the buffering action of high PZC alumina [22]. The rates of viscous flow in the impregnating solution as well as diffusion in the liquid are inversely proportional to the viscosity of the liquid. The high viscosity of ethylenediamine solutions impedes the convective flow of solution in the pores. During the drying step as more and more water is removed the viscosity of chelating solutions increases drastically (Figure 4) especially for Ni-C (acetate counter ion) solution. The advantage of increasing the viscosity of impregnating solution has already been reported [20, 23]. For Ni-A, as almost all active species is precipitated or reacted with alumina surface and hence there is no much redistribution. But for the Ni-en complexes, there is slight redistribution as the chelated complexes are intact which prevents an early precipitation. But because of high solution viscosity during drying the convective flow is less and the distribution profile is almost maintained intact. However it should be noted that for Ni-D sample (chloride counter ion) the redistribution was more as its precipitation volume is less. For Ni-C sample (acetate counter ion) a very uniform profile was obtained after drying which may be due to the diffusion.

4.3.2 Wet impregnation

The distribution profiles obtained for wet impregnation after a period of 30 minutes are shown in Figure 5. During wet impregnation there is no imbibition (convective flow of solution) as the support is already wet and the impregnation front moves by processes of adsorption and diffusion. It takes more time for the active species to diffuse from the bulk solution through the pores in to the core of the support. Thus among the two operative processes namely adsorption and diffusion, the slowest step determines the impregnation profile. If adsorption is faster than diffusion, impregnation front moves slow. This results in eggshell profile, while slow adsorption and fast diffusion gives uniform profile. In the present study the impregnation front for Ni-C moves much faster than that of others, and this slow adsorption and fast diffusion may be due to the presence of acetate counter ions. The impregnation depth is in order NiA < NiB < NiD < NiC. Thus counter ions have a definite influence on impregnation depths.

During drying again three forces are in action, namely convection (capillary flow towards outer surface), metal diffusion (towards the center) and adsorption (on the pore walls). If the adsorption is sufficiently strong, there would not be any redistribution during drying [12] and such strong adsorption occurs during the impregnation step. If adsorption is weak, the final profile will be determined by the relative strength of convection and diffusion. The distribution profile of wet impregnated solids after drying is shown in Figure 6. There was an outward migration for sample Ni-A, which shows that the convective transport is dominant in this case when compared to diffusion. Komiyama *et al.* [24] found that a uniform profile obtained after the impregnation step can be transformed in to a decreasing egg shell profile when capillary forces are much active.

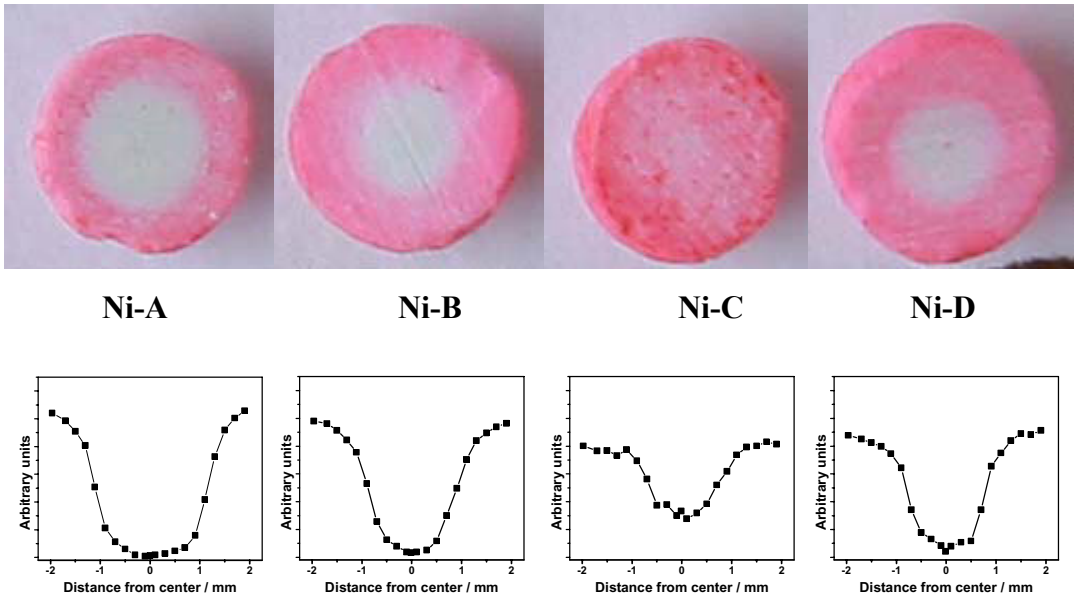

Figure 5. Optical micrographs and EDX spot analysis metal profiles of wet impregnated solids before drying.

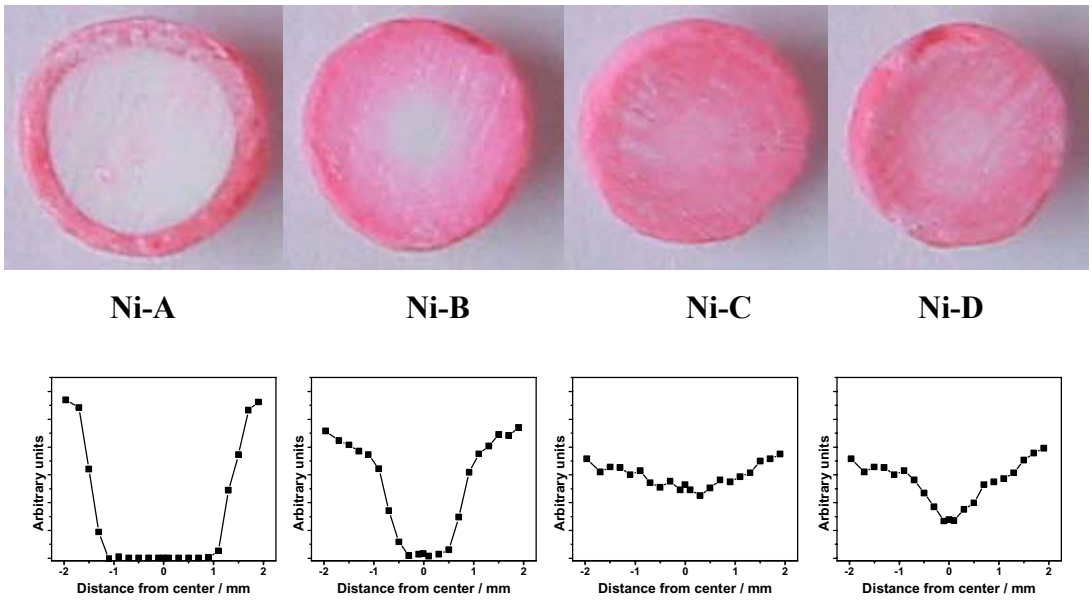

Figure 6. Optical micrographs and EDX spot analysis metal profiles of wet impregnated solids after drying at 200 °C after drying for four hours.

For ethylenediamine complexes the redistribution was almost intact, but shows a little inward migration and hence the final distribution became more uniform. The sluggish redistribution can be either due to a strong adsorption on alumina surface or due to high viscosity of solution during the drying stage which suppresses the convective flow. The major transport process therefore would be diffusion. An inward migration occurs in these cases as diffusion happens from a region of higher concentration to lower concentration resulting in the movement of the impregnation front deeper in to the centre. The adsorption of ethylenediamine complexes, although slow, is strong enough to restrict the redistribution. Che *et al.* [25] have shown that secondary interactions are possible between ethylenediamine ligands and alumina surface by grafting, thus increasing its adsorption strength. Generally for preparation of Ni/γ-Al_2O_3 catalysts, nickel nitrate is used and mostly an eggshell distribution results. Li *et al.* [26] used nickel ammonia complexes and obtained uniform distribution for the impregnation step. But the redistribution during drying caused the nickel species to migrate outwards and an eggshell distribution resulted. They concluded that only eggshell distribution of the activity component would be achieved for one component impregnation, and the distribution after the wet impregnation would not be maintained during the normal drying process. The present work suggests that by using ethylenediamine ligands with proper choice of counter ions, uniform distribution could be achieved with very less or no migration of the active species during drying.

4.3.3 Cyclohexanol decomposition

The cyclohexanol decomposition was carried out on bare γ-Al_2O_3 support, powdered nickel oxide, eggshell catalyst (derived from Ni-A by pore volume impregnation) and uniform catalyst (derived from Ni-B by pore volume impregnation). The final nickel loading was adjusted to be 3 wt% on eggshell and uniform pellets. The reaction was carried out at both low temperature (250 °C) and high temperature (400 °C).

The major products of cyclohexanol decomposition are cyclohexene and cyclohexanone. On γ-Al_2O_3 the major product is cyclohexene [27] whereas on nickel oxide the major product is cyclohexanone [28]. Incorporation of nickel oxide to γ-Al_2O_3, changes the selectivity towards cyclohexanone. The conversion and selectivity on the three samples at 250 °C and 400 °C are shown in Figure 7 (a) and (b). At low temperature, the reaction will be slow and diffusion of reactants will be fast and whole of the pellet will be active. Uniform pellets gave high cyclohexanone selectivity at low temperature which can be either due to high intrinsic activity of nickel oxide or due to the uniform distribution of nickel oxide in γ-Al_2O_3 pellet. For eggshell catalyst pellets, NiO is distributed as thin shell on the outer surface. When the whole pellet is active the reactants 'see' only a small layer of NiO phase; whereas it 'sees' more γ-Al_2O_3 as it diffuses deeply inside the pellet giving higher selectivity for cyclohexene. The events are more clearly demonstrated in Figure 8.

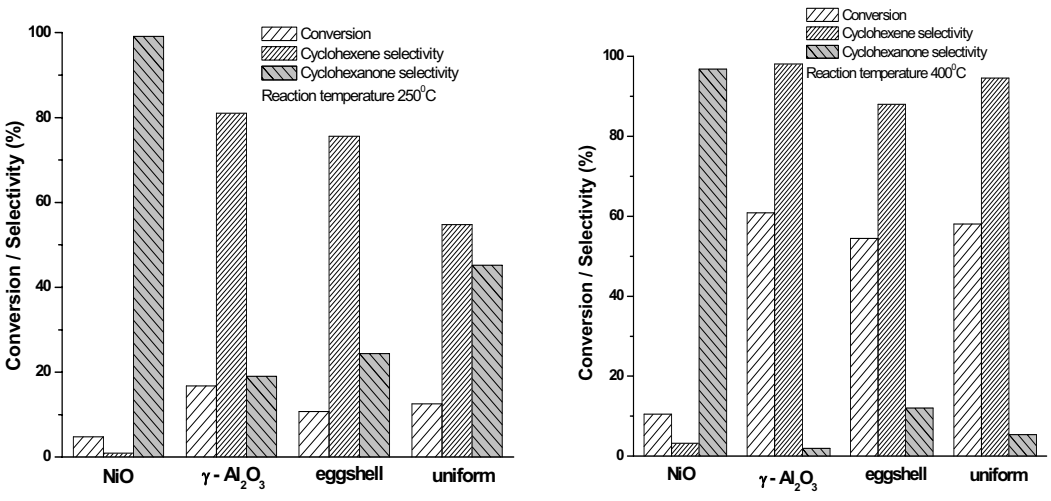

(a) (b)

Figure 7. Results of cyclohexanol decomposition on catalysts at temperatures (a) 250 °C and (b) 400 °C.

An increase of temperature increases the intrinsic activity of the pellets. As the reaction rate becomes faster; diffusion of reactants becomes slow compared to

the reaction and becomes the rate limiting process. At these conditions the surface of the pellet will be more active, and some times under drastic conditions the core of the pellet becomes inactive. For cyclohexanol decomposition an increase of temperature drives the reaction towards selective formation of cyclohexene. The temperature sensitivity towards cyclohexene selectivity is less for nickel oxide compared to γ-Al_2O_3 pellets (Figure 7). At 400 °C the cyclohexene selectivity increased on all the four samples. But it can be seen that the highest cyclohexanone selectivity was for the eggshell pellets. At diffusion limited conditions (surface layer is more active), on the eggshell catalysts the reactants come in to contact with a higher number of nickel oxide crystallites, as most of the nickel oxide is deposited near the outer surface. As nickel oxide's cyclohexanone selectivity is more, the eggshell catalyst gives more cyclohexanone than on uniform pellets, on which, the number of nickel oxide crystallites on the surface is almost similar to that in bulk phase.

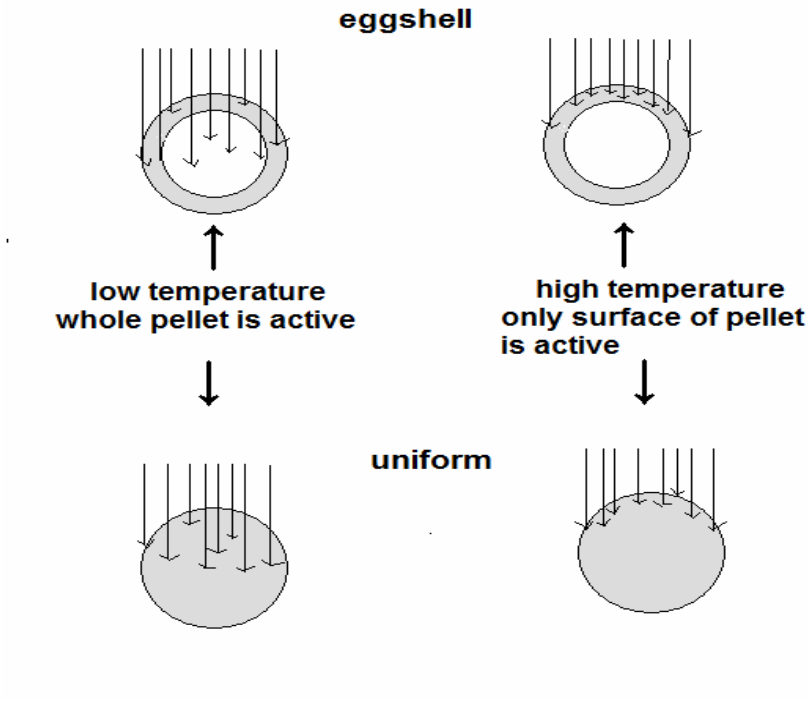

Figure 8. Pictorial representation of different activity for eggshell and uniform pellets at low and high temperature.

4.4 Conclusions

i) For pore volume impregnations with ethylenediamine complexes a diffuse eggshell or uniform distribution happens due to high viscosity of the chelating complexes.

ii) In case of nickel nitrate solution due to low viscosity of impregnating solution and high rate of precipitation an eggshell distribution results.

iii) The distribution profiles after drying are directly related to the viscosity and precipitation volumes of the impregnating solutions.

iv) For wet impregnation, the ethylenediamine complexes show a higher impregnation rate compared to the usual nickel nitrate impregnation due to fast diffusion and slow adsorption.

v) The counter ions in the complexes are found to have a significant effect during impregnation and drying, resulting in different impregnation depths. Acetate counter ion is more promising to obtain a uniform distribution having less effect on drying.

vi) The prepared eggshell and uniform pellets gave different product distributions for cyclohexanol decomposition reaction.

References

[1] J.M. Thomas, W.J. Thomas., Introduction to the principles of heterogeneous catalysis. Academic Press, London, 1967

[2] Y. Qiu, J. Chen, J. Zhang., Influence of nickel distribution on properties of spherical catalysts for partial oxidation of methane to synthesis gas., *Catal. Commun.* 8 (2007) 508-512

[3] J.F. Roth, T.E. Richard., Determination and effect of platinum concentration profiles in supported catalysts., *J. Res. Inst. Catalysis, Hokkaido Univ.* 20 (1972) 85-94

[4] M. Morbidelli, A. Servida, S. Carra, A. Varma., Optimal catalyst activity profiles in pellets. 3. The nonisothermal case with negligible external transport limitations., *Ind. Eng. Chem. Fundam.* 24 (1985) 116-119

[5] M. Komiyama, K. Ohashi, Y. Morioka, J. Kobayashi., Effects of the intrapellet activity profiles on the selectivities in consecutive Reactions : 1,3-Butadiene hydrogenation over Pt/Al_2O_3., *Bull. Chem. Soc. Jpn.* 70 (1997) 1009-1013

[6] T. Fujitani, O. Ueki, E. Echigoya., The effect of starting source on the concentration distribution of nickel supported on alumina., *Bull. Chem. Soc. Jpn.* 62 (1989) 2753-2755

[7] A. Lekhal, B.J. Glasser, J.G. Khinast., Influence of pH and ionic strength on the metal profile of impregnation catalysts., *Chem. Eng. Sci.* 59 (2004) 1063-1077

[8] S-Y. Lee, R. Aris., The Distribution of active ingredients in supported catalysts prepared by impregnation., *Catal Rev-Sci. Eng.* 27 (1985) 207-340

[9] P. Papageorgiou, D.M. Price, A. Gavriilidis, A. Varma., Preparation of $Pt/\gamma\text{-}Al_2O_3$ pellets with internal step-distribution of catalyst: experiments and theory., *J. Catal.* 158 (1996) 439-451

[10] R.C. Vincent, R.P. Merril., Concentration profiles in impregnation of porous catalysts., *J. Catal.* 35 (1974) 206-217

[11] Y. Uemura, Y. Hatate, A. Ikari., Formation of nickel concentration profile in nickel/alumina catalyst during post-impregnation drying., *J. Chem. Eng. Jpn.* 20 (1987) 117-123

[12] A. Lekhal, B.J. Glasser, J.G. Khinast., Impact of drying on the catalyst profile in supported impregnation catalysts., *Chem. Eng. Sci.* 56 (2001) 4473-4487

[13] E. Marceau, A. Lofberg, J.M. Giraudon, F. Negrier, M. Che, L. Leclercq., From Al_2O_3-supported Ni(II)–ethylenediamine complexes to CO hydrogenation catalysts: Characterization of the surface sites and catalytic properties., *Appl. Catal. A: General.* 362 (2009) 34-39

[14] S. Schimpf, C. Louis, P. Claus., Ni/SiO_2 catalysts prepared with ethylenediamine nickel precursors: Influence of the pretreatment on the catalytic properties in glucose hydrogenation., *Appl. Catal. A: General.* 318 (2007) 45-53

[15] F. Negrier, E. Marceau, M. Che, J.M. Giraudon, L. Gengembre, A. Lofberg., From Al_2O_3-supported Ni(II)-ethylenediamine complexes to CO hydrogenation catalysts: importance of the hydrogen post-treatment evidenced by XPS., *Catal. Lett.* 124 (2008) 18-23

[16] L. Espinosa-Alonso, K.P. de Jong, B.M. Weckhuysen., Effect of the nickel precursor on the impregnation and drying of γ-Al_2O_3 catalyst bodies: A UV−vis and IR microspectroscopic study., *J. Phys. Chem. C.* 112 (2008) 7201-7209

[17] J.S. Noh, J.A. Schwarz., Estimation of the point of zero charge of simple oxides by mass titration., *J. Colloid. Interface. Sci.* 130 (1980) 157-164

[18] E.M. Assaf, L.C. Jesus, J.M. Assaf., The active phase distribution in Ni/Al_2O_3 catalysts and mathematical modeling of the impregnation process., *Chem. Eng. J.* 94 (2003) 93-98

[19] J.F. Le Page. Applied Heterogeneous Catalysis: Design, Manufacture, Use of Solid Catalysts, Editions Technip, Paris, 1987.

[20] J.W. Geus., in: J.R. Regalbuto (Eds.), Catalyst Preparation: Science and Engineering, CRC Press, New York, 2007, ch. 15.

[21] A. Lekhal, B.J. Glasser, J.G. Khinast., in: J.R. Regalbuto (Eds.), Catalyst Preparation: Science and Engineering, CRC Press, New York, 2007, ch. 16.

[22] J. Park, J.R. Regalbuto., A simple, accurate determination of oxide PZC and the strong buffering effect of oxide surfaces at incipient wetness., *J. Colloid Interface. Sci.* 175 (1995) 239-252

[23] M. Kotter, L. Riekert., in: B. Delmon, P. Grange, P. Jacobs and G. Poncelet. (Eds.), Preparation of Catalysts II, Scientific bases for the Preparation of Heterogeneous Catalysts, Elsevier Scientific Publishing Company, Amsterdam, 1979, p. 51.

[24] M. Komiyama, R.P. Merill, H.F. Harnsberger., Concentration profiles in impregnation of porous catalysts: Nickel on alumina., *J. Catal.* 63 (1980) 35-52

[25] F. Negrier, E. Marceau, M. Che., Interplay of anions and ligands on the nature and reducibility of NiO_x/Al_2O_3 catalysts prepared by impregnation., *Chem. Commun.* (2002) 1194-1195

[26] W.D. Li, Y.W. Li, Z.E. Qin, S.Y. Chen., Theoretical prediction and experimental validation of the egg-shell distribution of Ni for supported Ni/Al_2O_3 catalysts., *Chem. Eng. Sci.* 49 (1994) 4889-4895

[27] R.D. Srivastava, J. Onuferko, J.M. Schultz, G.A. Jones, K.N. Rai, R. Athappan., Characterization and activity of nickel oxide supported on γ- Alumina., *Ind. Eng. Chem. Fundam.* 21 (1982) 457-463

[28] C.P. Bezouhanova, M.A. Al-Zihari., Cyclohexanol conversion as a test of the acid-base properties of metal oxide catalysts., *Catal. Lett.* 11 (1991) 245-248

Chapter 5

PREPARATION AND CHARACTERIZATION OF SUPPORTED NICKEL CATALYSTS.

Contents

This chapter deals with the preparation of supports, supported nickel catalysts and the details of the characterization methods used in subsequent chapters.

5.1 Preparation of supports

5.1.1 Preparation of α-Al_2O_3

Nano crystalline α-alumina was made by solution combustion synthesis [1]. $Al(NO_3)_3.9H_2O$ (Merck 99+%) (20g) and Urea (BDH India 99+%) (8g) (oxidant (metal salt) /fuel (urea) ratio =1) were together dissolved in 75 mL distilled water

and was then evaporated to a syrupy solution. This solution was then placed in a preheated furnace (450 °C) for five minutes, which yielded the fluffy product. The α-alumina derived by this process is phase pure as indicated by XRD (Figure 1a) (surface area = 5.9 m^2 g^{-1}, Average crystallite size = 37 nm and pore volume <0.1 mL g^{-1}). Scanning electron micrograph (SEM) (Figure 1b) indicated the formation of sheet like structures.

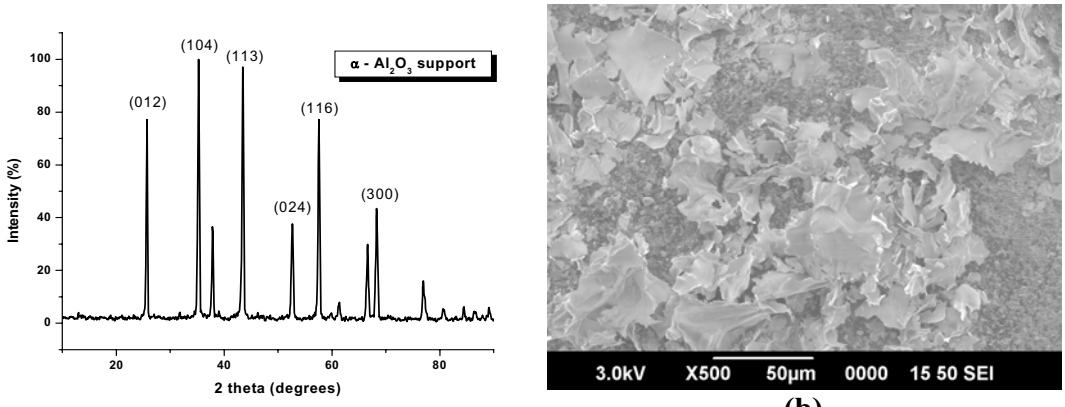

(a) **(b)**

Figure 1. (a) XRD and (b) SEM of α-Al_2O_3

5.1.2 Preparation of γ-Al_2O_3

The γ-Al_2O_3 used was a gift sample from Research and Development Division of Sud Chemie India Ltd. The sample had a surface area of 199 m^2 gm^{-1}, pore volume 0.57 mL gm^{-1} and an average pore diameter of 96 Å. The XRD pattern and adsorption desorption isotherm are given in Figure 2 (a) and (b).

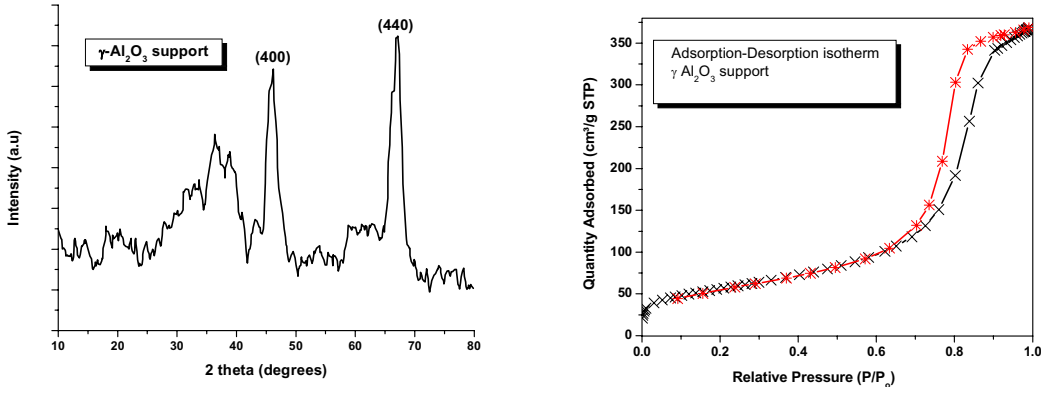

(a) **(b)**

Figure 2. (a) XRD and (b) Adsorption-desorption isotherm of γ-Al_2O_3

5.1.3 Preparation of MgO

Magnesium hydroxide ($Mg(OH)_2$) was precipitated from 0.1 molar solution of magnesium nitrate at a constant pH of 9 and temperature of 70 °C using 20% ammonia solution. The precipitate was then washed well to remove the nitrate ions, and then dried in an air oven at 120 °C overnight. The dried cakes were then powdered and calcined at 600 °C in a muffle furnace for four hours to obtain crystalline MgO. The XRD pattern and the SEM of calcined MgO are given in Figure 3 (a) and (b).

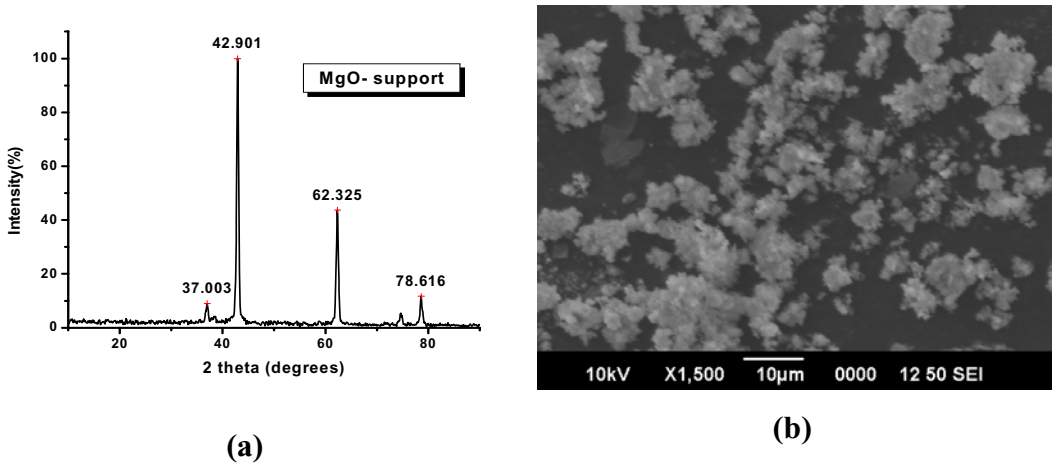

Figure 3. (a) XRD and (b) SEM of calcined MgO

5.2 Preparation of supported nickel catalysts-impregnation deposition

Metal loading was fixed to be 20 wt% nickel on all the catalysts. The method of catalyst preparation is outlined in the following block diagram (Figure 4). Solutions of the nickel complexes were prepared first. To this solution (volume of the solution should be much larger than pore volume) calcined support (which was dried at 200 °C for two hours prior to the preparation of catalyst) was added and stirred well. The slurry was then slowly dried on a water bath with occasional stirring to obtain dried cakes. It was then dried in an air oven at 120 °C overnight. The cakes were then powdered well and calcined in a muffle furnace at 600 °C for four hours. The heating program was set in such a way that material was heated from room temperature to 600 °C at the rate of 6 °C min^{-1}.

This method of preparation enables loading of higher metal percentages on the support and the targeted metal loading is easily achieved. During the preparation, the following events take place

i.) As the supports are dried, pore volume impregnation (filling of void volume with impregnating solution) takes place.

ii.) An excess solution (much more than pore volume) is used to make impregnating solution, so some nickel complex ions will be ion exchanged with the surface groups.

iii.) The remaining metal salts (complexes) will be deposited on the surface during the drying step.

This method thus involves *impregnation* and *deposition*.

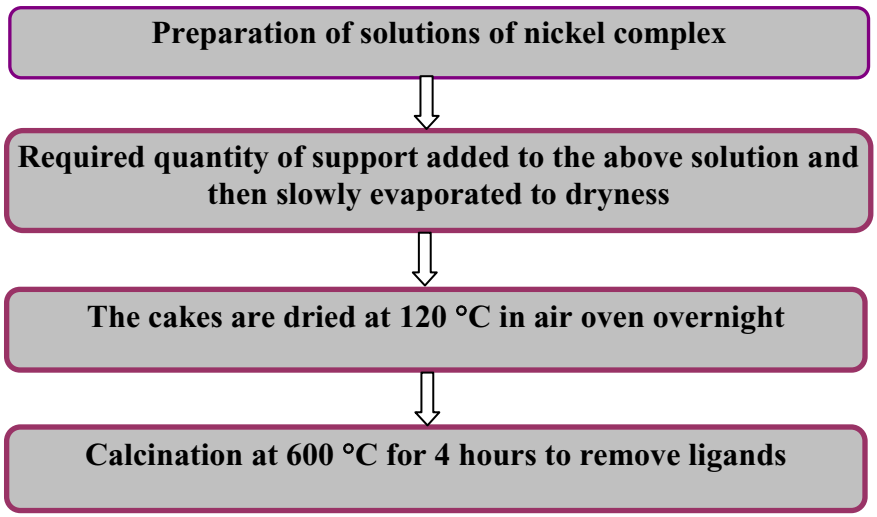

Figure 4. Scheme for the preparation of supported catalysts

Procedure for the preparation (for 5g of support) is as follows. The impregnating solution of $[Ni(H_2O)_6](NO_3)_2$ (Ni-A), was prepared by dissolving 4.956g $Ni(NO_3)_2.6H_2O$ in 100mL distilled water. The impregnating solution of $[Ni(en)_2(H_2O)_2](NO_3)_2$ (Ni-B) was prepared by adding ethylenediamine at a mol

ratio of en/Ni = 2 to a solution of $Ni(NO_3)_2.6H_2O$ (4.956 g) dissolved in distilled water (100 mL). The impregnating solutions, Ni-C and Ni-D were prepared in a similar way by using $Ni(CH_3COO)_2.4H_2O$ (4.240g) or $NiCl_2.6H_2O$ (4.050g) respectively. As an example for the preparation of α-Al_2O_3 supported catalysts, 5g of α-Al_2O_3 was added to the impregnating solution Ni-A, slowly evaporated to dryness with constant stirring on a water bath. It was then dried at 120 °C overnight in an air oven and the resulting sample was named as Ni-α-A-d. It was then calcined in a static furnace at 600 °C for 4 hours, with a heating rate of 6 °C min^{-1} and the resulting sample was named as Ni-α-A-c. Further the sample was reduced at 500 °C for four hours and was named as Ni-α-A-r. The other supported Ni/NiO catalysts were named in a similar way and the nomenclatures for the catalysts are as follows.

en= ethylenediamine

Metal Complex	NiO	Ni/α-Al_2O_3	Ni//γ-Al_2O_3	Ni/MgO
$[Ni(H_2O)_6](NO_3)_2$ (A)	NiO-A	Ni-α-A-x	Ni-γ-A-x	Ni-M-A-x
$[Ni(en)_2(H_2O)_2](NO_3)_2$ (B)	NiO-B	Ni-α-B-x	Ni-γ-B-x	Ni-M-B-x
$[Ni(en)_2(H_2O)_2](CH_3COO)_2$ (C)	NiO-C	Ni-α-C-x	Ni-γ-C-x	Ni-M-C-x
$[Ni(en)_2(H_2O)_2]Cl_2$ (D)	NiO-D	Ni-α-D-x	Ni-γ-D-x	Ni-M-D-x

x = d for dried, c for calcined, and x = r for reduced

5.3 Characterization techniques

5.3.1 Chemical analysis- AAS

The metal percentages on the calcined catalysts were estimated by atomic absorption spectrophotometry (AAS) on a Thermo Electron Corporation MMK_2 system. The catalyst (0.5g) was mixed well with potassium hydrogen sulphate

($KHSO_4$, 3g) in a small china dish. It was then fused in a muffle furnace set at 450 °C. The fused mixture was extracted by boiling with dilute sulfuric acid (50:50 solution) and was made up to 200 mL with distilled water. The solution was then analyzed for nickel content on AAS.

The chloride content on the catalysts was determined by titration with standardized silver nitrate solution following Volhard's method [2].

5.3.2 Thermal studies on precursors

The thermal decomposition patterns of the dried precursors were recorded on a Pyris Diamond TG of Perkin Elmer make. An air flow of 200 mL min^{-1} was maintained and the heating rate employed was 10 °C min^{-1} from 100 °C to 800 °C. The same instrument measured the DTA responses simultaneously.

5.3.3 N_2 physisorption

The adsorption desorption characteristics of the calcined catalysts were determined on a Micromeritics Tristar Surface area Analyzer. Prior to adsorption, the samples were degassed in the Flowprep unit of the system at a temperature of 350 °C for three hours under nitrogen flow.

5.3.4 Powder XRD

X-ray diffraction patterns of the calcined and reduced catalysts were recorded on Bruker model D8 (CuKα source) and X-ray line broadening analysis (XLBA) was done with the well known Scherrer equation.

5.3.5 UV-vis DRS

The UV-vis diffuse reflectance spectra were recorded on a Labomed UV-Vis spectrophotometer equipped with a diffuse reflectance accessory and integrating sphere in the range 200 to 900 nm. $BaSO_4$ was used as blank for the measurements. The percentage reflectance values were converted to absorbance using the Kubelka Munk function (equation) [3].

$$F(R_\alpha) = \frac{(1-R_\alpha)^2}{2R_\alpha}$$

R_α = reflectance of sample

5.3.6 TCD-TPR

The temperature programmed reduction (TPR) of NiO/α-Al_2O_3 (chapter 6) and NiO/MgO catalysts (chapter 8) were done on Micromeritics Pulse Chemisorb 2705 system. The calcined samples were heated in a flow of helium at 300 °C for two hours to remove any adsorbed moisture. It was then cooled to room temperature. The gas was switched to 5% H_2 in helium and the temperature was raised to 950 °C. A heating rate of 5 °C min^{-1} was used for NiO/α-Al_2O_3 and a heating rate of 10 °C min^{-1} was used for NiO/MgO catalysts. A thermal conductivity detector (TCD) was used to measure the hydrogen consumption. Moisture from the reduction reaction was trapped by a moisture trap before passing the gases through TCD. The TCD was calibrated by injecting pulses of pure hydrogen gas.

5.3.7 TG-TPR

The reduction characteristics of NiO/γ-Al_2O_3 catalysts (chapter 7) were studied by the technique of TG-TPR. The weight change accompanying the reduction reaction is monitored by a thermogravimetric balance. This method has been used by some researchers to identify the nickel species on supported nickel catalysts [4, 5].

The experiment was done on a Pyris Diamond TG of Perkin Elmer make. The sample was dried *ex situ* in flowing nitrogen at 200 °C for three hours. The sample (20-22 mg) was weighed in to the alumina crucible of the TG balance. Temperature was raised to 200 °C for 30 minutes to remove any adsorbed moisture and then it was increased at a rate of 10 °C min^{-1} to 800 °C in flow of 10% H_2 in N_2 (200 cc hr^{-1}) gas. Weight loss corresponding to the reduction was measured.

5.3.8 H_2 Chemisorption

The hydrogen chemisorption studies were done on a Quantachrome Autosorb system. Around 0.1g of catalysts was loaded in to the reactor and was reduced in a flow of hydrogen (20 vol %) at 500 °C for two hours. It was allowed to cool to 40 °C in a flow of Argon. After one hour, hydrogen chemisorption was done at 40 °C to determine the monolayer uptake in μmols of hydrogen adsorbed per gram of catalyst. From the monolayer uptake, % metal dispersion and active metal surface area were calculated as

$$\% \text{ dispersion} = (Ni_{surface} / Ni_{total}) \times 100$$

$$\text{Active metal surface area} = \text{Ni surface area } (m^2\ gm^{-1}) = m \times N \times 2 \times a / 10^{20}$$

$Ni_{surface}$ = number of surface nickel atoms = μmols of hydrogen adsorbed $\times 10^{-6} \times 2 \times N$

Ni_{total} = no of total nickel atoms = wt of catalyst × N × % Ni loading ⁄ (mol wt of nickel (58.69) × 100

$N = 6.022 \times 10^{23}$ molecules

chemisorption stoichiometry; one mol of hydrogen = 2 mols of nickel = 2

m = μmols of hydrogen adsorbed gm^{-1}

surface area of nickel atom = 6.49 $Å^2$ = a

Total area = number of nickel atoms × surface area of one nickel atom

NB: As precursors change, the morphology (shape) of the particles changes; so no attempt was done to calculate the Ni crystallite diameter, as such calculations include the assumptions about the shape of the crystallites.

5.3.9 TPD of CO_2

The temperature programmed desorption of carbon dioxide (for NiO/MgO catalysts, Chapter 8) was done on Micromeritics Pulse Chemisorb 2705 system under Helium atmosphere. The sample (≈ 0.1 g) was heated under helium flow at 300 °C for two hours to remove and adsorbed gases. It was then cooled to room

temperature. Three pulses of pure CO_2 (size of 100μL) was injected consecutively through the injection port to the sample. The sample was then allowed to stabilize under helium flow for another one hour. It was then heated from room temperature to 600 °C with a heating rate 10 °C min^{-1}. The desorbed CO_2 was monitored by TCD response. Quantitative calibration of CO_2-TPD peak area was made by monitoring the decomposition of known amounts of $CaCO_3$.

5.3.10 TPD of cyclohexylamine

The acidity of Ni/γ-Al_2O_3 catalysts (Chapter 7) was determined by temperature programmed desorption of cyclohexylamine (CHA) using thermogravimetry. The sample was treated with liquid cyclohexylamine for 20 minutes. It was then slowly heated to 150 °C in oven for two hours, cooled and 20 mg was weighed to the TG balance. Desorption thermograms were recorded at a heating rate of 10 °C min^{-1} under nitrogen flow (200 cc hr^{-1}). The mass loss between 200 and 420 °C was used to determine the acid content of the samples (in mmols CHA g^{-1} adsorbent) [6].

5.3.11 Scanning Electron Micrographs

The Scanning electron micrographs (SEM) of the samples were taken on a scanning electron microscope, model Jeol JSM-6390 LA. The powdered samples were spread on a carbon tape and then mounted on the microscope. The details of the magnification are present on the micrographs.

5.4 Activity studies

The details of the reaction conditions of vapor phase reactions are given in this section. Exploratory experiments were done to arrive at the reaction conditions.

5.4.1 Benzene hydrogenation / cyclohexane dehydrogenation

The benzene hydrogenation reaction (for Ni/α-Al_2O_3 catalysts, Chapter 6) was performed in a conventional glass reactor (10mm id) operated at atmospheric pressure. Benzene (99+%; Loba Chemie, India) was introduced with a precalibrated

syringe pump and H_2 flow was controlled by Bronkhaurst mass flow controller. Before the activity tests, the catalysts were reduced at atmospheric pressure with H_2 (flow rate 40mL min^{-1}) at 500 ° C for 4 hours. The liquid products were collected at the bottom of the reactor in an ice cooled trap. Products were analysed after 30 min (to ensure mass balance) on a gas chromatograph (Chemito 8510) equipped with a carbowax column and flame ionization detector. The selectivity was 100% towards cyclohexane. (Reaction conditions were: WHSV = 2.8 hr^{-1}, mol ratio $[H_2]/[C_6H_6]$ = 4, temperature 220 °C).

The cyclohexane dehydrogenation (for Ni/γ-Al_2O_3 catalysts, Chapter 7) was done in same apparatus as mentioned above. After reduction with hydrogen, the gas was changed to pure nitrogen at a flow rate of 20 mL min^{-1}. The cyclohexane feed rate was set at 2.4 mL hr^{-1} and temperature of the reaction was set at 300 °C. The catalyst weight used was 1.5g. The products were analyzed with the same GC used for benzene hydrogenation. The time on stream was only 30 minutes (Exploratory experiments indicated there was rapid deactivation for this reaction).

5.4.2 Cyclohexanol decomposition

The cyclohexanol dehydrogenation was performed on calcined and reduced samples of Ni/α-Al_2O_3, reduced Ni/γ-Al_2O_3 and reduced Ni/MgO, in a conventional glass reactor (10 mm id, fixed bed, down flow) operated at atmospheric pressure. Cyclohexanol was introduced with a pre calibrated syringe pump (at a flow rate of 3 mL hr^{-1}), and a flow of N_2 (20 mL min^{-1}) was maintained in the reactor by Bronkhaurst mass flow controller. The amount of catalyst was 0.8g. For the reactions on reduced catalysts, prior to the reaction the samples were reduced at atmospheric pressure with H_2 (flow rate 40 mL min^{-1}) at 500 °C for 4 hours. However, for Ni/MgO catalysts (Chapter 8) the reduction was done at higher temperature of 550 °C for 4 hours. The reaction was done at a temperature of 270 °C for Ni/α-Al_2O_3 and Ni/γ-Al_2O_3 catalysts, and at 350 °C for Ni/MgO catalysts. The reaction was conducted for two hours and the integral conversion was measured. The liquid products were collected at the bottom of the reactor in an ice cooled trap.

Products were analysed after 30 minutes (to ensure mass balance) on a gas chromatograph (Chemito 8510) equipped with a carbowax column and flame ionization detector.

5.4.3 Reactions of n-butanal and hydrogen

The Ni/MgO samples (Chapter 8) were reduced in a flow of hydrogen (20 mL min^{-1}) prior to the reaction at 550 °C for four hours. It was then cooled to the reaction temperature. n-Butanal was injected with the precalibrated syringe pump at a flow rate of 3.2 mL hr^{-1}. Catalyst weight was fixed as 1.0g. The exploratory experiments indicated that a higher contact time increases the trimers. Increase of temperature resulted in formation of light fractions (mainly C3's). The reaction conditions selected were WHSV = 2.78 hr^{-1}, mol ratio $[H_2]/[C_6H_6]$ = 6 (H_2 flow = 80 mL min^{-1}); temperature = 150 °C, and time on stream (TOS) = 45 minutes. The outlet of the reactor was connected to a condenser followed by ice trap. The condenser was circulated with a super cooled water-ethylene glycol mixture (70-30) and the ice trap was filled with sodium chloride and crushed ice. The condensed products were analyzed by a gas chromatograph (Chemito 8510) equipped with a 15% carbowax (on DMDS) column (1/8″, 12 ft) and flame ionization detector. The temperature conditions of the GC were

Carrier gas N_2 pressure = 0.8 bar; injector temperature = 210 °C; detector temperature = 260 °C; oven programme = 90 °C (for 8 minutes) — 2 °C min^{-1} to 120 °C — stay at 120 °C (10 minutes) — 5 °C min^{-1} to 180 °C — stay at 180 °C (10 minutes).

Occasionally the products were identified on a GC-MS (Shimadzu, Model – QP2010, equipped with universal capillary column).

References

[1] J.J. Kingsley, K.C. Patil., A novel combustion process for the synthesis of fine particle α-alumina and related oxide materials., *Mater. Lett.* 6 (1988) 427-432

[2] Vogel's Textbook of Quantitative Inorganic Analysis., ELBS, Longman, 1985, pg. 342.

[3] P. Kubelka, F. Munk., *Z. Tech. Phys.* 12 (1931) 593

[4] E. Heracleous, A.F. Lee, K. Wilson, A.A. Lemonidou., Investigation of Ni-based alumina-supported catalysts for the oxidative dehydrogenation of ethane to ethylene: structural characterization and reactivity studies., *J. Catal.* 231 (2005) 159–171

[5] Y. Cesteros, P. Salagre, F. Medina, J.E. Sueiras., Preparation and characterization of several high-area $NiAl_2O_4$ spinels. Study of their reducibility., *Chem. Mater.* 12 (2000) 331-335

[6] M. Polverejan, T.R. Pauly, and T.J. Pinnavaia., Acidic porous clay heterostructures (PCH): intragallery assembly of mesoporous silica in synthetic saponite clays., *Chem. Mater.* 12 (2000) 2698-2704

……✵…….

Chapter 6

STRUCTURE AND REACTIVITY OF Ni/α-Al_2O_3 CATALYSTS.

Contents

6 INTRODUCTION

The use of metal complexes as precursors for the preparation of the supported metal catalysts is gaining importance; as such precursors dramatically influence the final properties of the catalysts. The solid- state reactions occurring between active phase and support during calcinations are crucial in controlling the structural properties or the reactivity of supported oxide catalysts. Nickel supported on α-alumina are versatile catalysts used in steam reforming of hydrocarbons [1]. The global demand for processes like GTL (gas to liquid) and DME (dimethyl ether) has renewed interest in improvement of steam reforming catalysts. Steam reforming of gaseous hydrocarbons is seen as a potential way to provide fuel for fuel cells. The high temperature (700 – 1100 °C) of steam reforming requires robust catalyst and α-Al_2O_3 is a best option. α-Alumina is a refractory oxide formulated at high temperatures. They have low surface area, but have high mechanical and thermal stability suitable for the demanding conditions of steam reforming.

Co-precipitation route yields Ni catalysts with some of the active species getting converted to "hard to reduce" nickel aluminate. The most convenient method for preparation is impregnation with nickel salts, followed by calcination to oxide precursors. α-Alumina is considered to be an 'inert support' which provides little or no interaction to the metal supported on it. The stable structure of α-Al_2O_3 prevents migrations of metal ions into it. However calcinations at high temperature can force the NiO and α-Al_2O_3 to react to form refractory $NiAl_2O_4$. Gavalas *et al.* conducted a series of studies on impregnated 2.2 wt% NiO/α-Al_2O_3, employing hydrogen chemisorption, scanning electron microscopy and X-ray photoelectron spectroscopy [2, 3]. The studies indicated that above 850 °C a precursor of $NiAl_2O_4$ forms which is insoluble in acid and difficult to reduce. Molina *et al.* and Richardson *et al.* have reported $NiAl_2O_4$ formation at low temperatures [4, 5]. They argue that during impregnation, a part of Al_2O_3 dissolves in the impregnating solution and gets incorporated to NiO structure. Even by low temperature calcinations this can transform to $NiAl_2O_4$ like species.

Mostly nickel nitrate salt is used to prepare the $NiO_{x\ (x=0,1)}/Al_2O_3$ catalysts by impregnation method. Multiple impregnations are required to achieve the required metal concentrations. Conversion to nickel aluminate cannot be avoided even in these cases. In high temperature applications, the nickel particles agglomerate and reduce the active surface area for the reaction. So there is much interest in preparing easily reducible, highly active and stable NiO_x/α-Al_2O_3 catalysts. Previously reported studies have established that chelating ligands of the acetyl acetonate are good candidates for the preparation of easily reducible nickel and vanadia catalysts [6, 7].

Use of ethylenediamine metal complexes to prepare supported metal catalysts is gaining much importance because of the ease of preparation of the complexes and formation of smaller metal particles, which are held strongly to the support [8, 9]. Che *et al.* [10-12] have conducted a series of studies on impregnation

and drying of these nickel complexes on silica and gamma alumina. However, the reports on the catalytic activities are very rare [13].

In the present chapter the structure and reactivity of NiO_x/α-Al_2O_3 composite catalysts prepared by the wet impregnation of ethylenediamine complexes of nickel(II) is discussed. The main objective was to study the influence of counter ions on the physiochemical properties of the final catalyst and their influence on activity. Benzene hydrogenation and cyclohexanol decomposition were carried out on the catalysts. Benzene hydrogenation reaction has been used as a test reaction to check the metal support interaction [14].

6.1 Thermal decomposition of dried precursors, chemical analysis and surface area

The TG curves of the thermal decomposition of the dried precursors are shown in Figure 1. The decomposition of Ni-α-B-d is complete before 300 °C and this type of exothermic decomposition of complexes is because of the close proximity of NO_3^- counter ion and ethylenediamine ligand. The total weight loss corresponds to the removal of ethylenediamine ligands and NO_3^- ions in a rapid oxidation-reduction reaction. For the precursor with chloride counter ion (Ni-α-D-d), the decomposition was complete only at high temperature 590 °C. Ni-α-A-d followed almost a same decomposition pattern as the parent compound, nickel nitrate (Chapter 2). The DTG-DTA patterns of the precursors are given from Figures 2 to 5. A small weight increase corresponding to the oxidation of nickel can be found for Ni-α-B-d. This indicates metallic nickel has been formed during the decomposition. The decomposition of Ni-α-B-d is complete in a single step which is highly exothermic. The decomposition of Ni-α-C-d is also exothermic, but in two stages. Endothermic and exothermic weight losses are registered in the DTG-DTA pattern of Ni-α-D-d.

The counter ions present can influence the heat generated or absorbed, amount of heat energy and speed of the decomposition. During decompositions the

nickel ions can interact with the support and the strength of decomposition will be affected by above factors. The differences in decomposition patterns will affect the interactions of nickel ions with the support affecting the final structure and activity of the catalyst.

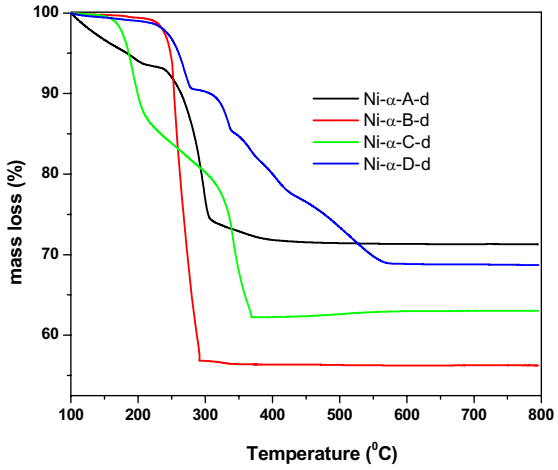

Figure 1. TG curves of dried precursors

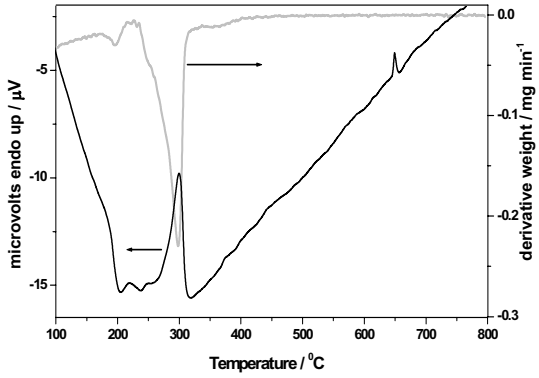

Figure 2. DTG-DTA of Ni-α-A-d

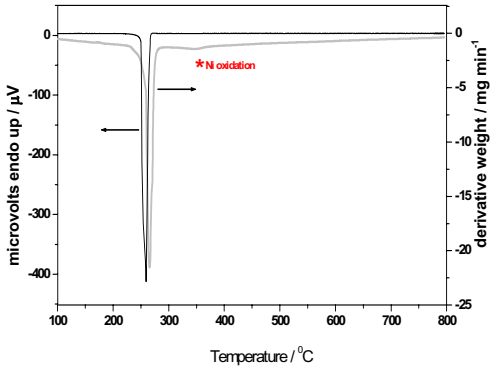

Figure 3. DTG-DTA of Ni-α-B-d

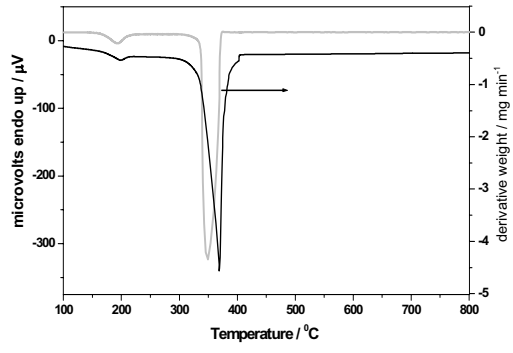

Figure 4. DTG-DTA of Ni-α-C-d

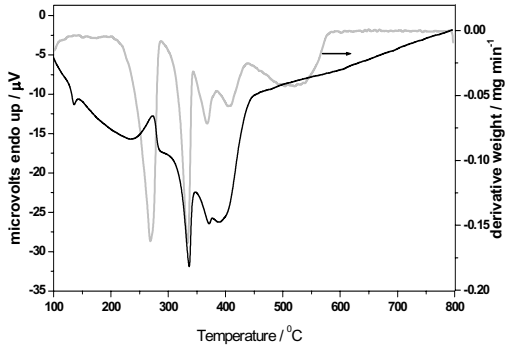

Figure 5. DTG-DTA of Ni-α-D-d

The results of chemical analysis and surface area for the calcined catalysts are given in Table 1.

Table 1. Chemical analysis and BET surface areas of calcined catalysts.

Sample	BET surface area ($m^2 g^{-1}$)	Ni (weight %)	Cl (weight %)
Support	5.9	--	
Ni-α-A-c	7.5	19.8	
Ni-α-B-c	23.8	19.6	
Ni-α-C-c	11.0	20.1	
Ni-α-D-c	3.6	20.0	0.9

The highest surface area obtained was for Ni-α-B-c. The surface areas for Ni-α-A-c, Ni-α-B-c and Ni-α-C-c were higher than the support. The increase of surface can be of two reasons; i) the formed NiO are of high surface area ii) the α-Al_2O_3 would have dissolved during impregnation and formed high surface area forms like gamma or eta alumina. The single stage exothermic decomposition of Ni-α-B-d resulted in formation of high surface area NiO supported on α-Al_2O_3. This decomposition happens at low temperatures compared to others. Also the process is very fast and the heat developed can dissipate fast avoiding the thermal sintering of the formed nickel oxide crystallites. The low surface area obtained for Ni-α-D-c is due to the exothermic decompositions at high temperatures (Figure 5 indicates decomposition of Ni-α-D-d is complete only at 590 °C) which might have resulted due to sintering.

6.2 XRD and UV-vis DRS studies

The XRD patterns of the support and samples before and after reduction are shown in Figure 6, and the crystallite sizes and lattice parameters are given in Table 2. The most intense NiO reflections are at 37.3˚ due to NiO (111) and 43.3˚ due to NiO (200). In the present system they are almost completely overlapped with the

(113) and (104) reflections of α-alumina at 37.8˚ and 43.4˚ respectively. Therefore the XLBA (X-ray line broadening analysis) was done on the 62.8˚ (220) peak of NiO for the calcined samples. The XLBA was done for the reduced catalysts for the peaks at 44.4˚ $Ni^{(0)}$ (111) and at 51.8˚ $Ni^{(0)}$ (200). The Ni-α-B-c derived from nitrate anion has the smallest crystallite for NiO and shows the maximum change in the lattice parameter also. The low crystallite size might have achieved because of the single stage exothermic decomposition during the calcination step. Ni-α-D-c derived from chloride anion has the largest crystallite size. The crystallite sizes for the reduced Ni systems did not vary much except for the Ni-α-D-r sample which shows a larger crystallite size. The Ni-α-D system shows no variation from the theoretical value thus indicating the formation of bulk NiO and Ni grains in this system. None of the catalysts showed reflections due to nickel aluminate formation.

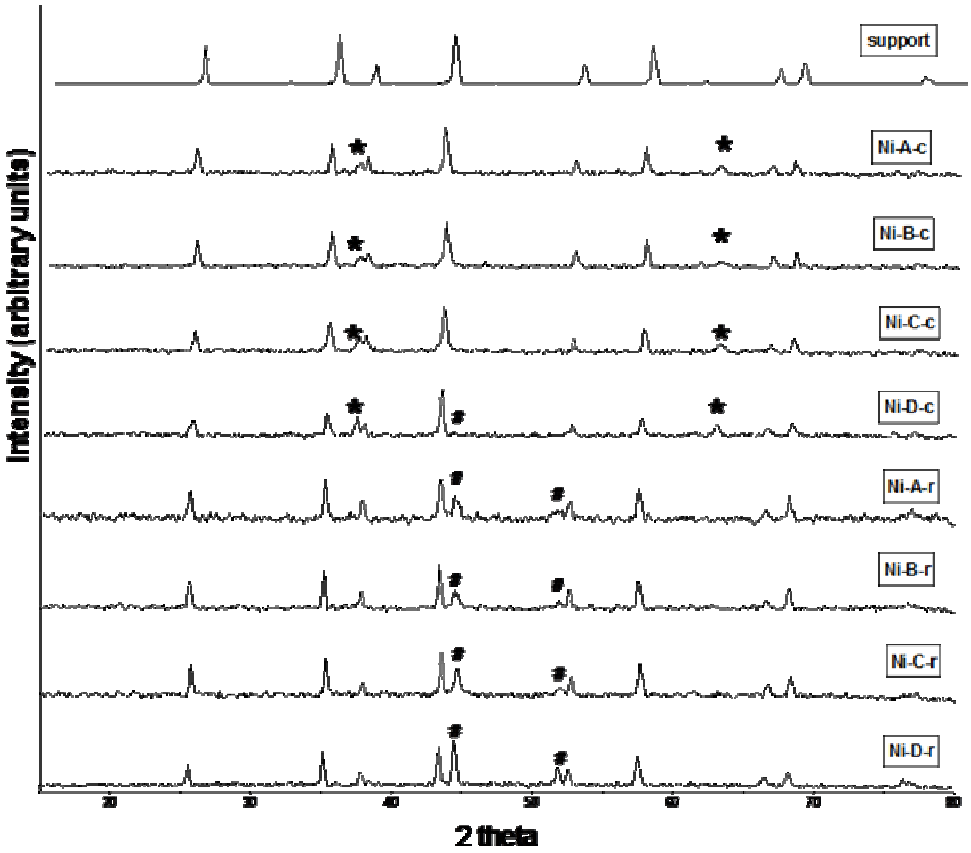

Figure 6. XRD patterns of support, calcined and reduced catalysts.

∗ NiO # Ni

Table 2. Crystallite sizes and lattice constants of calcined and reduced samples.

Samples	Crystallite size NiO nm	Crystallite size Ni nm	Cell constant NiO nm	Cell constant Ni nm	% Change in lattice parameter NiO	% Change in lattice parameter Ni
Ni-α-A-c	17	--	0.4175	--	0.034	--
Ni-α-B-c	9	--	0.4184	--	0.197	--
Ni-α-C-c	14	--	0.4179	--	0.068	--
Ni-α-D-c	20	--	0.4176	--	0.001	--
Ni-α-A-r	--	20	--	0.3526	--	0.046
Ni-α-B-r	--	18	--	0.3535	--	0.322
Ni-α-C-r	--	20	--	0.3524	--	0.012
Ni-α-D-r	--	33	--	0.3525	--	0.039

Theoretical NiO lattice parameter- 0.4176 nm

Theoretical Ni lattice parameter- 0.3524 nm

The UV-vis DRS spectra (Figure 7) of the calcined samples exhibit charge transfer band at 280 nm and the d-d transitions, $^3A_{2g} \rightarrow {}^1T_{1g}$, $^3A_{2g} \rightarrow {}^3T_{1g}$(P) and $^3A_{2g} \rightarrow {}^3T_{1g}$ (F) at 377 nm, 425 nm and 714 nm respectively. These transitions are due to nickel(II) in octahedral structure [15]. The transitions at 590 and 620 nm are not seen indicating the absence of Ni(II) in tetrahedral structures. This again points out the non formation of nickel aluminate, which is in agreement with the observation from XRD. The peaks of Ni-α-D-c are intense than others and it's less intense charge transfer band indicates the formation of bulk NiO. TPR and SEM results agree with this observation. The high intensity of charge transfer band, high absorption along the entire wavelength and low intensity of Ni[O] bands suggest the formation of black Ni_2O_3 on the Ni-α-C-c sample [16]. In general the DRS spectrum reveals the formation of NiO with less interaction with the support and is similar to the spectrum obtained by Lisboa *et al.* for the Ni/α-alumina catalysts [17]. Due to

the dark color and high absorbance in the entire range, more information could not be extracted from UV-vis DRS spectra.

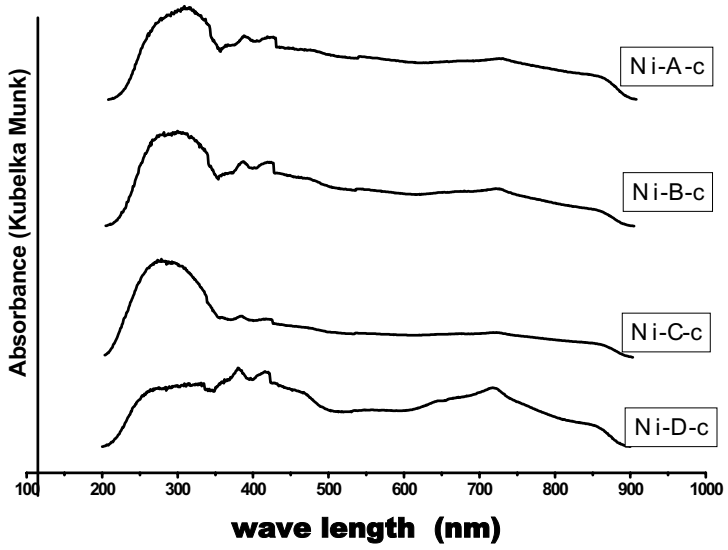

Figure 7. UV-vis diffuse reflectance spectra of calcined catalysts

6.3 TCD-TPR

Metal support interactions appreciably affect the surface properties of these catalysts and, hence, their catalytic properties. It is well known that the interaction between nickel oxide and support can affect the reduction temperature [18]. The reduction temperature mainly depends on the support interaction, Ni species, particle size and rate of nucleation of metallic nickel. The nickel species having weak interaction can be reduced at low temperature than those having strong interaction. Small particle sizes generally result in high reduction temperatures than large particle sizes. The TPR spectra of Ni-α-A-c and Ni-α-B-c (Figure 8) show major peaks at 620 and 450 °C. The peak at 620 °C is due to surface nickel aluminate, while the peak at 450 °C is due to small NiO crystallites having interaction with the support (supported NiO). The peak at 390 °C for Ni-α-D-c is due to the reduction of bulk NiO [19].

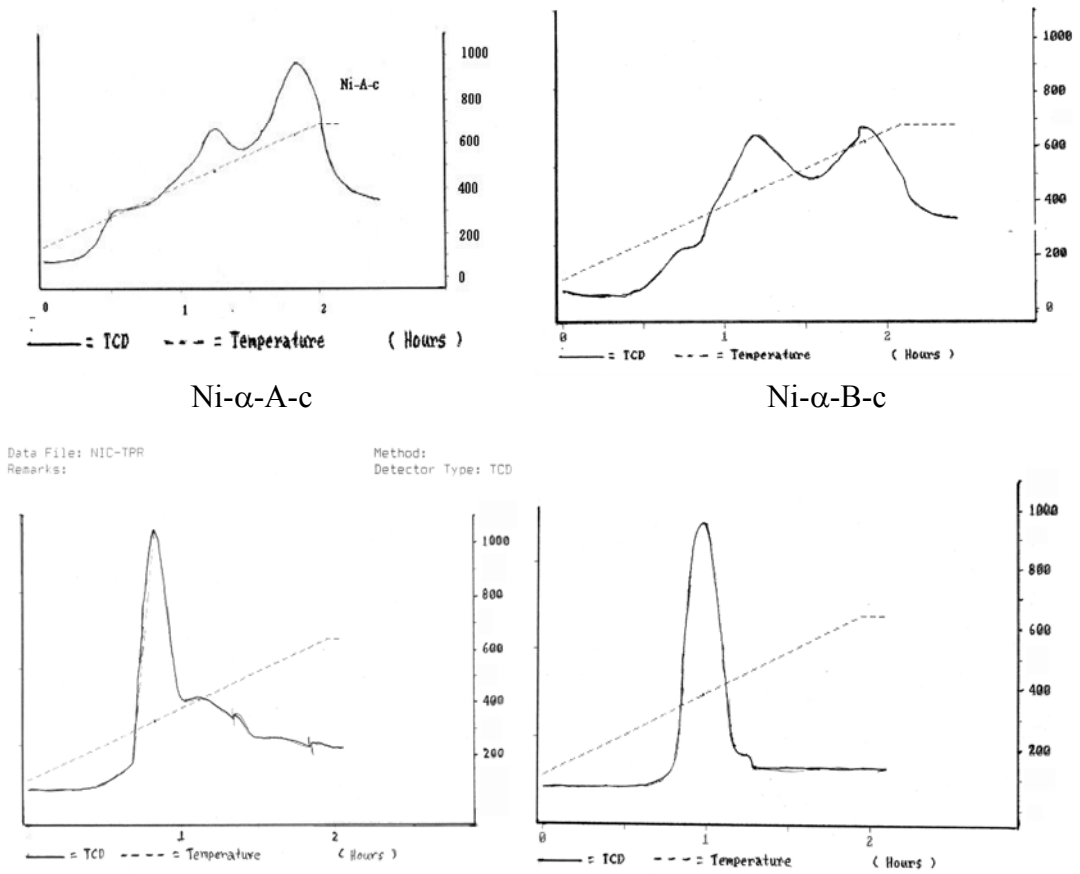

Figure 8. Temperature programmed reduction profiles of calcined catalysts

The reduction peak of Ni-α-C-c at 320 °C agrees with that reported for the pure Ni_2O_3 by Ho *et al.* who calcined their catalysts at low temperature and under inert atmosphere [20]. Such low reduction peak is very uncommon in nickel supported systems and is attributed to the formation of Ni_2O_3 in which Ni is in the +3 state. The samples Ni-α-A-c and Ni-α-B-c also show the presence of this Ni^{3+} species by the low intense peaks below 300 °C. Table 3 shows the different species present on the catalysts. It can be seen that the major species present on Ni-α-B-c is supported NiO crystallites. The use of ethylenediamine ligands in general resulted in formation of easily reducible nickel species. This may be due to the presence of chelating ligands which favour the formation of bulk NiO. During decomposition, the chelating ligands protect the nickel ions from interacting with the support.

Table 3. Different nickel species present on calcined catalysts.

Catalyst	Nickel Species			
	Ni_2O_3 (320 °C)	free NiO (390 °C)	supported NiO (450 °C)	surface $NiAl_2O_4$ (620 °C)
Ni-α-A-c		√	√	√ (major)
Ni-α-B-c		√	√ (major)	√
Ni-α-C-c	√ (major)	√		
Ni-α-D-c		√ (major)		

6.4 SEM

SEM results (Figure 9) show a striking difference in the morphologies of reduced catalysts. The SEM image of support indicates sheet like structures. Ni-α-A-r and Ni-α-A-r show smaller Ni grains embedded on the sheet like surface of α-alumina thus giving the support a rough nature. Morphology of Ni-α-D-r shows bulk Ni grains with nearly cubic shapes; whereas Ni-α-C-r contains flower shaped Ni grains which seems to be formed by loose aggregates of nickel crystallites. Both Ni-α-C-r and Ni-α-D-r are loosely bound to support surface resulting in very low metal support interaction. TPR results are in accordance with this observation. Variations in morphologies of NiO on changing the metal precursors were also noted by Estelle *et al.* [21].

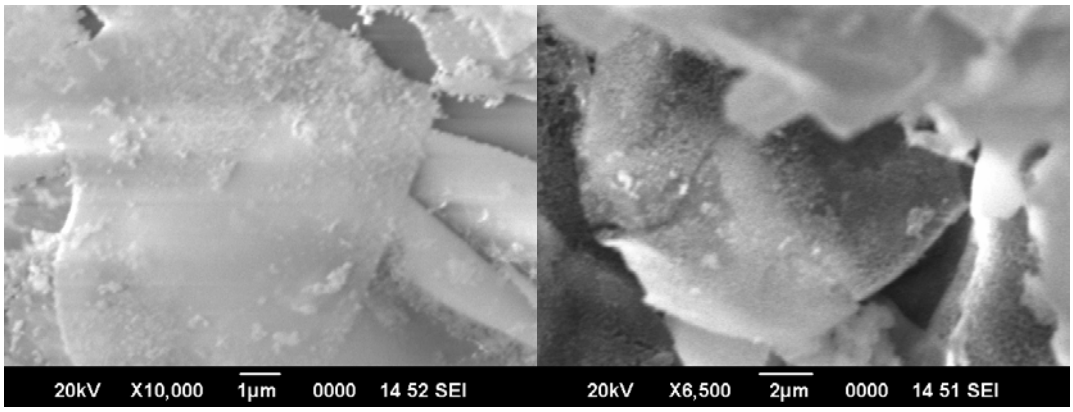

Ni-α-A-r Ni-α-B-r

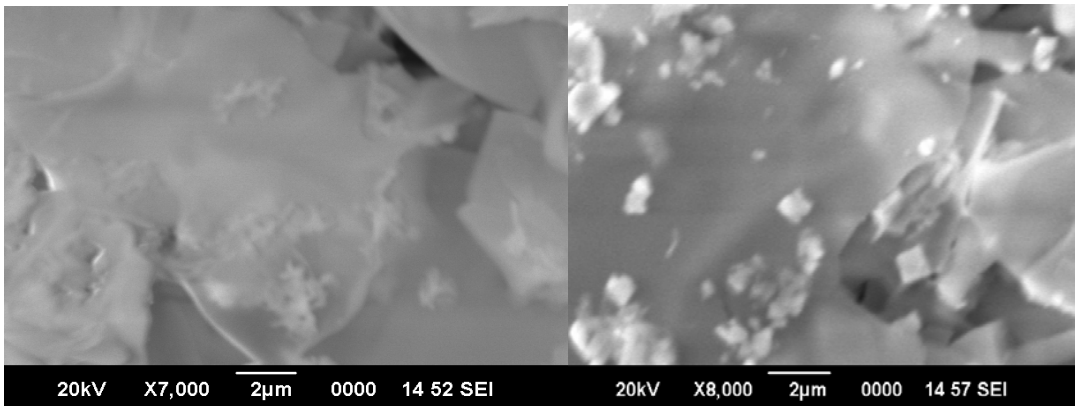

Ni-α-C-r Ni-α-D-r

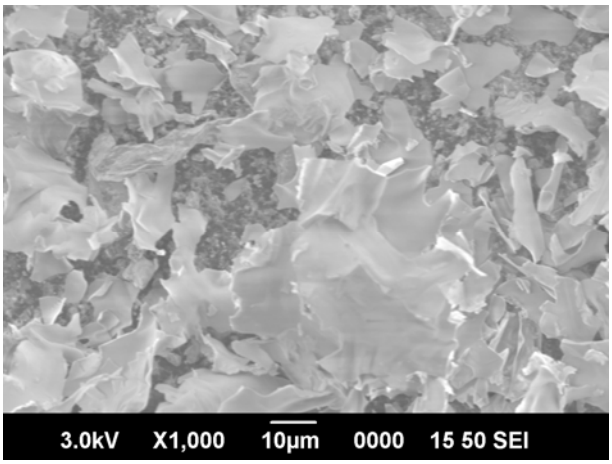

α-Al_2O_3 - support

Figure 9. Scanning Electron Micrographs of reduced catalysts and support

6.5 Benzene hydrogenation

The results of benzene hydrogenation on reduced catalysts are shown in Figure 10. Ni-α-C-r shows the highest conversion. The catalyst with lowest crystallite size, Ni-α-B-r did not show much activity. The special flower like morphology present on Ni-α-C-r may be the reason for its high activity.

Figure 10. Percentage conversion for benzene hydrogenation on reduced catalysts

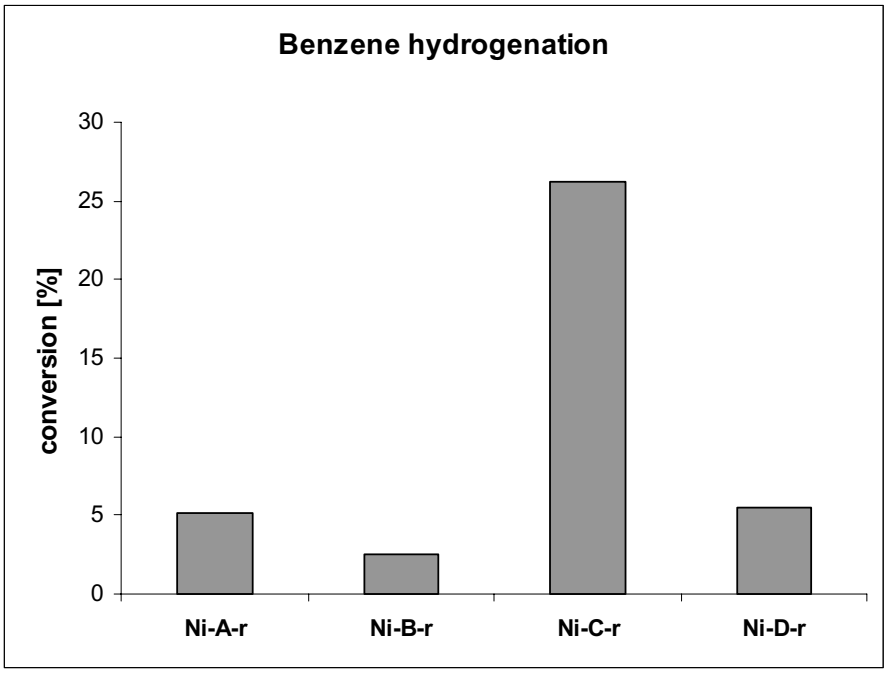

Such special morphology has found to give unexpected activity in nickel supported systems [22, 23]. For supported catalysts, when metal supported interaction is more, the benzene hydrogenation activity will be less [14].

6.6 Cyclohexanol dehydrogenation

The results of cyclohexanol dehydrogenation on the bare support, calcined samples and reduced catalysts are shown in the Table 4. All the catalysts yielded cyclohexanone and cyclohexene as the major products; however, using reduced catalysts trace quantities of benzene, cyclohexane and phenol were also obtained. These trace secondary products were less than 1%; so they were neglected in

selectivity and yield calculations. The calcined catalysts are highly selective towards cyclohexanone even though their activities were low.

Table 4. Results of cyclohexanol dehydrogenation

Sample	%(wt) conversion of Cyclohexanol	% selectivity	
		Cyclohexanone	Cyclohexene
Support	2	72	28
Ni-α-A-c	8	98	2
Ni-α-B-c	6	97	3
Ni-α-C-c	7	96	4
Ni-α-D-c	6	96	4
Ni-α-A-r	28	95	5
Ni-α-B-r	45	99	1
Ni-α-C-r	18	98	2
Ni-α-D-r	12	98	2

The increase in selectivity on these calcined catalysts, compared to the bare support is due to introduction of NiO, which always gives more selectivity towards cyclohexanone [24]. The reduced catalysts are reasonably active towards the dehydrogenation reaction. The Ni-α-B-r with the smallest nickel crystallite size and largest BET surface area gave the maximum yield for cyclohexanone, while the Ni-α-C-r gave least yield.

The TPR data indicate that different types of NiO having different interactions with the support has been formed, while XRD shows different crystallite size formation on the alpha alumina surface. Even though these different NiO did not show any difference in their performance for their reaction, upon reduction they yielded nickel metal crystallites differing in size and strength of interaction with support. The evolution of the active phase from the precursors during the

calcination stage determines the final properties of the catalysts. Cyclohexanol dehydrogenation to cyclohexanone is a reaction which depends on the metal crystallite size [25]. The high activity of Ni-α-B-r sample derived from the $[Ni(en)_2(H_2O)_2](NO_3)_2$ for cyclohexanol dehydrogenation to cyclohexanone is because of its low metal crystallite size and high surface area. And this low crystallite size resulted from the exothermic decomposition of the ligands in single step at a low temperature compared with the conventional preparation method. However, this highly exothermic decomposition resulted in formation of supported NiO crystallites with moderate interaction with the support.

The difference in reactivity of Ni-α-B-r and Ni-α-C-r towards the studied reactions indicate the difference in reactivity of the species present. Ni-α-C-r which have high amount of 'free Ni', having special flower like morphology is highly active for hydrogenation. Ni-α-B-r which contains high amount of 'Ni interacting moderately with support' (or small Ni crystallites) is highly active for cyclohexanol dehydrogenation. Thus, change of counterions resulted in formation of different types of nickel species on alpha alumina with varying activities towards chemical transformations.

6.7 Conclusions

i.) TG studies of dried precursors indicate that low temperature exothermic decomposition for Ni-α-B-d, results in formation of catalyst with high surface area and small supported NiO crystallites.

ii.) The acetate counter ion results in formation of nickel metal with special morphology highly active for benzene hydrogenation

iii.) The use of different counter ions results in catalysts with different metal-support interactions.

iv.) The model reactions studied indicate that aromatic hydrogenation sites are different from the sites for cyclohexanol dehydrogenation.

References

[1] T. Namaguchi., Highly Active Steam Reforming Catalyst for Hydrogen and Syngas Production., *Catal. Surv. Jpn.* 5 (2001) 59-63

[2] G.R. Gavalas, C. Phichitkul, G.E. Voecks., Structure and activity of NiO/α-Al_2O_3 and NiO/ZrO_2 calcined at high temperatures : I. Structure., *J. Catal.* 88 (1984) 54-64

[3] G.R. Gavalas, C. Phichitkul, G.E. Voecks., Structure and activity of NiO/α-Al_2O_3 and NiO/ZrO_2 calcined at high temperatures: II. Activity in the fuel-rich oxidation of methane., *J. Catal.* 88 (1984) 65-72

[4] R. Molina and G. Poncelet., α-Alumina-supported nickel catalysts prepared with nickel acetylacetonate. 2. A study of the thermolysis of the metal precursor., *J. Phys. Chem. B.* 103 (1999) 11290-11296

[5] J.T. Richardson, M. Lei, B. Turk, K. Forster, M.V. Twigg., Reduction of model steam reforming catalysts: NiO/α-$A1_2O_3$., *Applied Catalysis A: General.* 110 (1994) 217-237

[6] R. Molina, G. Poncelet., α-Alumina-supported nickel catalysts prepared from nickel acetylacetonate: A TPR Study., *J. Catal.* 173 (1998) 257-267

[7] M. Baltes, P. van der Voort, B.M. Weckhuysen, R. R. Rao, G. Catana, R.A. Schoonheydt, E.F. Vansant., Synthesis and characterization of alumina-supported vanadium oxide catalysts prepared by the molecular designed dispersion of $VO(acac)_2$ complexes. *Phys. Chem. Chem. Phys.* 2 (2000) 2673-2680

[8] S. Schimpf, C. Louis, P. Claus., Ni/SiO_2 catalysts prepared with ethylenediamine nickel precursors: Influence of the pretreatment on the catalytic properties in glucose hydrogenation *Appl. Catal. A: General.* 318 (2007) 45-53

[9] R. Zanella, A. Sandoval, P. Santiago, A.V. Basiuk, M.J. Saniger., New preparation method of gold nanoparticles on SiO_2., *J. Phys. Chem. B.* 110 (2006) 8559-8565

[10] F. Negrier, E. Marceau, M. Che, J.M. Giraudon, L. Gengembre, A. Lofberg., A systematic study of the interactions between chemical partners (metal, ligands, counterions, and support) involved in the design of Al_2O_3-supported nickel catalysts from Diamine−Ni(II) chelates., *J. Phys. Chem. B.* 109 (2005) 2836-2845

[11] K.Q. Sun, E. Marceau, M. Che., Evolution of nickel speciation during preparation of Ni–SiO_2 catalysts: effect of the number of chelating ligands in $[Ni(en)_x(H_2O)_{6-2x}]^{2+}$ precursor complexes., *Phys. Chem. Chem. Phys.* 8 (2006) 1731-1738

[12] S. Boudjay, J.F. Lambert, M. Che., Evidence for interfacial molecular recognition in transition metal complexes adsorption on amorphous silica surfaces., *J. Phys. Chem. B.* 107 (2003) 651-654

[13] F. Negrier, E. Marceau, M. Che, J-M. Giraudon, L. Gengembre, A. Lofberg., From Al_2O_3-supported Ni(II)-ethylenediamine complexes to CO hydrogenation catalysts: Importance of the hydrogen post-treatment evidenced by XPS., *Catal. Lett.* 124 (2008) 18–23

[14] R. Molina, G. Poncelet., Hydrogenation of benzene over alumina-supported nickel catalysts prepared from Ni(II) acetylacetonate., *J.Catal.* 199 (2001) 162-170

[15] B. Scheffer, J.J. Heijeinga, J.A. Moulijn., An electron spectroscopy and x-ray diffraction study of nickel oxide/alumina and nickel-oxide-tungsten trioxide/alumina catalysts., *J.Phy.Chem.* 91(1987) 4752-4759

[16] F.S. Stone in: J.P Bonnelle, B. Delmon, E. Derouane (Eds.), Surface Properties and Catalysis by Non metals, Reidel, Dordrecht, 1983, pg 237.

[17] S.J. Lisboa, C.R.M.D. Santos, B.F. Passos, B.F. Noronha., Influence of the addition of promoters to steam reforming catalysts., *Catal. Today.* 101 (2005) 15-21

[18] S. Wang, G.Q. Lu., Reforming of methane with carbon dioxide over Ni/Al_2O_3 catalysts: Effect of nickel precursor., *Appl. Catal. A: General.* 169 (1998) 271-280

[19] G. Li, L. Hu, J.M. Hill., Comparison of reducibility and stability of alumina-supported Ni catalysts prepared by impregnation and co-precipitation., *Appl. Catal. A: General.* 301 (2006) 16-24

[20] S.C Ho, T.C Chou., The role of anion in the preparation of nickel catalyst detected by TPR and FTIR spectra., *Ind. Eng. Chem. Res.* 34 (1995) 2279-2284

[21] J. Estelle, P. Salagre, Y. Cesteros, M. Serra, F. Medina, J.E. Sueiras., Comparative study of the morphology and surface properties of nickel oxide prepared from different precursors., *Solid State Ionics.* 156 (2003) 233– 243

[22] A.G. Boudjahem, S. Monteverdi, M. Mercy, M.M. Bettahar., Nanonickel particles supported on silica. Morphology effects on their surface and hydrogenating properties., *Catal. Lett.* 97 (2004) 177-183

[23] A.G. Boudjahem, S. Monteverdi, M. Mercy, M.M. Bettahar., Study of support effects on the reduction of Ni^{2+} ions in aqueous hydrazine., *Langmuir.* 20 (2004) 208-213

[24] R.D. Srivastava, J. Onuferko, J.M. Schultz, G.A. Jones, K.N. Rai, R. Athappan., Characterization and activity of nickel oxide supported on gamma-alumina., *Ind. Eng. Chem. Fundam*. 21 (1982) 457-463

[25] K. V. R. Chary, G.V. Sagar, C. S. Sreekanth, V. V. Rao., Characterization and catalytic functionalities of copper oxide catalysts supported on zirconia., *J. Phys. Chem B*. 111 (2007) 543-550

……✵…….

Chapter 7

STRUCTURE AND REACTIVITY OF Ni/γ-Al_2O_3 CATALYSTS.

Contents

7. INTRODUCTION

Thermal dehydration of bohemite (γ- AlOOH) to α-alumina through γ-alumina is well known [1]. γ- Al_2O_3 is an intermediate in the above transition and is a versatile support material due to its easily controllable physical properties. The surface area and pore structure can be varied by adjusting the preparation parameters, and catalyst supports with varying structure can be easily made. γ- Alumina is one of the supports which give excellent nickel dispersion. Also the moderate metal-support interaction present in the Ni/γ- Al_2O_3 system gives stability for the nickel crystallites. However the thermal stability of γ- Alumina is less. At high temperature very soon it gets transformed to θ-Al_2O_3 and then to more stable, low surface area hexagonal α-Al_2O_3. This fact restricts its use in high temperature applications. Nickel supported on γ- Al_2O_3 finds its use in hydrogenation [2], hydrodechlorination [3], natural gas reforming for syngas and hydrogen production [4, 5], methanation [6], and oxidative dehydrogenation [7].

Selective gas phase hydrogenation of p-chloronitrobenzene was studied on supported nickel catalysts and a high specific rate was obtained for γ- Al_2O_3 supported catalysts due to the smaller diameter of nickel crystallites obtained [8]. Promoted Ni/γ- Al_2O_3 catalysts were used for the oxidative dehydrogenation of ethane by Heracleous *et al.* [9]. Their studies revealed that the different species formed on the final catalysts had differing activity and selectivity. XPS studies indicated that NiO particles were chemically modified on interaction with alumina, and this modification made them selective for oxidative dehydrogenation of ethane to ethene. The unsupported NiO or those with least interaction with γ- Al_2O_3 were not selective for the reaction. Such studies show that species with different activity and selectivity could be prepared controlling the diffusion of Ni^{2+} to γ- Al_2O_3 structure. During the preparation Ni^{2+} ions can enter in to the defect lattice structure of γ- Al_2O_3. At high temperature the solid state reaction between NiO and γ- Al_2O_3 results in formation of the spinel nickel aluminate ($NiAl_2O_4$). Ni^{2+} ions can occupy the tetrahedral or octahedral vacancies of γ- Al_2O_3 and these nickel ions are very hard to reduce. High temperatures (above 700 °C) are often required to reduce nickel aluminate. This makes some of the Ni^{2+} ions 'non-usuable' in certain reactions, such as low temperature hydrogenations. However, the formation of nickel aluminate is desirable in certain reactions. The nickel crystallites in contact with nickel aluminate are thermally stable and can be used for high temperature applications like oxidative dehydrogenation.

The formation of nickel aluminate can be controlled by selecting appropriate preparation conditions, especially the drying and calcination temperature. Another approach is to use suitable precursors. Metal chelate precursors can restrict the formation of nickel aluminate, making use of the chelating behavior of the ligands. Use of ethylenediamine metal complexes to prepare supported metal catalysts is gaining much importance because of the ease of preparation of the complexes and formation of smaller metal particles, which are held strongly to the support [10]. Che *et al.* [11, 12] conducted a series of studies on impregnation and drying of the nickel

complexes on silica and γ- alumina. However, the evolution of the active phase and catalytic activities of such catalysts are investigated rarely [13]. We prepared Ni / γ-Al_2O_3 (containing 20 wt% Ni) catalysts employing the ethylenediamine complexes with varying counter ions. The preparation part has been already presented in Chapter 5. The first part of this chapter contains the discussion on the evolution of the catalysts from the precursors, and the physicochemical properties. The catalytic activities of these samples for decomposition of cyclohexanol and dehydrogenation of cyclohexane are discussed in the second part.

7.1 Thermal decomposition of dried precursors

Figure 1 shows the TG patterns of the dried precursors. The highest temperature for complete decomposition was recorded for Ni-γ-D-d. For Ni-γ-B-d the decomposition was complete at a low temperature of 350 °C. Figures 2 to 5 shows the DTG-DTA patterns of the dried samples. The major endothermic decomposition of Ni-γ-A-d occur at 265 °C and the decomposition temperature is low compared to nickel nitrate (chapter 1) and Ni-α-A-d (chapter 6). The exothermic decompositions of Ni-γ-B-d happen in two stages at 215 °C and 320 °C. Both the events are merged and the decomposition is complete early. The sample Ni-γ-C-d decomposed in two highly exothermic events at 182 °C and 355 °C. These two events are widely separated. For Ni-γ-D-d decompositions occur in several exothermic stages from 180 °C to 580 °C. From the thermolysis studies it can be seen that the shortest temperature span of decomposition was for Ni-γ-B-d.

7.2 Nitrogen physisorption studies and Chemical analysis

The textural properties of the calcined catalysts were investigated by N_2 physisorption studies. The adsorption-desorption iosotherms given in Figure 6 can be classified as type IV isotherms with H1 hysteresis [14].

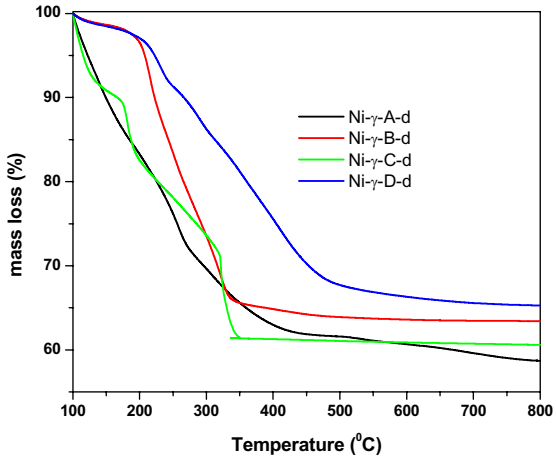

Figure 1. TG curves of dried precursors

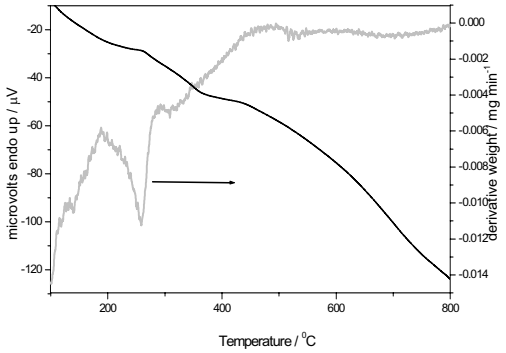

Figure 2. DTG-DTA of Ni-γ-A-d

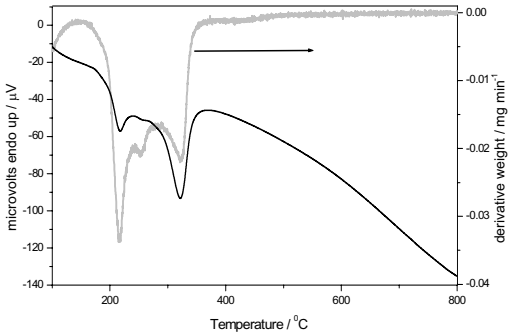

Figure 3. DTG-DTA of Ni-γ-B-d

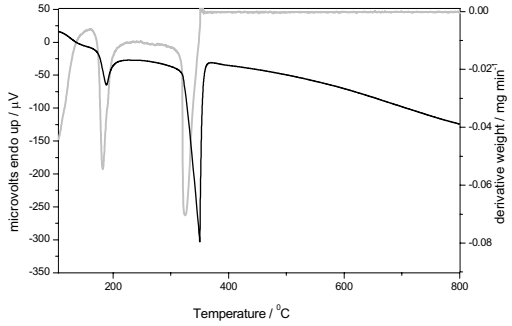

Figure 4. DTG-DTA of Ni-γ-C-d

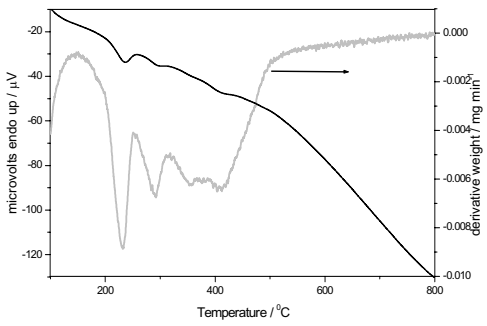

Figure 5. DTG-DTA of Ni-γ-D-d

The shapes of the hysteresis loops were similar to that of support indicating that pore structure has not changed much. For catalysts Ni-γ-A-c, Ni-γ-C-c and Ni-γ-D-c the isotherm shows higher absorption at high p/p_0 values (the isotherm is convex at $p/p_0 > 0.95$) suggesting that some pores with very high pore diameter has been formed. Pore size distribution (PSD) of the support and the calcined catalysts are given in Figure 7. Wider pores (in the range 2000 Å) are formed in Ni-γ-A-c, Ni-γ-C-c and Ni-γ-D-c. These new pores are formed from NiO present on these catalysts. Figures 8 A and B shows the adsorption isotherm and the PSD of a NiO sample prepared from nickel nitrate (Chapter 2).

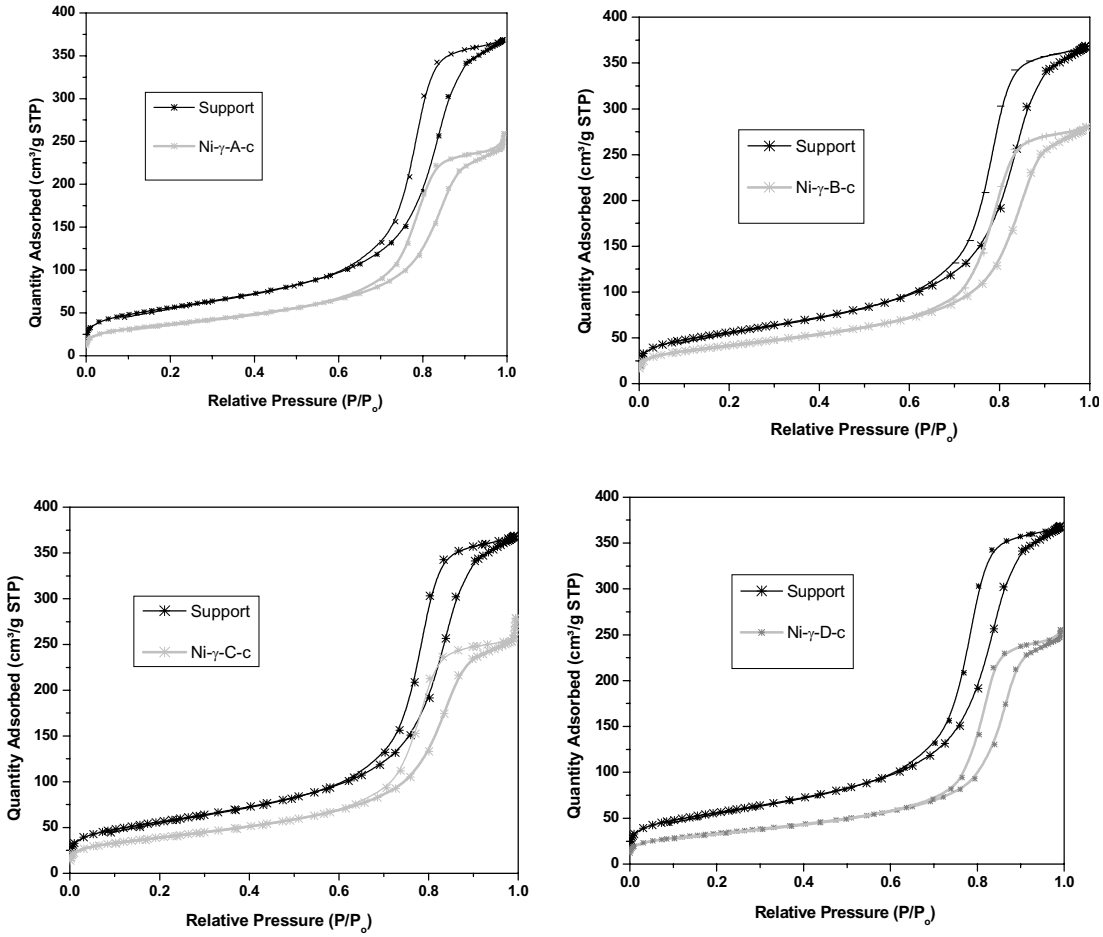

Figure 6. Adsorption – Desorption isotherms of calcined catalysts; support isotherm is provided for comparison.

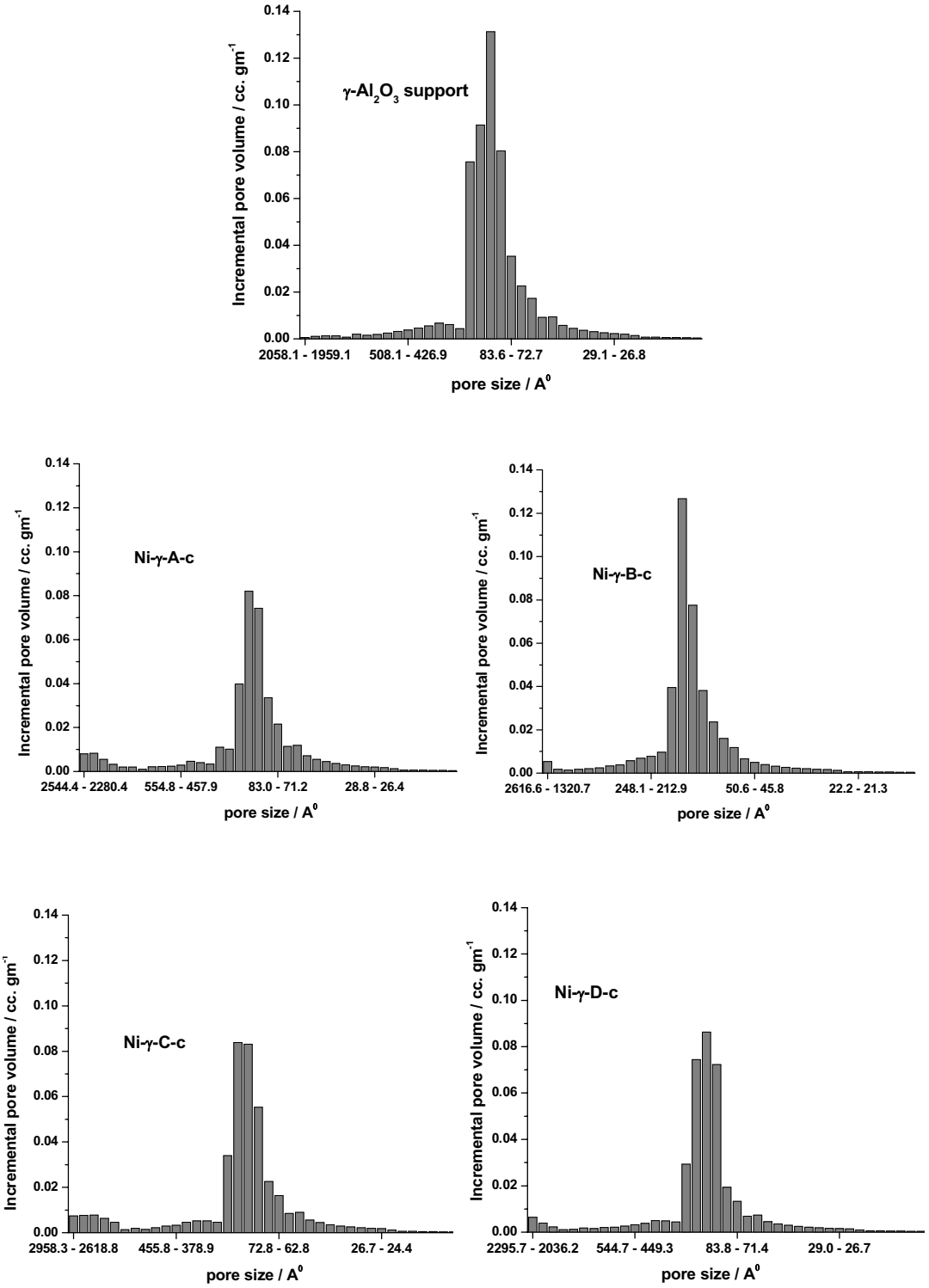

Figure 7. Pore size distributions of support and calcined catalysts

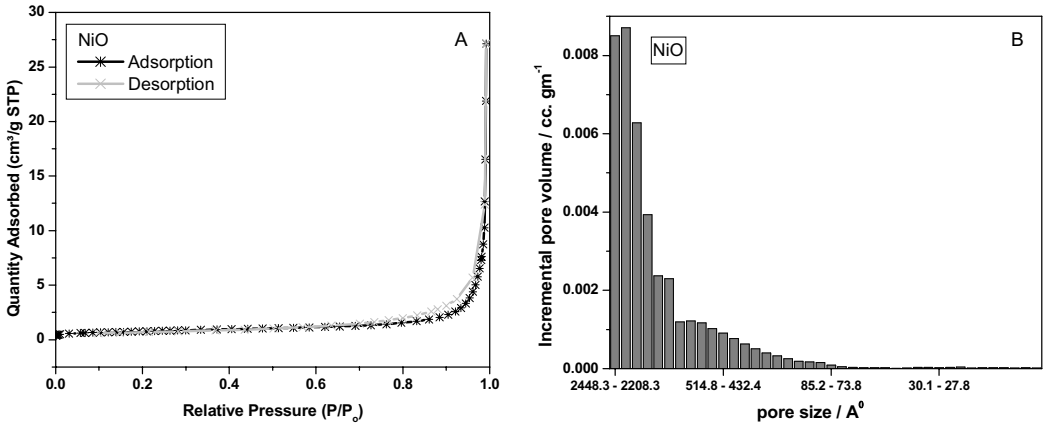

Figure 8. A- isotherm of NiO, B- PSD of NiO

Comparing the isotherms of above samples and NiO, it can be suggested that some free NiO would have been formed. Whereas, in Ni-γ-B-c, the pore volume due to wider pores is very less, which may be an indication of lower concentration of free NiO present on them. The summary of N_2 physisorptions are given in Table 1. All samples have a lower surface area than that of the support. However, the surface area of Ni-γ-B-c was not reduced, when compared to the other samples.

Table 1. Summary of Nitrogen physisorption experiments and Chemical analysis

Sample	γ-Al$_2$O$_3$	Ni- γ-A-c	Ni- γ-B-c	Ni- γ-C-c	Ni- γ-D-c
BET SA (m^2 gm^{-1})	199	133	149	140	120
PV (mL gm^{-1})	0.57	0.40	0.44	0.43	0.40
Avg Pore Dia (Å)	84	89	89	91	101
Nickel (wt %)	--	19.3	19.3	19.3	19.4
Chlorine	--	--	--	--	1.3

The low temperature exothermic decomposition of the complex results in the dissipation of heat energy more effectively which reduces the sintering and leads to high surface area materials [15]. The total pore volume and Average pore size are almost similar for all samples. The reduction in surface area of Ni-γ-D-c is due to high temperature exothermic decomposition.

7.3 XRD and UV-vis DRS studies – formation of nickel aluminate.

The diffraction angles from JCPDS files of NiO (JCPDS-47-1049), γ-Al_2O_3 (JCPDS-10-0425) and $NiAl_2O_4$ (JCPDS-10-341) are given in Table 2.

Table 2. Diffraction angles from JCPDS files

Diffraction angles		
γ-Al_2O_3	**NiO**	**$NiAl_2O_4$**
45.84 **(400)**	37.29 **(111)**	37.01 **(311)**
67.10 **(440)**	43.30 **(200)**	45.10 **(400)**
	62.91 **(220)**	65.70 **(440)**

The X' ray diffraction patterns of the support and the calcined catalysts are shown in Figure 9.

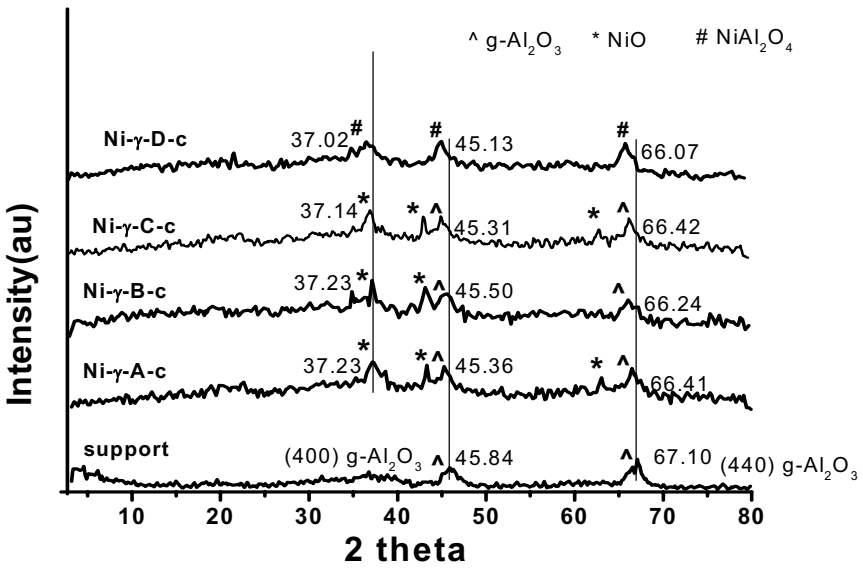

Figure 9. X-ray Diffraction patterns of support and calcined catalysts

Table 3 gives the diffraction angles of NiO, Al_2O_3 and $NiAl_2O_4$ of the calcined samples.

Table 3. Diffraction angles of samples and phases identified.

Diffraction angles of samples				
γ-Al_2O_3	Ni-γ-A-c	Ni-γ-B-c	Ni-γ-C-c	Ni-γ-D-c
45.84 **(400)**	37.13 **(111)** NiO	37.27 **(111)** NiO	37.18 **(111)** NiO	37.01 **(311)** **$NiAl_2O_4$**
67.10 **(440)**	43.34 **(200)** **NiO**	43.39 **(200)** **NiO**	43.30 **(200)** **NiO**	--
	45.29 **(400)**	45.70 **(400)**	45.26 **(400)**	45.48 **(400)** **$NiAl_2O_4$**
	63.01**(220)** **NiO**	--	63.04**(220)** **NiO**	--
	66.50 **(440)**	66.25 **(440)**	66.48 **(440)**	66.27 **(440)** **$NiAl_2O_4$**

The diffraction peaks due to free NiO is not seen in the XRD pattern of Ni-γ-D-c. Moreover the 2θ values of this sample are closer to that of $NiAl_2O_4$. These facts suggest that during calcination, much of NiO reacts with Al_2O_3 forming $NiAl_2O_4$. For Ni-γ-B-c the absence of (220) peak and the higher fwhm value of (200) peak indicate the formation of very small crystallites of NiO.

γ-Alumina has a defect spinel structure. Hence, the divalent metal cation like Ni^{2+} can occupy the tetrahedral and octahedral sites in its structure. For unsupported γ-Al_2O_3 the lattice constant is 0.7900 nm. Ni^{2+} ion have larger ionic radii compared to Al^{3+} ion. As Ni^{2+} enter the lattice, the lattice constant of γ-Al_2O_3 increases. The lattice constants of γ-Al_2O_3 were calculated and are tabulated in the Table 4.

Table 4. Lattice constant of γ-Al_2O_3

Cell constant of gamma alumina (theoretical 0.7900 nm)			
	(400)	**(440)**	Average
support	0.7912	0.7890	0.7901
Ni-γ-A-c	0.7991	0.7957	0.7974
Ni-γ-B-c	0.7968	0.7975	0.7971
Ni-γ-C-c	0.7999	0.7956	0.7978
Ni-γ-D-c	0.8030	0.7993	0.8011

It can be seen that the largest change was observed for Ni-γ-D-c, which indicates much proportion of Ni^{2+} ions enters the alumina lattice. The least change is noted for Ni-γ-B-c, which shows that Ni^{2+} ions occur on the surface. The chloride counter ion of Ni-γ-D-d has enhanced the formation of $NiAl_2O_4$ due to its decomposition at high temperature.

UV- vis DRS measurements can also identify the $NiAl_2O_4$ formation. Jacono *et al.* identified the formation of 'surface spinel' during calcinations of NiO/γ-Al_2O_3 system employing XRD, reflectance spectroscopy and magnetic measurements [16]. Ni^{2+} ions can occupy either tetrahedral or octahedral vacant sites of γ-Al_2O_3 and the relative occupancy depends on heat treatment and nickel loading. Figure 10 shows the correlation diagram between the energy levels of the Ni^{2+} free ion and the ion subjected to tetrahedral and octahedral symmetry [17].

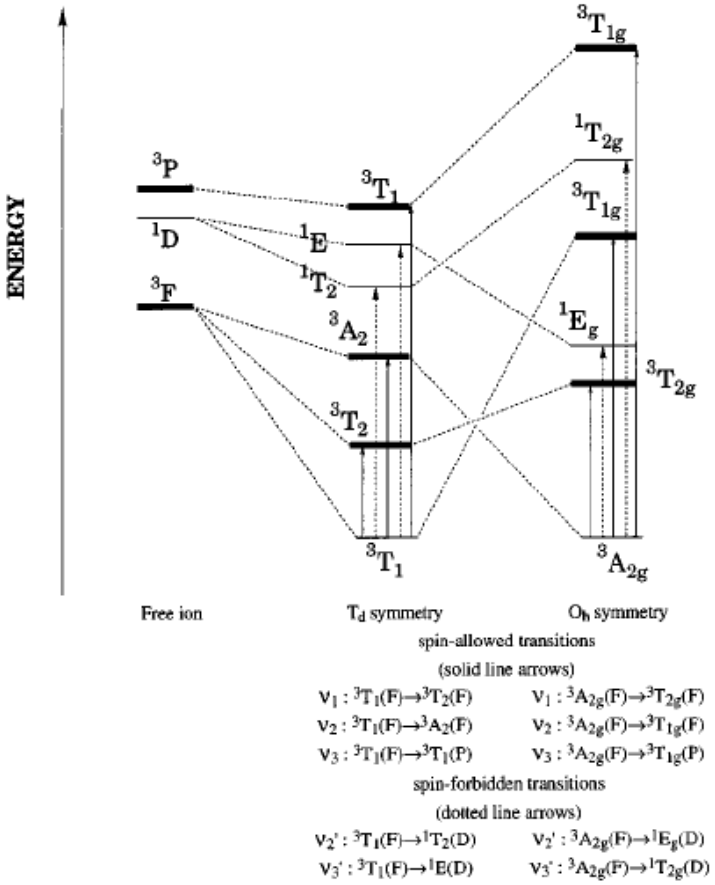

Figure 10. Correlation diagram of Ni^{2+} free ion and ion subjected to octahedral and tetrahedral symmetry. [from Ref:-17]

The three spin-allowed electronic transitions are referred to as ν_1, ν_2, and ν_3, whereas ν'_2 and ν'_3 are spin-forbidden transitions. All these d-d bands are expected to be weak since they are forbidden by the Laporte rule for the nickel(II) in octahedral site. This parity selection rule may, however, be relaxed (i) if any distortion occurs so that the effective group to which the molecule belongs is therefore no longer O_h or (ii) by the mechanism of vibronic coupling, which is in practice most important. The presence of spin-forbidden transitions, such as ν'_2, has been ascribed to the influence of the spin-orbit coupling in "mixing" a spin singlet (^1E_g) with the $^3T_{1g}(F)$ spin triplet, thereby allowing the spin-forbidden transition to gain intensity from the spin-allowed transition. UV- vis DRS spectra of calcined samples are given in Figure 11 and the results are summarized in Table 5.

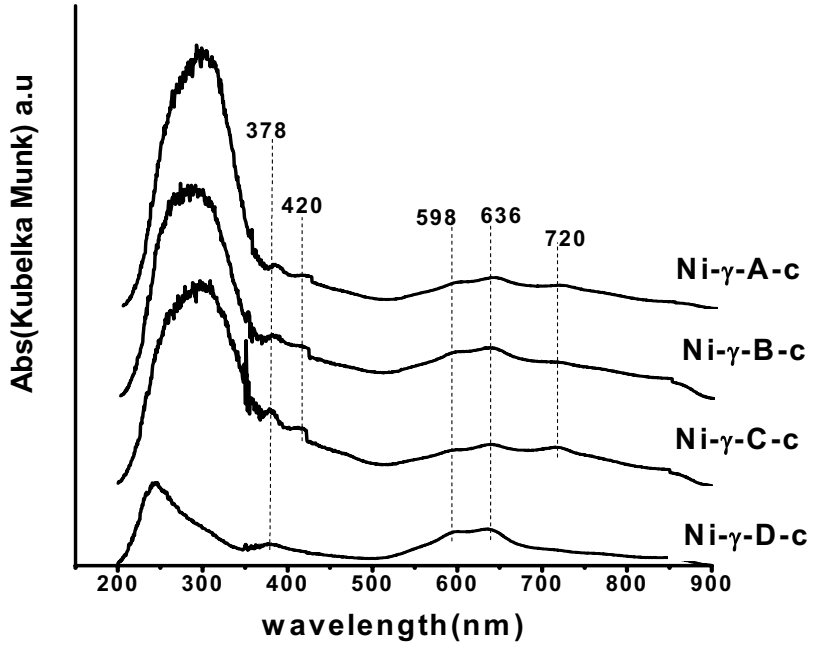

Figure 11. UV-DRS spectra of calcined catalysts

The bands at 598 and 636 nm are indication of Ni^{2+} in tetrahedral sites [9]. All the samples show these bands indicating the presence of Ni^{2+} ions in the tetrahedral vacant sites of γ-Al_2O_3. Even though the XRD studies indicate no $NiAl_2O_4$ formation on Ni-γ-A-c, Ni-γ-B-c, Ni-γ-C-c, the DRS studies clearly suggest the formation of 'surface $NiAl_2O_4$' through the bands at 598 and 636 nm [16]. For Ni-γ-D-c these peaks are of much intense, and in accordance with XRD studies 'bulk $NiAl_2O_4$' formation can be confirmed. The peaks at 420 and 720 nm are characteristics of NiO crystals [18] and they are missing in the spectrum of Ni-γ-D-c. The band at 720 nm arises from octahedral Ni^{2+} in bulk NiO [19]. So the appearance and intensity of this band could give an idea about the presence of bulk unsupported NiO. The bands due to NiO crystals are much pronounced on Ni-γ-C-c, which indicates higher proportion of free NiO in the sample.

7.4 TG-TPR and H_2 chemisorption studies

TPR is a very important characterizing tool to study the metal oxide-support interactions, and catalyst preparation methods can be tuned accordingly. Different types of species and their amounts can be qualitatively and quantitatively identified by this technique. Wu and Hercules identified three different nickel species on NiO/γ-Al_2O_3 catalysts using X-ray photoelectron and ion scattering spectroscopies [20]. Four different species were identified using TPR, XRD and XPS in a recent study by Yang *et al.* [21]. They classified the species as amorphous NiO, crystal NiO, $NiAl_2O_4$ and $NiAl_xO_y$ (x > 2).

Table 5. UV-vis DRS spectral data of the calcined catalysts.

Catalyst	transitions	wavelength 'nm'	Ni species
Ni- γ-A-c	Charge transfer	286	
	$^3A_{2g}\rightarrow{}^3T_{1g}(P)$	378	Ni[O]
	$^3A_{2g}\rightarrow{}^3T_{1g}(F)$	420	Ni[O]
	$^3A_{2g}\rightarrow{}^1E_g$ (D)	714	Ni[O]
	$^3T_1(F)\rightarrow{}^3T_1(P)$	598	Ni[T]
	$^3T_1(F)\rightarrow{}^1E$	636	Ni[T]
Ni- γ-B-c	Charge transfer	286	
	$^3A_{2g}\rightarrow{}^3T_{1g}(P)$	378	Ni[O]
	$^3A_{2g}\rightarrow{}^3T_{1g}(F)$	420	Ni[O]
	$^3A_{2g}\rightarrow{}^1E_g$ (D)	714	Ni[O]
	$^3T_1(F)\rightarrow{}^3T_1(P)$	598	Ni[T]
	$^3T_1(F)\rightarrow{}^1E$	636	Ni[T]
Ni- γ-C-c	Charge transfer	286	
	$^3A_{2g}\rightarrow{}^3T_{1g}(P)$	378	Ni[O]
	$^3A_{2g}\rightarrow{}^3T_{1g}(F)$	420	Ni[O]
	$^3A_{2g}\rightarrow{}^1E_g$ (D)	714	Ni[O]
	$^3T_1(F)\rightarrow{}^3T_1(P)$	598	Ni[T]
	$^3T_1(F)\rightarrow{}^1E$	636	Ni[T]
Ni- γ-D-c	Charge transfer	240	
	$^3A_{2g}\rightarrow{}^3T_{1g}(P)$	378	Ni[O]
	$^3A_{2g}\rightarrow{}^3T_{1g}(F)$	--	--
	$^3A_{2g}\rightarrow{}^1E_g$ (D)	--	--
	$^3T_1(F)\rightarrow{}^3T_1(P)$	598	Ni[T]
	$^3T_1(F)\rightarrow{}^1E$	636	Ni[T]

In the present study we employed TG-TPR to identify the different nickel species. Before going to further discussion, a discussion on the different types of interactions possible between NiO and Al_2O_3 would be useful.

Types of NiO-Al_2O_3 interactions

When any metal oxide and support are contacted together and allowed to react, different types of interactions can occur between them, depending on heat treatment and other conditions. In case of NiO-Al_2O_3 system as Al_2O_3 gets incorporated in to NiO the reduction temperature increases [22]. Depending upon the strength of interaction different TPR peaks will be resulted.

Type 1

If the interaction between NiO and Al_2O_3 is very low, the NiO remains as such (no mixing) and retains its bulk character. In such cases TPR peaks of bulk NiO is expected. However, the reduction characteristics of nickel oxides formed from different precursors will be different because of the changes in crystallite size, strain, defects and morphology. This type of NiO with no interaction is termed as 'free NiO'.

Type 2

During the preparation which involves solution and heat treatment, the small Al_2O_3 particles can migrate inside the bulk NiO structure. This can result in formation of a solid solution in which concentration of bulk NiO is very high. Although the incoming alumina has very low interaction with NiO in such a solid solution, the TPR peaks shifts to higher temperatures due to the electronic interaction of Al^{3+} ions. This solid solution in which NiO is in excess is termed as 'NiO rich NiO-Al_2O_3 solid solution'

Type 3

The another possibility is that during preparation conditions NiO can enter in to the loose surface structure of alumina forming a solid solution of 'Al_2O_3 rich

NiO-Al_2O_3' solid solution. As the concentration of Al_2O_3 is high, the interaction will be more and a TPR peak of higher temperature compared to type 2 is expected. Also during heat treatment, NiO crystallites of very small size can be deposited on the surface of Al_2O_3. Due to the small size of NiO crystallites, their area of interaction with Al_2O_3 will be high, and as a result the strength of interaction increases. The TPR peak again shifts to higher temperature, and this type of sites are termed as 'NiO crystallites supported on alumina surface'. These two species will have almost similar reduction temperatures and are termed as type 3.

Type 4

As the temperature of drying/calcinations increases further, the NiO and Al_2O_3 reacts at the interface forming nickel aluminate. The Ni^{2+} ions should enter the tetrahedral vacant sites of Al_2O_3 to form nickel aluminate, and for this high energy is needed.

$$NiO + Al_2O_3 \rightarrow NiAl_2O_4$$

This nickel aluminate formed on the interfacial surface is termed 'surface nickel aluminate'.

Type 5

The final form of interaction between NiO and Al_2O_3 is the one which results in the formation of 'bulk $NiAl_2O_4$', which is a refractory spinel. More Ni^{2+} ions enter in to the tetrahedral sites of γ- Al_2O_3 to form bulk nickel aluminate. As the vacancies are filled it forms a stable structure. As the nickel ions in the bulk nickel aluminate are very difficult to be reduced, and temperatures higher than 700 °C are generally required. Therefore it is highly recommended to study the TPR patterns of pure compound to identify various types of interactions. In the present study we have recorded the TPR patterns of following reference samples.

i) Pure nickel oxides NiO-A, NiO-B NiO-C and NiO-D obtained from decomposition of complexes (chapter 2)

ii) NiO containing 0.2 mol% of Al_2O_3, (NiO rich-NiO-Al_2O_3 solid solution) prepared by calcining a mixture of nickel nitrate and aluminium nitrate at 600 °C

iii) $NiAl_2O_4$ prepared by solution combustion synthesis (Ni^{2+} = 0.17 M, Al^{3+} = 0.34 M; oxidant/fuel ratio = 1; preparation procedure similar to that of α-Al_2O_3., Chapter 5)

TPR patterns of the reference samples are presented in Figure 12.

The nickel oxides formed from different precursors have different structural and morphological properties [Chapter 2]. It can be seen that the T_{max} (the maximum of DTG peak), $T_{initial}$ (the initial temperature of DTG peak), T_{final} (the final temperature of DTG peak) and ΔT ($T_{final} - T_{initial}$) differ for each samples. The T_{max} of the individual oxides can be used to identify the formation of 'free NiO' in supported systems. Addition of 0.2 mol% of Al_2O_3 shifted the reduction peak to higher temperature [23]. An additional peak at 410 °C is seen corresponding to formation of 'Al_2O_3 rich NiO-Al_2O_3' solid solution. The TPR pattern of 'NiO rich' $NiAl_2O_4$ shows three peaks at 380, 590 and 774 °C corresponding to 'Al_2O_3 rich NiO-Al_2O_3 s-s', 'surface $NiAl_2O_4$' and 'bulk $NiAl_2O_4$'.

Once the reduction temperatures of individual species are determined, they can be used to identify the different species present on an unknown sample. The TPR patterns of the calcined samples are given in Figure 13. The nickel species identified in comparison with Figure 12 are tabulated in Table 6.

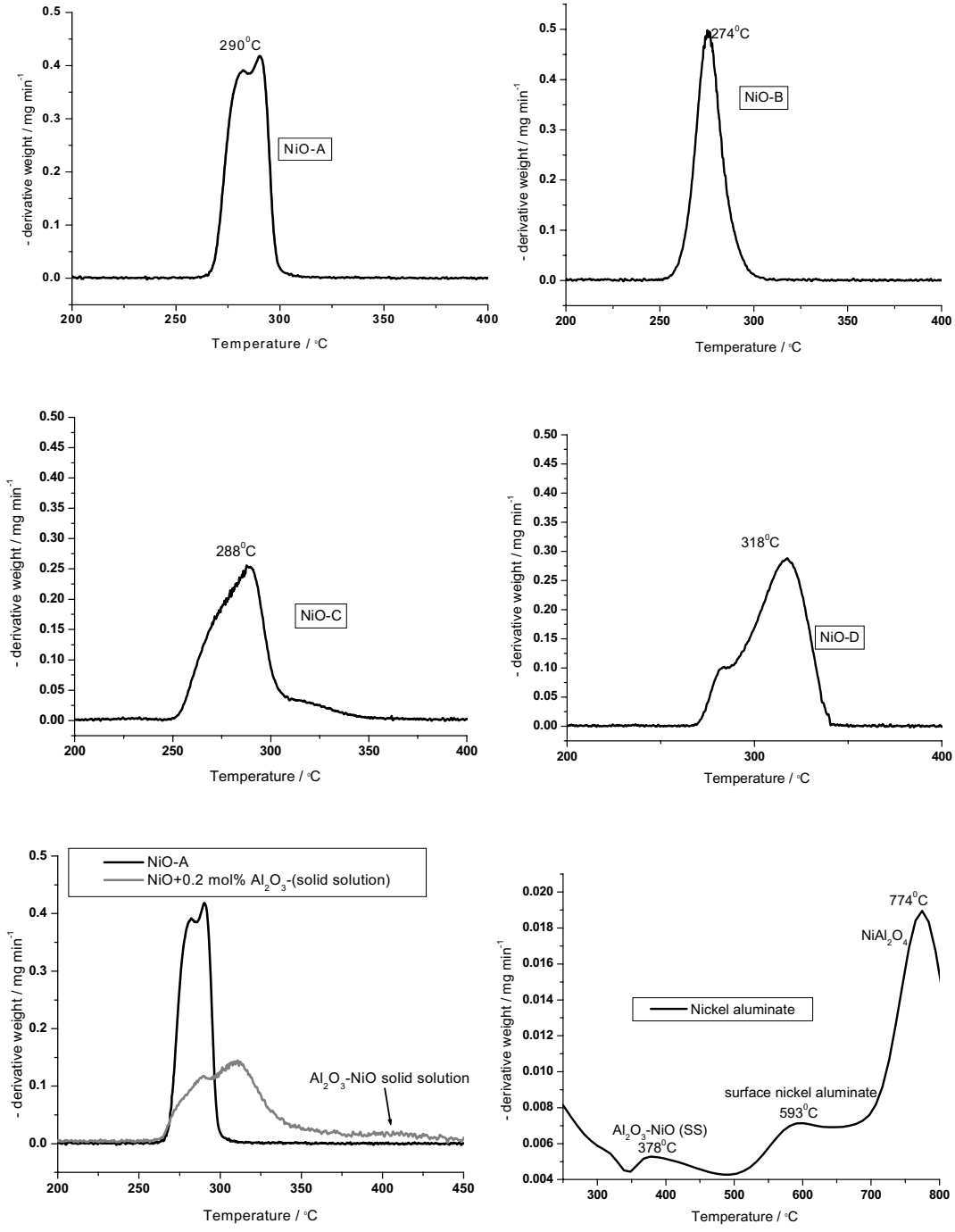

Figure 12. TPR patterns of the reference samples

Large amount of Type 1 species (free NiO) is present on Ni-γ-C-c. This result is in accordance with the UV-DRS results. Type 2 species (NiO rich NiO-Al_2O_3 solid solution) has been formed on catalysts derived from ethylenediamine complexes. The low temperature decomposition of ethylenediamine ligands would have resulted in formation of 'free NiO'. The alumina dissolved in the alkaline impregnating solutions would have migrated to 'free NiO' during the calcinations to form the solid solution. The 'supported NiO crystallites' (Type 3) are present in large amounts on Ni-γ-A-c and Ni-γ-B-c. As crystallite size decreases the interfacial area increases, which increases the metal support interaction and consequently the reduction temperature increases. For Ni-γ-B-c the reduction of type 3 specie starts from 390 °C and extends up to 600 °C. The shoulder at 546 °C corresponds to very small NiO crystallites. The type 4 species ('surface $NiAl_2O_4$') is present on all samples. On samples prepared by ethylenediamine complexes it occurs as a shoulder to the 'bulk $NiAl_2O_4$'-type 5 species. It can be seen that 'bulk $NiAl_2O_4$' has been formed on all samples and also its presence is very high on Ni-γ-D-c. The Ni-γ-D-c had a low reducibility because of the nickel aluminate formation. The different species formed on the catalysts are a direct consequence of the decomposition properties of the dried precursors. As the decomposition temperature increases more and more, Ni^{2+} ions enter the tetrahedral sites of γ-Al_2O_3 forming nickel aluminate. Figure 14 shows a pictorial representation of 5 different species formed on our calcined catalysts.

The results of H_2 chemisorption are given in Table 7. Ni dispersion and Ni specific surface area were high on Ni-γ-B-r catalyst. The surface area was high for the unreduced catalyst. TPR studies indicate the presence of smaller NiO crystallites on the unreduced sample. These smaller NiO crystallites on high surface area alumina can give smaller nickel crystallites on reduction resulting in high nickel dispersion and specific surface area.

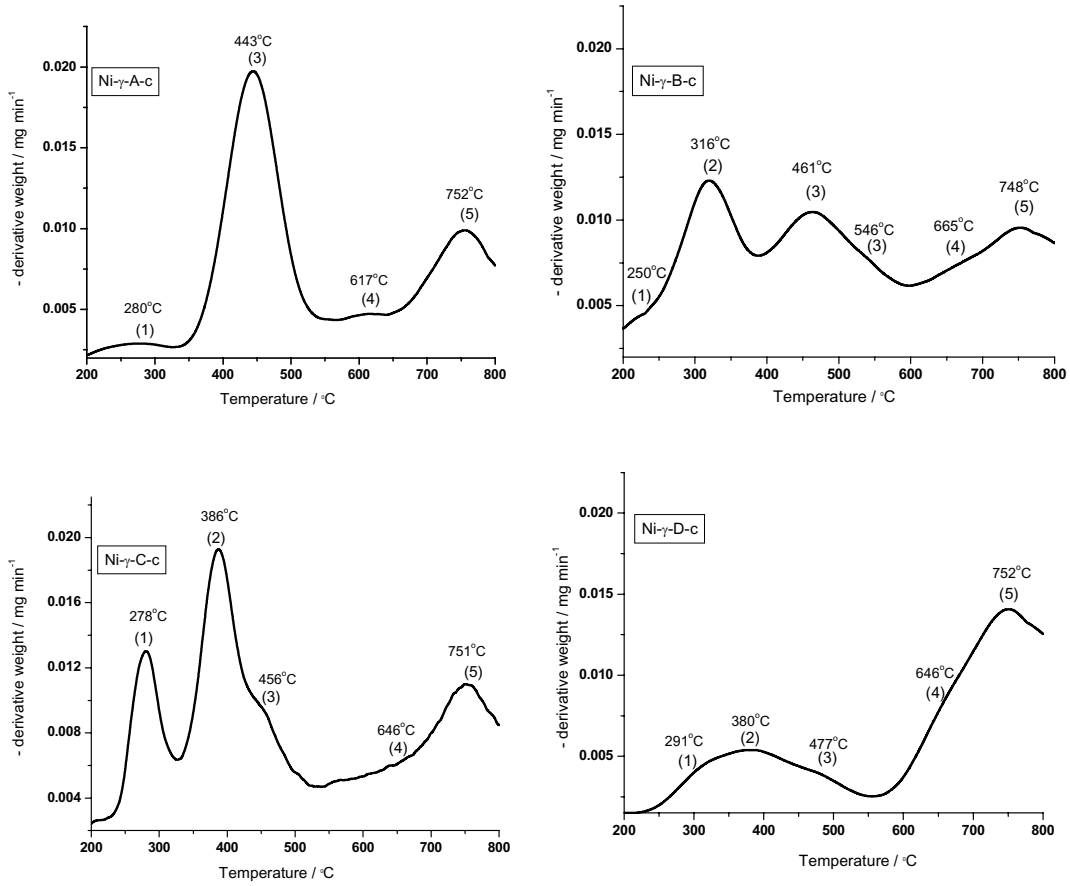

Figure13. TPR patterns of calcined catalysts.

Table 6. Percentage reducibility and reduction temperatures of different species

Catalysts	Reducibility at 800°C (%)	Nickel species Reduction Temperature °C				
		Type 1	Type 2	Type 3	Type 4	Type 5
Ni-γ-A-c	81	280	--	443	617	752
Ni-γ-B-c	84	250	316	461, 546	665	748
Ni-γ-C-c	80	278	386	456	646	751
Ni-γ-D-c	67	291	380	477	646	752

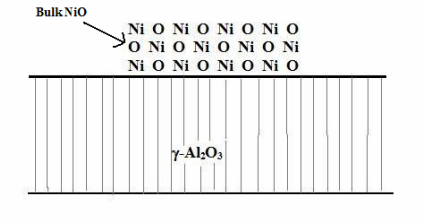

Type 1

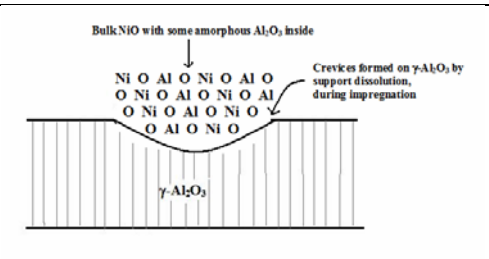

Type 2

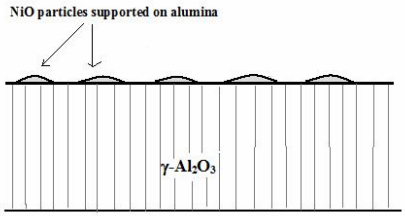

Type 3

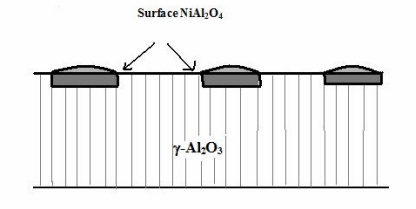

Type 4

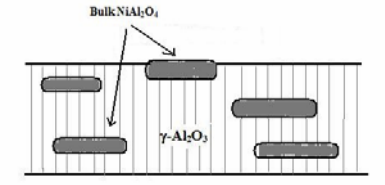

Type 5

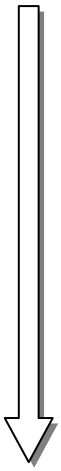

Increase of temperature pushes the Ni^{2+} ions in to the alumina structure

Figure 14. Pictorial representation of different nickel species formed after calcination.

Table 7. H_2 chemisorption results on reduced catalysts

Catalyst	μmols of H_2	% Ni dispersion	Ni surface area $m^2\ gm^{-1}$
Ni-γ-A-r	174	10.5	13.7
Ni-γ-B-r	210	14.7	18.8
Ni-γ-C-r	134	7.7	10.5
Ni-γ-D-r	98	5.7	7.7

7.5 TPD of cyclohexylamine -acidity determination

The Bronsted acid sites present on a sample can be easily estimated by temperature programmed desorption of adsorbed cyclohexylamine [24]. Cyclohexylamine is a strong base (pK_b = 3.3) and can interact with weak and strong acid sites. This method determines the number of protons capable of interacting with the base. The weight loss between 150 °C and 400 °C is used to quantify the acidity in mmol of cyclohexylamine desorbed.

The desorption patterns of support and calcined catalysts are given in Figure 15. The support shows three types of acid sites; whereas in calcined catalysts only two types of acid sites are seen. The introduction of NiO would destroy the stronger acid sites of alumina support. The peaks were deconvoluted to have an idea of different acid sites and the results are shown in Table 8. The total acidity was almost similar to that for the calcined catalysts. Strong acid sites are more on the Ni-γ-D-c; whereas on the other samples weak acid sites are more. Chemical analysis [Table 1] shows that 1.3 wt% of chlorine is present on this catalyst. It is well known that chlorine adsorbed on alumina increases the bronsted acid sites [25]. The strength of acid sites are similar on all catalysts as indicated by desorption peak temperatures.

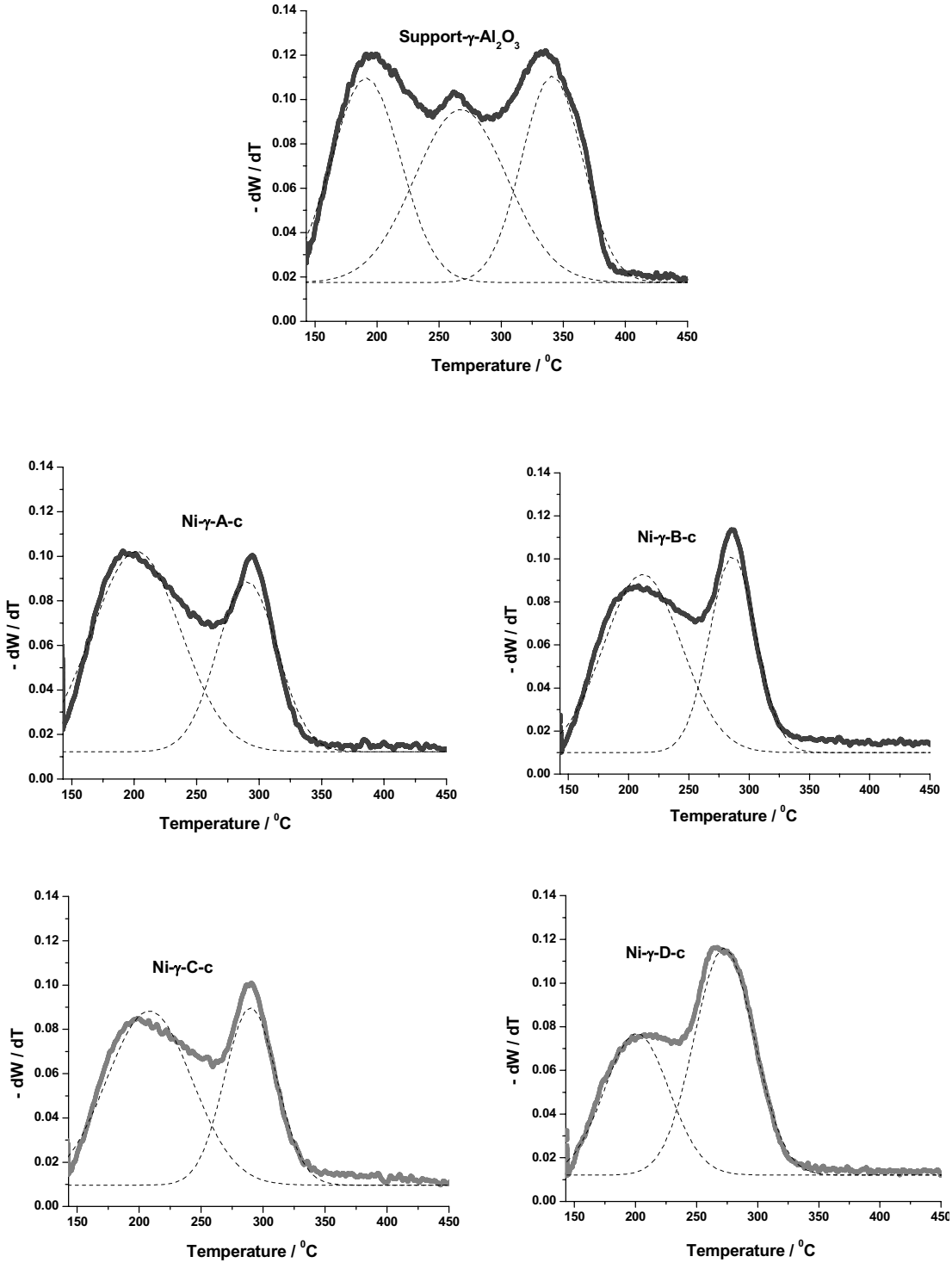

Figure 15. TPD of cyclohexyl amine on support and calcined catalysts.

Table 8. Results of TPD studies

Sample	Total acidity mmol CHA gm^{-1}	% weak acid sites	% strong acid sites
γ-Al_2O_3*	0.496	33	35
Ni-γ-A-c	0.333	70	30
Ni-γ-B-c	0.312	59	41
Ni-γ-C-c	0.313	62	38
Ni-γ-D-c	0.310	39	61

* Support contains 32 % of stronger acid sites

7.6 Cyclohexanol decomposition

Catalytic transformations on group VIII metal catalysts were studied in detail by Dobrovolszky *et al.* [26]. Cyclohexanone was the major product and they classified the metals as selectively d*ehydrogenating* metals and a*romatizing* metals. The aromatizing metals, which include Pt, Pd and Ni, dehydrogenate the cyclohexanone further to phenol. Hydrogenolytic splittic of phenol yields benzene as secondary product. When acidic metal oxides are used, cyclohexene is yielded as the main product from the dehydration pathway. On basic oxides, dehydrogenation is the major reaction pathway and cyclohexanone is obtained as major product [27]. Catalytic system used in the present work involves group VIII metal (Ni) supported on acidic oxide (γ-Al_2O_3). The results of the activity for support and reduced catalysts are given in Table 9.

Table 9. Activity for cyclohexanol decomposition

Catalyst	Conversion (%)	Selectivity (%)				
		cyclohexene	cyclohexanone	benzene	cyclohexane	phenol
Support	56	91.7	8.3	0	0	0
Ni-γ-A-r	60	22.9	67.7	6.1	1.2	2.2
Ni-γ-B-r	76	11.6	76.3	7.0	2.4	2.8
Ni-γ-C-r	68	19.8	65.0	11.8	2.6	0.8
Ni-γ-D-r	78	79.7	16.8	2.5	0.5	0.5

Cyclohexene, cyclohexanone, benzene, cyclohexane and phenol were detected in the product stream. The support (γ-Al_2O_3) had a very high selectivity for cyclohexene because of its high acidity. Reduced catalysts, except Ni-γ-D-r exhibited major selectivity for cyclohexanone. The highest cyclohexanone selectivity was for Ni-γ-B-r which had a high BET surface area and nickel specific surface area. Chlorine present on the Ni-γ-D-r increased the acidity of γ-Al_2O_3 support. TPD studies has revealed that Ni-γ-D-r contains higher proportion of stronger acid sites. Moreover it has lowest nickel specific surface area. These factors contributed towards high cyclohexene selectivity on Ni-γ-D-r. Reaction Scheme 1 shows the different routes to product formation on the active sites of the catalysts.

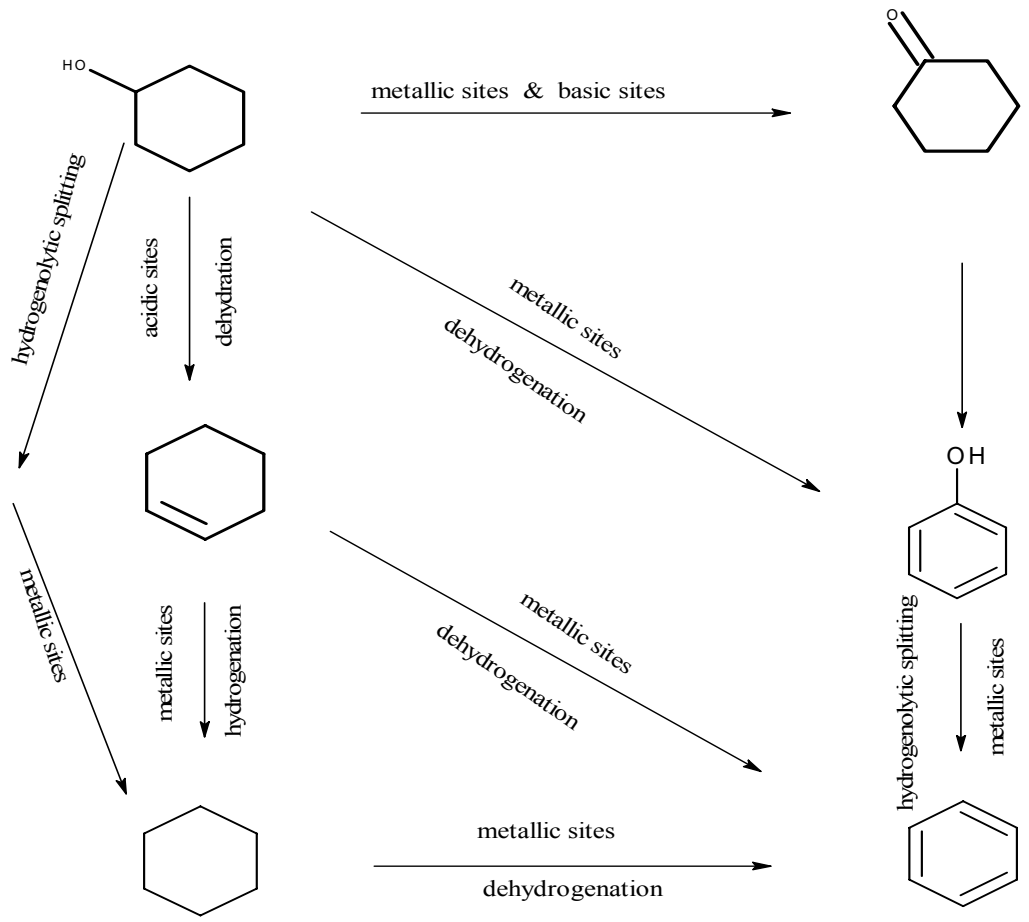

Scheme 1. Reaction routes of cyclohexanol decomposition on reduced catalysts.

Benzene formation was high on Ni-γ-C-r. According to Scheme 1 benzene can be formed either by dehydrogenation-hydrogenation pathway from cyclohexene or by hydrogenolytic splitting of phenol. Based on the temperature, reaction conditions (inert atmosphere) and product distribution obtained, the more probabilistic pathway for benzene formation would be dehydrogenation of cyclohexene. If we compare Ni-γ-A-r and Ni-γ-C-r, both had similar selectivity for cyclohexene and cyclohexanone. But the higher selectivity for benzene implies that Ni-γ-C-r had different sites for cyclohexene dehydrogenation. This was confirmed by cyclohexane dehydrogenation reaction discussed in the next section.

7.7 Dehydrogenation of cyclohexane

Cycloalkane dehydrogenation reactions are technologically important as they can be used for storage and transportation of hydrogen at room temperature. The high hydrogen content in cycloalkanes makes them attractive feed stock for dehydrogenation processes. The endothermal (ΔH = 49.3 kcal mol^{-1}) cyclohexane dehydrogenation to benzene has been studied over Ni/Al_2O_3 catalysts [28].

The dehydrogenation activities of the reduced catalysts are shown in Figure 16.

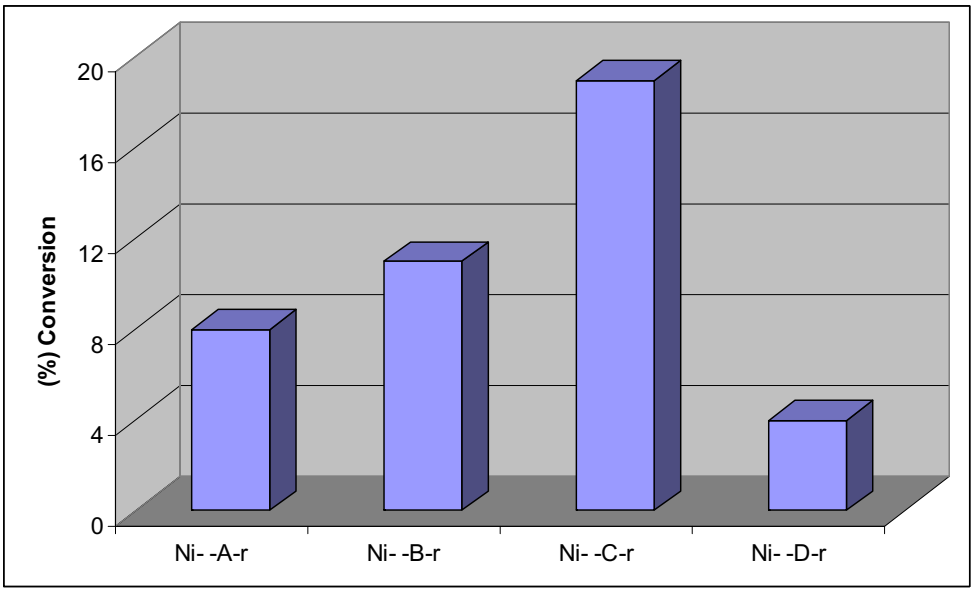

Figure 16. Percentage conversions for cyclohexane dehydrogenation on reduced catalysts

The catalysts were selective towards benzene and trace amounts of methane formed were neglected [29, 30].

The Ni-γ-C-r catalyst had the highest dehydrogenation activity. The catalyst with high nickel specific surface area, Ni-γ-B-r had only moderate activity for the reaction. But it had a high selectivity and conversion of cyclohexanol decomposition. This clearly indicates that the active sites for both reactions are different. Metallic nickel crystallites generated from reduction of bare NiO clusters are reported to have high activity in hydrogenation-dehydrogenation [6]. TPR studies have shown high

proportion of bulk NiO formation on Ni-γ-C-c. Up on reduction, this bulk NiO clusters would have generated highly active metallic nickel crystallites responsible for high dehydrogenation activity.

7.8 Conclusions

i.) Thermal decomposition studies show that Ni-γ-B-d (derived from the complex with nitrate counter ion) decomposed in a short temperature range, while Ni-γ-D-d (derived from the complex with chloride counter ion) decomposed slowly.

ii.) The decomposition properties are very crucial, as they had a profound influence on the final structure and activity of catalyst.

iii.) During calcination, bulk nickel aluminate was formed on Ni-γ-D-c (derived from the complex with chloride counter ion).

iv.) The use of nitrate counter ion resulted in the formation of catalysts with high BET surface area, high nickel surface area and low nickel aluminate.

v.) Five different nickel species were detected by TPR studies on the calcined catalysts.

vi.) The acetate counter ion resulted in formation of free (bulk) NiO.

vii.) The model reactions studied indicates aromatic hydrogenation-dehydrogenation sites are different from sites for cyclohexanol dehydrogenation.

References

[1] A.B Stiles., *Catalyst manufacture*., 1983 Marcel Dekker Inc, New York

[2] R. Yang, X. Li, J. Wu, X. Zhang, Z. Zhang., Promotion effects of copper and lanthanum oxides on nickel/gamma-alumina catalyst in the hydrotreating of crude 2-Ethylhexanol., *J. Phys. Chem. C.* 113 (2009) 17787–17794

[3] K.V.R. Chary, P.V.R. Rao, V.V. Rao., Catalytic functionalities of nickel supported on different polymorphs of alumina., *Catal. Commun.* 9 (2008) 886–893

[4] E. Ruckenstein, Y.H. Hu., Role of Support in CO_2 reforming of CH_4 to syngas over Ni Catalysts., *J. Catal.* 162 (1996) 230-238

[5] J. G. Seo, M.H. Youn, S. Park, Ji. C. Jung, P. Kim, J. S. Chung, In.K. Song., Hydrogen production by steam reforming of liquefied natural gas (LNG) over nickel catalysts supported on cationic surfactant-templated mesoporous aluminas., *J. Power Sources.* 186 (2009) 178–184

[6] K.B. Kester, E. Zagli, J. L. Falconer., Methanation of carbon monoxide and carbon dioxide on Ni/Al_2O_3 catalysts: Effects of Nickel loading., *Appl. Catal.* 22 (1986) 311-319

[7] Y. Schuurman, V. Ducarme, T. Chen, W. Li, C. Mirodatos, G.A. Martin., Low temperature oxidative dehydrogenation of ethane over catalysts based on group VIII metals., *Appl. Catal. A: General* 163 (1997) 227-235

[8] F. Cardenas-Lizana, S. Gomez-Quero, M.A. Keane., Clean production of chloroanilines by selective gas phase hydrogenation over supported Ni catalysts., *Appl. Catal. A: General* 334 (2008) 199–206

[9] E. Heracleous, A.F. Lee, K. Wilson, A.A. Lemonidou., Investigation of Ni-based alumina-supported catalysts for the oxidative dehydrogenation of ethane to ethylene: structural characterization and reactivity studies., *J. Catal.* 231 (2005) 159–171

[10] S. Schimpf, C. Louis, P. Claus., Ni/SiO_2 catalysts prepared with ethylenediamine nickel precursors: Influence of the pretreatment on the catalytic properties in glucose hydrogenation *Appl. Catal. A: General.* 318 (2007) 45-53

[11] F. Negrier, E. Marceau, M. Che, J.M. Giraudon, L. Gengembre, A. Lofberg., A systematic study of the interactions between chemical partners (metal, ligands, counterions, and support) involved in the design of Al_2O_3-supported nickel catalysts from Diamine−Ni(II) chelates., *J. Phys. Chem. B.* 109 (2005) 2836-2845

[12] K.Q. Sun, E. Marceau, M. Che., Evolution of nickel speciation during preparation of $Ni–SiO_2$ catalysts: effect of the number of chelating ligands in $[Ni(en)_x(H_2O)_{6-2x}]^{2+}$ precursor complexes., *Phys. Chem. Chem. Phys.* 8 (2006) 1731-1738

[13] F. Negrier, E. Marceau, M. Che, J-M. Giraudon, L. Gengembre, A. Lofberg., From Al_2O_3-supported Ni(II)-ethylenediamine complexes to CO hydrogenation catalysts:

Importance of the hydrogen post-treatment evidenced by XPS., *Catal. Lett.* 124 (2008) 18–23

[14] K. S. W. Sing, D. H. Everett, R. A. W. Haul, L. Moscou, R. A. Pierotti, J. Rouquerol, T. Siemieniewska., Reporting physisorption data for gas/solid systems with special reference to the determination of surface area and porosity., *Pure & App. Chem*. 57 (1985) 603-619

[15] G. Trimmel, C. Lembacher, G. Kickelbick and U. Schubert., Sol-gel processing of alkoxysilyl-substituted nickel complexes for the preparation of highly dispersed nickel in silica., *New J. Chem*., 26 (2002) 759–765

[16] M. Lo Jacono, M. Schiavello, and A. Cimino., Structural, Magnetic, and Optical Properties of Nickel Oxide Supported on η- and γ-Aluminas., *J. Phys. Chem.* 76 (1971) 1044-1050

[17] Lever, A. B. P. *Inorganic Electronic Spectroscopy, 2nd ed.;* Studies in Physical Theoretical Chemistry, Vol. 33; Elsevier: Amsterdam, 1984, pg. 82

[18] J. Wang, L. Dong, Y. Hu, G. Zheng, Z. Hu, Y. Chen., Dispersion of NiO Supported on γ-Al_2O_3 and TiO_2/γ-Al_2O_3 Supports., *J. Solid State Chem.* 157 (2001) 274-282

[19] Schoonheydt, R. A. In *Characterization of Heterogeneous Catalysts*; Delannay, F., Ed.; Marcel Dekker: New York, 1984; p 151

[20] M. Wu, D.M. Hercules., Studies of Supported Nickel Catalysts by X-Ray Photoelectron and Ion Scattering Spectroscopies., *J.Phys. Chem.* 83 (1979) 2003-2008

[21] R. Yang, X. Li, J. Wu, X. Zhang, Z. Zhang, Y. Cheng, J. Guo., Hydrotreating of crude 2-ethylhexanol over Ni/Al_2O_3 catalysts: Surface Ni species-catalytic activity correlation., *Appl. Catal. A: General.* 368 (2009) 105–112

[22] J.T. Richardson, B. Turk, M. Lei, K. Forster, M.V. Twigg., Effects of promoter oxides on the reduction of nickel oxide., *Appl. Catal. A: General.* 83 (1992) 87-101

[23] M.V. Twigg, J.T. Richardson., Effects of alumina incorporation in coprecipitated $NiO–Al_2O_3$ catalysts., *Appl. Catal. A: General.* 190 (2000) 61–72

[24] R. Mokaya, W. Jones, Z. Luan, M.D. Alba, Jacek Klinowski., Acidity and catalytic activity of the mesoporous aluminosilicate molecular sieve MCM-41., *Catal. Lett.* 37 (1996) 113-120

[25] A. V. Jain, N. C. Pradhan, A. K. Dalai, N. N. Bakhshi., Studies on Chlorided Pt/Al_2O_3 Catalysts: Preparation, Characterization and *n*-Butane Isomerization Activity., *Catal. Lett.* 86 (2003) 221-227

[26] M. Dobrovolszky, P. Tetenyi, Z. Paal., Catalytic Transformations of Cyclohexanol on Group VIII Metal catalysts., *J. Catal.* 74 (1982) 31-43

[27] C.P. Bezouhanova, M.A. Al-Zihari., Cyclohexanol conversion as a test of the acid-base properties of metal oxide catalysts., *Catal. Lett.* 11 (1991) 245-248

[28] P. H. Desai, J. T. Richardson., Crystallite size effects in nickel catalysts: Cyclohexane dehydrogenation and hydrogenolysis., *J. Catal.* 98 (1986) 392-400

[29] J. Escobar, J.A. De Los Reyes, T. Viveros, M.C. Barrera.,Cyclohexane Dehydrogenation over Wet-Impregnated Ni on Al_2O_3-TiO_2 Sol-Gel Oxides., *Ind. Eng. Chem. Res.* 45 (2006) 5693-5700

[30] G. Perez, T. Viveros., Hydrogenation and Dehydrogenation of Hydrocarbons Over Ni Supported on Alumina- and Silica-Promoted Titania. In *Studies of Surface Science and Catalysis*; A.Corma, F.V. Melo, S.Mendioroz, J.L.G. Fierro., Eds.; Elsevier: Amsterdam, 2000; Vol.130, p 2501

……✸…….

Chapter 8

STRUCTURE AND REACTIVITY OF Ni/MgO CATALYSTS.

Contents

8. INTRODUCTION

The discovery of natural gas reserves world wide during the last decades has renewed the interest to convert natural gas to more value added products. The major component of natural gas is methane which is the least reactive hydrocarbon and this fact makes the up gradation of natural gas a difficult task. Oxidative coupling of methane to heavier hydrocarbons was considered to be an attractive route, but the high rate of CO_2 formation which is thermodynamically more favorable, makes it economically and environmentally non-feasible. Now attention has been focused to the indirect process of converting methane to syngas, followed by Fischer-Tropsch and methanol syntheses. The three major catalytic routes for conversion of methane to syngas are

i) steam reforming $CH_4 + H_2O \rightarrow CO + 3H_2$ $\Delta H^0_{298} = 206$ kJ mol^{-1}

ii) partial oxidation $CH_4 + 1/2O_2 \rightarrow CO + 2H_2$ $\Delta H^0_{298} = -36$ kJ mol^{-1}

iii) CO_2 reforming $CH_4 + CO_2 \rightarrow 2CO + 2H_2$ $\Delta H^0_{298} = 247$ kJ mol^{-1}

The carbon dioxide reforming also called as dry reforming is of a great interest for environmental protection, since the reaction consumes two important green house gases, to convert them in to more valuable chemicals [1, 2].

Moreover the gas fields which contain a higher CO_2 content could be directly used as the feed stock. Although Ni catalysts and noble metals have been reported to be active for this reaction, former is considered to be more feasible due to availability and economic considerations. Despite of many years of research no adequate technology could be developed for the process of CO_2 reforming. Coking is the main problem which quickly deactivates the catalysts when operated in absence of steam. Coking or carbon deposition occurs at high rate when metal clusters of catalysts are of higher size and when support used is acidic in nature. The acidity of support can be controlled by choosing a basic oxide like MgO, CaO or BaO. A strong interaction between the reduced metal and the support can stabilize the size of metal clusters and prevent coke formation. MgO is a support which can provide good interaction with nickel metal clusters and very often the supported nickel particles formed are of low size. Nickel-support interaction will be high when NiO forms a solid solution with the support. The lattice constant of MgO is very close to that of NiO which makes it an ideal choice of support which forms solid solution.

Supported nickel catalysts are highly active for hydrogenation of aromatics, alkenes and carbonyl compounds. MgO is a highly basic oxide (pKa = 26) which can catalyze the aldol condensation reactions [3]. The product of aldol condensation usually the α, β unsaturated aldehyde can be hydrogenated if a metal catalyst is present and hydrogen is available. If one could combine the aldol condensation properties of MgO and hydrogenation properties of Ni metal by making a Ni/MgO catalyst, higher aldehydes can be synthesized in a single step starting from lower aldehyde and hydrogen. Ni/MgO catalysts are already known to be active for one step preparation of methyl isobutyl ketone (MIBK) from acetone and hydrogen gas [4]. Bergada *et al.* reported a clean obtention of 2-phenyl ethanol on Ni/MgO catalysts by styrene oxide hydrogenation owing to the basic character of MgO [5].

The ease of solid solution formation between NiO and MgO is sometimes disadvantageous as most of the nickel becomes irreducibile when a true solid solution forms, thus making them non usuable [6].

Thus, synthesis of Ni/MgO catalysts, which are highly reducible, is a difficult task. In the present chapter the structure of Ni/MgO catalysts prepared with the ethylenediamine complexes is discussed in the first part. The activity of these catalysts for cyclohexanol decomposition and reactions of n-butyraldehyde with hydrogen are discussed in the second part.

8.1 Chemical analysis, surface area of calcined samples and thermal decomposition of dried precursors

The results of chemical analysis and surface area on calcined materials are given in Table 1. The results of thermal decompositions of dried precursors are illustrated in Figures 1 to 5.

Table 1. Results of chemical analysis and BET surface area of the calcined catalysts

	Ni (weight) %	**Cl (weight) %**	**Surface area $m^2\ gm^{-1}$**
Support	--	--	25
Ni- *M* –A-c derived from $[Ni(H_2O)_6](NO_3)_2$	20.3	--	22
Ni- *M* –B-c derived from $[Ni(en)_2(H_2O)_2](NO_3)_2$	20.5	--	41
Ni- *M* –C-c derived from $[Ni(en)_2(H_2O)_2](CH_3COO)_2$	19.7	--	34
Ni- *M* –D-c derived from $[Ni(en)_2(H_2O)_2]Cl_2$	20.1	0.5	15

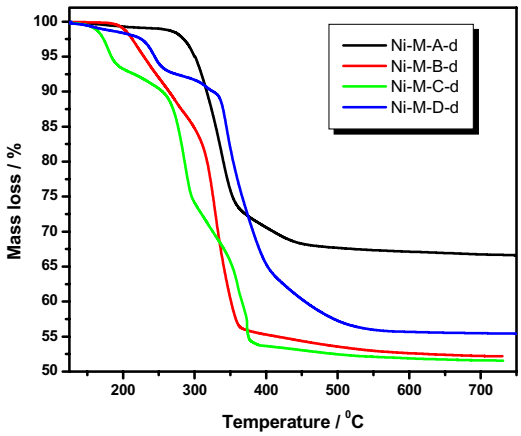

Figure 1. TG curves of dried precursors

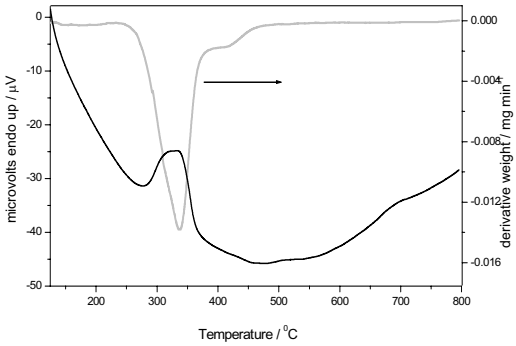

Figure 2. DTG-DTA of Ni-M-A-d

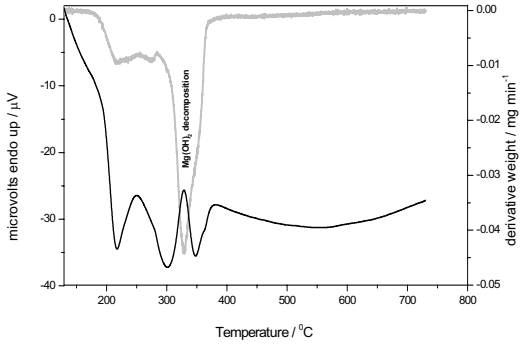

Figure 3. DTG-DTA of Ni-M-B-d

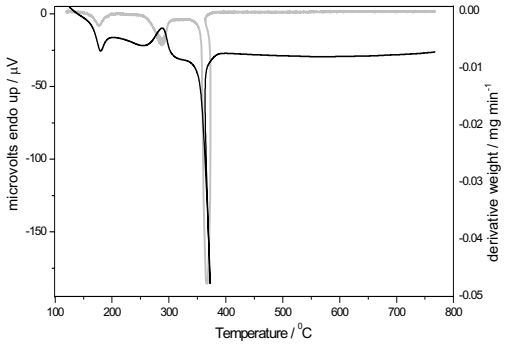

Figure 4. DTG-DTA of Ni-M-C-d

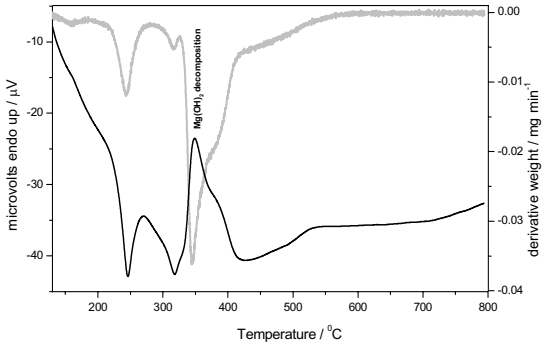

Figure 5. DTG-DTA of Ni-M-D-d

The most widely studied procedures to obtain NiO catalytic precursors are through the decomposition of nickel nitrate hexahydrate [7]. When the decomposition is done under static atmosphere, the surface area obtained is much

less, because of the sintering of magnesia due to the significant pressure of water vapor over the sample [8]. MgO is a highly hygroscopic material and readily forms $Mg(OH)_2$ or 'hydrated magnesia' when contacted with water [9, 10].

$$MgO + H_2O \rightarrow Mg(OH)_2$$

Considering our preparation condition (which involves contacting MgO with aqueous solutions of nickel complexes); the dried precursor will be a mixture of hydrated magnesia and nickel complex. Thus the reaction happening during calcinations can be written as

$$Mg(OH)_2 + \text{Ni complex} \rightarrow MgO + NiO + NiMgO_2$$

Hydrated magnesia decomposes (endothermic) at ≈ 325 °C. Depending upon the decomposition temperature of the nickel complex three conditions can arise

i) Ni complex decomposes before decomposition of hydrated magnesia
ii) Ni complex decomposes together with hydrated magnesia
iii) Ni complex decomposes after decomposition of hydrated magnesia

When the Ni complex decomposes early, the MgO formed by decomposition of hydrated magnesia will cover the already formed NiO. The formed NiO will be then embedded inside MgO. If the Ni complex decomposes after the formation of MgO, the NiO will be deposited on the outer surface of MgO and formation of free NiO could not be avoided.

In the case of simultaneous decomposition, intermediate interactions between NiO and MgO would be expected. The TG of dried precursors for are given in Figure.1 and DTG-DTA patterns are given in Figure 2 to 5 Inspection of the TG pattern (Figure 1) shows that the precursor Ni-M-B-d decomposes completely at 365 °C. The DTG-DTA pattern of Ni-M-B-d shows that much of the complex has been decomposed prior to decomposition of hydrated magnesia. For Ni-M-C-d and Ni-M-D-d, the most part of the nickel complex decomposes after the decomposition of

hydrated magnesia, whereas for Ni-M-A-d simultaneous decomposition occurs. Moreover for Ni-M-D-d the decomposition is complete only at a higher temperature of 550 °C. The surface area results (Table 1) is a direct consequence of this decomposition patterns. The higher surface area of Ni-M-B-c is due to the early decomposition of nickel complex at lower temperatures. The decomposition of Ni-M-D-d at high temperatures (after decomposition of hydrated magnesia) reduces its surface area. The water vapor and other gases evolved at higher temperatures sinters the magnesia, reducing its surface area [11].

8.2 XRD studies – indication of solid solution formation

NiO and MgO have identical structures (rock salt – simple cubic) and the ionic radii of Ni^{2+} and Mg^{2+} are very close (Ni^{2+} = 69 picometer; Mg^{2+} = 72 picometer). Their lattice parameters are very close (NiO = 4.1684 Å; MgO = 4.2212 Å). For these reasons, the two oxides can easily form solid solutions in which the ratio between the components can vary without disturbing the homogeneity. In a MgO crystal, when Ni^{2+} diffuses in to the lattice the diffraction peaks of MgO slightly shift to higher angles. When Mg^{2+} diffuses to NiO crystal lattice, the diffraction peaks of NiO shift to lower angles. As solid solution forms, the individual XRD peaks of NiO and MgO merges together.

The XRD patterns of calcined samples are shown in Figure 6. No doublets are seen at respective 2θ values which indicate solid solution formation on all the samples. Figure 7 shows the expanded view of (200) peak which clearly shows the diffraction angles of samples are in between that of MgO (200) and NiO (200). The 2θ values given in Table 2 clearly indicate the formation of solid solution.

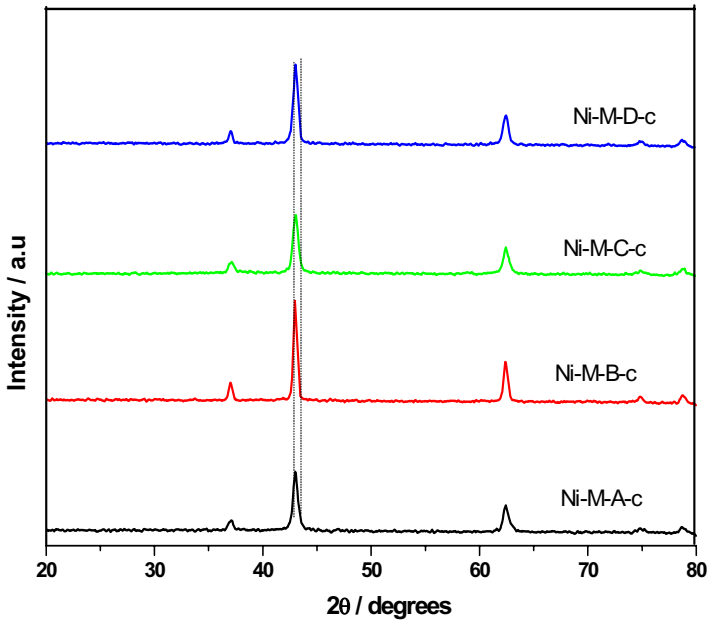

Figure 6. XRD patterns of calcined samples

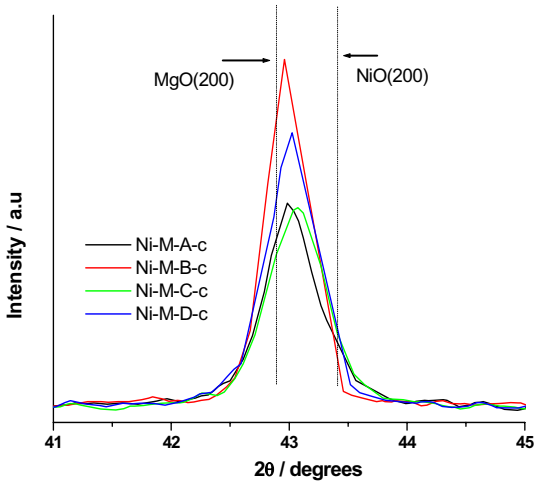

Figure 7. Expanded view of (200) peak of solid solution

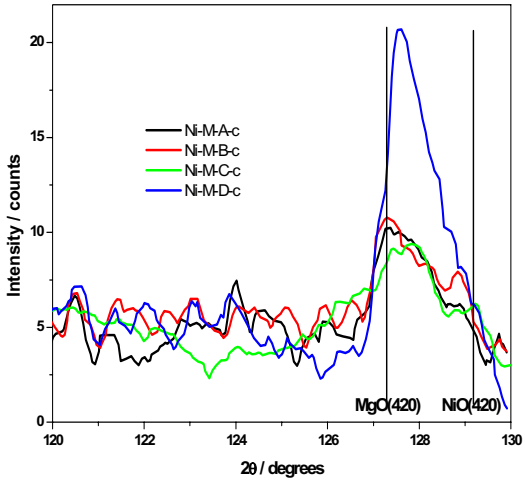

Figure 8. High angle XRD of (420) peak of solid solution

Table 2. Diffraction angles of MgO, NiO and calcined catalysts

d_{hkl}	MgO	NiO	Ni-M-A-c	Ni-M-B-c	Ni-M-C-c	Ni-M-D-c
(111)	37.003	37.453	37.102	36.996	37.146	37.058
(200)	42.901	43.454	42.985	42.961	43.075	43.025
(220)	62.325	63.010	62.425	62.360	62.455	62.462
(311)	74.576	75.510	74.778	74.750	74.885	74.755
(222)	78.616	79.503	78.670	78.700	78.900	78.764

An XRD pattern was recorded at high 2θ (120° to 130°) and the results are shown in Figure 8. For Ni-M-D-c, the MgO (200) peak has been shifted to 127.58° which clearly indicate diffusion of Ni^{2+} to MgO lattice. No peak of NiO(420) could be detected indicates the absence of the free NiO or the formation of a complete solid solution. The peak height shows the sample is well crystalline. For Ni-M-B-c sample, the MgO (420) peak occurs at the theoretical value but the NiO (420) peak has shifted to lower angles (128.84°). This indicates the migration of Mg^{2+} ions to NiO lattice. Such a structure is termed as NiO based NiO-MgO solid solution [12]. Samples Ni-M-A-c and Ni-M-C-c show intermediate values indicating formation of free NiO and MgO based NiO-MgO solid solution.

The thermal decomposition studies of Ni-M-B-d have shown that the nickel complex decomposes earlier than hydrated magnesia. The hydrated magnesia decomposes over the formed NiO forcing some of Mg^{2+} ions to enter in to the NiO lattice. The high temperature decomposition of Ni-M-D-d has facilitated the NiO-MgO solid solution formation.

8.3 TPR and H_2 chemisorption studies

When NiO and MgO are contacted together and allowed to react, different types of interactions can occur depending up on the heat treatment. Reducibility of Ni^{2+} in NiO–MgO solid solution depends on the position of Ni^{2+} in MgO lattice and the interaction between Ni^{2+} and MgO [13]. Reduction peak of NiO generally occurs

in the range 400 °C to 450 °C under hydrogen atmosphere with a heating rate of 10 °C min^{-1}. As Ni^{2+} ions migrate to MgO lattice, its reduction temperature increases.

The TPR patterns of the four calcined samples are shown in Figure 9. The peaks were deconvoluted to have an idea of the different species present in the samples. Reduction patterns indicate that reduction is not complete even at a high temperature of 950 °C.

The percentage of 'reducible nickel' present on samples were calculated at 950 °C and 550 °C from the peak areas (after TCD calibration). The summary of TPR results is given in Table 3. The reduction temperatures of different species are tabulated.

Species 1 is 'free NiO', or bulk NiO crystallites with negligible interaction with MgO. The reduction temperature corresponds to that of bare NiO [7]. As some Mg^{2+} ions enter in to the NiO lattice, the reduction temperature of NiO increases as Mg^{2+} retards the reduction of NiO by its electropositive character [14]. This species can be termed as NiO based NiO-MgO solid solution and is named as species 2. The species 3 corresponds to small NiO crystallites supported on MgO. Zecchina *et al.* assigns this species as 5 coordinated square pyramidal Ni ions [15]. When the NiO crystallites are small in size the interfacial area between NiO and MgO will be high resulting in high interaction between them. The peak maxima of this species give an idea of size of nickel crystallites. The results from Table 3 and Figure 9, implies that Ni-M-B-c contains a large number of smaller NiO crystallites, when compared to other catalysts.

During impregnation Ni^{2+} ions can diffuse in to MgO lattice and form solid solution. When Ni^{2+} moves in to the sub surface region of MgO, Ni^{2+} is surrounded wholly by Mg ions and the reduction temperature increases. This species assigned as species 4 corresponds to MgO based NiO-MgO solid solution. Its reduction happens between 800 °C and 900 °C. At high temperatures of calcinations, the above solid solution changes to almost crystalline and can be termed as complete or true solid solution (species 5).

The description of different species and the temperature ranges of their reduction can be given as follows.

Description	'Free or Bulk NiO'	'NiO based NiO-MgO solution'	'surface NiO'	'MgO based NiO-MgO solution'	'true solid solution'
Ni species	Type 1	Type 2	Type 3	Type 4	Type 5
Temp range	300-500 °C	500-600 °C	600-800 °C	800-900 °C	> 950 °C

The Ni^{2+} corresponding to this species are situated deeply inside the MgO lattice and high reduction temperatures are necessary for hydrogen gas to reach these Ni^{2+} ions. Based on the above discussion the highlights of TPR results can be summarized as follows.

i.) The percentage reducibility is more for Ni-M-B-c.

ii.) Species 1 (free or bulk NiO) is almost absent in Ni-M-B-c.

iii.) The presence of reduction peaks above 500 °C is an indication of solid solution formation [12].

iv.) The formation of NiO based NiO-MgO solid solution (species 2) is evident for Ni-M-B-c which is in agreement with the XRD results.

v.) A large number of smaller NiO crystallites (species 3) are formed on Ni-M-B-c.

vi.) Ni-M-D-c has very low reducibility, and its reduction peaks indicate formation of true solid solution (species 5). This result is also in accordance with XRD results.

vii.) Species 4 (MgO based NiO-MgO solid solution) is present in all catalysts.

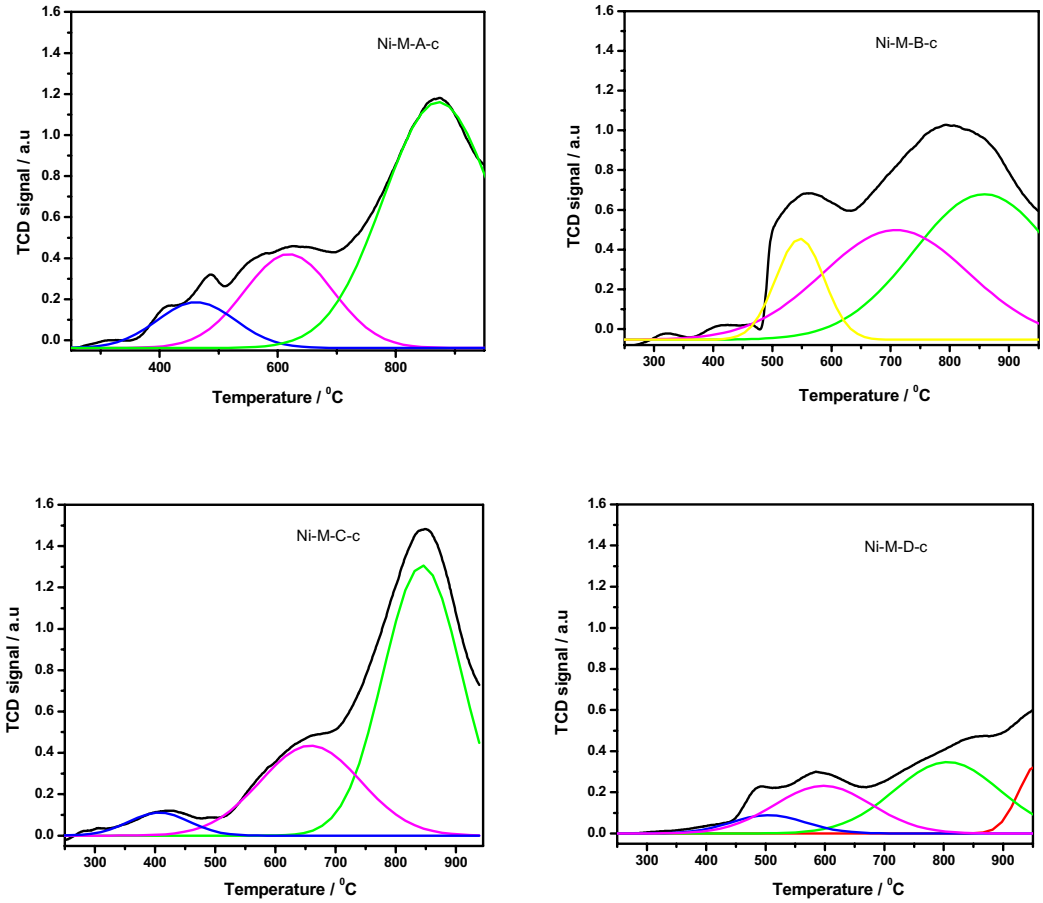

Figure 9. TPR patterns of calcined catalysts

Table 3. Reducibility of catalysts and peak maxima of different species

Catalysts	Reducibility at 950 °C (%)	Reducibility at 550 °C (%)	Nickel species				
			1	2	3	4	5
Ni-M-A-c	64	48	463		624	871	
Ni-M-B-c	75	60		549	710	860	
Ni-M-C-c	67	36	407		658	849	
Ni-M-D-c	32	21	488		602	810	>950

The results of H_2 chemisorption on the reduced (550 °C for two hours) catalysts are given in Table 4.

Table 4. H_2 Chemisorption results on reduced catalysts

Catalyst	μmols of H_2	% Ni dispersion	Ni surface area m^2 gm^{-1}
Ni-M-A-r	38	2.2	3.0
Ni-M-B-r	73	4.2	5.7
Ni-M-C-r	28	1.6	2.2
Ni-M-D-r	15	0.86	1.2

Ni dispersion and Ni specific surface area were high on Ni-M-B-r catalyst. The high BET surface area, high reducibility and large amount of supported NiO crystallites (species 3) are the reasons for the high Ni specific surface area of this catalyst.

8.4 TPD of CO_2 - basicity determination

Studies had already revealed that MgO surface contains Lewis basic sites with different electron pair donor (EPD) strength [16]. Three types of basic sites namely, low strength, medium strength and high strength, are classified on MgO surface depending on the adsorption modes of carbon dioxide. Adsorbed CO_2 forms bicarbonate species on low strength basic site, while bidentate carbonate and mono dentate carbonate are formed on medium and high strength basic sites respectively [17]. The TPD spectra of the support (MgO) and samples are given in Figure 10 and the results are summarized in Table 5.

In general the pattern consists of two peaks, (i) a low temperature peak corresponding to desorption of bicarbonate species and (ii) a high temperature peak corresponding to desorption of various carbonate species. The amount of CO_2 desorbed is high on Ni-M-B-c catalyst, which may be because of its high surface area.

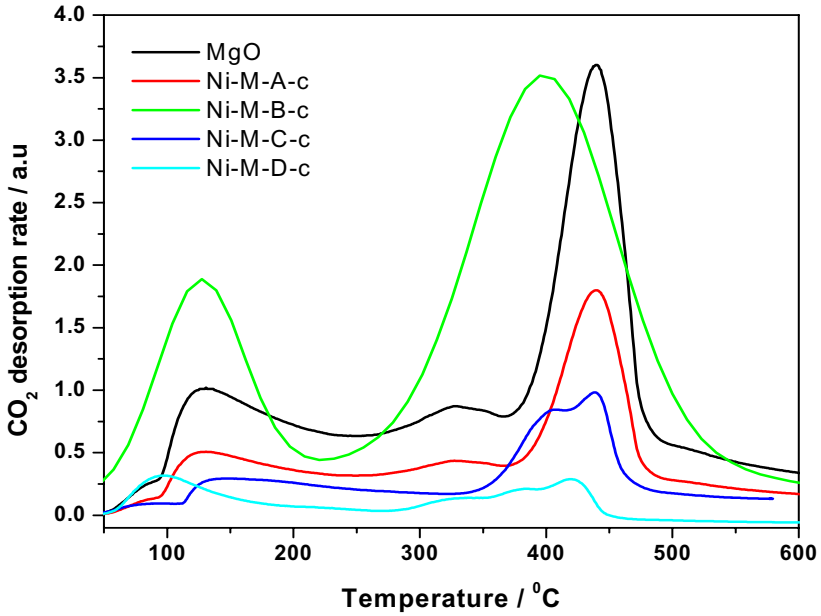

Figure 10. TPD Spectra of support and calcined catalysts

Table 5. Results of CO_2 - TPD studies

Sample	Low temp peak °C	High temp peak °C	mmol CO_2 gm^{-1}	µmol CO_2 m^{-2} (surface basicity)
MgO	128	439	0.57	22.8
Ni-M-A-c	127	436	0.38	17.3
Ni-M-B-c	127	398	0.78	19.0
Ni-M-C-c	137	438	0.28	8.2
Ni-M-D-c	94	420	0.19	12.7

The density of basic site is better expressed as surface basicity (µmols of CO_2 desorbed per m^2). Introduction of NiO has reduced the surface density of basic sites on all samples. The high temperature peak of Ni-M-B-c has been shifted considerably (from 439 °C of MgO to 398 °C). TPR studies had revealed that on this sample, NiO is covered with MgO particles (see TPR Figure 9 and Table 3). The reducibility is also high for this sample, which indicates that NiO is near to the surface. The large number of Ni^{2+} ions under the MgO surface can perturb the electronic structure of MgO and reduce the strength of basic sites [18].

The incoming Ni^{2+} ions on the surface of MgO, not only reduces the number of basic sites but also reduces the basic strength. Thus on Ni-M-B-c, large number low strength basic sites are present.

8.5 SEM images

Figure 11 (SEM images) shows the morphology of samples differ considerably.

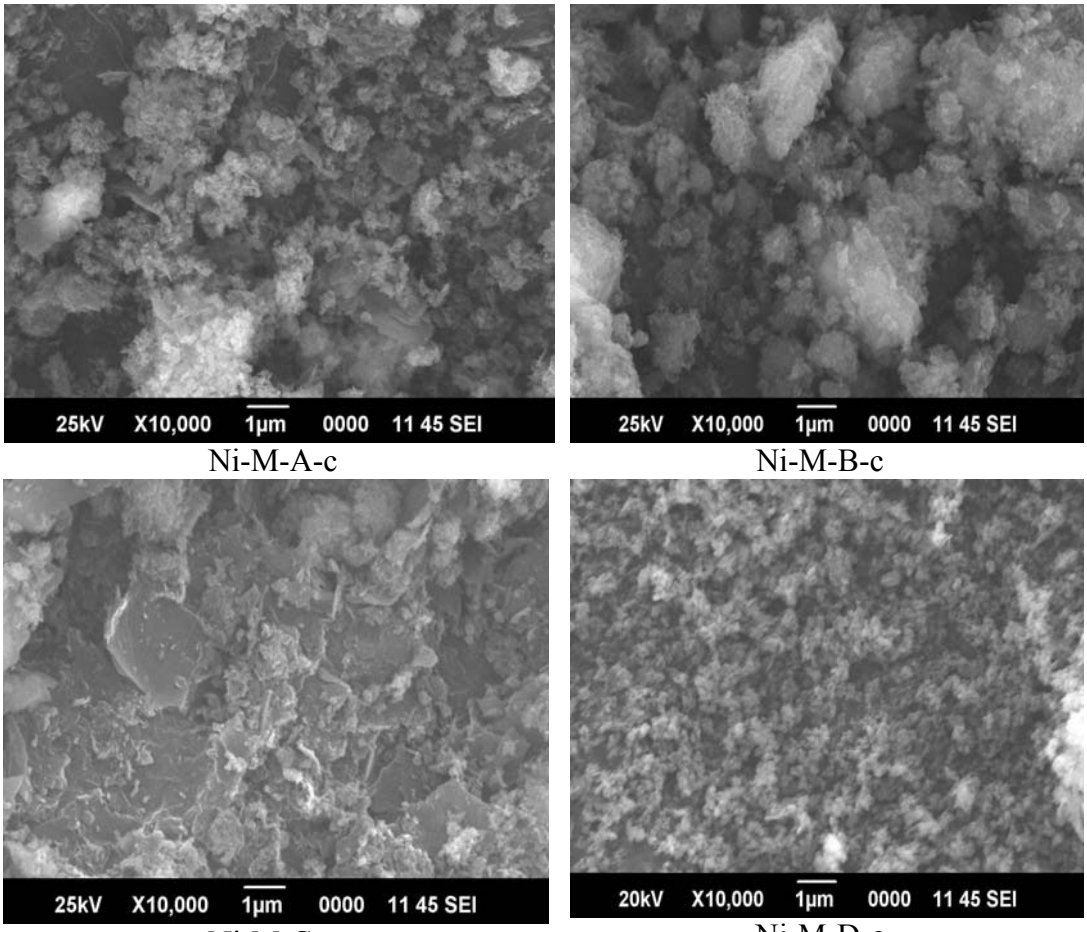

Ni-M-A-c Ni-M-B-c

Ni-M-C-c Ni-M-D-c

Figure 11. Scanning Electron Micrographs of the calcined catalysts

The particle size of sample Ni-M-D-c is considerably lower than others. Sheet like structure has been formed on Ni-M-A-c and Ni-M-C-c, while the sample Ni-M-B-c the structure has been formed by build up of irregularly shaped small particles (amorphous). The difference in the decomposition properties of the precursors should be the reason for the difference in morphology.

8.6 Cyclohexanol decomposition

Cyclohexanol decomposition proceeds selectively to cyclohexanone formation on MgO catalysts [19]. The basic sites present on MgO direct the reaction towards formation of cyclohexanone. Literature reports [19, 20] reveal that NiO is highly active for this decomposition reaction; but selectivity towards cyclohexanone is relatively low. Although metallic nickel is more active for the reaction, by products like phenol and benzene are formed on nickel metal [21]. The results of cyclohexanol decomposition are given in Table 6.

Table 6. Results of cyclohexanol decomposition on reduced catalysts

Catalyst	Conversion (%)	Selectivity to cyclohexanone (%)
Ni-M-A-r	33	83
Ni-M-B-r	48	85
Ni-M-C-r	19	68
Ni-M-D-r	14	60

Reduction = 550°C for four hours; Reaction temperature = 350°C; Time on stream = two hours; WHSV = 2.7 hr^{-1}; N_2 flow = 20 ml min^{-1}

The only byproduct formed was cyclohexene on the catalysts. Ni-M-B-r exhibits high activity and selectivity for the reaction. The percentage conversion on these catalysts shows a direct relationship with the BET surface areas and nickel specific surface areas. Cyclohexanol decomposition to cyclohexanone is a reaction which depends on the % dispersion when studied on supported Cu catalysts [22, 23]. Our studies establish that same relation exists for these Ni/MgO catalysts.

8.7 Reactions of n-butanal in presence of hydrogen

2-Ethyl hexanol is an important chemical used world wide as plasticizer. Current industrial syntheses of this chemical is a multistage process which involves liquid phase aldol condensation of n-butanal to 2-ethyl-2hexenal and further hydrogenation of c=c and c=o to yield 2-ethyl hexanol. The replacement of liquid bases for aldol condensation by solid base catalyst would provide environmental advantages to industrial processes. The use of solid base catalysts would result in decreased reactor corrosion, easier separation of product and catalyst, and the process could be continuous [24]. Aldol condensation of normal aldehydes to higher α-β unsaturated aldehydes on solid base catalysts has been studied in detail [25, 26]. Introduction of a hydrogenating component to the catalyst and the presence of hydrogen can direct the reaction to form saturated aldehyde and then to alcohol. 2-Ethyl hexanal was obtained in good selectivity on Pd supported on basic zeolites from a mixture of n butanal and hydrogen [27]. One pot synthesis of 2-ethyl hexanal and 2-ethyl hexanol starting from syngas has been reported by Srivastava *et al.* [28].

In the present study, the hydrogenating function of the nickel metal and aldolization (basic properties) function of MgO has been coupled to form the Ni/MgO bifunctional catalyst. The details of the reaction procedure are given in chapter 5. The product mixture after the reaction was analyzed by GC and the composition is given in Table 7. The major products obtained are n-butanol, 2-ethyl-2-hexenal, 2-ethyl hexanal and 2-ethyl hexanol. Nickel metal can hydrogenate both n-butanal and also the aldol condensation products (scheme 1).

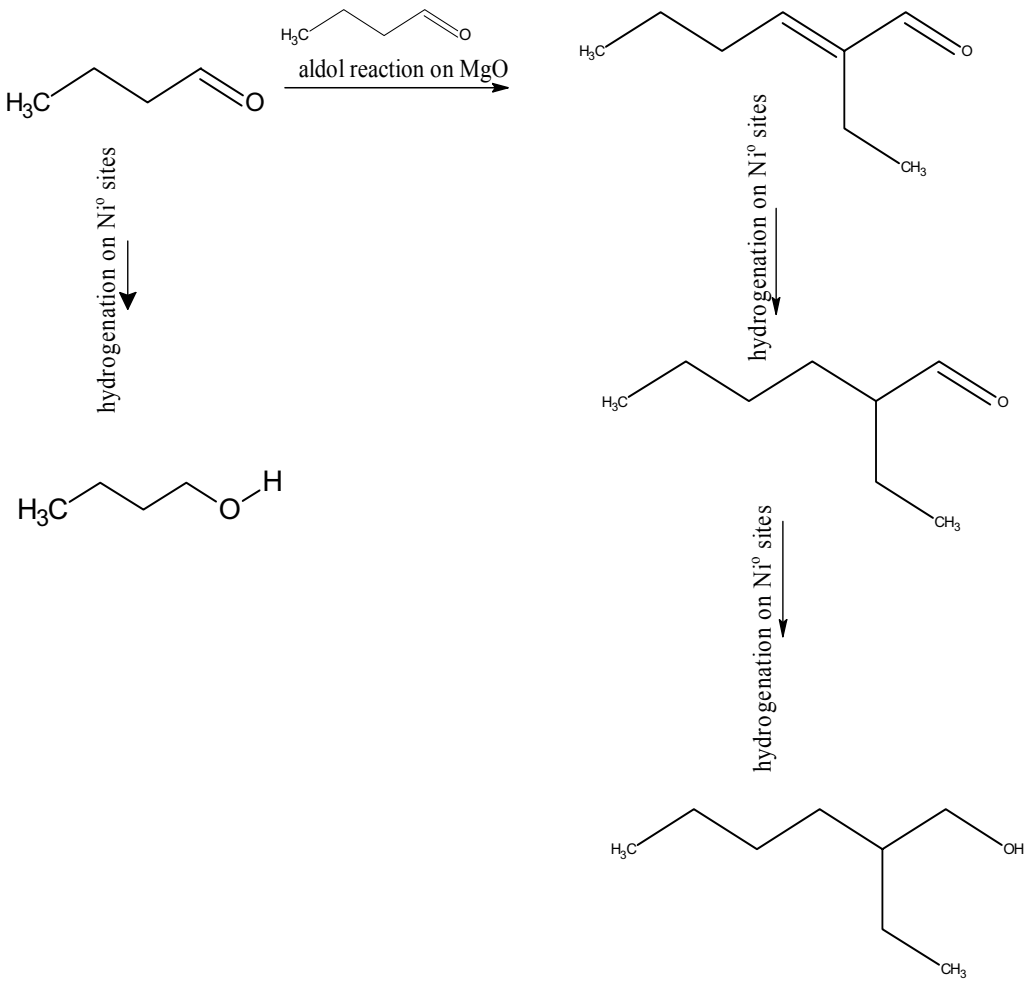

Scheme 1. Major reactions of n butanal on Ni/MgO catalysts

It can be seen that (from Table 7) the product mixture contains high amounts of hydrogenated aldol products (or low n-butanol- direct hydrogenated product) when Ni-M-B-r was used as the catalyst.

The reason for this behaviour can be correlated from the structure of Ni-M-B-c. TPR studies indicate formation of bulk NiO on all catalysts except on Ni-M-B-c. Up on reduction the free NiO forms exposed nickel crystallites which are active for direct hydrogenation. n-butanol was formed (by direct hydrogenation of n-butanal) in higher percentages on these catalysts. Where as, on Ni-M-B-c, Ni^{2+} ions are covered with MgO. On reduction nickel metal crystallites are formed inside the MgO particles. During reaction the incoming n-butanal feed has to meet the basic

sites of MgO first, and undergo aldol condensation. The aldol product then gets hydrogenated on the Ni sites. Figure 12 shows a pictorial representation of catalysts structure and their role in the reaction. CO_2-TPD study has shown that Ni-M-B-c has a high basicity.

Table 7. Analysis of product mixture.

Products	MgO	Ni-M-A-r	Ni-M-B-r	Ni-M-C-r	Ni-M-D-r
n-butanal	45.5	46	38.1	36.2	62.6
n-butanol	0.8	26.7	17.3	34.3	14.6
4-heptanone	0.2	0.8	0.3	0.4	0.8
butyl ether	0.2	1.7	0.5	2.2	3.5
2 ethyl hexanal	0.5	16.5	29.3	14.8	9.1
2ethyl2hexenal	47.1	1.4	0.1	2.6	0.4
2 ethyl hexanol	nd	2.2	10.8	3.6	0.3
butyl butanoate	0.8	0.3	nd	1.7	3
Butanoic acid	0.3	2.1	0.8	1.6	2.7
Trimer	4.6	2.3	2.8	2.6	3

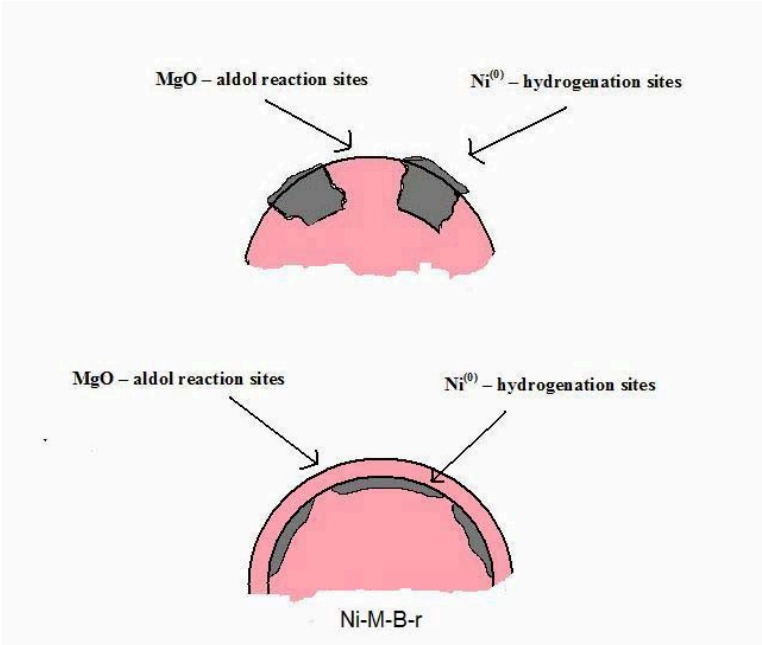

Figure 12. Pictorial representation of reactive sites on Ni/MgO catalysts

Recent study by Chen *et al.* has indicated that reduced Ni/MgO catalysts exhibit higher basicity than that of unreduced NiO/MgO catalysts [29]. As Ni-M-B-c had a high reducibility, upon reduction the basicity would have increased considerably favoring aldol reaction.

8.8 Conclusions

i) The sequence of decomposition of hydrated magnesia and the Ni complex is very important in determining the final physicochemical properties of NiO/MgO catalysts.

ii) The early decomposition of the nickel complex (as in case of Ni-M-B-c) results in formation of high surface area catalysts, which are also highly reducibile and devoid of free NiO.

iii) XRD studies indicate formation of NiO based NiO-MgO solid solution on Ni-M-B-c sample. True solid solution was detected on Ni-M-D-c.

iv) The complex with chloride counter ion leads to the sample (Ni-M-D-c) with lowest surface area and bulk NiO-MgO solid solution formation due to the high temperature required for the decomposition.

v) For cyclohexanol dehydrogenation, high rate was observed on Ni-M-B-r because of high reducibility, basicity and surface area.

vi) For n-butanal reactions, hydrogenated aldol products are formed more on Ni-M-B-r because of its different structure.

vii) The decomposition properties of the complexes having counter ions are very important in deciding the final structure and performance of the catalysts.

References

[1] Y-H. Wang, H-M. Liu, B-Q. Xu., Durable Ni/MgO catalysts for CO_2 reforming of methane: Activity and metal–support interaction., *J. Mol. Catal. A: Chemical* 299 (2009) 44–52

[2] Y-H. Hu and E. Ruckenstein., The characterization of a highly effective NiO/MgO solid solution catalyst in the CO_2 reforming of CH_4., *Catal. Lett.* 43 (1997) 71-77

[3] H. Tsuji, F. Yagi, H. Hattori and H. Kita., Self-condensation of n-Butyraldehyde over solid base catalysts., *J. Catal.* 148 (1994) 759-770

[4] L.M. Gandía, M. Montes., Highly selective one-step formation of methyl isobutyl ketone from acetone with a magnesia supported nickel catalyst., *Appl. Catal. A: General.* 101 (1993) L1-L6

[5] O. Bergadà, P. Salagre, Y. Cesteros, F. Medina, J.E. Sueiras., High-selective Ni-MgO catalysts for a clean obtention of 2-phenylethanol., *Appl. Catal. A: General.* 272 (2004) 125-132

[6] A. Djaidja, S. Libs, A. Kiennemann, A. Barama., Characterization and activity in dry reforming of methane on NiMg/Al and Ni/MgO catalysts., *Catal. Today.* 113 (2006) 194–200

[7] J. Estellé, P. Salagre, Y. Cesteros, M. Serra, F. Medina, J.E. Sueiras., Comparative study of the morphology and surface properties of nickel oxide prepared from different precursors., *Solid State Ionics*. 156 (2003) 233-243

[8] P.L. Llewellyn, V. Chevrot, J. Ragaï, O. Cerclier, J. Estienne, F. Rouquérol., Preparation of reactive nickel oxide by the controlled thermolysis of hexahydrated nickel nitrate., *Solid State Ionics*. 101-103 (1997) 1293-1298

[9] G.C. Bond, S.P. Sarsam., Reduction of nickel/magnesia catalysts., *Appl. Catal.* 38 (1988) 365-377

[10] S. Narayanan, G. Sreekanth., Problems involved in the reducibility of the NiO–MgO system as evidenced by X-ray diffraction, electron paramagnetic resonance, electron spectroscopy for chemical analysis and adsorption techniques., *J. Chem. Soc., Faraday Trans*. 89 (1993) 943-949

[11] M. Serra, P. Salagre, Y. Cesteros, F. Medina and J.E. Sueiras., Design of NiO–MgO materials with different properties., *Phys. Chem. Chem. Phys.* 6 (2004) 858-864

[12] Y-H. Wang, H-M. Liu and B-Q. Xu., Durable Ni/MgO catalysts for CO_2 reforming of methane: Activity and metal–support interaction., *J. Mol. Catal. A: Chemical.* 299 (2009) 44–52

[13] F. Arena, B.A. Horrell, D.L. Cocke, A. Parmaliana, N. Giordano., Magnesia-supported nickel catalysts I. Factors affecting the structure and morphological properties., *J. Catal*. 132 (1991) 58–67

[14] G. Parravano., The reduction of nickel oxide by hydrogen., *J. Am. Chem. Soc.*, 74 (1952) 1194-1198

[15] A. Zecchina, G. Spoto, S. Coluccia, E. Guglielminotti., Spectroscopic study of the adsorption of carbon monoxide on solutions of nickel oxide and magnesium oxide. Part 2.—Samples pretreated with hydrogen., *J. Chem. Soc., Faraday Trans. 1* 80 (1984) 1891-1901

[16] J.A Lercher, C. Clombier, H. Noller., Acid-Base Properties of Alumina-Magnesia Mixed Oxides. Part 4.-Infrared Study of Adsorption of Carbon Dioxide., *J. Chem. Soc. Faraday Trans*. I , 80 (1984) 949-959

[17] J.I. Di Cosimo, V.K. Diez, M. Xu, E. Iglesia, C.R. Apesteguia., Structure and surface and catalytic properties of Mg-Al Basic Oxides., *J. Catal.* 178 (1998) 499-510

[18] F. Arena, A. Parmaliana,, J.N. Mondello, F. Frusteri, N. Giordanot., Influence of the calcination treatment on the surface chemical properties of Ni/MgO catalyst: A CO_2 temperature programmed desorption approach., *Langmuir* 7 (1991) 1555-1557

[19] C.P. Bezouhanova, M.A. Al-Zihari., Cyclohexanol conversion as a test of the acid-base properties of metal oxide catalysts., *Catal. Lett.* 11 (1991) 245-248

[20] R.D. Srivastava, J. Onuferko, and J.M. Schultz., Characterization and activity of nickel oxide supported on γ- Alumina., *Ind. Eng. Chem. Fundam*. 21 (1982) 457-463

[21] M. Dobrovolszky, P. Tetenyi and Z. Paal., Catalytic transformations of cyclohexanol on Group VIII metal catalysts., *J. Catal.* 74 (1982) 31-43

[22] K.V.R. Chary, G.V. Sagar, C.S. Sreekanth, V.V. Rao., Characterization and catalytic functionalities of copper oxide catalysts supported on zirconia., *J. Phys. Chem. B*. 111 (2007) 543-550

[23] H-Fu. Chang, M.A Saleque, W-S. Hsu, W-H. Lin., Characterisation and dehydrogenation activity of Cu/Al_2O_3 catalysts prepared by electroless plating technique., *J. Mol. Catal. A: Chemical*. 109 (1996) 249-260

[24] H. Hattori., Basic catalysts and fine chemicals., *Stud. Surf. Sci. Catal*. 78 (1993) 35-50.

[25] H. Tsuji, F. Yagi, H. Hattori, H. Kita., Self-Condensation of *n*-Butyraldehyde over solid base catalysts., *J. Catal.* 148 (1994) 759-770

[26] H. E. Swift, J. E. Bozik, F. E. Massoth., Vapor-phase aldol condensation of *n*-butyraldehyde using a reduced tin-silica catalyst., *J. Catal.* 15 (1969) 407-416

[27] A-N. Ko, C. H. Hu, J-Y Chen., Efficient direct synthesis of 2-ethylhexanal from *n*-butyraldehyde and hydrogen using palladium modified base catalysts., *Appl. Catal. A: General.* 184 (1999) 211-217

[28] V.K. Srivastava, S.K. Sharma, R.S. Shukla, R.V. Jasra., The 'single-pot' synthesis of C_{2n+2}-aldol derivatives from C_n-alkenes using multi-functional catalyst., *Catal. Commun.* 7 (2006) 879–884

[29] H. Chen, M. Xue, J. Shen., Surface Properties of Ni/MgO Catalysts for the hydrogenation of lauronitrile., *Catal. Lett.* 135 (2010) 246–255

Chapter 9

GENERAL CONCLUSIONS AND SUGGESTIONS FOR FURTHER RESEARCH

Contents

9.1 General conclusions

The general conclusions arrived from the previous chapters are discussed here.

The literature survey conducted in Chapter 1 indicates the importance of supported nickel catalysts in the chemical industry. Some new areas of application for supported nickel catalysts are discussed. Previous investigations which indicate the importance of '*selections of precursors' are* cited. The effect of chelating ethylenediamine precursors in catalyst preparation is discussed in detail. The chapter ends with the significance of the present work.

The work presented in Chapter 2 shows that the counter ions can influence the decomposition properties of the complexes. The products obtained (nickel or nickel oxide) also depends on the counter ions. Phase pure nickel metal obtained by the decomposition of $[Ni(en)_2(H_2O)_2](NO_3)_2$ was characterized and its oxidation properties were discussed. The structural and morphological properties of the nickel oxides were different. In general, the results indicate that, the complex with fast decomposition at low temperatures gives high surface area, while the sample with

slow decomposition at high temperature gives low surface area and high crystallite size.

Chapter 3 gives the details of kinetics of temperature programmed reduction of nickel oxides obtained from thermolysis of the complexes. The kinetic triplets were obtained by following procedure of non isothermal analysis and Malek's procedure. Crystallite size has a strong influence on the reduction mechanism. Increase of crystallite size leads to increase in reduction temperature and increase in activation energy. The NiO sample with chlorine impurity reduces at higher temperature but with low activation energy. In general as the precursors are changed, the product's reduction properties change.

The four metal complexes were used to impregnate γ-Al_2O_3 spheres. The macrodistributions obtained after wet impregnation and pore volume impregnation are discussed in Chapter 4. Nearly uniform profiles were obtained for ethylenediamine complexes. The low strength of adsorption of ethylenediamine complexes and high viscosity of the impregnating solution are the reasons for achieving uniform profiles. As the counter ions are changed, the viscosity changes which affects the impregnation depths. The prepared egg shell and uniform pellets gave different product distributions for cyclohexanol decomposition reaction.

Details the preparation of supports and supported metal complexes are presented in Chapter 5. The details on instruments and procedures used to characterize the supported catalysts are also given. The ethylenediamine complexes of nickel were used to prepare catalysts and the supports used were α-Al_2O_3, γ-Al_2O_3 and MgO. The influence of the counter ions on the structure and activity of the catalysts are discussed in the remaining chapters.

The use of different counter ions results in formation of different nickel species on α-Al_2O_3. Details of the structure and reactivity of Ni/α-Al_2O_3 catalysts are given in Chapter 6. The catalyst formed by decomposition of metal complex with nitrate counter ion had high surface area and intermediate metal support interaction. The different nickel species formed after reduction gave different

reactivity for the model reactions studied. The decomposition properties of the precursors are identified to be the main factor determining the final properties of the catalysts.

Structure and reactivity of Ni/γ-Al_2O_3 catalysts are discussed in Chapter 7. The precursor having chloride counter ion decomposes at high temperature. This high temperature decomposition forced the nickel ions to migrate to γ-Al_2O_3 lattice leading to formation of nickel aluminate. The low temperature, sudden exothermic decomposition of ethylenediamine precursor having nitrate counter ion gave catalyst with high surface area. Different nickel precursors gave different nickel species as identified by UV-DRS and TPR. The product distribution of cyclohexanol decomposition depends up on the different species formed on the catalysts.

The counter ions influence the extent of NiO-MgO solid solution formation, when the precursors were used to prepare Ni/MgO catalysts. The details of this study are presented in Chapter 8. The sequence of decomposition of hydrated magnesia and the nickel precursors is the major factor determining the final structure of the catalyst. The nitrate counter ion results in the early decomposition of precursor leading to formation of highly reducibile catalyst. This catalyst gave more hydrogenated aldol products for the reactions of n-butanal and hydrogen because of its different structure.

9.2 Outcome of present work

One of the important parameters which determines the final properties of the catalysts are the decomposition properties of the catalyst precursors. The counter ions present on the metal complexes influences their decomposition. They can accelerate or decelerate the decomposition, make the reaction exothermic or endothermic and can shift the decomposition temperatures. These properties can influence the location of nickel on the support (metal migration to support). The activity and selectivity of the catalyst depends upon this location as metal support interactions are crucial for the supported metal catalysts. The nickel complex, $[Ni(en)_2(H_2O)_2](NO_3)_2$ exhibits lowest temperature of decomposition in both the

supported and unsupported form. Furthermore, the exothermic decomposition of this complex occurs at a fast rate (before reaching high temperature). As the exothermic events are limited to a small time period, the sintering of particles is avoided resulting in materials with high surface area. If the decomposition happens in a wide temperature range (as in case of $[Ni(en)_2(H_2O)_2](Cl)_2$), the particles are subjected to high temperature while forming the final phase. This creates sintering and also migration of metal ions to the support structure.

In final I would like to end the discussion with a single sentence

"The selection of the catalyst precursor with suitable decomposition properties is an important step in determining the final properties of the catalyst"

9.3 Suggestions for further research

i.) Nickel oxides with different morphologies are formed by the decomposition of the complexes having different counter ions(Chapter 2). The catalytic activities of these nickel oxides having different morphologies will be an interesting subject for further studies [1].

ii.) The EGA (Evolved gas analysis) and EXAFS (Extended X-ray Absorption Fine Structure) studies of the decomposition can give further details about the precursor decomposition.

iii.) Only three counter ions were selected for the present study. The work can be extended to other water soluble metal complexes with different counter ions. In future a database containing the decomposition properties and the extent of metal migration to the support may be prepared, which would certain help in better design and development of new catalysts.

iv.) The bimetallic or trimetallic catalysts of nickel are an emerging field of research [2-4]. The chelating ligands can be used to prepare bimetallic complexes. The alloy formation in such catalysts will definitely depend on the decomposition properties of the precursors.

References

[1] M.M. Natile, A. Glisenti., Surface Reactivity of NiO: Interaction with Methanol., *Chem. Mater.* 14 (2002) 4895-4903

[2] J.A. lvarez-Rodriguez, M. Cerro-Alarcon, A. Guerrero-Ruiz, I. Rodriguez-Ramos, A. Arcoya., Effect of nickel precursor and the copper addition on the surface properties of Ni/KL-supported catalysts for selective hydrogenation of citral., *Appl. Catal. A: General* 348 (2008) 241–250

[3] B. Bridier, J. Perez-Ramirez., Cooperative Effects in Ternary Cu-Ni-Fe Catalysts lead to enhanced alkene selectivity in alkyne hydrogenation., *J. Am. Chem. Soc.* 132 (2010) 4321-4327

[4] S.K. Singh, Q. Xu., Bimetallic Ni-Pt nanocatalysts for selective decomposition of hydrazine in aqueous solution to hydrogen at room temperature for chemical hydrogen storage., *Inorg. Chem.* (2010). doi: 10.1021/ic1007654

List of Publications

1. **P.P. Robinson**, V. Arun, S. Manju, C.U. Aniz, K.K.M. Yusuff, "Oxidation kinetics of nickel nano crystallites obtained by controlled thermolysis of diaqua-bis(ethylenediamine)nickel(II) nitrate" *J. Therm. Anal. Calorim.* 100 (2010) 733-740

2. **P.P. Robinson**, V. Arun, S. Manju, C.U. Aniz, K.K.M. Yusuff , "The active phase distribution in Ni/γ-Al_2O_3 catalysts prepared by impregnation of bis(ethylenediamine)nickel(II) complexes" (under review: *Chemical Engineering Communications*)

3. ***** V. Arun, N. Sridevi, **P.P. Robinson**, S. Manju, K.K.M. Yusuff, "Ni(II) and Ru(II) Schiff base complexes as catalysts for the reduction of benzene" *J. Mol. Catal. A: Chem.* 304(1-2) (2009) 191-198

4. ***** V. Arun, **P.P. Robinson**, S. Manju, P. Leeju, G. Varsha, V. Digna, K.K.M. Yusuff, "A novel fluorescent bisazomethine dye derived from 3-hydroxyquinoxaline-2- carboxaldehyde and 2,3-diaminomaleonitrile" *Dyes and Pigments.* 82(3) (2009) 268-275

***** Not related to the thesis

O' Lord, It was good for me to suffer,

so that I might learn your statutes.

(Psalm 119:71). The Bible.